Sujata K. Bhatia

Biomaterials for Clinical Applications

Springer

Biomaterials for Clinical Applications

Sujata K. Bhatia

Biomaterials for Clinical Applications

Springer

Sujata K. Bhatia
Central Research and Development
DuPont Company
Wilmington, DE 19880-0262, USA
sujata.k.bhatia@usa.dupont.com

ISBN 978-1-4419-6919-4 e-ISBN 978-1-4419-6920-0
DOI 10.1007/978-1-4419-6920-0
Springer New York Dordrecht Heidelberg London

Library of Congress Control Number: 2010934220

Preface

The field of biomaterials science currently faces an unprecedented opportunity to improve and save the lives of millions worldwide. A unique integration of chemistry, biology, engineering, and medicine, biomaterials science brings novel materials to bear on medical problems. The past few years have witnessed an explosion in the field of biomaterials, with an expansion of both the compositions and the applications of medical implant materials. While traditional biomaterials have been designed from polymers, ceramics, and metals, the newest generation of biomaterials incorporates biomolecules, therapeutic drugs, and living cells. At the same time that biomaterials science is advancing in the laboratory, the incidence of serious diseases is rising in the global community. The increasing proportion of older people in the global population is contributing to the increase of age-associated chronic diseases, including heart disease and cancer. Infectious diseases also represent a significant burden to global health; mortality from HIV/AIDS, tuberculosis, and infectious gastrointestinal diseases remains high. Physicians and biomedical researchers must be ready to address growing healthcare needs in every part of the world. Innovative biomedical materials will only reach the clinic if these technologies solve pressing clinical problems.

Biomaterials scientists who wish to impact global health must first understand where the most urgent clinical needs lie. Translation of innovative technologies into clinical usage will require close collaboration between physicians and biomaterials scientists, so that scientists can address unmet clinical needs and physicians can appreciate novel technologies. The present volume aspires to bridge the gap between the laboratory and the clinic, by identifying needs for biomedical materials in the context of the most prevalent diseases worldwide. The book is organized according to the World Health Organization's report of the top 10 causes of death worldwide and lays out opportunities for both biomaterials scientists and physicians to tackle each of these leading contributors to mortality. The introductory chapter discusses the global burden of disease. Each of the subsequent 10 chapters focuses on a specific disease process, beginning with the leading cause of death worldwide, cardiovascular disease. Every chapter begins by describing the underlying pathology of the disease and then discusses prospective research areas for novel biomaterials to modify the disease process. Diseases addressed in the book include coronary

artery disease, HIV/AIDS, pneumonia, cancer, stroke, and gastrointestinal disease, as well as traumatic injuries. The book also covers a wide range of technologies necessary to defeat these diseases, including imaging agents, drug delivery platforms, biosensors, tissue engineered constructs, antimicrobials, and vaccines.

Several excellent biomaterials books describe novel technologies in biomedical materials and proceed to envision potential applications for such technologies. The present volume is not intended to replace those books. Rather, this book aims to provide a complementary perspective to the existing biomaterials literature; while other books take a technology-centered approach to biomaterials, this book takes a disease-centered approach. The book addresses the question, *"Where are clinical needs most urgent, and how can biomaterials be designed to meet those needs?"* The book provides detailed descriptions of relevant disease pathologies, both to provide necessary background for biomaterials development and to inspire new innovations in medical technology. This perspective may provide useful insights for biomaterials scientists and engineers, as well as physicians and surgeons who utilize emerging biomedical materials technologies in their clinical practice. Such an approach can aid researchers and administrators in allocating resources and setting research priorities, to ensure that biomaterials advances and new technologies actually fulfill an unmet clinical need. In addition, the disease-centered approach is valuable for science and engineering education, as it conveys to students the excitement and relevance of materials science to solving the world's most pressing healthcare problems. Finally, this approach enables scientists and engineers to converse knowledgeably with clinicians regarding disease processes and technological solutions.

It is indeed an exciting time to work in the field of biomaterials science. The emerging class of biomedical materials, including surface-modified biomaterials, smart biomaterials, bioactive biomaterials, and tissue engineered materials, will have improved properties of biocompatibility, tunability, and biological functionality. This book advocates for disease-oriented biomaterials research, so that emerging technologies can be most effectively deployed from "bench to bedside" to defeat existing diseases. If appropriately designed, innovative new biomedical materials will have the capacity to lower morbidity and mortality, lessen suffering, and improve the quality of life for patients worldwide. The global imperative for novel biomedical materials is clear, now more than ever.

Acknowledgments

First and foremost, I would like to thank Dr. Ken Howell, Senior Editor at Springer, for believing in the importance of biomaterials and giving me the opportunity to publish this book. I would also like to thank my family for their support and encouragement during the composition of this book. I am thankful to my parents, Kamlesh and Kanak Bhatia, and my three siblings, Sunita, Surita, and Krishan Bhatia, for their love. I am additionally thankful to my niece Indira and my three nephews, Julian, Evan, and Kumar, for their constant inspiration. I am grateful to my high school biology teacher, Mr. Harry Dillner, for first providing me with the confidence and knowledge to enter biomedical sciences. I am grateful to my advisors in graduate school, Dr. Daniel Hammer and Dr. Skip Brass, for imparting me with the necessary skills to pursue a career in biomaterials research. I am additionally blessed with wonderful scientific colleagues at DuPont and the University of Delaware. Finally, I am thankful to all of the brilliant and dedicated biomaterials researchers, whose innovations form the basis for this book. I am confident that their work can alleviate suffering, eliminate disease, and change lives. For that reason, I have written this book.

Contents

About the Author

Sujata K. Bhatia is a physician-scientist at DuPont Applied BioSciences and an affiliated faculty member in the Department of Chemical Engineering at the University of Delaware. She earned three bachelor's degrees, in biology, biochemistry, and chemical engineering, and a master's degree in chemical engineering at the University of Delaware. She then attended the University of Pennsylvania School of Medicine, where she earned her MD and PhD in bioengineering. She currently contributes to medical biomaterials projects, as well as health and nutrition programs at DuPont. She teaches biochemical engineering and biomedical engineering courses at the University of Delaware.

Chapter 1
Introduction

One of the most important means for gauging the effectiveness of the global healthcare system, as well as the biomedical research enterprise, is to measure how many people die each year and track the causes of death. Such numbers provide a meaningful, concrete basis for guiding not only public health actions but also biomedical science and technology development. In late 2008, the World Health Organization (WHO) published the most recent update to its Global Burden of Disease study, which gives the leading causes of death for the year 2004 (World Health Organization 2008). Prepared by the WHO Department of Health Statistics and Informatics, the study presents comprehensive, comparable, and internally consistent estimates of mortality and burden of disease by cause for all regions of the world. The data are further classified by age, sex, and region. These figures are critical for improving health and reducing preventable deaths in both the developing and the developed world.

Indeed, the Global Burden of Disease study has already served as an important input to health decision-making and planning processes. For instance, the results from the year 2001 study provided a framework for cost-effectiveness and priority setting analyses for the Disease Control Priorities Project, a joint project of the World Bank, WHO, and the National Institutes of Health and funded by the Bill and Melinda Gates Foundation. The WHO Director-General, Dr. Margaret Chan, noted in her speech to the World Health Assembly in May 2007, "Reliable health data and statistics are the foundation of health policies, strategies, and evaluation and monitoring"; she additionally stated, "Evidence is also the foundation for sound information for the general public." Accurate epidemiological assessments can focus the allocation of finite, limited healthcare resources toward the most significant healthcare needs.

Biomaterials scientists are uniquely positioned to improve the health of the general population, through the clinical application of novel therapeutic technologies. Yet the actual impact of biomaterials on the overall burden of disease and death has not been systematically examined. Similarly, the role of health statistics in shaping biomaterials research directions has not been previously considered. If many children are dying of infectious diseases, for example, then biomaterials development can be aimed toward technologies such as biomolecules for pathogen detection, peptides for microbial control, and polymeric constructs for vaccination. The worldwide

S.K. Bhatia, *Biomaterials for Clinical Applications*,
DOI 10.1007/978-1-4419-6920-0_1, © Springer Science+Business Media, LLC 2010

burden of disease is a useful starting point for reviewing progress in biomaterials science and evaluating the current status of research efforts. More importantly, the global disease burden lends insights for future biomaterials thrusts and the effective deployment of scientific and engineering capital. Such an approach ensures that biomaterials science remains relevant and beneficial to human needs.

1.1 The Worldwide Burden of Disease

An estimated 58.8 million people died worldwide in 2004 according to the Global Burden of Disease study (World Health Organization 2008). Of these deaths, 27.7 million were females and 31.1 million were males. The study classifies causes of death into three broad cause groups:

- Group I – communicable, maternal, perinatal, and nutritional conditions
- Group II – non-communicable diseases
- Group III – injuries

Group I causes are conditions that typically occur in poorer populations. Globally, these conditions are responsible for 3 out of 10 deaths in both males and females (Fig. 1.1). Group II conditions result in the most deaths among men and women; they account for approximately 6 out of 10 deaths globally. Group III

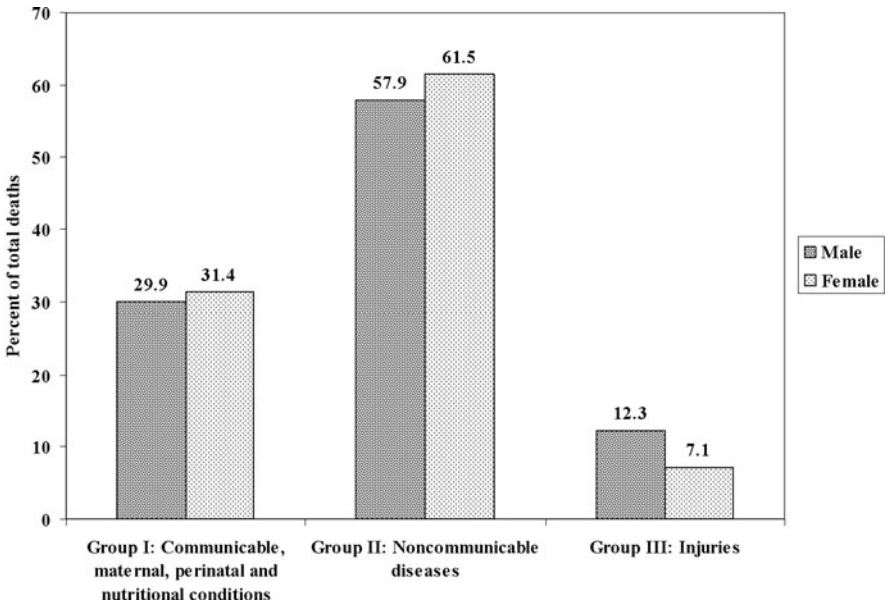

Fig. 1.1 Distribution of deaths in the world by sex in 2004

Table 1.1 The top 10 causes of death worldwide in 2004

Cause of death	Deaths in millions	Percentage of deaths
Coronary heart disease	7.20	12.2
Stroke and other cerebrovascular disease	5.71	9.7
Lower respiratory infections	4.18	7.1
Chronic obstructive pulmonary disease	3.02	5.1
Diarrheal diseases	2.16	3.7
HIV/AIDS	2.04	3.5
Tuberculosis	1.46	2.5
Trachea, bronchus, lung cancers	1.32	2.3
Road traffic accidents	1.27	2.2
Prematurity and low birth weight	1.18	2.0

World Health Organization (2008)

causes are the source of 1 out of 10 deaths worldwide. There is a notable difference in sexes for Group III, with injuries causing 1 in 8 male deaths and 1 in 14 female deaths.

The 10 leading causes of death worldwide in 2004 are given in Table 1.1. Of these top 10 causes of death, 5 are Group I communicable and perinatal conditions: lower respiratory infections, diarrheal diseases, HIV/AIDS, tuberculosis, and diseases of prematurity and low birth weight. Four are Group II non-communicable diseases: coronary artery disease, stroke and cerebrovascular diseases, chronic obstructive pulmonary disease , and lung cancers. One is a Group III condition, injuries from road traffic accidents. From the perspective of organ systems affected, it is remarkable that 4 of the top 10 causes of death involve the pulmonary system: lower respiratory infections, chronic obstructive pulmonary disease, tuberculosis, and lung cancers (Fig. 1.2). Two of the top 10, coronary heart disease and stroke, primarily involve the vasculature.

Coronary artery disease and cerebrovascular disease are the most frequent causes of death. These are followed by lower respiratory infections (including pneumonia), chronic obstructive pulmonary disease, and diarrheal disease. The infectious diseases HIV/AIDS and TB are the sixth and seventh leading causes of death, respectively. Globally, lung cancers (including tracheal and bronchial cancers) are the most common cause of cancer death among men and the second most common cause of cancer death among women; lung cancers are the eighth leading cause of death worldwide. Traumatic injuries from road traffic accidents are the ninth leading cause of death, and neonatal diseases of prematurity and low birth weight are the tenth most frequent cause of death.

The distribution of age at death reveals a striking pattern (Fig. 1.3). Globally a total of 30.2 million deaths (more than half of all deaths) occurred in people aged 60 years and older. At the same time, almost one in five deaths in the world was of a child under the age of 5 years. Different regions of the world demonstrate remarkable differences in the distribution of deaths by age (Figs. 1.4 and 1.5). In high-income countries, only 1% of deaths occurred in children under 15 years of

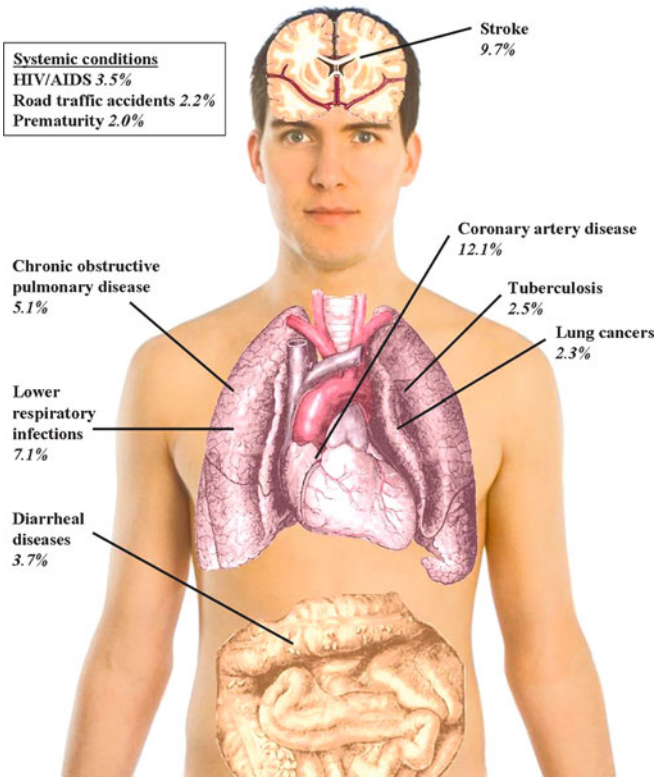

Fig. 1.2 The top 10 causes of death worldwide in 2004 and affected organ systems

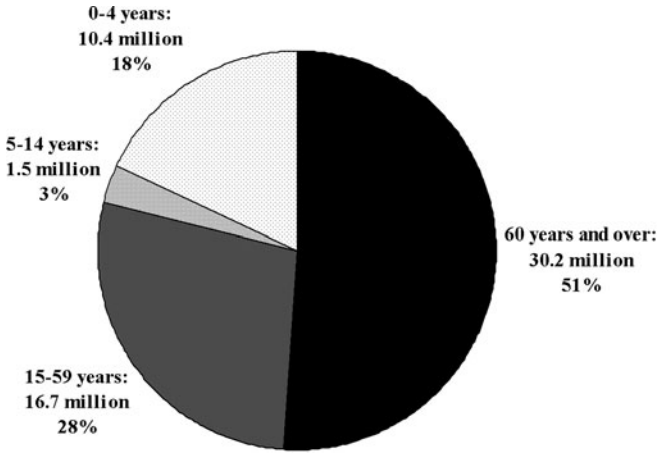

Fig. 1.3 Distribution of age at death and numbers of deaths worldwide in 2004

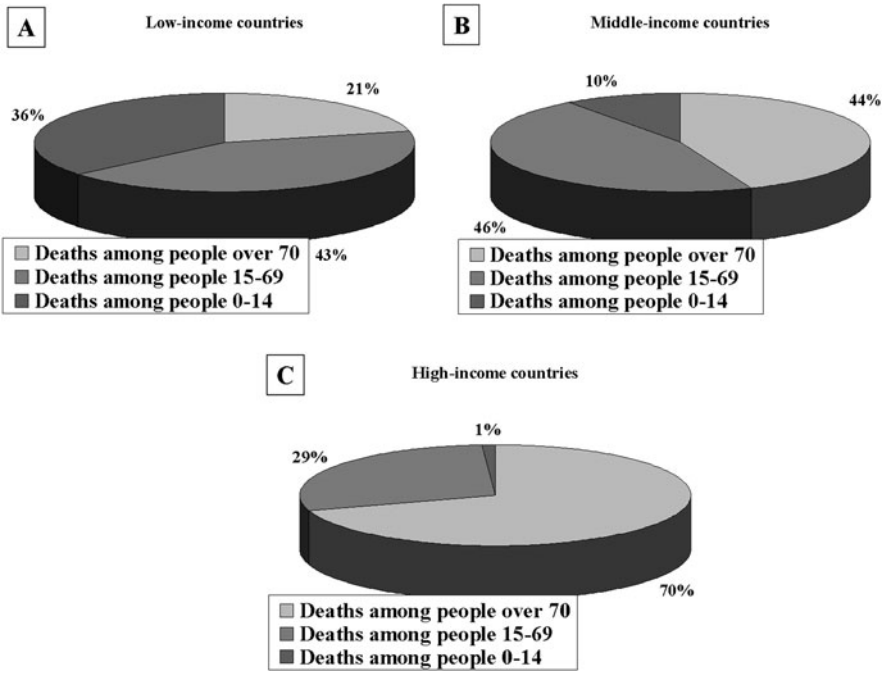

Fig. 1.4 Death distribution by age and income in 2004

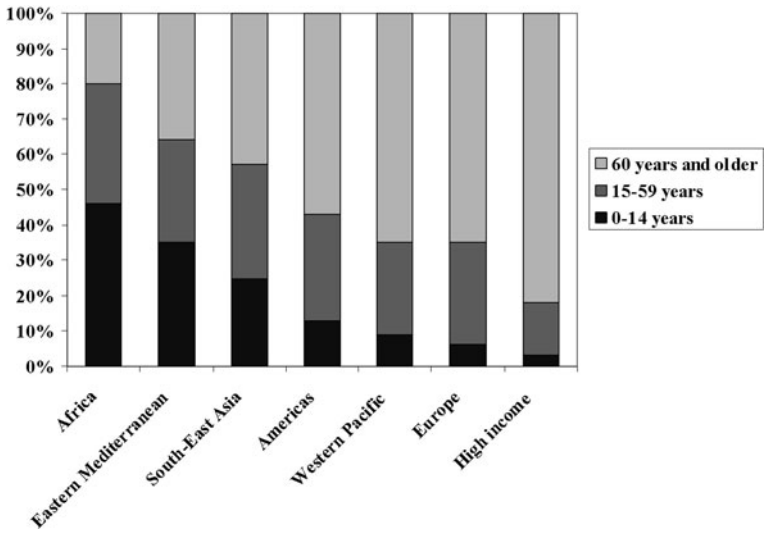

Fig. 1.5 Death distribution by age and region in 2004

age, while 84% of deaths were people aged 60 years and older. In contrast, in the African region, 46% of all deaths were in children under 15 years of age, while only 20% of deaths occurred in people aged 60 years and older. As the Global Burden of Disease study notes, "In Africa, death takes the young; in high-income countries, death takes the old" (World Health Organization 2008). More than 7 out of every 10 child deaths are in Africa and Southeast Asia, and 99% of child deaths occur in low-income and middle-income countries. Deaths in the neonatal period (0–27 days) account for more than one third of all child deaths.

There are significant differences in the leading causes of death between affluent nations and poorer nations. The Global Burden of Disease study classifies countries as high income, middle income, or low income based on the gross national income per capita, as shown in Table 1.2. For every 1,000 people who died in 2004, approximately 138 would have come from high-income countries, 415 from middle-income countries, and 447 from low-income countries. The top 10 causes of death in high-income, middle-income, and low-income countries are given in Table 1.3. In low-income countries, the predominant causes of death are infectious and parasitic disease (including malaria) and perinatal conditions; 7 of the top 10 causes of death in low-income nations are Group I communicable and perinatal conditions. In high-income countries, 9 of the 10 leading causes of death are Group II non-communicable conditions, including four types of cancer. Diabetes mellitus also emerges as a leading cause of death in high-income countries; this chronic disease imparts a dramatically increased risk for cardiovascular disease and stroke and is strongly correlated with the top two causes of death worldwide. In middle-income countries, the 10 leading causes of death are again dominated by Group II non-communicable diseases; they additionally include Group III injuries from road traffic accidents as the sixth most common cause of death and the communicable disease tuberculosis as the ninth leading cause of mortality.

The main differences between rich and poor countries with respect to aging and mortality are summarized in Table 1.4. Beyond economic differences in the major causes of death, it is essential to recognize regional distinctions in the leading causes of mortality. HIV/AIDS is the main cause of adult mortality in Africa; 35% of adult deaths in Africa are attributable to HIV/AIDS. Injuries and cardiovascular disease are the leading causes of death among men in the low-income and middle-income countries of Europe; together these two conditions are responsible for two-thirds of adult male mortality in this region. Injuries are the main cause of death for adult men in the low-income and middle-income countries of the Americas, including Latin America and the Caribbean.

The relative impact of various diseases and conditions worldwide is thus reflected in the leading causes of death. A related metric for assessing the effects of various conditions is the Years of Life Lost (YLL). The YLL is a measure of premature mortality that incorporates both the frequency of deaths and the age at which death occurs. This analysis results in major shifts in the relative importance of the leading causes of death (Fig. 1.6), as it assigns weight to the age at death. The main causes of YLL are neonatal conditions (prematurity and low birth weight, birth asphyxia and birth trauma, and other perinatal conditions), lower respiratory infections, diarrheal diseases, and HIV/AIDS. Because of economic and regional disparities with regard

Table 1.2 Countries grouped by income per capita in 2004

Income group	Countries included
High income (Gross national income of US $10,065 or more per capita)	Andorra, Aruba, Australia, Austria, Bahamas, Bahrain, Belgium, Bermuda, Brunei Darussalam, Canada, Cayman Islands, Channel Islands, Cyprus, Denmark, Faeroe Islands, Finland, France, French Polynesia, Germany, Greece, Greenland, Guam, Iceland, Ireland, Isle of Man, Israel, Italy, Japan, Kuwait, Liechtenstein, Luxembourg, Malta, Monaco, The Netherlands, The Netherlands Antilles, New Caledonia, New Zealand, Norway, Portugal, Puerto Rico, Qatar, Republic of Korea, San Marino, Saudi Arabia, Singapore, Slovenia, Spain, Sweden, Switzerland, United Arab Emirates, United Kingdom, United States of America, Virgin Islands
Upper middle income (Gross national income of US $3256–10,065 per capita)	American Samoa, Antigua and Barbuda, Argentina, Barbados, Belize, Botswana, Chile, Costa Rica, Croatia, Czech Republic, Dominica, Equatorial Guinea, Estonia, Gabon, Grenada, Hungary, Latvia, Lebanon, Libyan Arab Jamahiriya, Lithuania, Malaysia, Mauritius, Mexico, Northern Mariana Islands, Oman, Palau, Panama, Poland, Russian Federation, Saint Kitts and Nevis, Saint Lucia, Saint Vincent and the Grenadines, Seychelles, Slovakia, South Africa, Trinidad and Tobago, Turkey, Uruguay, Venezuela (Bolivarian Republic of)
Lower middle income (Gross national income of US $826–3255 per capita)	Albania, Algeria, Angola, Armenia, Azerbaijan, Belarus, Bolivia, Bosnia and Herzegovina, Brazil, Bulgaria, Cape Verde, China, Colombia, Cuba, Djibouti, Dominican Republic, Ecuador, Egypt, El Salvador, Fiji, Georgia, Guatemala, Guyana, Honduras, Indonesia, Iran (Islamic Republic of), Iraq, Jamaica, Jordan, Kazakhstan, Kiribati, Maldives, Marshall Islands, Micronesia (Federated States of), Morocco, Namibia, Paraguay, Peru, Philippines, Romania, Samoa, Serbia and Montenegro, Sri Lanka, Suriname, Swaziland, Syrian Arab Republic, Thailand, The former Yugoslav Republic of Macedonia, Tonga, Tunisia, Turkmenistan, Ukraine, Vanuatu, West Bank, and Gaza Strip
Low income (Gross national income of US $825 or less per capita)	Afghanistan, Bangladesh, Benin, Bhutan, Burkina Faso, Burundi, Cambodia, Cameroon, Central African Republic, Chad, Comoros, Congo, Côte d'Ivoire, Democratic People's Republic of Korea, Democratic Republic of the Congo, Eritrea, Ethiopia, Gambia, Ghana, Guinea, Guinea-Bissau, Haiti, India, Kenya, Kyrgyzstan, Lao People's Democratic Republic, Lesotho, Liberia, Madagascar, Malawi, Mali, Mauritania, Moldova, Mongolia, Mozambique, Myanmar, Nepal, Nicaragua, Niger, Nigeria, Pakistan, Papua New Guinea, Rwanda, Sao Tome and Principe, Senegal, Sierra Leone, Solomon Islands, Somalia, Sudan, Tajikistan, Timor-Leste, Togo, Uganda, United Republic of Tanzania, Uzbekistan, Viet Nam, Yemen, Zambia, Zimbabwe

World Health Organization (2008)

to age at death, an individual born in the more developed regions is now expected to outlive by almost 12 years an individual born in the less developed regions of the world (United Nations 2001). If the individual is born in one of the least developed countries, the life expectancy disadvantage doubles to almost 24 years.

Table 1.3 The top 10 causes of death by broad income group in 2004

Cause of death	Deaths in millions	Percentage of deaths
High-income countries		
Coronary heart disease	1.33	16.3
Stroke and other cerebrovascular disease	0.76	9.3
Trachea, bronchus, lung cancers	0.48	5.9
Lower respiratory infections	0.31	3.8
Chronic obstructive pulmonary disease	0.29	3.5
Alzheimer and other dementias	0.28	3.4
Colon and rectum cancers	0.27	3.3
Diabetes mellitus	0.22	2.8
Breast cancer	0.16	2.0
Stomach cancer	0.14	1.8
Middle-income countries		
Stroke and other cerebrovascular disease	3.47	14.2
Coronary heart disease	3.40	13.9
Chronic obstructive pulmonary disease	1.80	7.4
Lower respiratory infections	0.92	3.8
Trachea, bronchus, lung cancers	0.69	2.9
Road traffic accidents	0.67	2.8
Hypertensive heart disease	0.62	2.5
Stomach cancer	0.55	2.2
Tuberculosis	0.54	2.2
Diabetes mellitus	0.52	2.1
Low-income countries		
Lower respiratory infections	2.94	11.2
Coronary heart disease	2.47	9.4
Diarrheal diseases	1.81	6.9
HIV/AIDS	1.51	5.7
Stroke and other cerebrovascular diseases	1.48	5.6
Chronic obstructive pulmonary disease	0.94	3.6
Tuberculosis	0.91	3.5
Neonatal infections	0.90	3.4
Malaria	0.86	3.3
Prematurity and low birth weight	0.84	3.2

World Health Organization (2008)

1.2 Global Population Aging and the Burden of Disease

Population aging will have a significant effect on the worldwide burden of disease in the coming decades. The older population is growing at a much faster rate than that of the world's total population; the annual growth rate of the population aged 60 or older is currently 1.9%, while the growth rate of the total population is 1.2% (United Nations 2001). The United Nations projects that by 2025–2030, the population over 60 will be growing 3.5 times as rapidly as the total population (annual growth rate of 2.8% for older population versus 0.8% for total population). In the 50-year period from 1950 to 2000, the number of persons aged 60 or older tripled from 205 million

Table 1.4 Characteristics of aging and mortality in rich and poor countries

Income group	Main characteristics
High income (Gross national income of US $10,065 or more per capita)	More than two-thirds of people live beyond the age of 70 People predominantly die of chronic diseases: cardiovascular disease, chronic obstructive lung disease, cancers, diabetes, or dementia Lung infection remains the only leading infectious cause of death
Middle income (Gross national income of US $826–10,065 per capita)	Nearly half of all people live beyond the age of 70 Chronic diseases are the major killers, as in high-income countries Unlike in high-income countries, tuberculosis and road traffic accidents are also leading causes of death
Low income (Gross national income of US $825 or less per capita)	Less than a quarter of all people live to the age of 70 and more than a third of all deaths are among children under 14 People predominantly die of infectious diseases: lung infections, diarrheal diseases, HIV/AIDS, tuberculosis, and malaria Complications of pregnancy and childbirth together continue to be leading causes of death, claiming the lives of both infants and mothers

World Health Organization (2008)

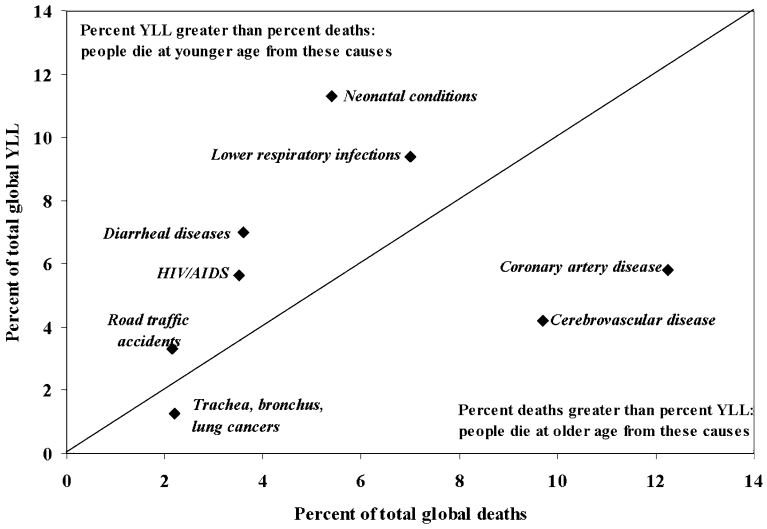

Fig. 1.6 Comparison of the proportional distribution of deaths and YLL by leading cause of death in 2004

to 606 million worldwide (Fig. 1.7). According to the United Nations report on World Population Aging: 1950–2050, the number of persons aged 60 or older will triple again in the 50-year period from 2000 to 2050, to reach a total of 2 billion older persons worldwide by 2050 (United Nations 2001). In relative terms, the percentage of older persons is projected to more than double worldwide by 2050.

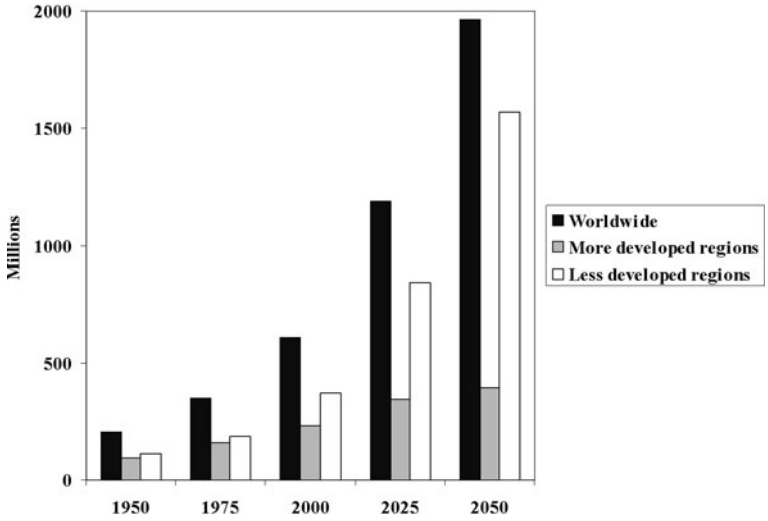

Fig. 1.7 Population aged 60 and over, 1950–2050

The WHO's Global Burden of Disease study projects trends in global mortality from 2004 to 2030 based on demographic shifts. The study predicts that aging of populations in low-income and middle-income countries will result in significant increases in total deaths due to most Group II non-communicable diseases over the next 25 years (World Health Organization 2008). Global cardiovascular deaths are projected to rise from 17.1 million in 2004 to 23.4 million in 2030, and global cancer deaths are projected to rise from 7.4 million in 2004 to 11.8 million in 2030. The four leading causes of death worldwide in 2030 are projected to be coronary artery disease, cerebrovascular disease (stroke), chronic obstructive pulmonary disease, and lower respiratory infections (mainly pneumonia). Finally, road traffic accidents are projected to rise from the ninth leading cause of death globally in 2004 to the fifth leading cause in 2030.

1.3 The Global Economic Impact of Disease

Current levels of disease and disability, along with aging populations and the concomitant rise in chronic diseases, will negatively affect global economic growth if left unchecked. While developing countries face pressing priorities in providing basic health services to their populations, they are also increasingly struggling to manage epidemic rates of non-communicable diseases; the prolonged and costly care of such diseases draws significant resources away from basic priorities (Boutayeb and Boutayeb 2005). Low-income and middle-income countries in particular must deal with a "double burden" of infectious and chronic diseases, as well as the practical realities of limited resources (World Health Organization 2006).

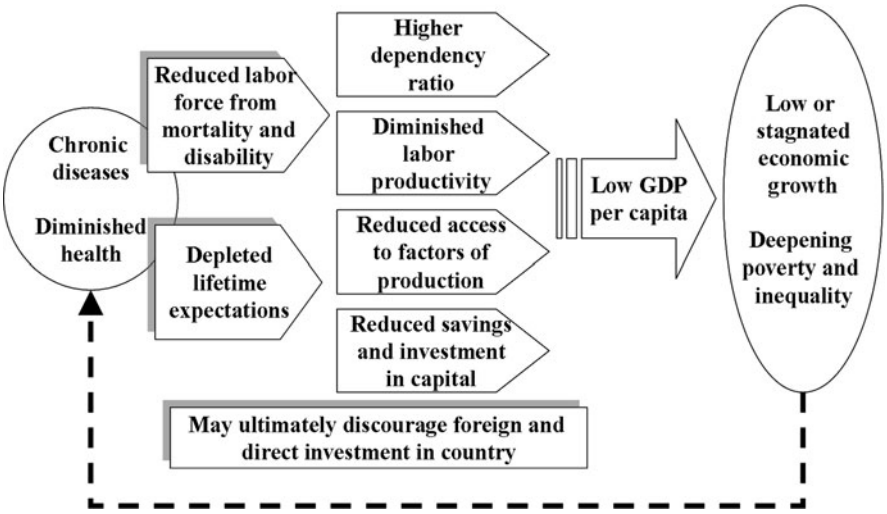

Fig. 1.8 Linkages between disease and the economy

Disease is linked to the economy through a variety of channels (Fig. 1.8). All diseases deprive individuals of their health and productive potential, and the majority of deaths from chronic diseases occur in the most productive age groups. From the perspective of affected individuals and families, diseases and death challenge household income and savings and lessen investment activity. Diseases can cause individuals and families to fall into poverty, creating a downward spiral of worsening poverty and disease. From the perspective of affected nations, diseases reduce life expectancy and ultimately economic productivity, depleting the quality and quantity of a nation's labor force. This leads to lower gross domestic product (GDP) and lower gross national income (GNI). Additionally, diseases and premature death reduce the intergenerational transfer of knowledge, skills, and wealth; the schooling of children is adversely affected, propagating the cycle of ill health and poverty (World Health Organization 2006). Disease and death thus undermine the macroeconomic development of countries.

Conversely, health positively influences economic well-being, growth, and wealth. Good health improves levels of human capital, which in turn positively affect individual productivity and ultimately affect economic growth rates (Lopez-Cassanovas et al. 2005). On an individual level, good health increases individuals' economic opportunities and levels of education (schooling and scholastic performance). On a national level, health increases workforce productivity by reducing incapacity, disability, and workdays lost. Good health frees resources, which would otherwise be used to pay for treatment and disease management. A reduction in disease and death thus reduces the likelihood of poverty. Countries would benefit economically from the absence of morbidity and mortality from infectious diseases, chronic diseases, and traumatic injuries.

A few studies provide evidence of the impact of chronic diseases on economic growth. Empirical evidence from Eastern Europe and Asia demonstrates that an annual increase in economic growth of between 0.3 and 0.4% is associated with a 10% increase in life expectancy (World Health Organization 2005); this life expectancy increase is mainly attributed to a reduction in the burden of cardiovascular diseases. Life expectancy gains of as much as 7.75 years have been credited to the control of cardiovascular disease in Europe and Central Asia (The World Bank 2004). These studies suggest that control of chronic diseases could yield substantial life expectancy gains and economic returns for countries.

National income and GDP are meaningful outcome measures for assessing the macroeconomic consequences of disease and death. The Department of Chronic Diseases and Health Promotion at the WHO estimated the impact of deaths from heart disease, stroke, and diabetes on national income and GDP for nine countries in 2005 (World Health Organization 2006). The nine nations in the WHO analysis represent low-income, middle-income, and high-income regions of the world; the results of this analysis are presented in Tables 1.5 and 1.6. Notably, the estimated loss in national income in 2005 from heart disease, stroke, and diabetes deaths was $18 billion in China, $11 billion in the Russian Federation, $8.7 billion

Table 1.5 Effects of heart disease, stroke, and diabetes deaths on national income

	Brazil	Canada	China	India	Nigeria	Pakistan	Russia	UK	Tanzania
Numbers in billions of US dollars									
Income loss in 2005	−$2.7	−$0.5	−$18	−$8.7	−$0.4	−$1.2	−$11	−$1.6	−$0.1
Income loss in 2015	−$9.3	−$1.5	−$13	−$54	−$1.5	−$6.7	−$6.6	−$6.4	−$0.5
Average annual income loss	−$5.1	−$0.9	−$53	−$23	−$0.8	−$3.0	−$30	−$3.4	−$0.2

World Health Organization (2006)

Table 1.6 Effects of heart disease, stroke, and diabetes deaths on GDP

	Brazil	Canada	China	India	Nigeria	Pakistan	Russia	UK	Tanzania
Estimated loss in GDP/projected GDP (%)									
Percent GDP loss in 2005	0.19	0.07	0.31	0.35	0.23	0.30	1.13	0.10	0.29
Percent GDP loss in 2015	0.48	0.15	1.18	1.27	0.65	1.02	5.34	0.32	0.86
Average annual percent GDP loss	0.3	0.1	0.7	0.7	0.4	0.6	2.7	0.2	0.3

World Health Organization (2006)

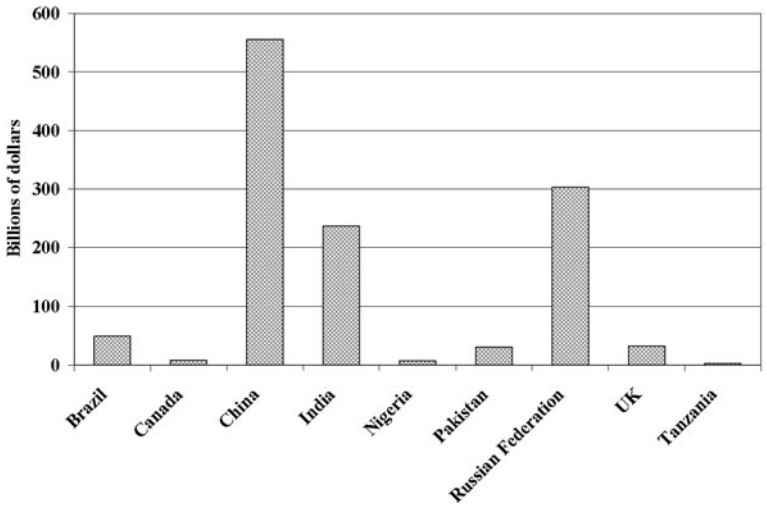

Fig. 1.9 Cumulative loss in national income due to deaths from heart disease, stroke, and diabetes, 2005–2015

in India, and $2.7 billion in Brazil. In terms of percentage reduction in GDP, chronic disease deaths were estimated to reduce GDP by 1% in the Russian Federation and 0.1–0.5% in other countries in 2005.

The WHO further predicts income losses from heart disease, stroke, and diabetes deaths through 2015 for the same nine countries. Estimates for income loss in 2015 are between three and seven times those of 2005. By 2015, the percentage reduction in GDP will be over 5% in the Russian Federation and approximately 1% in other countries. The cumulative losses in national income from 2005 to 2015 as a result of mortality from chronic disease are substantial (Fig. 1.9). For instance, China stands to lose $556 billion over the 10-year period, India will lose over $236 billion, and the Russian Federation will lose $303 billion, due to premature deaths from heart disease, stroke, and diabetes.

The WHO attributes these dramatic forecasts of national income loss to two main factors: the labor units lost as a result of deaths from chronic disease and the direct medical costs of treating chronic disease. Medical expenditures for disease management continue to increase annually. Healthcare expenses are initially covered by current earnings, then by savings, and eventually from accumulated capital assets. The combination of depleted savings and lost labor units exacts a huge macroeconomic toll on nations.

The above estimates include only the effects of mortality from heart disease, stroke, and diabetes. The collective economic impact of deaths from all causes is even greater; these estimates are summarized in Table 1.7. In 2005, all-cause deaths reduced GDP by approximately 3% in the Russian Federation and 1% in most other countries. By 2015, the loss in GDP due to all-cause deaths will be over 12% in the Russian Federation and 3–5% in most other countries. This indicates a clear

Table 1.7 Effects of all-cause deaths on GDP

	Brazil	Canada	China	India	Nigeria	Pakistan	Russia	UK	Tanzania
Estimated loss in GDP/projected GDP (%)									
Percent GDP loss in 2005	0.92	0.38	1.08	1.27	1.11	0.84	2.73	1.11	1.57
Percent GDP loss in 2015	3.21	0.64	3.94	5.04	3.07	3.08	12.35	5.18	4.19
Average annual percent GDP loss	1.4	0.4	1.6	2.0	1.6	1.3	4.5	1.8	2.2

World Health Organization (2006)

economic imperative to reduce deaths from chronic diseases, infectious diseases, and traumatic injuries.

The WHO has proposed a global goal of an additional 2% annual reduction in chronic disease death rates; this corresponds to preventing 36 million premature deaths over a 10-year period. Novel biomedical technologies can play a central role in helping nations reach this target. If the global goal is achieved, the averted deaths will translate into substantial labor supply gains in all countries. From 2005 to 2015, this would result in an accumulated income gain of over $36 billion in China, $15 billion in India, and $20 billion in the Russian Federation. This can be regarded as income that would otherwise be lost to chronic diseases if the global goal were not achieved.

Table 1.8 summarizes the potential economic gains from achieving the global goal. A modest 2% reduction in deaths from chronic disease would increase the annual GDP of China by 0.04%, India by 0.05%, and the Russian Federation by 0.2%. Medical interventions that decrease deaths, even by small amounts, can therefore catalyze enormous economic growth. Indeed, several countries have recognized the need for chronic disease prevention and control and have adapted their Millennium Development Goal targets and indicators to include chronic diseases in addition to infectious diseases and child mortality (World Health Organization 2005).

Table 1.8 GDP gain from 2% reduction in chronic disease deaths in 2005–2015

	Brazil	Canada	China	India	Nigeria	Pakistan	Russia	UK	Tanzania
Estimated gain in GDP/projected GDP (%)									
Average annual percent GDP gain	0.03	0.01	0.04	0.05	0.03	0.03	0.19	0.01	0.01

World Health Organization (2006)

1.4 The Role of Novel Biomaterials in Alleviating Disease

Given the growing burden of disease worldwide and the grave economic consequences of disease, innovative biomaterials are urgently needed to address a multitude of conditions – infectious diseases, chronic diseases, and traumatic injuries. While lifestyle changes and increased healthcare access are important mechanisms for decreasing the prevalence of diseases, new biomaterials will be essential for managing complex diseases and injuries. Novel technologies that decrease mortality fulfill not only a humanitarian role by alleviating suffering but also a practical role in generating the economic benefits of decreased mortality. As the editor of the medical journal *The Lancet* has asserted, "There is an unusual opportunity before us to act now to prevent the needless deaths of millions" (Horton 2005).

Before discussing the unique potential of biomaterials for disease prevention and treatment, it is important to define the scope of biomaterials science and describe the ideal biomaterial. A commonly used definition of a biomaterial, endorsed by a consensus of biomaterials experts, is "a nonviable material used in a medical device, intended to interact with biological systems" (Williams 1987). An essential characteristic of biomaterials is biocompatibility, defined as "the ability of a material to perform with an appropriate host response in a specific application" (Williams 1987). Typical biomaterials are composed of metals, glasses, ceramics, polymers, carbons, and composite materials. However, the newest biomaterials employ traditional materials in combination with small-molecule drugs, protein therapeutics, biological molecules, and living cell populations. In addition, emerging biomaterials are rationally designed to interact with living systems and react to biological and environmental stimuli. Modern biomaterials science includes the following subspecialties:

- Surface-modified biomaterials – biomaterials engineered with surface modifications to control cell attachment and protein adsorption
- Smart biomaterials – biomaterials that change their properties in response to environmental triggers such as pH, temperature, and chemical species
- Bioactive biomaterials – biomaterials that incorporate pharmacological agents, growth factors, antibodies, cytokines, adhesion factors, or enzyme recognition sites to render the materials biologically active
- Tissue engineering and regenerative medicine – biomaterials that replace lost tissues or organs with polymer constructs that contain specific populations of living cells, with the goal of regenerating tissues to restore normal function

These categories of biomaterials are not mutually exclusive, and the ideal biomaterial may integrate many or all of the above features. The perfect biomaterial not only defends against disease and supports weakened tissues or organs, it also provides the elements required for healing and repair, stimulates the body's intrinsic immunologic and regenerative capacities, and seamlessly interacts with the living

body (Greenwood et al. 2006). Contemporary biomaterials science encompasses a wide range of technologies, including imaging agents, drug delivery platforms, biosensors, tissue engineered constructs, antimicrobials, and vaccines.

Biomaterials are increasingly being recognized as a beneficial means for lessening the global disease burden. For example, biomaterials for tissue engineering and regenerative medicine have recently been investigated for their potential to advance global health (Greenwood et al. 2006). An international panel of 44 experts, including researchers in disciplines contributing to regenerative medicine and clinicians working in fields at the forefront of applying regenerative medicine therapies, participated in a technology foresight study to identify the top 10 most promising applications of regenerative medicine for improving health in developing countries. Seventy-seven percent of the panelists lived in developing countries. The results of the study are presented in Table 1.9. Importantly, the applications identified by the panel can impact most all of the world's leading causes of death. Novel methods for insulin replacement and pancreatic islet regeneration can address diabetes; autologous cells for heart muscle regeneration can address coronary artery disease; and nerve regeneration technologies can be utilized to treat stroke. Engineered vaccines can protect against infectious diseases such as tuberculosis, pneumonia, HIV/AIDS, and diarrheal diseases. Skin substitutes and growth factors can prevent deaths from traumatic injuries. These applications indicate the versatility of biomaterials for treating chronic diseases, infectious diseases, and injuries.

Table 1.9 Top 10 regenerative medicine applications for improving health in developing countries

Ranking (score)[a]	Applications of regenerative medicine	Examples
1 (415)	Novel methods of insulin replacement and pancreatic islet regeneration for diabetes	• Bone marrow stem cell transplantation for pancreatic regeneration • Microencapsulation for immune isolation of transplanted pancreatic islet cells • Cultured insulin-producing cells from embryonic stem cells, pancreatic progenitor cells, or hepatic stem cells • Genetically engineered cells to stably express insulin and contain a glucose-sensing mechanism
2 (358)	Autologous cells for the regeneration of heart muscle	• Myocardial patch for cardiac regeneration • Direct injection of autologous bone marrow mononuclear cells for cardiac repair • Stromal cell injection for myocardial regeneration • Localized angiogenic factor therapy through controlled release systems or gene therapy
3 (339)	Immune system enhancement by engineered immune cells and novel vaccination strategies for infectious disease	• Genetically engineered immune cells to enhance or repair immune function • Single injection DNA vaccines

Table 1.9 (continued)

Ranking (score)[a]	Applications of regenerative medicine	Examples
4 (272)	Tissue-engineered skin substitutes, autologous stem or progenitor cells, intelligent dressings, and other technologies for skin loss due to burns, wounds, and diabetic ulcers	• Bilayered living skin constructs • Engineered growth factors applied in conjunction with topical treatments • Intelligent dressings composed of a slow-releasing growth hormone polymer • Epithelial cell sprays
5 (238)	Biocompatible blood substitutes for transfusion requirements	• Polyhemoglobin blood substitutes for overcoming blood shortages and contamination issues
6 (200)	Umbilical cord blood banking for future cell replacement therapies and other applications	• Preserved umbilical cord blood stem cells to provide future cell replacement therapies for diseases such as diabetes, stroke, myocardial ischemia, and Parkinson disease • Pooled cord blood for the treatment of leukemia
7 (157.5)	Tissue-engineered cartilage, modified chondrocytes, and other tissue engineering technologies for traumatic and degenerative joint disease	• Matrix-induced autologous chondrocyte implantation for cartilage repair • Tissue-engineered cartilage production using mesenchymal stem cells
8 (121.5)	Gene therapy and stem cell transplants for inherited blood disorders	• Genetically engineered hematopoietic stem cells to restore normal blood production in beta-thalassemic patients
9 (105.5)	Nerve regeneration technologies using growth factors, stem cells, and synthetic nerve guides for spinal cord and peripheral nerve injuries	• Synthetic nerve guides to protect regenerating nerves • Embryonic stem cell therapy for spinal cord regeneration • Growth factor-seeded scaffolds to enhance and direct nerve regeneration
10 (80)	Hepatocyte transplants for chronic liver diseases or liver failure	• Microencapsulation of hepatocytes to prevent immunological reaction • Derivation of hepatocytes for transplantation from embryonic stem cells • Transdifferentiation of hepatocytes for transplantation from bone marrow cells

[a]Applications were scored based on six criteria: disease burden, therapeutic impact, feasibility, affordability, acceptability, and indirect benefits. The maximum total score an application could receive was 440

Greenwood et al. (2006)

In many cases, biomaterial solutions may be more cost-effective and accessible than existing treatments for disease (Greenwood et al. 2006). In the case of traumatic injuries, the existing method for managing blood loss is transfusion, which is associated with costly screening measures and a risk of viral transmission. Modern biomaterials such as tissue adhesives and sealants can minimize blood loss, to avoid the need for transfusion and screening. In the case of coronary artery disease, the

existing treatment for advanced heart failure is cardiac transplantation. Biomaterial innovations such as autologous cells for cardiac regeneration could be much less costly than cardiac transplantation; cell-based biomaterial therapies will also be technically much simpler than traditional transplantation. In addition, cell-based biomaterial treatments will carry the advantage of avoiding immune rejection and costly immunosuppressive regimens. In the case of diabetes, the existing therapy is repeated administration of insulin; such treatments are costly and inaccessible to many patients in developing countries. Biomaterial therapies, such as microencapsulated pancreatic islet cells, could increase access by providing a permanent regenerative solution and avoiding the financial burden caused by the purchase of insulin. The coming generation of biomaterials can enable healthcare that is both more effective and more affordable.

1.5 Practical Considerations for Modern Biomaterials

Modern biomaterials must meet stringent performance requirements and overcome difficult practical challenges. A number of technical factors must be considered in the selection and development of new biomaterials. First, biomaterials must demonstrate sufficient physical and mechanical properties to survive the physiological environment. Second, novel biomaterials must meet biocompatibility specifications. The biomaterial must be biocompatible to the target site, performing in its desired application without causing adverse effect. Both the biomaterial construct and any residuals or degradation products must be non-cytotoxic, non-hemolytic, and non-inflammatory; undesirable responses such as irritation and sensitization must be avoided. The biomaterial must not interfere with wound healing or induce fibrosis or a foreign body response; it is also necessary that the material does not act as a hospitable environment for bacteria, so that it does not propagate an infection.

In many clinical situations, it may be advantageous for the biomaterial to be degradable; such instances include biomaterials for wound closure and tissue regeneration. For these applications, degradable biomaterials must meet the requirements of physiological metabolism, and degradation should be achieved via hydrolysis or enzymatic cleavage. The degradation time should be tuned such that the material remains on the target site until physiological wound healing has taken place and degrades soon afterward to avoid material encapsulation by immune cells. Indeed, the success of a degradable biomaterial can be judged by how well the tissue is replaced. Moreover, the degradation products must be easily excreted by the kidneys. The molecular weight cut-off for kidney elimination of native globular proteins is considered to be 70,000, which is close to the molecular weight of serum albumin (Lote 2000). Hydrophilic polymers utilized in biomaterials may have a higher molecular volume than compact globular proteins; because of the larger effective size of polymers, the molecular weight cut-off for kidney excretion of polymers may be even more stringent. An additional consideration is that polymers with higher molecular weights will exhibit longer retention times in the blood.

Finally, biomaterials must satisfy commercial requirements and clinical needs. The ideal biomaterial for medical usage should be readily delivered through a user-friendly device. The system should demonstrate adequate shelf stability, and an optimal system should be storable at room temperature, requiring minimal advance preparation time. Production of the biomaterial must be scalable to allow cost-effective manufacture; this quality is particularly critical for global health, as low-income and middle-income countries carry 80% of the worldwide disease burden. The reality is that biomaterials will be most needed in low-resource settings, where staffing and facilities are severely limited. As shown in Table 1.10, most developing countries have few physicians and nurses relative to the developed world. Biomaterials that are of low cost and easy-to-use will have the largest impact on public health.

Table 1.10 WHO figures for national physician and nurse density

Country	Physician density (per 1,000 population)	Nurse density (per 1,000 population)
Malawi	0.02	0.59
Mozambique	0.03	0.21
Uganda	0.08	0.61
Kenya	0.14	1.14
India	0.60	0.80
South Africa	0.77	4.08
Brazil	1.15	3.84
Bolivia	1.22	3.19
United States	2.56	9.37
Denmark	2.93	10.36
Spain	3.30	7.68
Cuba	5.91	7.44

Yager et al. (2008)

Throughout the development process, new biomaterials must be assessed to ensure their suitability for medical applications; characterization should include mechanical properties, physical/chemical properties, biological properties, shelf stability, and usability. A listing of recommended tests for biomaterials is presented in Table 1.11. The precise properties required of each biomaterial are determined to a large extent by the surgical target. Clinician input is an essential component of the design process, so that surgeon needs and patient needs can be translated into technical specifications. The clinical target should continually guide and inspire the creation of a biomaterial.

In summary, biomaterials carry a great deal of hope for lightening the heavy burden of disease and death worldwide. Both developing and developed nations are battling poverty and ill health; the situation demands innovative biomaterial solutions. The following 10 chapters explore the promise of biomaterials for addressing each of the world's top 10 causes of death. Each chapter focuses on a specific disease

Table 1.11 Methods for characterization of biomaterials

Mechanical characterization	*Biological characterization*
Mechanical strength	Sterility properties
Tensile strength	Bioburden
Shear strength	Bacterial endotoxin assay
Impact strength	Tissue compatibility
Cohesive and adhesive strength	Cytotoxicity
Physical/chemical characterization	Cellular inflammation
Curing and reaction properties	Cell and protein attachment
Extent of reaction	Tissue irritation
Residual sutarting materials	Tissue implantation response
Heat of reaction	Wound healing
Degradation properties	Hemolysis testing
Degradation rate	Systemic effects
Degradation products	Pyrogenicity
Swelling determination	Sensitization
Drug release properties	Toxicokinetic evaluation
Drug delivery rate	Metabolic fate
Drug bioactivity	Antimicrobial effects
Device characterization	Encapsulated live cell viability
Accelerated shelf stability test	*Clinical characterization*
Physical integrity	Ease-of-use
Device functionality	Patient and clinician acceptance
Device preparation time	Clinical efficacy
	Cost-effectiveness

process identified in the WHO report of the Global Burden of Disease. Every chapter will describe the underlying pathology of the disease; discuss the latest advances in biomaterials for treating the disease; and identify prospective research areas for novel biomaterials to modify the disease process. The discussion begins with the world's leading cause of death, cardiovascular disease.

References

Boutayeb A, Boutayeb S (2005) The burden of noncommunicable diseases in developing countries. Int J Equity Health 4:2

Greenwood HL, Singer PA, Downey GP et al (2006) Regenerative medicine and the developing world. PLoS Med 9:e381

Horton R (2005) The neglected epidemic of chronic disease. Lancet 366:1514

Lopez-Cassanovas G, Rivera B, Currais L (2005) Health and economic growth: findings and policy implications. MIT Press, Cambridge, MA

Lote CJ (2000) Principles of renal physiology. Springer, New York, NY

The World Bank (2004) Millennium development goals for health in Europe and Central Asia: relevance and policy implications. The World Bank, Washington, DC

United Nations (2001) World population ageing: 1950–2050. United Nations Publications, New York, NY

Williams DF (1987) Definitions in biomaterials. Proceedings of a Consensus Conference of the European Society for Biomaterials. Elsevier, New York, NY

World Health Organization (2005) Preventing chronic diseases: a vital investment. WHO Press, Geneva
World Health Organization (2006) An estimation of the economic impact of chronic noncommunicable diseases in selected countries. WHO Working Paper, Geneva
World Health Organization (2008) The global burden of disease: 2004 update. WHO Press, Geneva
Yager P, Domingo GJ, Gerdes J (2008) Point-of-care diagnostics for global health. Annu Rev Biomed Eng 10:107

Chapter 2
Coronary Artery Disease

Coronary artery disease, also known as ischemic heart disease, is the leading killer of men and women worldwide. In 2004, coronary artery disease was responsible for 7.2 million deaths, or 12.2% of all deaths globally and 5.8% of all years of life lost (World Health Organization 2008). The disease is highly prevalent: at any given time, 54 million people in the world suffer from angina pectoris (the characteristic chest pain of ischemic heart disease), and 23.2 million people experience moderate to severe disability as a result of ischemic heart disease (World Health Organization 2008). Thirty-day mortality after an acute heart attack is extremely high at 33%; even in a hospital with a coronary care unit where advanced care options are available, mortality is still 7%. Approximately 4% of patients who survive initial hospitalization die in the first year following a heart attack (Antman et al. 2004). Congestive heart failure, the end stage of many heart diseases, carries a 1-year mortality rate as high as 40% and a 5-year mortality between 26 and 75%; the prognosis for patients with congestive heart failure is worse than for those with most malignancies or AIDS (McMurray and Stewart 2000). Pharmacologic therapy, metallic stents, and coronary artery bypass grafts have been mainstays of treatment for ischemic heart disease. However, new biomaterial devices are on the horizon that will enable optimal treatment of coronary artery lesions, as well as regeneration of damaged cardiac tissue.

2.1 Historical Perspective on Coronary Artery Disease

Atherosclerosis, the "hardening of the arteries," was first described by the Italian anatomist Giovanni Morgagni in 1761. Seven years later, the English doctor William Heberden observed a painful "disorder of the breast, marked with strong and peculiar symptoms. . .and sense of strangling and anxiety" (Jay 2000). Heberden coined the name *angina pectoris* for this syndrome; it was British physicians Edward Jenner and Caleb Parry who linked this excruciating "disorder of the breast" to the "hardening" of arteries that had been described by Morgagni (Ashley and Niebauer 2004). In 1856, the German pathologist Rudolf Virchow, known as the "father of pathology," delineated the three physiological elements that interact to precipitate blood clotting

S.K. Bhatia, *Biomaterials for Clinical Applications*,
DOI 10.1007/978-1-4419-6920-0_2, © Springer Science+Business Media, LLC 2010

(thrombosis) within the vascular system: the blood vessel wall, the components of the blood, and the flow characteristics of the blood (Virchow 1856). Specifically, Virchow identified the triad of risk factors that predispose arteries and veins to thrombus formation: vascular wall injury, blood hypercoagulability, and flow stasis. Virchow's triad remains a relevant precept in modern medicine for explaining the development of thrombotic occlusion. However, a good description of myocardial infarction, commonly known as heart attack, was not forthcoming until the twentieth century.

Throughout the nineteenth and early twentieth century, sudden death and temporary invalidism from heart disease were occurring commonly, and pathologists were finding evidence of scars in the heart and other indications of serious coronary disease (White 1942). In 1912, the American doctor James Herrick put the facts together and proposed that thrombotic occlusion of the coronary arteries plays a central role in myocardial infarction (Herrick 1912). Herrick's paper was the first to suggest that clots, rather than a slow accrual of atherosclerotic plaque, are responsible for the complete arterial occlusion that could result in death. Herrick was also the first to link the pathology of coronary artery disease to symptoms in living patients and to suggest that patients can survive complete arterial blockage. As he asserted, "even large branches of the coronary arteries may be occluded – at times acutely occluded – without resulting death Even the main trunk may at times be obstructed and the patient live" (Herrick 1912). The pathophysiological basis of coronary artery disease was thus established. Herrick provided an insight regarding the therapeutic strategy for coronary artery disease that remains relevant today: "The hope for the damaged myocardium lies in the direction of securing a supply of blood through friendly neighboring vessels so as to restore so far as possible its functional integrity" (Herrick 1912).

2.2 Pathology of Coronary Artery Disease

Coronary artery disease is a multi-factorial condition, resulting from the convergence of genetics, environment, diet, and lifestyle. Recognized risk factors for the development of ischemic heart disease include family history, high blood pressure, smoking, elevated low-density lipoprotein (LDL) cholesterol, diabetes, physical inactivity, and obesity. Tables 2.1 and 2.2 list risk factors for coronary artery disease that have been identified and classified by the American Heart Association and the European Society of Carbdiology, respectively.

Atherosclerosis begins at the vascular walls of the coronary arteries, the blood vessels which run over the surface of the heart. Each coronary artery is critical for supplying oxygenated blood to the highly active cardiac muscle, also known as myocardium (Fig. 2.1). In a normal artery, the wall is composed of three distinct layers: the intima, the media, and the adventitia (Fig. 2.2). The intima is the innermost layer and consists of a single layer of endothelial cells lining the vessel, supported by a layer of connective tissue. The media is composed of smooth muscle

Table 2.1 American Heart Association guide to risk factors for coronary artery disease

Major independent risk factors	Predisposing risk factors	Possible risk factors
• Cigarette smoking • Hypertension • Elevated total and LDL cholesterol • Low HDL cholesterol • Diabetes mellitus • Older age	• Physical inactivity • Obesity • Family history of premature coronary disease • Ethnicity • Psychosocial factors	• Fibrinogen • C-reactive protein • Homocysteine • Lipoprotein-a [Lp(a)]

HDL, high-density lipoprotein; LDL, low-density lipoprotein

Table 2.2 European Society of Cardiology table of lifestyles and characteristics associated with an increased risk of a future coronary heart disease event

Lifestyle	Biochemical or physiological characteristics (modifiable)	Personal characteristics (non-modifiable)
• Diet high in saturated fat, cholesterol, and calories • Tobacco smoking • Excess alcohol consumption • Physical inactivity	• Elevated blood pressure • Elevated plasma total and LDL cholesterol • Low plasma HDL cholesterol • Elevated plasma triglycerides • Hyperglycemia/ diabetes • Obesity • Thrombogenic factors	• Older age • Male gender • Family history of coronary heart disease or other atherosclerotic vascular disease at early age (men <55, women <65) • Personal history of coronary heart disease or other atherosclerotic vascular disease

HDL, high-density lipoprotein; LDL, low-density lipoprotein

cells and is surrounded by the internal and external elastic laminae. The adventitia is the outermost layer and consists mainly of collagen fibers that protect the blood vessel.

Atherosclerosis is initiated by a combination of circulating cholesterol, inflammatory white blood cells, and hemodynamic forces; common sites for atherosclerosis are areas where arteries branch (Ashley and Niebauer 2004). Low-density lipoprotein (LDL) cholesterol and blood-borne leukocytes adhere to the vascular wall and penetrate the wall at areas of high shear stress and turbulent flow. The oxidized form of LDL cholesterol is atherogenic; in its oxidized form, LDL cholesterol enters macrophages and converts them to foam cells, which will eventually become the center of the atherogenic plaque. Oxidized LDL cholesterol also enhances the migration of monocytes and smooth muscle cells to the intima; the smooth muscle cells will eventually differentiate to form the fibrous coating of the atherosclerotic plaque.

A mature atherosclerotic plaque contains a core of dead form cells (lipid-engorged macrophages) and smooth muscle cells. The core of the plaque is covered

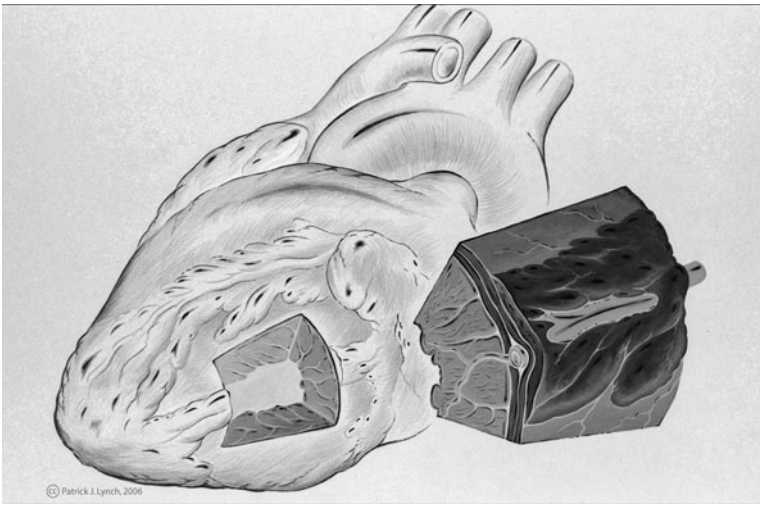

Fig. 2.1 Location of the coronary arteries in the surface of the highly active cardiac muscle (Patrick J. Lynch, medical illustrator)

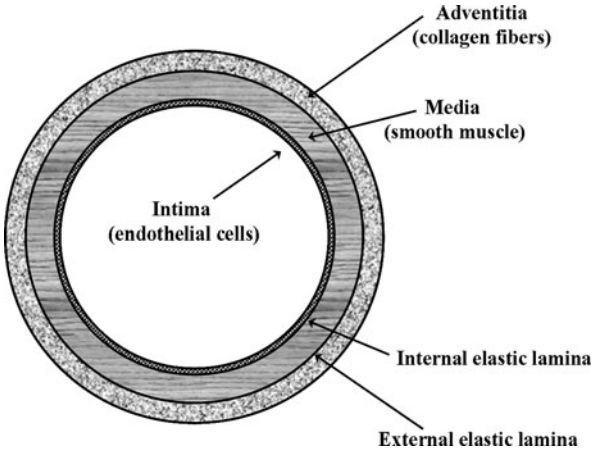

Fig. 2.2 Diagram of the layers of a normal arterial wall

by a fibrous cap, a region of the intimal layer that has become thickened as a result of medial smooth muscle cells depositing collagen fibers. The thickening artery wall of an atherosclerotic plaque gradually encroaches on the arterial lumen and narrows the inner diameter of the artery, resulting in a restriction to blood flow (Fig. 2.3) and compromised blood supply to the myocardium (Fig. 2.4). A flow-limiting atherosclerotic plaque is typically visible as an arterial narrowing on a coronary angiogram (Fig. 2.5).

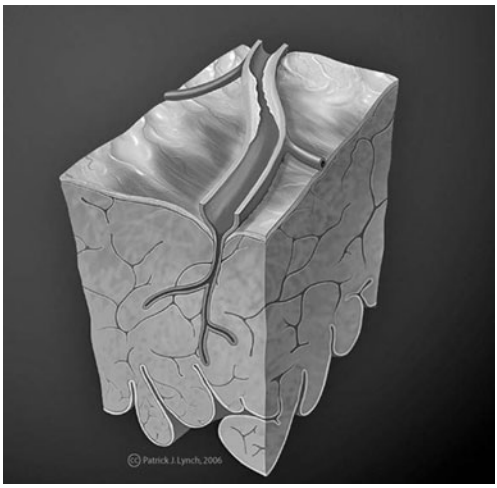

Fig. 2.3 Atherosclerotic plaque formation in the coronary artery (Patrick J. Lynch, medical illustrator)

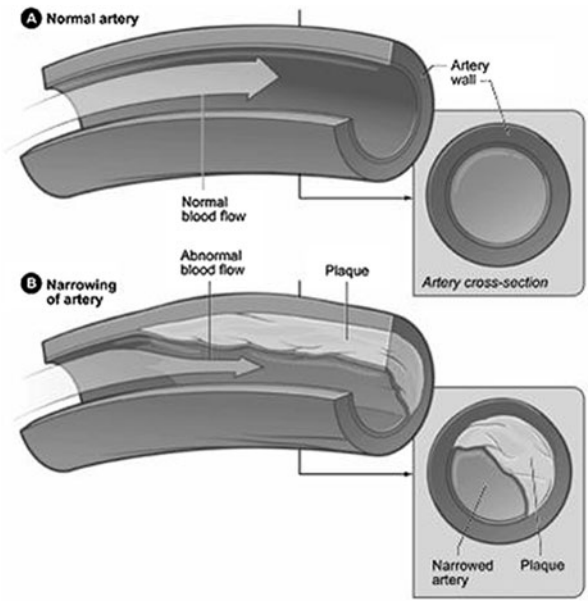

Fig. 2.4 Effects of arterial plaque formation on blood flow (National Heart, Lung, and Blood Institute)

Coronary artery disease therefore represents the culmination of cholesterol accumulation, cellular capture, vascular injury, and inflammatory activation. The cellular composition of an atherosclerotic plaque determines whether it will be stable or unstable, and consequently how it will manifest clinically. A stable plaque has abundant smooth muscle cells at its core, with a thick fibrous cap. Patients with stable

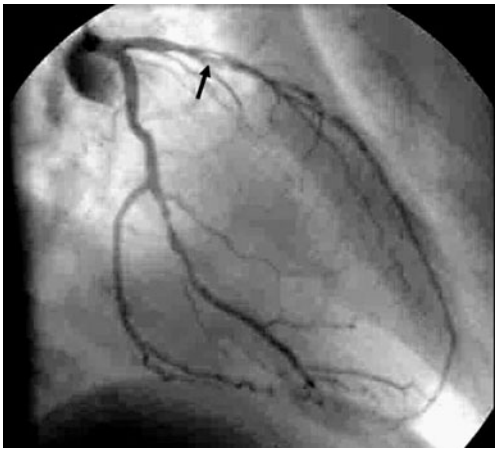

Fig. 2.5 Appearance of arterial narrowing on coronary angiography (Ashrafian et al. 2006)

arterial plaque display predictable chest pain that occurs transiently during exercise or physical exertion when the cardiac muscle is taxed; the pain disappears at rest. An unstable plaque has abundant lipid-rich macrophages at its core, with a thinner fibrous cap; the softer unstable plaque is more susceptible to rupture. Patients with unstable plaque can experience transient or incomplete blockage of the coronary artery and present clinically with unpredictable chest pain that may occur at rest. Plaque rupture may trigger the formation of a blood clot, which can completely block the flow of blood through the artery, resulting in a myocardial infarction. Patients with complete occlusion of the coronary arteries demonstrate symptoms of a heart attack, including severe chest pain, anxiety, sweating, shortness of breath, and weakness. The clinical syndromes associate with stable atherosclerotic plaque, unstable atherosclerotic plaque, and complete occlusion are summarized in Table 2.3. However, atherosclerosis and acute myocardial infarction can sometimes be clinically silent with no apparent symptoms, particularly in patients with coexisting diabetes. This makes coronary artery disease an even more insidious killer of men and women.

Acute myocardial infarction compromises the blood supply to the cardiac muscle, deprives the heart of oxygen and nutrients, and leads to substantial cardiac tissue

Table 2.3 Manifestations of coronary artery disease

Symptomatic presentation	Pathological vascular event
Stable angina – chest pain occurs predictably with activity or stress and disappears at rest	No plaque rupture, but stable vascular occlusion that limits perfusion
Acute coronary syndromes, unstable angina – chest pain occurs unpredictably, without identifiable precipitating factors	Plaque rupture with transient or incomplete vascular occlusion
Acute myocardial infarction (heart attack) – sudden crushing chest pain with shortness of breath, weakness, nausea, anxiety, or fatigue	Plaque rupture with complete occlusion and tissue damage

destruction. Different areas of the heart may be affected, depending on the specific coronary artery branches that are occluded. The anterior wall of the heart is fed by the left anterior descending (LAD) artery; obstruction of the LAD artery results in anterior wall damage and dysfunction (Fig. 2.6). The inferior wall of the heart is fed by the right coronary artery (RCA); obstruction of the RCA results in inferior wall damage and destruction (Fig. 2.7). Because the heart has limited intrinsic ability to

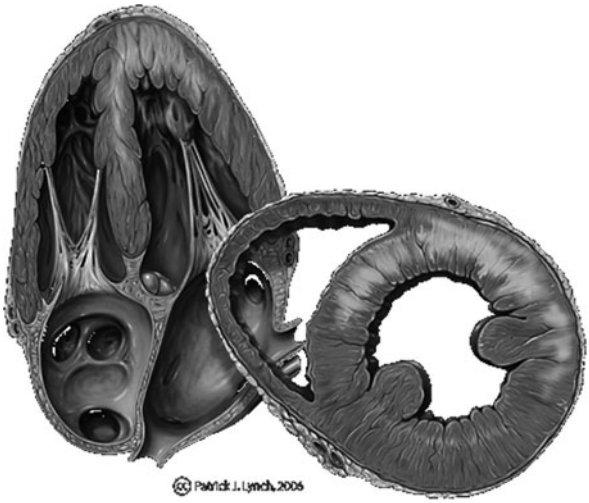

Fig. 2.6 Anterior wall damage and scarring in the heart as a result of obstruction of the left anterior descending artery (Patrick J. Lynch, medical illustrator)

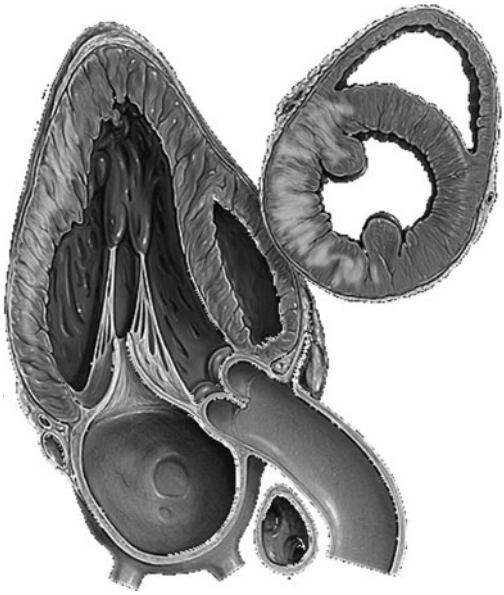

Fig. 2.7 Inferior wall damage and scarring in the heart as a result of obstruction of the right coronary artery (Patrick J. Lynch, medical illustrator)

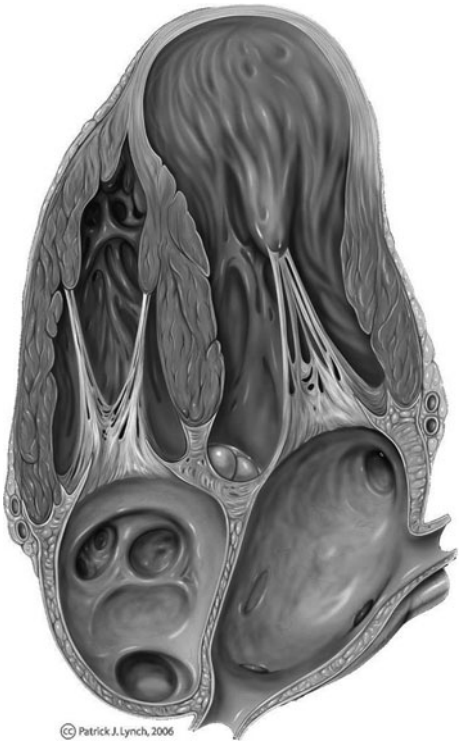

Fig. 2.8 Aneurysm of the cardiac wall resulting from myocardial infarction (Patrick J. Lynch, medical illustrator)

heal and repair damaged tissues, the injured site heals as scar tissue, and the functionality of the heart is seriously impaired. Extensive tissue necrosis and scarring may even lead to thinning of the heart wall and aneurysm formation (Fig. 2.8).

Severe or repeated insults to the cardiac tissue from myocardial infarctions can seriously impair the heart's ability to circulate blood. The ultimate consequence is congestive heart failure, a condition characterized by abnormalities in myocardial function and neuro-hormonal regulation, resulting in fatigue, fluid retention, and reduced longevity (Gaziano et al. 2006). Loss of the heart's pumping action causes blood to back up in other parts of the body, such as the lungs, liver, and extremities. The hallmark symptom of congestive heart failure is shortness of breath, due to excess fluid collection in the pulmonary system. Additional symptoms include swelling in the ankles and legs, fluid sequestration in the abdomen, effusions surrounding the lungs, and general weakness (Fig. 2.9). Heart failure progresses to affect almost every other organ in the body, and patients in heart failure carry a grim prognosis. The risk of developing congestive heart failure is two times greater in hypertensive men and three times greater in hypertensive women, compared to those who maintain normal blood pressure. Congestive heart failure is five times more common in those who have suffered an acute myocardial infarction than in those who have not (McMurray and Stewart 2000).

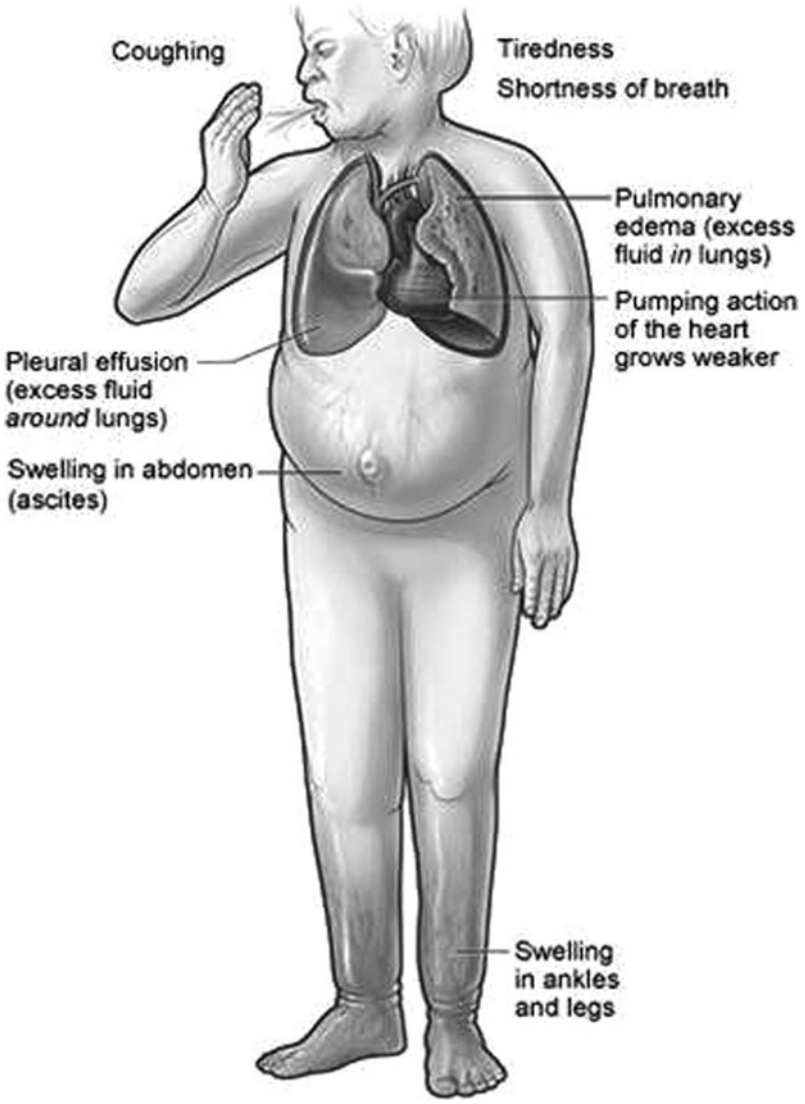

Fig. 2.9 Clinical symptoms of congestive heart failure (National Heart, Lung, and Blood Institute)

Coronary artery disease and myocardial infarctions are typically managed with both pharmacologic therapy and surgical intervention. Standard drug regimens utilize anti-thrombotic agents such as aspirin, cholesterol-lowering agents such as statins, and anti-hypertensives such as angiotensin-converting enzyme inhibitors and beta-adrenergic receptor blockers. This last class of pharmaceuticals is particularly useful for reducing the workload on the heart. The longtime surgical treatment for occluded coronary arteries has been coronary artery bypass surgery, in which a vein

is harvested from another part of the body, and grafted onto the affected artery to bypass the blockage. Bypass surgery is a sophisticated technique that has saved many lives since its development in the 1960s; and it continues to be a necessary procedure in the surgical armamentarium. However, bypass surgery is highly invasive, requiring the chest wall to be cracked open to expose the heart. Attendant complications include graft infection, chest wall dehiscence, and chest wound infection. Moreover, coronary artery bypass is technically difficult and costly, which limits patient access to the procedure. In addition, the procedure requires a long hospital stay of approximately 5 days post-procedure and an extended recovery time of 4–6 weeks.

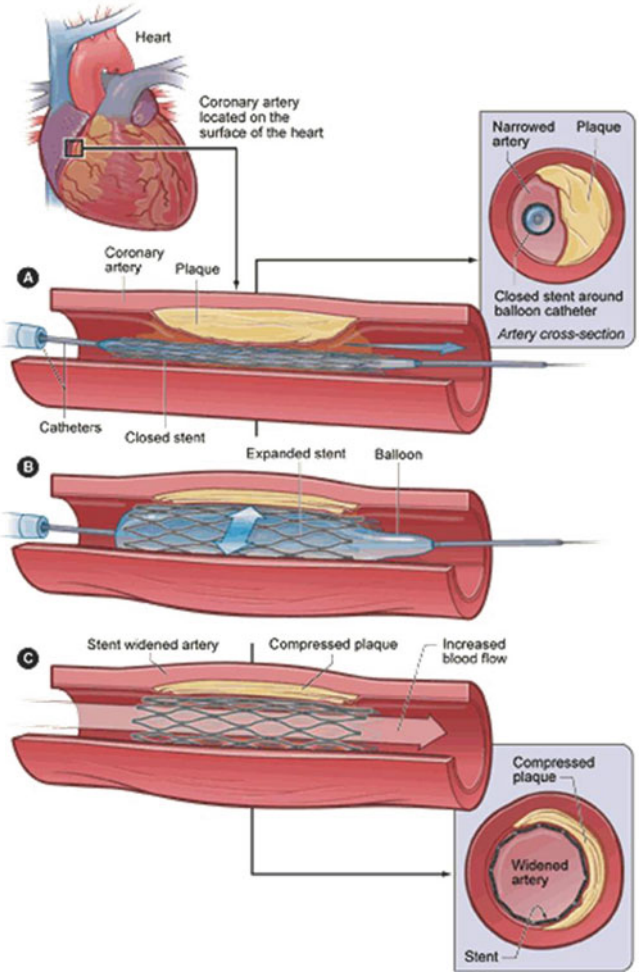

Fig. 2.10 Stent implantation for the treatment of coronary artery plaque (National Heart, Lung, and Blood Institute)

A minimally invasive device for opening blocked coronary arteries, known as the coronary stent, has been developed more recently to avoid many of the complications of bypass surgery. A typical stent is formed as a mesh tube, constructed from metal wire commonly made of stainless steel or other metals. The first widely used metallic stent, the Palmaz–Schatz stent, was clinically evaluated and commercialized in the early 1990s (Schatz et al. 1991). Since then, stent implantation has become the most common treatment for blocked coronary arteries; stents are now used in over 75% of all coronary artery procedures worldwide (Zimmer et al. 2002). During a stenting procedure (Fig. 2.10), the stent is mounted on a balloon catheter which is inserted through the femoral (leg) artery. The stent balloon system is then guided from the femoral artery to the affected coronary artery, using x-ray/fluoroscopy for visualization. Once the device is properly located at the narrowed lesion in the coronary artery, the balloon and stent are expanded, compressing the atherosclerotic plaque and opening up the arterial lumen. The balloon is withdrawn, and the expanded stent is permanently set in place. The stent becomes embedded into the vessel wall, as vascular endothelial cells populate the stent surface in a process known as endothelialization. The stent subsequently maintains the blood vessel in an enlarged state and prevents the vessel from recoiling. Stenting essentially allows a patient with coronary artery lesions to undergo surgery via a small puncture in the leg, rather than a large open surgical wound on the chest. The widespread adoption of coronary stents has enabled shorter hospital stays, faster recovery times, and lower hospitalization costs.

Patients suffering from coronary artery disease can now be treated with minimally invasive stents that are even more effective and biocompatible, as a result of biomaterial innovations. The following sections will discuss bioactive stents and degradable stents that demonstrate improved functionality compared to bare-metallic stents. The final section will discuss biomaterials for heart regeneration that can potentially benefit patients in congestive heart failure, a population for which few interventions currently exist.

2.3 Biomaterials as Bioactive Stents

Bioactive stents are biomaterials that combine the mechanical properties of coronary stents with the functional properties of biomolecules such as pharmaceuticals, cytokines, and antibodies. The main motivation for bioactive stent development is to reduce complications associated with stent implantation. Bare-metallic stents, while permitting targeted treatment for occluded coronary arteries, are associated with high rates of restenosis (i.e., re-narrowing of the coronary artery). Though the design of bare- metallic stents has been continually upgraded, up to 25% of patients treated with bare-metal stents experience restenosis (Zimmer et al. 2002). Restenosis is caused in part by the expanding balloon and stent, which leads to vascular wall injury and cellular over-proliferation. More complex arterial lesions such as lung lesions, smaller diameter lesions, vascular bifurcations, and ostial locations

Table 2.4 Specifications and requirements of a bioactive stent

Criteria	Specification
Crimping on traditional angioplasty balloon, and deployed with minimal recoil	Deformable material with minimal elasticity
Mechanical strength	Sufficiently strong to maintain artery open
Mechanical flexibility	Sufficiently flexible to allow stent deformation during navigation and minimal artery tonicity
Biostable	No release of toxic agents, predictable release of therapeutic agents
Hemocompatible	Non-thrombogenic surface
Endothelialization	Cell-compatible surface
Sterility	Properties not changed by sterilization

Sharkawi et al. (2007)

are more prone to restenosis (Mercado et al. 2001); the complication may occur in up to 30–60% of patients with complex lesions (Fattori and Piva 2003). Restenosis has proven to be intractable to the systemic administration of drugs. The rationale for incorporating biological agents into stents is to optimize the tissue response to stent implantation, prevent restenosis, and thereby improve patient outcomes.

An ideal bioactive stent must fulfill both mechanical and biological specifications, as listed in Table 2.4. First, the stent must have the ability to be crimped onto an angioplasty balloon catheter with a resulting diameter of approximately 1 mm; this is an absolute requirement for stent introduction into the body (Sharkawi et al. 2007). The stent must be flexible enough to deform, so that the stent on the balloon catheter can be inserted through the femoral artery and guided to the site of the coronary artery lesion. Once the balloon reaches the desired site, the stent must be deployed and retain its nominal diameter, typically between 2 and 4 mm. A stent must have enough radial strength to resist arterial spasm and maintain the artery in an open state; however, the strength must be finely tuned since exaggerated radial resistance will hinder the natural elasticity of the artery. In addition, an exceedingly rigid stent will encumber the deliverability of the device, since access to the artery usually goes through a tortuous vascular bed. In terms of biological properties, the bioactive stent must be compatible with the blood and its various constituents, as well as with the endothelium and other arterial wall cells. The surface properties are critical, since the initial compatibility with the blood elements will depend entirely on the stent surface properties. The surface must also encourage rapid embedding in the endothelial lining of the artery, to avoid possible thrombosis due to prolonged blood contact. If the bioactive stent releases a therapeutic agent, it must deliver the agent in a consistent and predictable manner to avoid overdose. Both the mechanical and biological components of the bioactive stent must withstand sterilization conditions.

Drug-eluting stents are bioactive stents that release small-molecule therapeutics directly into the vessel lumen to forestall restenosis. A drug-eluting stent is created by coating a metallic stent with a drug-loaded polymer. The stent wires, or

Table 2.5 Comparison of drug-eluting stent structures and compositions

	Cypher®	Taxus® Express	Xience™ V	Endeavor®
Stent thickness (μm)	140	132	81	91
Polymer thickness (μm)	14	16	7	6
Stent material	Stainless steel	Stainless steel	Cobalt–chromium	Cobalt–chromium
Chemical nature of polymer	PEVA and PEMA	Hydrocarbon-based elastomer	Biocompatible fluoropolymer	Hydrophilic phosphorylcholine
Bioactive drug	Sirolimus	Paclitaxel	Everolimus	Zotarolimus

struts, are configured in a specific geometry to optimize local delivery of pharmacologic agents; strut configurations include the "slotted tube" which produces diamond-shaped cells upon expansion or the corrugated tubular-like rings with bridging links. Once implanted, the stent releases a therapeutic amount of the drug over a short period of time (usually a few weeks). As discussed in Section 2.2, atherosclerotic plaque results from both lipid deposition and smooth muscle cell proliferation. Therefore, the pharmaceuticals utilized most commonly in drug-eluting stents are anti-proliferative agents. Table 2.5 compares the materials of construction, technical specifications, and therapeutic agents for four leading drug-eluting stents. Such stents have been realized through advances in drug delivery, cell biology, and polymer science.

The first generation of drug-eluting stents includes sirolimus-eluting stents and paclitaxel-eluting stents. The Cypher® sirolimus-eluting stent (Johnson & Johnson/Cordis, Miami Lakes, FL, USA) was the first drug-eluting stent to be made commercially available in 2003. This stent has been the most widely used drug-eluting stent in the world and is considered to be the standard of comparison for all drug-eluting stents (Maluenda et al. 2009). The Cypher® stent utilizes a stainless steel platform (Fig. 2.11), coated with poly(ethylene co-vinyl acetate) and poly(*n*-butyl methacrylate). The polymer releases sirolimus, an anti-proliferative drug that inhibits the G1 phase of the cell cycle and halts cell replication. Most of the drug is delivered in approximately 3 weeks post-implantation of the stent (Acharya and Park 2006). Sirolimus-eluting stents have achieved yearly restenosis rates as low as 6.8–7.9% (Weisz et al. 2006). The Cypher® stent is also associated with a significant reduction in both mortality and repeat revascularization procedures, compared to bare-metal stents (Groeneveld et al. 2008).

Fig. 2.11 The Cypher® sirolimus-eluting stent (Food and Drug Administration)

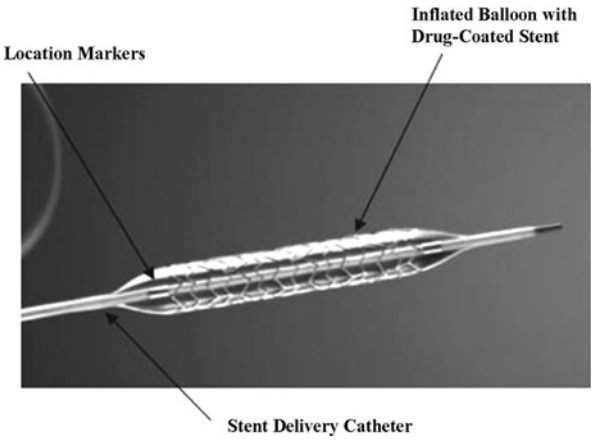

Fig. 2.12 The Taxus® paclitaxel-eluting stent (Food and Drug Administration)

The Taxus® paclitaxel-eluting stent (Boston Scientific, Natick, MA, USA) was also introduced commercially in 2003. As of 2009, nearly 5 million Taxus® drug-eluting stents had been implanted in patients worldwide (Maluenda et al. 2009). This stent is made with a stainless steel platform (Fig. 2.12), coated with the hydrocarbon-based elastomer poly(styrene-b-isobutylene-b-styrene). Embedded within the elastomer is the drug paclitaxel, an anti-proliferative agent that stabilizes microtubules and blocks intracellular signaling, inhibiting smooth muscle cell migration and growth (Axel et al. 1997). The elastomer–paclitaxel system is advantageous in that it is a diffusion-based controlled-release matrix, facilitating slow and very specific delivery of the drug (Acharya and Park 2006). Paclitaxel-eluting stents exhibit restenosis rates of 10% (Maluenda et al. 2009).

The second generation of drug-eluting stents includes everolimus-eluting stents and zotarolimus-eluting stents. This generation of devices incorporates flexible stent designs, more biocompatible polymers, and potent therapeutics; such biomaterials are now emerging in clinical use. The Xience^{TM} V everolimus-eluting stent (Abbott Vascular, Markham, Ontario, Canada) employs a cobalt–chromium alloy within the stent. The alloy is stronger than stainless steel, allowing for very thin struts. The open cells and nonlinear structure make the Xience^{TM} stent more flexible than previous stents. The stent is assembled onto a semi-compliant balloon with short tapers that are designed to minimize vascular injury outside the stent area (Maluenda et al. 2009). The polymer coating is a non-adhesive, durable, and biocompatible fluoropolymer composed of an outer layer of poly(*n*-butyl-methacrylate) and an inner layer of poly(vinylidene fluoride co-hexa-flu-oropropylene). The inner layer is a drug reservoir and contains everolimus, an anti-proliferative agent that inhibits the G1 phase of the cell cycle; everolimus is distinguished from previous agents by its high potency and high lipophilicity. The Xience^{TM} system releases approximately 80% of the drug by the first month and nearly all of it by 4 months post-implantation. The Endeavor® zotarolimus-eluting stent (Medtronic CardioVascular, Minneapolis,

MN, USA) uses a cobalt–chromium alloy stent coated with a phosphorylcholine-based polymer. The hydrophilic polymer is intended to be more biocompatible as phosphorylcholine is a naturally occurring phospholipid, and it delivers the drug zotarolimus, an analogue of sirolimus. The release kinetics of zotarolimus enables nearly complete drug delivery within the first month after stent placement.

In general, drug-eluting stents have demonstrated an advantage over bare-metal stents with regard to restenosis rates; drug-releasing stents allow the coronary arteries to remain patent longer and reducing the necessity for repeat interventions. Drug-eluting bioactive stents are now estimated to reach 75% of all stent procedures (Maluenda et al. 2009); currently available coronary stents permit the treatment of complex cases with a wide safety margin and a high likelihood of optimal acute results. Drug-eluting stents improve the cost-effectiveness of treatment for coronary artery disease, given the significantly fewer repeat revascularizations during the first year. These devices provide the means for a predictable interventional procedure, a function of both the mechanical properties of drug-eluting stents and their delivery systems (Lemos 2007).

Other types of bioactive stents, which rely on immune-stimulating cytokines or cell-specific antibodies to halt arterial narrowing, are also on the verge of clinical introduction. For instance, coating of stainless steel surfaces with meshwork containing the cytokine interferon-γ (IFN-γ) inhibits smooth muscle cell growth without affecting endothelial cell growth (Kipshidze et al. 2002). Because smooth muscle cell hyperproliferation is a main cause of recurrent stenosis following cardiovascular stent implantation, coating of metal stents with IFN-γ may be a promising strategy for stopping restenosis and maintaining cardiac perfusion.

Several classes of antibody-coated and antibody-eluting coronary artery stents have been developed to improve endothelialization and inhibit thrombogenesis on the inner stent surface, thereby increasing stent patency rates post-implantation. Coating of stainless steel stents with anti- CD34 antibody allows capture of circulating endothelial progenitor cells (EPCs) onto the stent surface to enhance endothelialization (Aoki et al. 2005); this may be a critical factor for success in certain patient populations, as the number of circulating EPCs and their migratory activity are reduced in patients with diabetes, coronary artery disease, or multiple coronary risk factors (Kawamoto and Asahara 2007). The Genous™ BioEngineered R stent™ (OrbusNeich, Hong Kong) utilizes anti-CD34 antibodies coated onto a stainless steel stent; the first human clinical investigation of this technology suggests that the EPC capture stent is safe and feasible for treatment of de novo coronary artery disease (Aoki et al. 2005). A multi-center, worldwide clinical study is currently underway to evaluate the efficacy of the Genous™ device in treating coronary artery disease.

Other receptor-targeting antibodies have been investigated for antibody-stent combinations. Abciximab (ReoPro, c7E3-Fab) inhibits the platelet glycoprotein IIb/IIIa receptor as well as the smooth muscle cell αvβ3 integrin receptor. Elution of abciximab from polymer-coated stents results in significantly lower platelet deposition. In human coronary arteries, abciximab-eluting stents are associated with significantly decreased neointimal hyperplasia as compared to control stents. In a

prospective randomized trial, the abciximab-coated stent demonstrated lower rates of restenosis and target vessel revascularization, indicating that the stent may be effective for prevention of coronary restenosis. In patients with acute myocardial infarction, the abciximab-coated stent is safe and effective without stent thrombosis (Kim et al. 2006).

Growth factor-targeting antibodies have also been incorporated into stents to modulate the tissue response to stent implantation. The VEGF-targeting antibody bevacizumab inhibits angiogenesis and neovascularization. Because neovascularization is associated with the destabilization of atheromatous plaque, inhibition of neovascularization may be a useful strategy for treatment of stable and vulnerable plaques. Delivery of bevacizumab from vascular stents results in decreased neointimal hyperplasia and decreased neovascularization in an iliac artery model, without compromising endothelialization (Stefanadis et al. 2007). Such devices show promise for preventing stent restenosis and stabilizing arterial plaque. The newest bioactive stents are thus mobilizing cellular pathways, biological receptors, and novel polymers, to improve patient outcomes and decrease mortality from coronary artery disease. The following section will describe how polymer science can be fully brought to bear on the construction of degradable stents.

2.4 Biomaterials as Degradable Stents

Though bioactive stents are making great strides in saving patients from coronary artery disease, there is evidence that their permanent implantation in the arterial wall can have adverse long-term consequences. For this reason, biomaterials researchers are increasingly turning their attention toward degradable stents. Clinicians generally agree that the mechanical reinforcement provided by a stent is needed only temporarily during the healing period. The artery heals between 3 and 6 months after stent implantation, after which arterial support is no longer needed (Sharkawi et al. 2007). A functional device that can disappear is clearly preferable over a permanent device that presents the risk of triggering late complications such as restenosis and thrombosis. Indeed, while some regard drug-eluting metal stents as the final technologic advancement in the treatment of coronary artery disease, others consider the development of degradable stents as the next logical step (Kohn and Zeltinger 2005).

A degradable stent can potentially overcome many of the shortcomings of permanent metallic stents, as summarized in Table 2.6. For example, there is a significant mechanical mismatch between a metal stent and the vessel wall, due to the excessive stiffness of the metal stents. Over time, the associated arterial stress can affect vessel perfusion and healing of the vessel wall. Metal stents also induce constrictive remodeling of the blood vessel, since it is not possible for the artery to increase its lumen past the original stent diameter. These problems are alleviated by the use of a degradable stent with mechanical strength and stiffness that decreases during the degradation process. A bioresorbable stent can permit an increase in lumen diameter once the stent is eliminated.

Table 2.6 Potential advantages and technical challenges of degradable stents

Advantages	Technical challenges to overcome
• Mechanically functional for required healing period • Better physiologic healing of the artery upon degradation • Permits positive remodeling of the artery • Allows repeated interventions • Disappears after healing is complete • Stent itself can be used as a drug delivery system (larger loads)	• Incompatibility due to poor polymer quality or processing (residual solvents, catalyst, monomer, etc.) • Inadequate degradation and resorption profile • Inflammatory degradation residues • Insufficient mechanical properties or radial strength • Inadequate release profile when used as a drug delivery system

Sharkawi et al. (2007)

Moreover, permanent metallic stents that are covered by drug-loaded delivery systems can sometimes trigger clotting in the longer term, because the anti-proliferative drugs delay the growth of healthy endothelium over stent struts and their durable polymer coatings (Finn et al. 2007). Such stents are exposed for a long period of time to the blood without being endothelialized, and the chance of stent thrombosis is increased. A degradable stent avoids such side effects by dissolving away, rather than leaving behind a permanent surface that can induce unwanted platelet or cell attachment. Stent degradation enables gradual restoration of the vessel's natural environment, which should produce a better functional tissue than in the case where a vessel heals in the presence of a permanent aid.

Finally, permanent stents are superfluous after the vessel has healed and make repeat interventions difficult if not impossible. When additional stents are needed to treat downstream lesions, it is sometimes not feasible to pass the new stents through the already implanted stents; surgical bypass is the only available treatment option in such cases. Unfortunately, bypass surgery can be difficult for patients with multiple metal stents within their coronary arteries. Permanent metal stents tend to block off or "jail" side arterial branches and impair non-invasive imaging of coronary arteries with standard CT and MRI. A degradable stent leaves no trace once absorbed and will not interfere with subsequent surgeries.

The design of polymers for degradable stents presents an incredible challenge to biomaterials scientists. A degradable polymer stent must meet all of the mechanical and biological specifications listed in Table 2.4 and must also be eliminated after accomplishing its function. The polymeric material must be resorbable under physiological conditions with a predictable time line; polymer degradation is affected by a multitude of structural, chemical, and processing parameters as listed in Table 2.7. Biocompatibility requires that the degradation products be well tolerated and readily excreted. As far as mechanical properties, degradable stents must match the strength and flexibility of metallic stents. While the high strength of metals enables designers to use ultra-thin stent struts in metallic stents, all polymer stents have stents that are substantially thicker, as polymers are mechanically weaker than metals. The intrinsically lower mechanical strength of degradable polymers relative to metal

Table 2.7 Factors affecting polymer degradation

1. Chemical composition and structure
– *Repeat unit distribution in multimers*
– *Molecular weight and distribution*
– *Morphology* (*crystallinity, microstructures, residual stresses)*
– *Adsorbed and absorbed compounds (water, lipids, ions, proteins, etc.*)
– *Physicochemical factors* (*ion exchange, pH*)
2. Processing conditions (force, solvents, catalysts, etc.)
3. Sterilization process (affecting crystallinity)
4. Physical factors (changes in shape, size, diffusion, and mechanical stress)
5. Implantation site (mechanical and biological environment)

must be overcome by substantial changes in stent design, to achieve an appropriate level of flexibility (Kohn and Zeltinger 2005). Balloon deployment conditions such as inflation time, temperature, and pressure have to be adapted for deploying plastic stents.

Bioresorbable polymers under investigation for degradable stents include aliphatic polyesters, polyorthoesters, and polyanhydrides (Eberhart et al. 2003). Bioresorbable aliphatic polyesters of the poly-lactic acid (PLA) family are the most extensively studied polymers in the biomaterials field, because of their known biocompatibility and physiological metabolites. The mechanical properties and degradation profiles of PLA-type polymers can by tuned by utilizing different combinations of stereocopolymers or copolymers with other monomers. The polymerization of the stereoisomers D-lactic acid and L-lactic acid in various proportions leads to a family of compounds, each having distinct resorption rates. Polymers of this family have been successfully used for drug delivery systems and orthopedic devices, making PLA-type polymers a natural starting point for degradable stents.

The first degradable stent to demonstrate clinical safety and efficacy was the Igaki-Tamai stent (Igaki Medical, Kyoto, Japan), which was successfully implanted in patients in 2000 (Tamai et al. 2000). This bioresorbable stent is made from a monofilament of poly-L-lactic acid (PLLA) shaped in a zigzag design. The self-expanding stent requires a covered sheet system and a heated balloon for deployment – a process that is non-standardized and potentially hazardous. The overall performance and the rate of adverse cardiac events following Igaki-Tamai stent implantation are similar to that for bare-metal stents. However, the lack of visibility and the need for a heated balloon have limited the clinical utility of the Igaki-Tamai stent.

An additional limitation is that semi-crystalline PLLA undergoes very slow hydrolytic degradation and may leave long-lasting crystalline particles which induce an inflammatory response. PLLA is the most stable member of the poly-lactic acid family, a disadvantage for degradable stent design. To address these issues, PLA stereocopolymers have been investigated as a means of varying the degradation rate of temporary stents (Lafont et al. 2006). Two stent compositions have been evaluated: poly-D,L-lactic acid with D:L ratio of 50/50 (PLA50) and poly-D,L-lactic acid

with D:L ratio of 8/92 (PLA92). Both demonstrated good biocompatibility properties in animal models, and the PLA50 stent achieved nearly complete resorption after 6 months (Lafont et al. 2006). Other degradable polymers have been synthesized for degradable stents as well. A tyrosine-derived polycarbonate stent is under development; this stent carries the unique advantage of excellent visibility by x-ray/fluoroscopy, by virtue of iodination of the tyrosine ring (Kohn and Zeltinger 2005).

Building on these accomplishments in resorbable stent design, degradable stents that also elute therapeutics are now being created. A degradable drug-eluting stent could potentially offer new and more efficacious treatment strategies, as compared to existing drug-eluting metallic stents. Polymer-coated metal stents have a relatively low total drug-loading capacity, as the polymer coatings are typically thin. A degradable drug-eluting stent can deliver a greater drug payload over a longer period of time. When the stent is entirely made up of a polymer, the whole stent can act as a drug-releasing matrix. Degradable drug-eluting stents could additionally provide greater options for timed delivery of multiple drugs, to modify the underlying disease state. Finally, a degradable drug-eluting stent combines pharmaceutical delivery capability with short-term scaffolding, while avoiding the chronic inflammation caused by metallic stents.

A bioresorbable everolimus-eluting stent system known as the BVS stent (Abbott Vascular, Santa Clara, CA, USA) has recently been investigated in a human clinical trial (Ormiston et al. 2008). The BVS stent consists of a backbone of semicrystalline poly-L-lactic acid (PLLA) coated with poly-D,L-lactic acid (PDLLA). The PDLLA in the coating is an amorphous, random copolymer of D-lactic acid and L-lactic acid. The PDLLA coating contains and controls the release of the antiproliferative agent everolimus. During bioresorption of the stent, the long chains of PLLA and PDLLA are progressively shortened by hydrolysis of ester bonds, producing small particles less than 2 μm in diameter that are phagocytosed by macrophage cells. Eventually, PLLA and PDLLA degrade to lactic acid, which is physiologically metabolized by the Krebs cycle. The in vivo degradation profile of a PLLA everolimus-eluting stent was established in a porcine model; the stent exhibits 30% mass loss at 12 months post-implantation and 60% mass loss at 18 months post-implantation (Ormiston et al. 2008). Importantly, the acute stent recoil of bioabsorbable everolimus-eluting stents is not different from that of everolimus-eluting metallic cobalt–chromium stents (Tanimotos et al. 2007), an indication that the bioabsorbable stent has adequate radial strength. In a human clinical trial, this degradable drug-eluting stent demonstrated a 94% success rate during implantation and excellent clinical safety up to 1 year after the procedure (Ormiston et al. 2008).

The success of the bioresorbable everolimus-eluting stent in early clinical trials suggests that degradable drug-eluting stents represent the future of interventional cardiology. It has been predicted that optimally designed degradable stents, combined with highly specific and potent therapeutic agent, will emerge in the next few years to effectively treat diseased vessels (Kohn and Zeltinger 2005). Degradable polymer stents have been envisioned that will elute more than one therapeutic agent, to treat heterogeneous and complex lesions such as unstable plaque or stenosis in

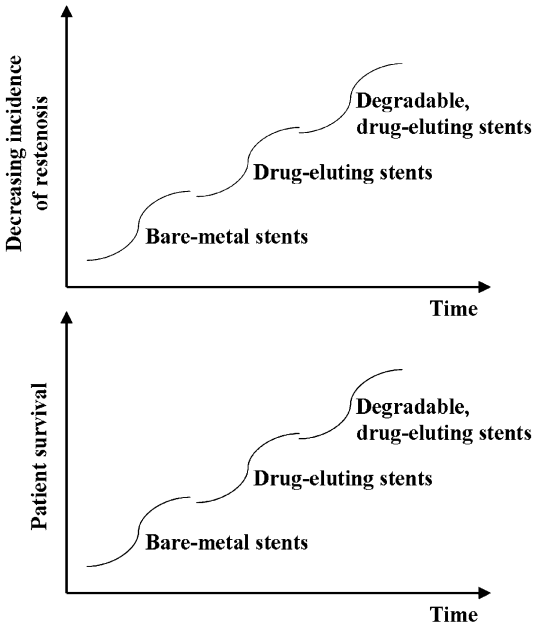

Fig. 2.13 Technological evolution of stents for treatment of coronary artery disease

diabetic patients. For example, a degradable stent could provide early and acute delivery of an anti-inflammatory agent, longer and subacute delivery of an anti-proliferative agent, and prolonged elution of a lipid-lowering agent (Kohn and Zeltinger 2005). The technology evolution for minimally invasive stents is summarized in Fig. 2.13. Just as drug-eluting metal stents have displaced bare-metal stents for treatment of coronary artery disease, it appears that degradable drug-eluting stents will gradually displace drug-eluting metal stents. The ease of placement of these devices, as well as the invasiveness to the blood vessel itself will be constantly improved. Patients with acute coronary artery blockage will continue to benefit from these innovative biomaterials and will experience lower restenosis rates and lower overall mortality.

2.5 Biomaterials for Cardiac Regeneration

While stenting is an effective minimally invasive method for opening occluded coronary arteries and re-establishing perfusion after an acute arterial blockage, stents have limited value for treating patients with long-standing cardiac muscle damage and chronic heart failure. A large number of cardiomyocytes (cardiac muscle cells), more than 10^9 cells, can be lost following a myocardial infarction. This cell death is irreversible; the adult heart cannot repair the damaged tissue even when blood flow is restored through the coronary arteries. The resultant fibrous scar tissue lacks the

contractile, mechanical, and electrical properties of normal cardiac muscle. Heart failure results from the loss of the heart's pumping efficiency. Current treatment options for patients in advanced heart failure are limited and include mechanical ventricular assist devices or heart transplantation. Ventricular assist devices are associated with high costs and high complication rates, while donor organs are in short supply. For these reasons, there is increasing interest in creating biomaterials for regeneration of native heart tissue; this field of biomaterials science is also known as cardiac tissue engineering.

The general strategy for cardiac tissue engineering is to combine a three-dimensional polymeric scaffold with cardiac or non-cardiac cells; the scaffold provides support and structure for the cells, while the cells contribute biological functionality. The scaffold may take the form of a mesh, patch, or foam, and it may incorporate growth factors to stimulate the expansion of desirable cell populations. Once implanted, the tissue-engineered construct guides the growth and development of new cardiac tissue, and the polymer scaffold degrades away to be replaced by healthy functioning tissue. An optimal biomaterial for cardiac regeneration enhances cell attachment, proliferation, and differentiation. To initiate tissue renewal, the biomaterial must integrate with the host tissue and promote in vivo revascularization to ensure adequate oxygen supply. At the same time, the implanted biomaterial must safely degrade at a rate similar to that of the new cardiac tissue formation, such that the biomaterial is eventually removed from the body by natural metabolic processes. In this respect, scaffolds for cardiac tissue engineering are like degradable stents: both devices are temporary structures which disappear once they have served their therapeutic function and healing is complete.

The basic physical requirements for myocardial engineered constructs are robust yet flexible mechanical properties, contractile ability, and electro-physiologic stability. Ideally, the elastic properties of the biomaterial should match the elastic properties of the native heart, to prevent cell detachment from the construct (Jawad et al. 2007). Table 2.8 lists the mechanical properties of some biomaterials used in cardiac regeneration.

Biomaterials for cardiac regeneration may be engineered either in vitro or in situ (Fig. 2.14). In vitro engineering entails culturing cells on a biomaterial scaffold in vitro and then implanting the tissue onto the affected cardiac surface. In situ engineering utilizes an injectable biomaterial to deliver cells directly into the infarct wall to increase cell survival. Table 2.9 summarizes the in vitro and in situ engineered tissue constructs which have been investigated for cardiac regeneration. Cardiac tissue engineering has employed synthetic degradable polymers such as poly-lactic acid and poly-glycolic acid, as well as natural polymers including collagen and alginate.

Cardiac tissue engineering may incorporate a wide variety of cellular populations, such as cardiomyocytes (cardiac muscle cells), fibroblasts (connective tissue cells), and myoblasts (muscle cells). For instance, cardiomyocytes can be encapsulated into collagen to create an engineered construct for cardiac regeneration (Fig. 2.15). Additionally, stem cells are becoming critical components of many cardiac repair strategies. Stem cells are cells with the potential to self-renew and

Table 2.8 Mechanical properties of biomaterials used in cardiac tissue engineering

Biomaterial	Young's modulus	Tensile strength
Synthetic polymers		
Polyglycolic acid (PGA)	7–10 GPa	70 MPa
Polylactic acid (PLLA or PDLLA)	1–6 GPa	30–80 MPa
Natural polymers		
Alginate	2.25–2.4 GPa	24.72 MPa
Collagen fiber (tendon/ cartilage/ligament/bone)	2–46 MPa	1–7 MPa
Collagen gel (calf skin)	0.002–0.022 MPa	1–9 kPa
Physiological tissue		
Myocardium of rat	0.14 MPa (end-diastole)	30–70 kPa
Myocardium of human	0.2–0.5 MPa (end-diastole	3–15 kPa

Jawad et al. (2007)

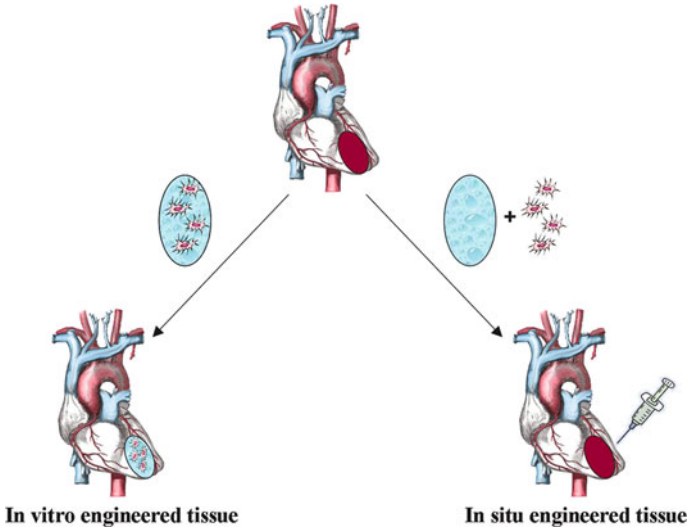

Fig. 2.14 In vitro and in situ methods for cardiac tissue engineering

differentiate along specific lineages (Fig. 2.16); they may be either embryonic or adult cells depending on their origin. Embryonic stem cells are formed from early embryos and possess the ability to differentiate into every cell type in the body. Adult stem cells reside in adult tissues and organs, and they have the capacity to differentiate into a restricted number of cell lineages. Adult stem cells include cardiac stem cells and hematopoietic and mesenchymal stem cells of the bone marrow. As seen in Table 2.9, biomaterials have also been transplanted without cellular populations, to provide mechanical support for the ventricular walls or to transfer growth factors to ischemic myocardium.

Table 2.9 Constructs utilized for cardiac tissue engineering

Material	Transplantation
In vitro *engineered tissue*	
Gelatin	Alone or with fetal cardiomyocytes
Alginate	With fetal cardiomyocytes
Polyglycolic acid/ polylactic acid	With dermal fibroblasts
Collagen type I and matrigel	With neonatal cardiomyocytes
Polytetrafluoroethylene (PTFE), polylactic acid mesh, collagen type I, and matrigel	Alone or with bone marrow-derived mesenchymal progenitor cells
Collagen type I	Alone or with embryonic stem cells
Poly-*N*-isopropylacrylamide (PNIPAAM)	Cell sheet of neonatal cardiomyocytes or adipose-derived mesenchymal stem cells
In situ *engineered tissue*	
Fibrin	Alone, with skeletal myoblasts, bone marrow mononuclear cells, or pleiotrophin plasmid
Collagen	Alone or with bone marrow cells
Alginate	Alone
Matrigel	Alone or with embryonic stem cells
Collagen type I and matrigel	Alone or with neonatal cardiomyocytes
Self-assembling peptides	Alone, with neonatal cardiomyocytes, or with platelet-derived growth factor BB
Gelatin	With basic fibroblast growth factor

Christman and Lee (2006)

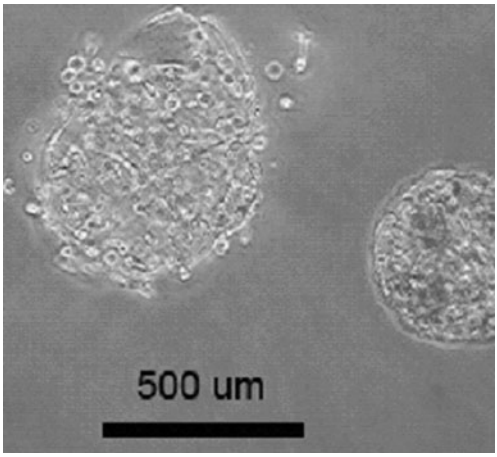

Fig. 2.15 Encapsulation of cardiomyocytes in collagen modules for tissue engineering (McGuigan et al. 2009)

The first demonstration of in vitro engineered cardiac tissue was reported in 1999, when fetal cardiomyocytes were seeded onto a biodegradable gelatin mesh in vitro and implanted on myocardial scar tissue in rat model (Li et al. 1999). Though the fetal cardiomyoctes survived on the grafts, there was no improvement in cardiac function. In a more recent study, a cardiac patch comprising dermal fibroblasts

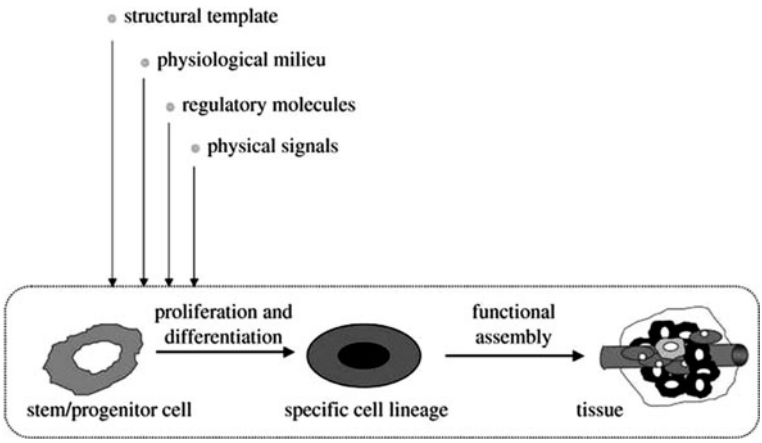

Fig. 2.16 Differentiation of stem cells into specific cell lineages and native tissue (Radisic et al. 2007)

seeded on knitted polyglycolic acid/polylactic acid showed efficacy in mouse models of myocardial infarction; the patch significantly increased ventricular pumping infarction; the patch significantly increased ventricular pumping function (Kellar et al. 2005). Another promising approach combined neonatal cardiomyocytes with liquid collagen type I and matrigel; this engineered tissue stimulated the formation of ~450-μm thick new myocardium in rat models and improved systolic and diastolic heart function (Zimmerman et al. 2006).

A unique and innovative method for in vitro cardiac tissue engineering utilizes a temperature-sensitive polymer, poly-*N*-isopropylacrylamide (PNIPAAM). This polymer is slightly hydrophobic and cell adhesive at 37°C, but becomes hydrophilic and cell resistant at 32°C due to rapid hydration and swelling. To create engineered cardiac biomaterials, PNIPAAM has been coated onto tissue culture plates and seeded with neonatal cardiomyocytes (Shimizu et al. 2002). Once the cells formed a monolayer, the temperature was dropped to release in intact sheet of cardiomyocytes. A three-dimensional pulsatile cardiac tissue construct was formed by layering six cell sheets upon each other (Shimizu et al. 2002). This cell-sheet technology has also been used to make monolayers of mesenchymal stem cells (Miyahara et al. 2006). Upon transplantation onto myocardial scar tissue in rat models, the monolayers expanded to produce new 600-μm thick tissue.

Though current methods for in vitro cardiac tissue engineering are exciting, they are unable to produce tissue constructs of sufficient thickness for human cardiac repair. The current maximum thickness of in vitro scaffolds is approximately half a millimeter; such a biomaterial is unlikely to produce noticeable changes in human myocardium. This represents a major obstacle for in vitro approaches, so that in situ engineered constructs are now being investigated as a possible alternative.

Because the in situ approach utilizes injectable biomaterials, it is less invasive than implanting an in vitro engineered mesh, sheet, or patch. Thus, in situ engineered biomaterials may be more clinically efficacious and more clinically appealing.

In many cases, in situ engineered cardiac tissues have drawn on the same polymers and cellular populations as in vitro engineered cardiac tissues, as seen in Table 2.9. In situ engineered scaffolds have already shown early success in animal models. In 2004, it was demonstrated that an injectable fibrin scaffold carrying skeletal myoblasts induced neovascularization in a rat model of myocardial infarction (Christman et al. 2004). The biopolymer scaffold improved cell survival, compared to the result when cells were injected alone. Injection of fibrin glue with skeletal myoblasts has even shown efficacy in treating chronic cardiac aneurysms in animal models of myocardial infarction (Christman and Lee 2006). In another interesting approach, a mixture of collagen type I and matrigel was introduced with neonatal cardiomyocytes into the heart wall of rat models; the injectable biomaterial preserved ventricular geometry and cardiac function (Zhang et al. 2006). Still another method involves self-assembling peptides that form nanofibers upon injection, to create a suitable environment for cellular and vascular ingrowth (Davis et al. 2005). Delivery of the self-assembling peptides with neonatal cardiomyocytes was found to enhance recruitment of host cells. Clearly, biomaterials for cardiac regeneration have the potential to reduce scar tissue, recruit new cells for healing, remodel cardiac muscle, and reconstruct broken hearts.

Many unanswered questions remain before regenerative cardiac biomaterials can be translated to human patients. The exact biological mechanism of each tissue engineering approach has not been well characterized. The best cell sources for cardiac repair have yet to be identified; one cell source may be unable to fully replenish all necessary cell types. The mechanical stability of the polymer scaffolds must still be optimized. Moreover, current studies often last 1–2 months and may not be indicative of long-term outcomes. There is no assurance that the benefits of engineered scaffolds will persist months or years after the polymer has degraded away. Clinical studies will need to demonstrate that these biomaterials not only improve cardiac pumping function, but also increase patient survival. Cardiac tissue engineering is a ripe area for future biomaterials research. An improved understanding of the biological function and mechanical properties of such biomaterials will speed their clinical implementation.

In general, novel biomaterials for the treatment of coronary artery disease have been well worth the investment. It has been estimated that approximately 70% of the survival improvement in heart attack mortality can be attributed to new technologies (Cutler and McClellan 2001). From an economic perspective, every $1 spent on technological innovations in heart attack care has produced an estimated $7 economic gain (Cutler and McClellan 2001). The potential benefits of innovative biomaterials for heart disease, such as stents and engineered tissue constructs, certainly outweigh the costs. Given that coronary artery disease is the leading cause of death worldwide, continued progress in cardiac biomaterials is essential. As William Harvey stated in 1628, “The heart of creatures is the foundation of life, the Prince

of all, the Sun of their micro-cosmos from where all vigour and strength does flow." In the next chapter, the discussion will turn to another disease that manifests from vascular injury and impaired circulation, stroke.

References

Acharya G, Park K (2006) Mechanisms of controlled drug release from drug-eluting stents. Adv Drug Deliv Rev 58:387

Antman EM, Anbe DT, Armstrong PW et al (2004) ACC/AHA guidelines for the management of patients with ST-elevation myocardial infarction – executive summary: a report of the American College of Cardiology/American Heart Association Task Force on practice guidelines (Writing Committee to Revise the 1999 Guidelines for the Management of Patients with Acute Myocardial Infarction). Circulation 110:588

Aoki J, Serruys PW, van Beusekom H et al (2005) Endothelial progenitor cell capture by stents coated with antibody against CD34: the HEALING-FIM (Healthy endothelial accelerated lining inhibits neointimal growth-first in man) Registry. J Am Coll Cardiol 45:1574

Ashley EA, Niebauer J (2004) Cardiology explained. Remedica, London

Ashrafian H, Dwivedi G, Senior R (2006) Assessing myocardial perfusion after myocardial infarction. PLoS Med 3:e131

Axel DI, Kunert W, Göggelmann C (1997) Paclitaxel inhibits arterial smooth muscle cell proliferation and migration in vitro and in vivo using local drug delivery. Circulation 96:636

Christman KL, Lee RJ (2006) Biomaterials for the treatment of myocardial infarction. J Am Coll Cardiol 48:907

Christman KL, Vardanian AJ, Fang Q et al (2004) Injectable fibrin scaffold improves cell transplant survival, reduces infarct expansion, and induces neovasculature formation in ischemic myocardium. J Am Coll Cardiol 44:654

Cutler DM, McClellan M (2001) Is technological change in medicine worth it? Health Affairs 20:11

Davis ME, Motion JP, Narmoneva DA et al (2005) Injectable self-assembling peptide nanofibers create intramyocardial microenvironments for endothelial cells. Circulation 111:442

Eberhart RC, Su SH, Nguyen KT et al (2003) Bioresorbable polymeric stents: current status and future promise. J Biomater Sci Polym Ed 14:299

Fattori R, Piva T (2003) Drug eluting stents in vascular interventions. Lancet 361:247

Finn AV, Joner M, Nakazawa G et al (2007) Pathological correlates of late drug-eluting stent thrombosis: strut coverage as a marker of endothelialization. Circulation 115:2435

Gaziano T, Reddy KS, Paccaud F (2006) Cardiovascular disease. In: Jamison DT, Breman JG, Measham AR et al (eds) Disease control priorities in developing countries, 2nd edn. IBRD/The World Bank and Oxford University Press, Washington, DC

Groeneveld PW, Matta MA, Greenhut AP et al (2008) Drug-eluting compared with bare-metal coronary stents among elderly patients. J Am Coll Cardiol 51:2017

Herrick JB (1912) Clinical features of sudden obstruction of the coronary arteries. JAMA 59:2015

Jawad H, Ali NN, Lyon AR et al (2007) Myocardial tissue engineering: a review. J Tissue Eng Regen Med 1:327

Jay V (2000) The legacy of William Heberden. Arch Pathol Lab Med 124:1750

Kawamoto A, Asahara T (2007) Role of progenitor endothelial cells in cardiovascular disease and upcoming therapies. Catheter Cardiovasc Interv 70:477

Kellar RS, Shepherd BR, Larson DF et al (2005) Cardiac patch constructed from human fibroblasts attenuates reduction in cardiac function after acute infarct. Tissue Eng 11:1678

Kim W, Jeong MH, Kim KH et al (2006) The clinical results of a platelet glycoprotein IIb/IIIa receptor blocker (abciximab: ReoPro)-coated stent in acute myocardial infarction. J Am Coll Cardiol 47:933

Kipshidze N, Moussa I, Nikolaychik V et al (2002) Influence of Class I interferons on performance of vascular cells on stent material in vitro. Cardiovasc Radiat Med 3:82
Kohn J, Zeltinger J (2005) Degradable, drug-eluting stents: a new frontier for the treatment of coronary artery disease. Expert Rev Med Devices 2:667
Lafont A, Li S, Garreau H et al (2006) PLA stereocopolymers as sources of bioresorbable stents: preliminary investigation in rabbit. J Biomed Mater Res B Appl Biomater 77:349
Lemos PA (2007) Polymeric stents: degradable but strong. Catheter Cardiovasc Interv 70:524
Li RK, Jia ZQ, Weisel RD et al (1999) Survival and function of bioengineered cardiac grafts. Circulation 100(suppl 19): II63
Maluenda G, Lemesle G, Waksman R (2009) A critical appraisal of the safety and efficacy of drug-eluting stents. Clin Pharmacol Ther 85:474
McGuigan AP, Bruzewicz DA, Glavan A et al (2009) Cell encapsulation in sub-mm sized gel modules using replica molding. PLoS One 3:e2258
McMurray JJ, Stewart S (2000) Heart failure: epidemiology, aetiology, and prognosis of heart failure. Heart 83:596
Mercado N, Boersma E, Wijns W et al (2001) Clinical and quantitative coronary angiographic predictors of coronary restenosis: a comparative analysis from the balloon-to-stent era. J Am Coll Cardiol 38:645
Miyahara Y, Nagoya N, Kataoka M et al (2006) Monolayered mesenchymal stem cells repair scarred myocardium after myocardial infarction. Nat Med 12:459
Ormiston JA, Serruys PW, Regar E et al (2008) A bioabsorbable everolimus-eluting coronary stent system for patients with single de-novo coronary artery lesions (ABSORB): a prospective open-label trial. Lancet 371:899
Radisic M, Park H, Gerecht S et al (2007) Biomimetic approach to cardiac tissue engineering. Philos Trans R Soc Lond B Biol Sci 362:1357
Schatz RA, Baim DS, Leon M et al (1991) Clinical experience with the Palmaz-Schatz coronary stent. Initial results of a multicenter study. Circulation 83:148
Sharkawi T, Cornhill F, Lafont A et al (2007) Intravascular bioresorbable polymer stents: a potential alternative to current drug eluting metal stents. J Pharm Sci 96:2829
Shimizu T, Yamato M, Isoi Y et al (2002) Fabrication of pulsatile cardiac tissue grafts using a novel 3-dimentional cell sheet manipulation technique and temperature-responsive cell culture surfaces. Circ Res 90: e40
Stefanadis C, Toutouzas K, Stefanadi E et al (2007) Inhibition of plaque neovascularization and intimal hyperplasia by specific targeting vascular endothelial growth factor with bevacizumab-eluting stent: an experimental study. Atherosclerosis 195:268
Tamai H, Igaki K, Kyo E et al (2000) Initial and 6-month results of biodegradable poly-L-lactic acid coronary stents in humans. Circulation 102:399
Tanimotos S, Serruys PW, Thuesen L et al (2007) Comparison of in vivo acute stent recoil between the bioabsorbable everolimus-eluting coronary stent and the everolimus-eluting cobalt chromium coronary stent: insights from the ABSORB and SPIRIT trials. Catheter Cardiovasc Interv 70:515
Virchow R (1856) Gesammalte abhandlungen zur wissenschaftlichen medtzin. Medinger Sohn & Co., Frankfurt
Weisz G, Leon MB, Holmes DR Jr (2006) Two-year outcomes after sirolimus-eluting stent implantation: results from the sirolimus-eluting stent in de Novo native coronary lesions (SIRIUS) trial. J Am Coll Cardiol 47:1350
White PD (1942) Book review: a short history of cardiology by Herrick JB. JAMA 202–203
World Health Organization (2008) The global burden of disease: 2004 update. WHO Press, Geneva
Zhang P, Zhang H, Wang H et al (2006) Artificial matrix helps neonatal cardiomyocytes restore injured myocardium in rats. Artif Organs 30:86
Zimmer S, Jacobs B, Levy T et al (2002) Med Tech 101: the medical device handbook. Deutsche Bank Securities, Inc., New York, NY
Zimmermann WH, Melnychenko I, Wasmeier G et al (2006) Engineered heart tissue grafts improve systolic and diastolic function in infarcted rat hearts. Nat Med 12:452

Chapter 3
Stroke

Stroke and other cerebrovascular diseases are the second leading cause of death worldwide. In 2004, stroke and cerebrovascular disease were responsible for 5.7 million deaths, or 9.7% of all deaths globally and 4.2% of all years of life lost (World Health Organization 2008). Cerebrovascular syndromes are highly prevalent, as evidenced by the worldwide population of stroke survivors. At any given time, there are 30.7 million survivors of stroke around the globe. Of these survivors, 12.6 million worldwide suffer moderate to severe disability as a result of stroke; such disabilities include loss of mobility, impaired speech, and cognitive problems. Each year, 9 million individuals worldwide experience a first-ever stroke (World Health Organization 2008). Acute mortality following a stroke is high: approximately 15% of patients die shortly after a stroke. Another 40% experience moderate to severe impairments that require special rehabilitative care, and 10% require care in a nursing home or other long-term care facility. About 25% recover with minor impairments, and only 10% of stroke patients recover completely (National Stroke Association 2002). Long-term mortality following a stroke is also significant: about a quarter of stroke patients are dead within a month, about a third by 6 months, and half by 1 year (Hankey et al. 2000). Immediate medical and surgical interventions are required to treat the patient experiencing an acute stroke, to maximize survival, and to minimize long-term consequences. Aggressive rehabilitation is typically applied to help patients recover from the chronic sequelae of stroke. The disease takes a physical and emotional toll on those it strikes, because survivors experience frustration and difficulty adapting to new limitations. There is hope that the prognosis for stroke sufferers will improve, as novel biomaterials are now emerging for brain imaging and nerve regeneration that will address both the acute and chronic effects of cerebrovascular disease.

3.1 Pathology of Stroke

Stroke, also known as cerebrovascular accident or "brain attack," is a clinical condition caused by disruption in blood flow to a portion of the brain. The traditional definition of stroke, delineated by the World Health Organization in the 1970s, is a "neurological deficit of cerebrovascular cause that persists beyond 24 hours or

S.K. Bhatia, *Biomaterials for Clinical Applications*,
DOI 10.1007/978-1-4419-6920-0_3, © Springer Science+Business Media, LLC 2010

Fig. 3.1 Diagram of ischemic stroke resulting from blood vessel blockage within the brain (National Institute of Neurological Disorders and Stroke)

is interrupted by death within 24 hours" (World Health Organization 1978). Like all other tissues of the body, the neural tissue of the brain requires oxygen and nutrients to perform its function. An interruption in blood supply to the brain leads to tissue destruction and cell death, almost instantaneously. Strokes are classified into two categories depending on the underlying pathological process: an ischemic stroke results from occlusion of a blood vessel (Fig. 3.1), while a hemorrhagic stroke results from rupture and subsequent leakage of a blood vessel (Fig. 3.2). In most parts of the world, about 70% of strokes are due to ischemia, 27% are due to

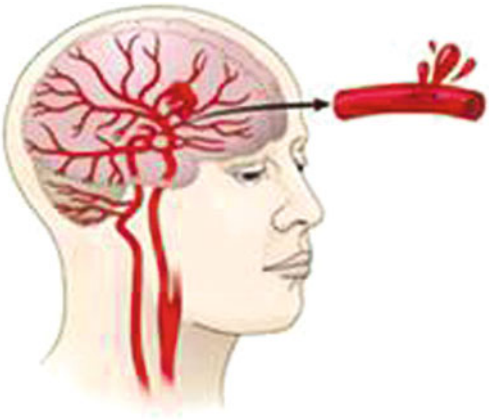

Fig. 3.2 Diagram of hemorrhagic stroke resulting from blood vessel rupture within the brain (National Institute of Neurological Disorders and Stroke)

hemorrhage, and 3% are of unknown cause (Gunatilake et al. 2001). In the United States, approximately 80% of strokes are ischemic in origin. However, in some countries such as China and Japan, hemorrhagic strokes are more common, accounting for 39.4% of all strokes in China (Zhang et al. 2003) and 38.7% of all strokes in Japan (Fukiyama et al. 2000).

Both ischemic stroke and hemorrhagic stroke are associated with multiple risk factors. Non-modifiable risk factors for stroke include increasing age; family history; male gender; and prior stroke, transient ischemic attack, or heart attack. The chance of having a stroke approximately doubles for each decade of life between the ages of 55 and 85 (National Institute of Neurological Disorders and Stroke 2009). However, strokes can occur in young children and neonates as well. Prior incidences of stroke or transient ischemic attack are also strongly predictive of stroke risk. A transient ischemic attack, sometimes called a "mini-stroke" or "warning stroke," produces temporary stroke-like symptoms lasting less than 24 h. An individual who experiences a transient ischemic attack has a 10–20% risk of having a full-blown stroke within the next 90 days. An individual who experiences a full-blown stroke has a 2–7% risk of having another stroke within the next 90 days (National Institute of Neurological Disorders and Stroke 2009).

Modifiable risk factors for stroke include hypertension; smoking; diabetes mellitus; peripheral artery disease and carotid artery disease; cardiac dysfunction such as heart failure and atrial fibrillation; sickle cell anemia; high cholesterol; poor diet; and physical inactivity and obesity. Notably, many of these risk factors for stroke are similar to those for coronary artery disease. Table 3.1 details the modifiable risk factors for stroke, the magnitude of their effect on stroke risk, and the underlying mechanisms relating each risk factor to stroke. Two additional risk factors are particularly important in developing countries. Rheumatic heart disease, leading to cardiac dysfunction and stroke, is a major cause of cerebrovascular accidents in developing countries. Dehydration in postpartum women can also lead to stroke, especially in remote areas where deliveries may not be conducted in a hospital setting (Chandra et al. 2006). Excess alcohol consumption and drug abuse may be potential risk factors for stroke as well.

Stroke, like coronary artery disease, is a condition created by vascular dysfunction. An ischemic stroke in the brain is analogous to ischemic heart disease in the myocardium, in that both maladies are caused by blood clots that obstruct critical blood vessels. The thrombotic clots that trigger ischemic stroke may originate in one of three locations: (1) the large arteries supplying blood to the brain (atherothrombotic stroke); (2) the heart (cardioembolic stroke); and (3) the small arteries within the brain (lacunar stroke). Ischemic stroke most commonly results from atherosclerosis of the large arteries that perfuse the brain. Just as cholesterol accumulation and vascular injury lead to atherosclerotic plaque formation in the coronary arteries, these factors can also trigger plaque formation in the arteries feeding the head and neck. For instance, the carotid arteries in the neck are an essential source of blood for the brain (Fig. 3.3). Plaque formation in the carotid artery (Fig. 3.4) causes a stroke in the corresponding brain tissue; such an ischemic stroke is called an atherothrombotic stroke. *(Biomaterials for targeted treatment of atherosclerotic*

Table 3.1 Modifiable risk factors for stroke

Risk factor	Magnitude of effect on stroke risk	Mechanism of effect on stroke risk
Hypertension	Hypertension causes a two- to fourfold increase in the risk of stroke before age 80	Hypertension promotes atherosclerosis and causes mechanical damage to the walls of blood vessels
Cigarette smoking	Smoking causes a twofold increase in the risk of ischemic stroke and a fourfold increase in the risk of hemorrhagic stroke	Smoking promotes atherosclerosis and aneurysm formation and stimulates blood clotting factors
Diabetes	In terms of stroke and cardiovascular disease risk, having diabetes is the equivalent of aging 15 years	In diabetes, glucose is not efficiently taken up by the body's tissues and accumulates in the blood. Excess glucose in the blood damages the vascular system. Hypertension is also common among diabetics and accounts for much of their increased stroke risk
Physical inactivity and obesity	A waist-to-hip ratio equal to or above the median for the population increases the risk of ischemic stroke threefold	Obesity is associated with hypertension, diabetes, and cardiovascular disease
Atrial fibrillation	Atrial fibrillation is responsible for one in four strokes after age 80 and is associated with high mortality and disability	Atrial fibrillation refers to irregular contraction of the atrium – the cardiac chamber where blood enters the heart. Atrial fibrillation can lead to blood stagnation and clotting
Cholesterol imbalance	High-density lipoprotein (HDL) cholesterol is protective against ischemic stroke, while low-density lipoprotein (LDL) cholesterol is considered harmful when present in excess	Excess LDL can cause cholesterol to accumulate in blood vessels, leading to atherosclerosis. HDL sends cholesterol to the liver to be eliminated

National Institute of Neurological Disorders and Stroke (2009)

plaque in coronary arteries could thus find utility for treating carotid artery plaque and preventing stroke. These biomaterials include bioactive stents and degradable stents and are discussed in Sections 2.3 and 2.4.) An ischemic stroke may also be initiated by blood clots that have migrated from the heart to the brain. Cardiac rhythm disturbances and pumping abnormalities allow blood to pool within the heart and form clots. Atrial fibrillation, a heart rhythm disorder in which the heart's upper chambers quiver instead of beating effectively, generates clots inside the cardiac chambers. A clot that breaks away into the bloodstream, known as an embolus, can subsequently lodge in the blood supply to the brain and spark an ischemic stroke. Such an ischemic stroke is called a cardioembolic stroke; approximately 25% of all ischemic strokes are due to cardioembolic causes (Chandra et al. 2006). Patients

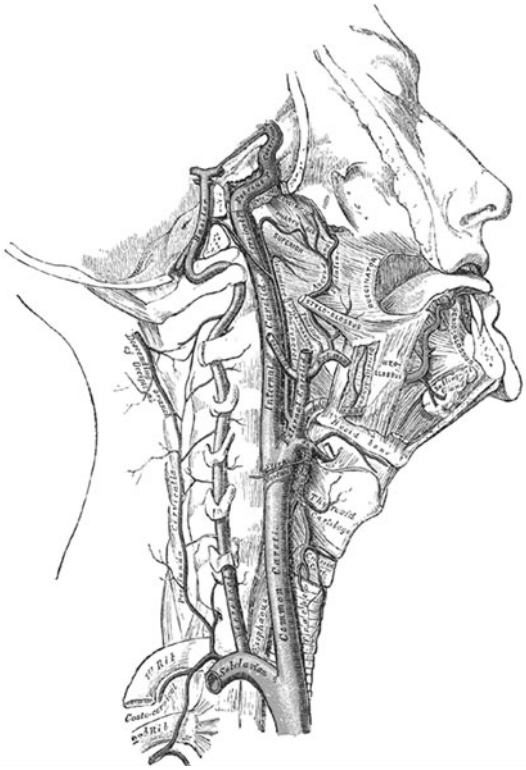

Fig. 3.3 Anatomic relationship of the carotid arteries to the brain

in heart failure are also prone to form cardiac emboli, due to pumping dysfunction in the heart. *(Biomaterials for cardiac regeneration could therefore be useful for healing weak cardiac muscle and thereby preventing stroke. These materials for cardiac tissue engineering are discussed in* Section 2.5) Finally, an ischemic stroke may begin in the small, deep penetrating arteries of the brain as a consequence of microatheroma. The stroke may produce tiny 3–15 mm fluid-filled cavities within the brain known as lacunes (Wardlaw 2008); such an ischemic stroke is called a lacunar stroke.

Irreversible damage to brain tissue commences immediately following an ischemic stroke. A few minutes of oxygen deprivation is sufficient to kill millions of neurons (National Institute of Neurological Disorders and Stroke 2009). The "ischemic core" is the area of brain tissue that experiences severe impairment in blood flow, and this core region is permanently injured after ischemic stroke. Cells in the core rapidly die as a result of energetic failure, lipid breakdown, protein breakdown, structural alterations, and disruption of ion homeostasis (Brouns and De Deyn 2009). Ischemic injury produces cellular necrosis, a fulminant form of cell death associated with destruction of cellular membranes; necrotic cells release toxins into the tissue environment, affecting neighboring neurons. As a result, the

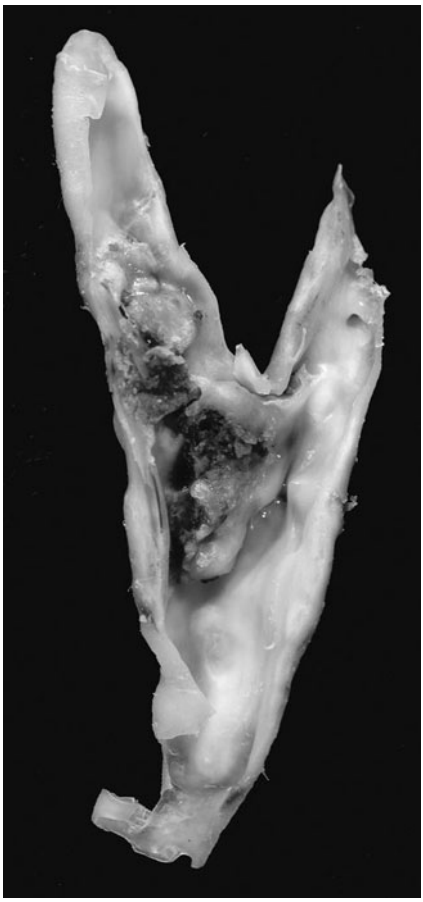

Fig. 3.4 Atherosclerotic plaque formation in the internal and external carotid arteries

brain tissue surrounding the ischemic core is susceptible to further damage. Cerebral injury to this surrounding region can continue for hours to days following the initial stroke, due to inflammation, swelling, and coagulation. This vulnerable adjoining area is known as the "ischemic penumbra," and it is functionally impaired yet structurally intact. The penumbra may be conceptualized as a "battlefield" between the lethally damaged core and the normal brain (Brouns and De Deyn 2009). Within the penumbra, a cascade of neurochemical events can induce lasting damage if blood flow is not quickly restored; Table 3.2 lists the biological processes involved in the ischemic cascade. The longer that perfusion to the brain is delayed, the more cells in the penumbra will die (Fig. 3.5). The region of brain tissue that is finally damaged is the infarct.

Indeed, many patients exhibit an expanding area of brain injury in the several days following an ischemic stroke. A study of 450 stroke patients who underwent a CT scan within 6 h of symptom onset and at days 1 and 7 revealed a significant

Table 3.2 Pathophysiological mechanisms of injury in acute ischemic stroke

Pathological process	Underlying mechanism
Cerebral cell damage	Ischemia induces cellular death (apoptosis and necrosis) of neuronal and glial cells
Bioenergetic failure	Cells are deprived of oxygen and glucose and fail to carry out normal metabolic processes
Excitotoxicity	Dying cells release excitatory neurotransmitters which overstimulate adjacent cells and push them to overdrive
Oxidative stress	Free radicals, including reactive oxygen and nitrogen molecules, overwhelm cellular antioxidant defenses
Blood–brain barrier dysfunction	Deterioration of blood–brain barrier allows blood leakage into brain and leads to intracranial swelling
Post-ischemic inflammation	Inflammatory white blood cells, signaling molecules, and adhesion molecules cause ongoing damage
Hemostatic activation	Vascular endothelial cells become activated and initiate coagulation, platelet aggregation, and fibrinolysis
Microvascular dysregulation	Both vasoconstriction and vasodilation occur in response to ischemia, further disrupting perfusion

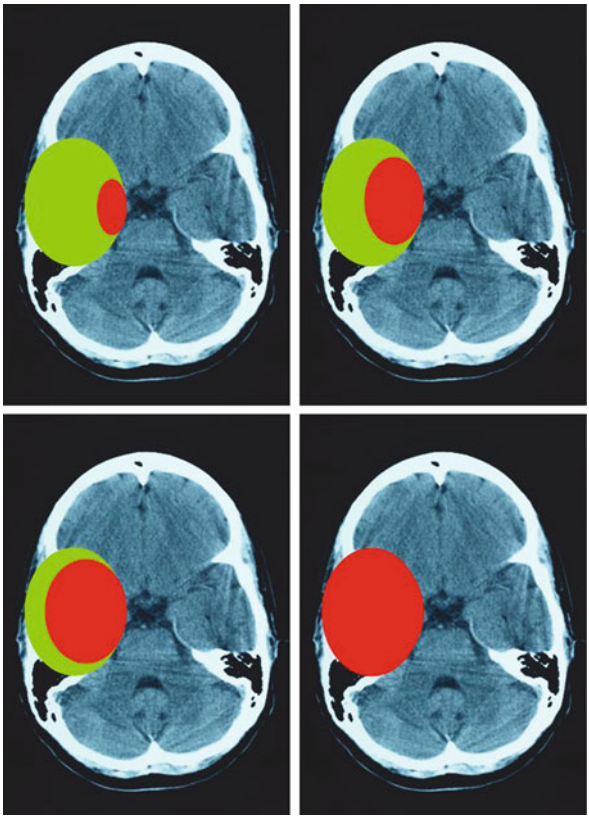

Fig. 3.5 Diagram of ischemic core and ischemic penumbra. Immediately after an ischemic stroke, a core of irreversibly damaged brain tissue (shown in *red*) is surrounded by an area of viable but at-risk tissue called the penumbra (shown in *green*). Unless blood flow is restored quickly, the brain tissue within the penumbra will be lost

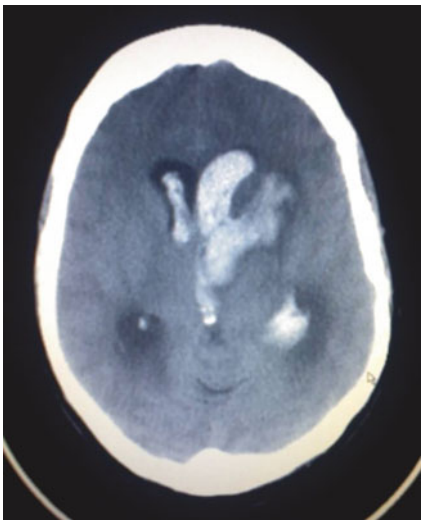

Fig. 3.6 Computed tomography (CT) scan of intracerbral hemorrhage

increase in infarct volume between day 1 and day 7 in almost a third of cases (Brown et al. 2006). The ischemic penumbra is salvageable only if treatment is instituted swiftly, and it is the target for rapid therapeutic interventions following an acute ischemic stroke. Early and accurate diagnosis of ischemic stroke is essential, as neurological recovery depends on rescue of brain tissue.

As noted previously, ischemic strokes account for approximately 70% of all strokes worldwide, while hemorrhagic strokes are responsible for roughly 30% of all strokes worldwide. In contrast to ischemic stroke, a hemorrhagic stroke occurs when a cerebral blood vessel ruptures and leaks into the intracranial space (Fig. 3.6). The most frequent cause of cerebral hemorrhage is hypertensive disease of the small cerebral vessels. High blood pressure damages the vascular walls and prompts the formation of small aneurysms that subsequently burst. About two-thirds of patients with primary cerebral hemorrhage have either pre-existing or newly diagnosed hypertension (Thrift et al. 1995). An additional risk factor for intracranial bleeding is poor clotting ability due to blood disorders or blood-thinning medications. Structural abnormalities in the brain, such as arteriovenous malformations and saccular aneurysms, also play a significant role in increasing the risk of hemorrhagic stroke. Saccular aneurysms are particularly dangerous in the subarachnoid space, a fluid-filled space between layers of connective tissue that surround the brain. Subarachnoid hemorrhage accounts for 5% of all strokes, and most subarachnoid hemorrhages are caused by rupture of saccular aneurysms (Donnan et al. 2008).

A hemorrhagic stroke compromises the blood–brain barrier, releasing cells and molecules from the blood into the delicate environment surrounding neurons. Destruction of the blood–brain barrier provokes ongoing injury and intracranial swelling (Fig. 3.7). Moreover, the accumulation of blood within the closed

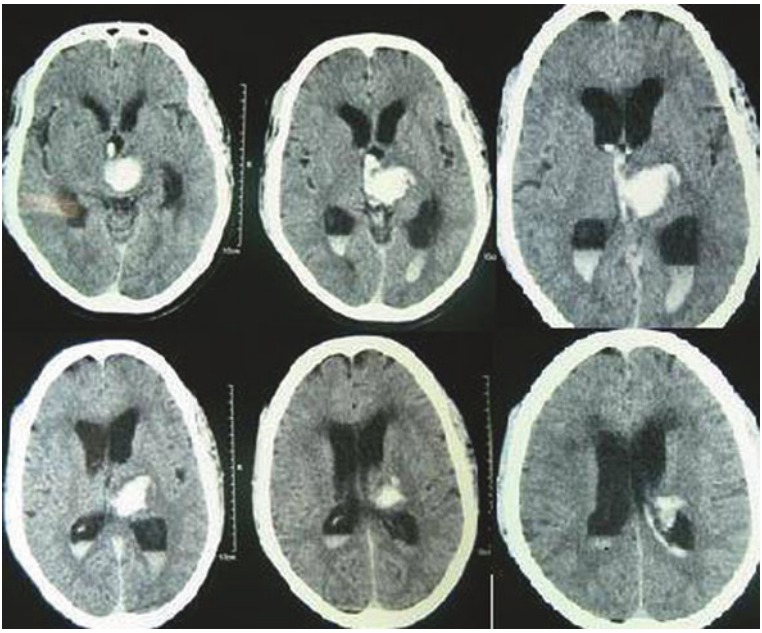

Fig. 3.7 CT scan of intracerebral hemorrhage, showing abnormal accumulation of fluid within the brain cavities (Yadav et al. 2007)

intracranial space (known as a hematoma) raises intracranial pressure and compresses the brain inside the skull. The hematoma expands with continued pooling of blood, further crowding the brain and impairing normal blood flow (Fig. 3.8). The hemorrhagic stroke will continue to devastate more brain tissue until bleeding is controlled. A third of patients with primary intracerebral hemorrhage have a rapid expansion of the hematoma within the first few hours after presentation, which is an independent predictor of poor outcome and mortality (Davis et al. 2006). Early and accurate diagnosis of hemorrhagic stroke is critical, since an optimal neurological outcome requires timely intervention.

Whether a stroke is ischemic or hemorrhagic, it is a medical emergency, and its effects manifest within seconds. The five most common symptoms of stroke are as follows (National Institute of Neurological Disorders and Stroke 2009):

- Sudden weakness or numbness of the face or limbs, especially on one side of the body
- Sudden confusion or difficulty speaking or understanding speech
- Sudden vision disturbance in one or both eyes
- Sudden dizziness, difficulty walking, or loss of balance or coordination
- Sudden severe headache (particularly characteristic of hemorrhagic stroke – a subarachnoid hemorrhage is associated with a “thunderclap” headache)

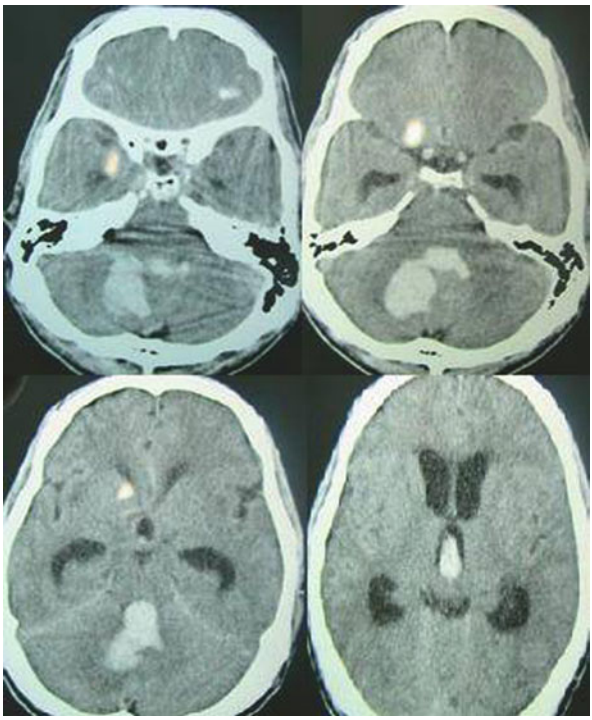

Fig. 3.8 CT scan of intracerebral hemorrhage, showing accumulation of both blood and fluid within the brain cavities (Yadav et al. 2007)

The exact neurological manifestations of a stroke are determined by the location of the vascular insult within the brain. In many cases, the stroke predominantly affects one cerebral hemisphere. Because each cerebral hemisphere controls the contralateral side of the body, a stroke in the left hemisphere causes motor and sensory deficits on the right side, and vice versa.

The long-term consequences of stroke depend on the severity of the initial insult, the type of stroke, the age of the affected patient, and the rapidity of intervention. Chronic disabilities that can result from stroke include

- Hemiplegia – paralysis on one side of the body
- Hemiparesis – weakness on one side of the body
- Hemineglect – lack of awareness of one side of the body or one side of the visual field
- Dysphagia – difficulty swallowing
- Dysarthria – difficulty talking, caused by facial weakness
- Aphasia – difficulty speaking or understanding speech, caused by damage to the brain's language centers
- Apraxia – altered voluntary movements
- Amnesia – deficits in short-term or long-term memory

Neurological deterioration is the major cause of early mortality following stroke with contributions from other causes such as infection. Patients experiencing intracerebral and subarachnoid hemorrhage have the worst prognosis, with a 1-month mortality approaching 50% (Hankey et al. 2000).

Current treatment for acute ischemic stroke includes "clot-busting" thrombolytic drugs such as tissue plasminogen activator (tPA) which dissolve occlusive blood clots. However, these therapeutics are efficacious only when administered soon after the stroke occurs. The therapeutic time window for tPA is particularly short at 3 h; ischemic stroke patients given tPA within the 3-h time window are more likely to have minimal or no disability 3 months after treatment (National Institute of Neurological Disorders and Stroke 2009). As a result, only 3% of all stroke patients receive thrombolysis (Fisher et al. 2006). Another mainstay of therapy for ischemic stroke is the anti-thrombotic drug aspirin; oral administration of aspirin within 48 h of onset of ischemic stroke reduces 14-day morbidity and mortality (International Stroke Trial Collaborative Group 1997). Contemporary management of hemorrhagic stroke may involve anti-hypertensive drugs to lower blood pressure and clotting factors to promote blood coagulation; optimal therapeutic regimens for hemorrhagic stroke are still under investigation.

Stroke must be diagnosed quickly and correctly, since time lost equals brain tissue lost. Accurate diagnosis of ischemic stroke versus hemorrhagic stroke is absolutely essential, since administration of clot-busting and anti-thrombotic agents to a patient with an intracerebral bleed will considerably worsen the hemorrhage; conversely, clotting agents will not benefit a patient with an ischemic stroke. Patients suffering from stroke are assessed using imaging technologies such as computed tomography (CT) and magnetic resonance imaging (MRI). Neither of these imaging modalities is perfectly sensitive. A CT scan without contrast is only 16% sensitive for diagnosing ischemic stroke in the emergency setting and is only 89% sensitive for diagnosing hemorrhagic stroke in an emergency. An MRI is only 83% sensitive for diagnosing ischemic stroke in the emergency setting and is only 81% sensitive for diagnosing hemorrhagic stroke in an emergency (Chalela et al. 2007). A significant proportion of stroke patients could thus be misdiagnosed with existing imaging modalities. Conventional imaging techniques also have shortcomings with regard to visualization of stroke pathology. For instance, even gadolinium-enhanced MRI and multimodal MRI comprising diffusion-weighted and perfusion-weighted imaging are unable to discriminate inflamed from non-inflamed brain infarcts (Schroeter et al. 2001). This is a significant limitation, since local brain inflammation is a pathologic hallmark of ischemic stroke lesions and is related temporally and spatially to the occurrence of delayed cell death (Braun et al. 1996). New biomaterial technologies for neurological imaging could enable more precise stroke diagnosis and finer characterization of stroke pathology, allowing prompt treatment.

Even with correct diagnosis and swift intervention, many patients with stroke still suffer long-term neurological deficits. Stroke rehabilitation includes physical therapy to restore movement and coordination; occupational therapy to improve activities of daily living; neurocognitive therapy; and speech and language therapy.

Patients may also receive psychiatric treatment, since depression, anxiety, and social isolation are common among stroke survivors (National Institute of Neurological Disorders and Stroke 2009). The inherent ability of the brain to repair itself is limited, and there is an urgent need for therapies that stimulate neural regeneration. Implantable biomaterials could play a role in guiding nerve growth and boosting post-stroke recovery.

Biomaterials can reduce morbidity and mortality from stroke, by improving both stroke diagnosis and stroke rehabilitation. In the early stages of a stroke, novel biomaterials for neurological imaging can enhance stroke diagnosis in the emergency setting. Moreover, new materials for neuroimaging might extend the time window for therapy in ischemic stroke by identifying persistent ischemic penumbra (Donnan et al. 2008). Once a stroke has occurred, biomaterials for nerve regeneration can promote brain tissue growth and restore function to those who struggle with disabilities. The following sections will discuss emerging biomaterials for brain imaging and neural regeneration.

3.2 Biomaterials for Brain Imaging

The newest biomaterials for brain imaging are designed for targeted interactions with particular cell populations and molecular receptors; such biomaterials enable specific biological processes to be imaged non-invasively with MRI. Advances in nanoparticle technology and molecular biology have made these materials possible. The major goals of biomaterials for MRI imaging are to image the presence of specific molecules with targeted contrast; to be able to monitor cell migration; and to develop strategies that permit MRI to monitor other specific biological pathways (Koretsky 2004). These innovative biomaterials shift imaging from the tissue level to the more detailed cellular and molecular levels and improve the ability of MRI to detect stroke pathology. Since inflammation plays a pivotal role in the evolution of stroke, many biomaterials for neuroimaging are constructed to selectively interact with inflammatory cells, such as monocytes and macrophages of the brain and bloodstream.

Much biomaterials research in the field of molecular imaging has been directed toward the development of superparamagnetic iron oxide nanoparticles. Each nanoparticle consists of an iron oxide nanocrystal interior, which is coated with a biocompatible polymer. The iron oxide nanocrystal is composed of magnetite (Fe_3O_4) and maghemite (Fe_2O_3), both of which are insoluble in water. Because of their nanoscale size, superparamagnetic agents have no magnetic properties outside an external magnetic field (Bonnemain 1998); this characteristic distinguishes superparamagnetic agents from ferromagnetic substances. Superparamagnetic nanoparticles exhibit a large magnetic moment in the presence of a static external magnetic field (Roch et al. 1999). Compared with contemporary gadolinium-containing compounds, iron oxide nanoparticles create very high local magnetic field gradients, which result in marked focal changes in signal.

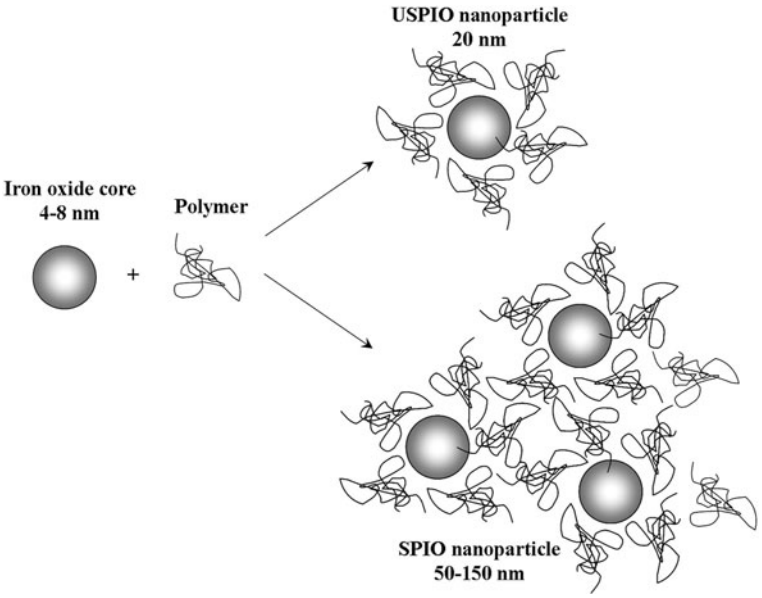

Fig. 3.9 Composition of superparamagnetic iron oxide (SPIO) and ultrasmall superparamagnetic iron oxide (USPIO) nanoparticles for MRI imaging

Thus, the sensitivity for iron oxide-containing contrast media is much higher than for gadolinium compounds at comparable tissue concentrations, permitting visualization of single iron-labeled cells at clinical magnetic field strength (Zhang et al. 2005). These nanoparticles not only have special physical properties by virtue of their size, but also possess useful biological properties: superparamagnetic nanoparticles are selectively taken up by monocyte and macrophage cells.

Superparamagnetic nanoparticles are classified into two different groups based on their hydrodynamic size (Fig. 3.9): superparamagnetic iron oxide (SPIO) particles having a mean particle diameter greater than 50 nm, and ultrasmall superparamagnetic iron oxide (USPIO) particles having a smaller hydrodynamic diameter (Corot et al. 2006). An individual SPIO particle contains several iron oxide cores that are collectively covered by a polymer coating; hence SPIO particles are sometimes referred to as polycrystalline magnetic nanoparticles. Each iron oxide core is 4–8 nm in diameter, and a typical SPIO particle is 50–150 nm in size. An individual USPIO particle contains a single iron oxide core that is covered by a polymer coating; therefore USPIO particles are also called monocrystalline iron oxide nanoparticles. A typical USPIO particle is 20 nm in size.

Both SPIO and USPIO nanoparticles require a polymer coating to prevent destabilization and aggregation of particles and to make the nanoparticles soluble in aqueous or biological media. A very high density of coating is often necessary to effectively stabilize iron oxide nanoparticles, and polymeric or monomeric coatings have been used (Corot et al. 2006). The most common polymeric coatings for

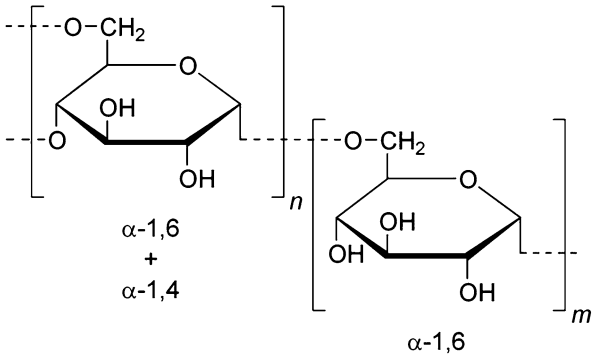

Fig. 3.10 Chemical structure of the natural polysaccharide dextran

iron oxide nanoparticles are dextran (Fig. 3.10) and dextran derivatives. Dextran is a natural polysaccharide and a known biocompatible neutrally charged polymer, with a long history of clinical use as a plasma expander (Larsen 1989). Other polysaccharide coatings for iron oxide nanoparticle imaging agents have included chitosan and starch (Lin et al. 2008). Hydrophilic polymeric coatings that incorporate poly(ethylene oxide) copolymers have also been investigated for imaging applications (Thunemann et al. 2006); these coatings resist protein adsorption and increase the blood circulation time of nanoparticles. In addition, polymer coatings of polyvinyl alcohol, thiol-functionalized polyvinyl alcohol, and carboxy-functionalized polyvinyl alcohol have been utilized to impart a negative charge to USPIO particles; particle coatings of amino-polyvinyl alcohol have been used to impart a positive charge to USPIO particles (Cengelli et al. 2006). Finally, small organic molecules, either cationic or anionic or neutral, may be useful as coatings.

The efficacy of SPIO and USPIO imaging agents is determined by multiple factors, including the size of the iron oxide nanocrystals, the particle charge, the nature of the coating, and the hydrodynamic size of the coated particle. These physicochemical properties affect not only the efficacy of the superparamagnetic particles in MRI, but also their biological behavior, including stability, biocompatibility, tissue distribution, cellular uptake, metabolism, and clearance from the vascular system (Corot et al. 2006). Particles with larger diameters tend to be eliminated more quickly and have a shorter half-life in circulation. Most SPIO particles, having diameters much greater than 50 nm, exhibit a plasma half-life of approximately 2 h. On the other hand, USPIO particles, having diameters much less than 50 nm, exhibit a longer plasma half-life of 24–40 h.

Table 3.3 summarizes the main physical and biological characteristics of SPIO and USPIO nanoparticles that are currently marketed. Commercially available SPIO particles for intravenous administration include Endorem® dextran-coated particles (Guerbet, Paris, France); Feridex® dextran-coated particles (Advanced Magnetics, Cambridge, MA, USA); and Resovist® carboxydextran-coated particles (Bayer Schering Pharma, Berlin, Germany). Commercially available USPIO

Table 3.3 Characteristics of iron oxide nanoparticles that are currently marketed

Product	Coating agent	Hydrodynamic size (nm)	Clinical dose (μmol Fe/kg)	Half-time in blood (h)
Superparamagnetic iron oxide (SPIO) particles				
Endorem®	Dextran T10	120–180	30	2
Feridex®	Dextran T10	120–180	30	2
Resovist®	Carboxydextran	60	8–12	2.4–3.6
Ultrasmall superparamagnetic iron oxide (USPIO) particles				
Sinerem®	Dextran T10, T1	15–30	45	24–36
Combidex®	Dextran T10, T1	15–30	45	24–36
Supravist®	Carboxydextran	21	6	40

Corot et al. (2006)

particles for intravenous administration include Sinerem® dextran-coated particles (Guerbet, Paris, France); Combidex® dextran-coated particles (Advanced Magnetics, Cambridge, MA, USA); and Supravist® carboxydextran-coated particles (Bayer Schering Pharma, Berlin, Germany). In general, these agents are clinically approved for liver imaging and are under clinical investigation for neurological imaging.

When SPIO or USPIO nanoparticles are injected intravenously, the particles are engulfed by both circulating macrophages in the bloodstream and tissue macrophages in the brain (Fig. 3.11). The resident microglia (brain macrophages) and blood-derived monocytes (infiltrating macrophages) are the most abundant cells involved in the post-ischemic inflammatory response; the inflammation that follows ischemic stroke is so strong that it resembles classical autoimmune disorders of the nervous system (Stoll et al. 1998). Macrophages therefore represent an attractive target for imaging ischemic stroke. Iron-labeled macrophages within inflammatory degenerative tissue appear as a dark signal on MRI (Fig. 3.12).

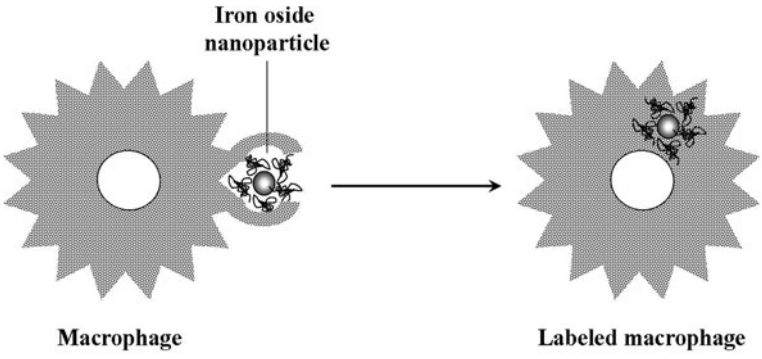

Fig. 3.11 Schematic diagram of macrophage engulfment of an iron oxide nanoparticle

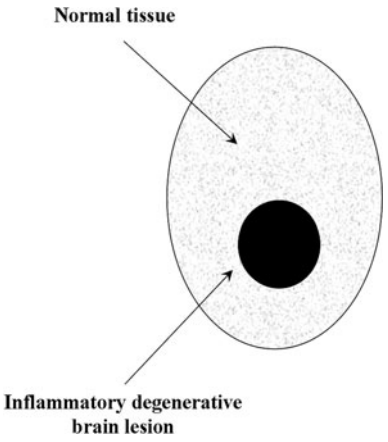

Fig. 3.12 Appearance of inflammatory degenerative lesion as a dark signal on nanoparticle-enhanced MRI

The use of USPIO particles for macrophage labeling and ischemic stroke imaging was first established in 2001. In this initial demonstration, ischemic stroke was induced in rats via occlusion of the middle cerebral artery, and Sinerem® USPIO particles were administered intravenously 5 h after the stroke (Rausch et al. 2001). The animals were followed by repeat MRI; the USPIO particles were detected around the ischemic lesion on day 1 and inside the lesion until day 4. In a later study, dextran-coated USPIO particles were injected into mice 5 h after permanent occlusion of the middle cerebral artery and revealed an inflammatory response within the brain that was distant from the site of injury (Wiart et al. 2007). The inflammatory damage was located in the opposite cerebral hemisphere from the arterial occlusion; the spread of inflammation from the initial site of injury to the contralateral hemisphere was detected within the first 36 h after stroke (Wiart et al. 2007). This was the first evidence of remote inflammation following ischemic stroke in a living mouse. Nanoscale biomaterials for brain imaging are thus uncovering new pathological processes in stroke. USPIO nanoparticles have additionally been evaluated as blood pooling agents, on the basis of their long blood half-life. The nanoparticles have been successfully used to track blood–brain barrier disruption (Zimmer et al. 1995), as well as cerebral blood flow and cerebral blood volume (Simonsen et al. 1999). Clearly, nanoparticle-enhanced MRI has the power to monitor both cellular migration and vascular perfusion into the brain.

The first clinical study of USPIO particles for MRI imaging was performed in 2004. In this investigation, dextran-coated USPIO particles were administered to 10 ischemic stroke patients at the end of the first week after symptom onset (Saleh et al. 2004). Two follow-up MRI scans were performed at 24–36 h and 48–72 h after USPIO injection and revealed brain infiltration by USPIO-laden macrophages. In a subsequent clinical investigation, dextran-coated USPIO particles were administered to 10 ischemic stroke patients at 6 days post-ischemia, followed by MRI at 72 h post-injection (Nighoghossian et al. 2007). This study confirmed USPIO-related MRI enhancement and exposed a late inflammatory response

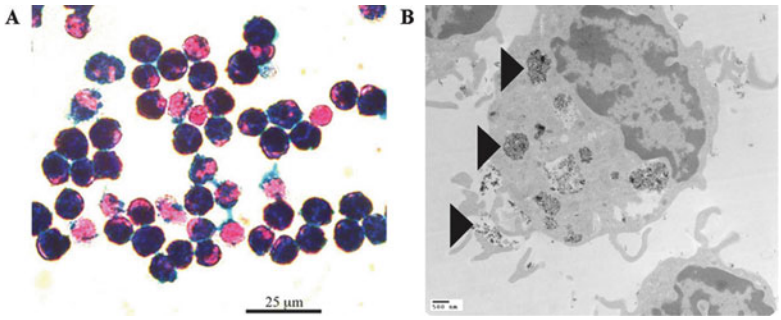

Fig. 3.13 Labeling of human monocytes with immunoglobulin-linked iron oxide nanoparticles. (**a**) Light microscopy image of iron-labeled monocytes, with iron stained by Prussian blue and monocytes counterstained by nuclear fast red; (**b**) Transmission electron microscopy of iron-labeled monocyte, showing internalization of iron oxide nanoparticles (Beduneau et al. 2009)

to ischemic stroke. Larger clinical studies will be necessary to validate the clinical benefit of nanoparticle-enhanced MRI for evaluating brain inflammation after stroke. The metabolism and elimination of iron oxide nanoparticles must also be completely elucidated, and non-toxicity of the particles must be established, before these biomaterials can achieve widespread usage.

A major advance in iron oxide nanoparticle technology has been the conjugation of biomolecules, such as proteins and antibodies, to the nanoparticle surface. Nanoparticle bio-functionalization is typically accomplished by coupling the biomolecule of interest to the polymer coating. Functionalized SPIO and USPIO nanoparticles further refine the sensitivity of MRI for stroke pathology. Antibody-coated SPIO particles are more efficiently engulfed by monocytes and macrophages (Fig. 3.13), increasing the efficacy of the particles for imaging inflammation (Beduneau et al. 2009). More importantly, functionalization allows the particle to selectively bind receptors on targeted cell membranes (Fig. 3.14). For example, antibody-conjugated iron oxide particles have been successfully used to visualize

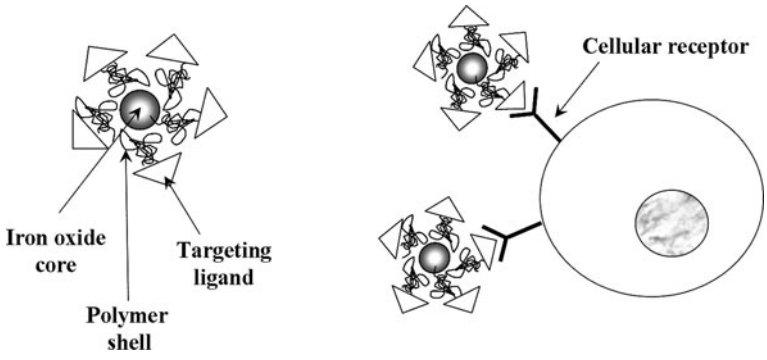

Fig. 3.14 Binding of bio-functionalized nanoparticles to specific receptors on a targeted cell

expression of vascular cell adhesion molecule 1 (VCAM-1) during acute brain inflammation in mouse models (McAteer et al. 2007). The presence of VCAM-1 on endothelial cells is an important marker of inflammatory foci within the brain, and the functionalized nanoparticles were able to delineate the architecture of cerebral blood vessels expressing activated VCAM-1. Iron oxide nanoparticles have also been linked to anti-E-selectin antibody, to facilitate MRI detection of the inflammatory adhesion molecule E-selectin on human endothelial cells (Kang et al. 2002). In addition, a library of 146 biomolecule-linked nanoparticles, each bearing different synthetic small ligands, has been developed to recognize apoptotic cell death (Weissleder et al. 2005).

Bio-functionalized nanoparticles may be useful not only for MRI imaging of inflamed vasculature and cellular death during stroke, but also for targeted delivery of therapeutics such as pharmaceuticals or genes. Notably, peptide-linked SPIO nanoparticles have even been utilized to guide the transplantation of stem cells into the injured brains of mice following stroke (Rice et al. 2007). In this investigation, dextran-coated SPIO particles were conjugated with poly-L-lysine, to enable the particles to label adipose-derived stem cells. Adult mice were subjected to middle cerebral artery occlusion, and the SPIO-labeled stem cells were implanted into brain tissue 2 weeks later. The labeled cells could be successfully visualized by MRI, ensuring the implantation of stem cells directly adjacent to brain infarct (Rice et al. 2007). Iron oxide nanoparticles linked with poly-L-lysine have also shown success in labeling and tracking bone marrow-derived stem cells within the brains of mice (Anderson et al. 2005). Nanoparticles linked with biomolecules may thus find applications for imaging of neural tissue engineering.

The use of nanoscale biomaterials, including SPIO and USPIO nanoparticles, will enable MRI to assess stroke damage; track blood leakage and blood flow; define complex pathology; and predict the efficacy of neuroprotective treatments. MRI techniques for detecting and monitoring macrophages may also stimulate the development of anti-inflammatory therapies and other novel treatment strategies for stroke patients. Nanoparticle-enhanced MRI may allow clinicians to "stage" a stroke in the same way that cancerous tumors are staged; stroke staging cannot yet be done with current imaging technologies (Koretsky 2004). SPIO and USPIO nanoparticles can reveal residual brain damage and neural reorganization after the acute insult and may help to elucidate the factors that influence clinical recovery from stroke. The nanoparticles may therefore find utility during stroke rehabilitation as well. Nanoparticles linked to biological peptides and proteins will push MRI resolution to the molecular level and will facilitate the visualization and delivery of drugs, genes, and regenerative cells to injured brain tissue. The following section will further explore how nanoscale biomaterials are being used to stimulate nerve regeneration after stroke.

3.3 Biomaterials for Nerve Regeneration

Both ischemic stroke and hemorrhagic stroke wreak destruction on delicate brain tissue, leaving behind the scars of neuronal deterioration and permanent neurological deficits. The central nervous system has little ability to regenerate and repair

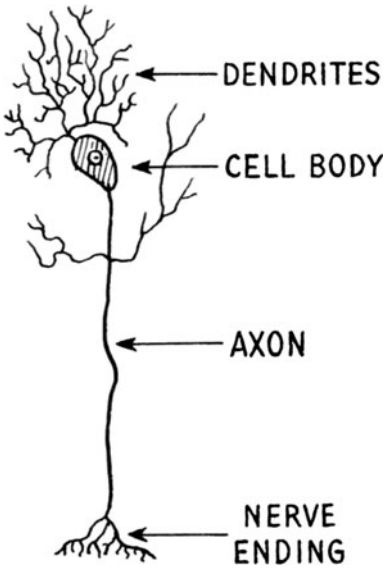

Fig. 3.15 Structure of a neuron, showing the long slender axon which conducts electrical impulses from one nerve cell to the next

damaged neurons; unlike the peripheral nervous system, the central nervous system lacks proliferative Schwann cells which are essential for recovering damaged neurons. Neural tissue regeneration following brain injury relies on the re-extension and re-innervation of axons, the long projecting arms of neurons that conduct electrical impulses from one nerve cell to the next (Fig. 3.15). While the peripheral nervous system can spontaneously sprout and re-grow axons through the action of proliferating Schwann cells, the brain cannot. As a consequence, there is a critical need for biomaterials that promote neural growth within the brain following stroke.

An ideal biomaterial for stimulating nerve regeneration should mimic the mechanical properties, physical dimensions, and electrical conductivity of native axons. The biomaterial must additionally have sufficient biocompatibility for successful brain implantation and must limit glial scar formation so that tissue functionality can be maximized. Nanoscale biomaterials are excellent candidates for neural regeneration, as nanomaterials can accurately simulate the dimensions of biological structures. Nanomaterials are unique among biomaterials in that only nanoscale scaffolds can mimic the surface properties and topography of natural tissues. Since physiological tissues and organs are nanometer in dimension and cells directly interact with and create nanostructured extracellular matrices, nanomaterials are appropriate biomimetics for inducing neuronal growth and guiding brain regeneration (Zhang and Webster 2009). A promising strategy for healing brain tissue after a stroke is to support and promote neurite and axonal growth by implanting nanometer-scale scaffolds.

Nanotubes and nanofibers are particularly applicable for neural regeneration, because these materials can recapitulate tubular structures found in nature, including axons and dendrites. Both nanotubes and nanofibers are low-dimensional nanostructures, having a very large axial ratio. The length-to-volume ratio of these

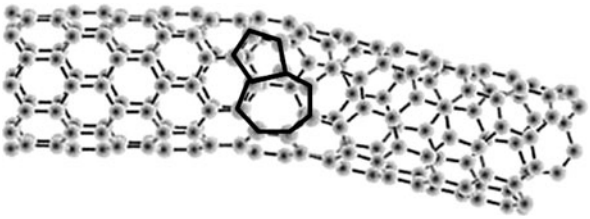

Fig. 3.16 Structure of a carbon nanotube composed of carbon atoms arranged in hexagonal rings, with five-membered and seven-membered rings providing curvature to the nanotube

nanomaterials can be manipulated during synthesis, and the diameter of semiconducting nanotubes and nanofibers can be reduced to enhance conductivity (Gilmore et al. 2008). Such nanomaterials additionally have a large surface area-to-volume ratio, which allows high exposure of the implanted material to the biological environment. This is an advantageous property for molecular recognition, surface functionalization, and drug delivery. Finally, the curvature of nanotubes and nanofibers can be adjusted to optimize their mechanical properties.

Nanosized carbon tubes, also known as carbon nanotubes, are the primary nanomaterials that have been investigated for nerve regeneration. Carbon nanotubes are composed of carbon atoms arranged in hexagonal ring structures similar to graphite (Baxendale 2003), with some five-membered and seven-membered rings providing curvature to the nanotube (Fig. 3.16). Multi-walled carbon nanotubes consist of multiple concentric layers of carbon nanotubes, a coaxial assembly of cylinders. Neuronal growth on carbon nanotubes was first demonstrated in 2000, when embryonic rat brain neurons were found to proliferate and branch when seeded on multi-walled carbon nanotubes (Mattson et al. 2000). Single-walled carbon nanotubes functionalized with polyethyleneimine have also been shown to support neurite outgrowth and branching (Hu et al. 2005).

Carbon nanotubes are compatible with biological tissues for scaffolding applications, and the surface charge of the nanotubes can be adjusted to control neurite outgrowth patterns. Cellular properties such as neurite length, branching, and the number of growth cones can be tuned via the charge of the nanotube scaffold. These morphological features are necessary for the establishment of connections between neurons and the formation of synapses after injury; these cellular properties directly reflect the potential capability in synaptic transmission. Positively charged multi-walled carbon nanotubes significantly increase the number of growth cones and neurite branches compared to neutral or negatively charged multi-walled carbon nanotubes (Hu et al. 2004). The surface functionalization of carbon nanotubes may thus be tailored for tissue repair in the clinical setting.

Multi-walled carbon nanotubes boost electrical signal transfer of neuronal networks, while allowing dendrite elongation and neuronal adhesion (Lovat et al. 2005). Further, carbon nanotubes can be functionalized with biological growth factors, including nerve growth factor and brain-derived growth factor, which stimulate the proliferation of neurons on the nanotube scaffold (Matsumoto et al. 2007).

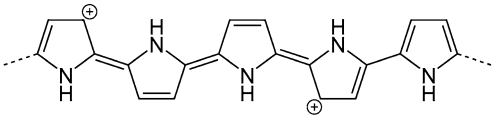

Fig. 3.17 Chemical structure of polypyrrole, an electrically conductive polymer

Nanotubes and nanofibers additionally may be combined with stem cells for neural tissue engineering and may encourage stem cell differentiation into neural structures. For instance, mouse embryonic neural stem cells have been found to differentiate into neurons on composites of single-walled carbon nanotubes and polyelectrolytes (Jan and Kotov 2007). Combination biomaterials consisting of nanofibers and stem cells have recently demonstrated efficacy for neural regeneration in animal models of stroke. Carbon nanofibers impregnated with stem cells have been injected into rat brains following stroke damage and have generated extensive neural stem cell differentiation with little glial scar tissue formation (Zhang and Webster 2009).

Although the majority of neural regeneration work has focused on carbon nanotubes and nanofibers, several new nanomaterials have been developed from synthetic polymers and natural proteins. These materials have superior properties of conductivity, biocompatibility, and neuronal growth capability. Nanotubes made of electrically conducting polymers, such as polypyrrole (Fig. 3.17), polyaniline, poly(3-hexylthiophene) , and poly(3,4-ethylenedioxythiophene) have been synthesized (Xiao et al. 2007); these polymers have significant potential for repairing and growing neural circuitry. Well-known biocompatible polymers including polylactic acid are also serving as substrates for neuronal growth. Biomaterial scaffolds composed of polylactic acid nanofibers have been shown to support neurite extension, as well as differentiation of neonatal mouse cerebellar progenitor cells into mature neurons (Yang et al. 2004). Finally, nanomaterials assembled from biologically active molecules such as peptides and proteins are being designed to mimic the extracellular matrix that surrounds neurons. Nanofibers composed of the self-assembling peptide IKVAV, derived from the extracellular matrix protein laminin, have been shown to promote and support neuronal regeneration (Silva et al. 2004). In a particularly exciting study, nanofiber scaffolds made of the self-assembling peptide RADA were found to be efficacious in repairing brain tissue and restoring functionality in hamster models of brain injury (Ellis-Behnke et al. 2006). The nanoscaffolds not only aided in axonal growth and synapse formation, but also effectively "knit" the brain tissue together.

Nanomaterials incorporating pharmaceuticals, growth factors, and stem cells may soon find clinical usage for stroke recovery. Nanoscaffolds for neural regeneration may be constructed from carbon, electrically conducting polymers, synthetic polymers, self-assembling peptides, or combinations of these materials. Future research on biomaterials for nerve regeneration must focus on optimizing the tissue response and defining the metabolic fate of nanomaterials. Importantly, nanomaterials for neural regeneration must be effective for both structural repair of the brain and functional recovery of the patient.

Nanoscale biomaterials, including nanoparticles and nanotubes, are demonstrating special capabilities for visualizing and healing the fine structures of the brain following a stroke. The development of new technologies for stroke detection and treatment is a wise investment: every additional dollar spent on the overall treatment of stroke has produced health gains valued at $1.55 (MEDTAP International 2004). Yet the proportion of research funds directed toward stroke remains disproportionately low; in most countries, stroke research receives less than one-tenth of the funding devoted to cancer research (Rothwell 2001). Improved therapies for stroke patients are necessary for preservation of the physical and mental health of populations worldwide. Novel nanomaterials for the brain can serve as platforms for MRI imaging, neural tissue engineering, and targeted pharmaceutical delivery. The next chapter will further explore biomaterial formulations for drug delivery in the context of the world's third leading killer, lower respiratory infection and pneumonia.

References

Anderson SA, Glod J, Arbab AS et al (2005) Noninvasive MR imaging of magnetically labeled stem cells to directly identify neovasculature in a glioma model. Blood 105:420

Baxendale M (2003) The physics and applications of carbon nanotubes. J Mater Sci Mater Electron 14:657

Beduneau A, Ma Z, Grotepas CB et al (2009) Facilitated monocyte-macrophage uptake and tissue distribution of superparamagnetic iron-oxide nanoparticles. PLoS One 4: e4343

Bonnemain B (1998) Superparamagnetic agents in magnetic resonance imaging, physicochemical characteristics, and clinical applications. A review. J Drug Target 6:167

Braun JS, Jander S, Schroeter M et al (1996) Spatiotemporal relationship of apoptotic cell death to lymphomonocytic infiltration in photochemically induced focal ischemia of the rat cerebral cortex. Acta Neuropathol (Berl) 92:255

Brouns R, De Deyn PP (2009) The complexity of neurobiological processes in acute ischemic stroke. Clin Neurol Neurosurg 111:483

Brown MM, Markus H, Oppenheimer S (2006) Stroke medicine. Taylor and Francis, Oxon

Cengelli F, Maysinger D, Tschudi-Monnet F et al (2006) Interaction of functionalized superparamagnetic iron oxide nanoparticles with brain structures. J Pharmacol Exp Ther 318:108

Chalela JA, Kidwell CS, Nentwich LM et al (2007) Magnetic resonance imaging and computed tomography in emergency assessment of patients with suspected acute stroke: a prospective comparison. Lancet 369:293

Chandra V, Pandav R, Laxminarayan R et al (2006) Neurological disorders. In: Jamison DT, Breman JG, Measham AR et al (eds) Disease control priorities in developing countries, 2nd edn. IBRD/The World Bank and Oxford University Press, Washington, DC

Corot C, Robert P, Idee J-M et al (2006) Recent advances in iron oxide nanocrystal technology for medical imaging. Adv Drug Deliv Rev 58:1471

Davis SM, Broderick J, Hennerici M et al (2006) Hematoma growth is a determinant of mortality and poor outcome after intracerebral hemorrhage. Neurology 66:1175

Donnan GA, Fisher M, Macleod M, Davis SM (2008) Stroke. Lancet 371:1612

Ellis-Behnke RG, Liang YX, You SW et al (2006) Nano neuro knitting: peptide nanofiber scaffold for brain repair and axon regeneration with functional return of vision. Proc Natl Acad Sci USA 103:5054

Fisher M, Davalos A, Rogalewski A et al (2006) Toward a multimodal neuroprotective treatment of stroke. Stroke 37:1129

Fukiyama K, Kimura Y, Wakugami K et al (2000) Incidence and long-term prognosis of initial stroke and acute myocardial infarction in Okinawa, Japan. Hypertens Res 23:127
Gilmore JL, Yi X, Quan L et al (2008) Novel nanomaterials for clinical neuroscience. J Neuroimmune Pharmacol 3:83
Gunatilake SB, Jayasekera BA, Premawardene AP (2001) Stroke subtypes in Sri Lanka – a hospital based study. Ceylon Med J 46:19
Hankey GJ, Jamrozik K, Broadhurst RJ et al (2000) Five-year survival after first-ever stroke and related prognostic factors in the Perth community stroke study. Stroke 31:2080
Hu H, Ni Y, Mandal SK et al (2005) Polyethyleneimine functionalized single-walled carbon nanotubes as a substrate for neuronal growth. J Phys Chem B 109:4285
Hu H, Ni Y, Montana V et al (2004) Chemically functionalized carbon nanotubes as substrates for neuronal growth. Nano Lett 4:507
International Stroke Trial Collaborative Group (1997) The international stroke trial (IST): a randomised trial of aspirin, subcutaneous heparin, both, or neither among 19435 patients with acute ischaemic stroke. Lancet 349:1569
Jan E, Kotov NA (2007) Successful differentiation of mouse neural stem cells on layer-by-layer assembled single-walled carbon nanotube composite. Nano Lett 7:1123
Kang HW, Josephson L, Petrovsky A et al (2002) Magnetic resonance imaging of inducible E-selectin expression in human endothelial cell culture. Bioconjug Chem 13:122
Koretsky AP (2004) New developments in magnetic resonance imaging of the brain. NeuroRx 1:155
Larsen C (1989) Dextran prodrugs – structure and stability in relation to therapeutic activity. Adv Drug Deliv Rev 3:103
Lin MM, Kim DK, El Haj AJ et al (2008) Development of superparamagnetic iron oxide nanoparticles (SPIONS) for translation to clinical applications. IEEE Trans Nanobioscience 7:298
Lovat V, Pantarotto D, Lagostena L et al (2005) Carbon nanotube substrates boost neuronal electrical signaling. Nano Lett 5:1007
Matsumoto K, Sato C, Naka Y (2007) Neurite outgrowths of neurons with neurotrophin-coated carbon nanotubes. J Biosci Bioeng 103:216
Mattson MP, Haddon RC, Rao AM (2000) Molecular functionalization of carbon nanotubes and use as substrates for neuronal growth. J Mol Neurosci 14:175
McAteer MA, Sibson NR, von Zur Muhlen C et al (2007) In vivo magnetic resonance imaging of acute brain inflammation using microparticles of iron oxide. Nat Med 13:1253
MEDTAP International (2004) The value of investment in health care: better care, better lives. MEDTAP, Bethesda, MD
National Institute of Neurological Disorders and Stroke (2009) Stroke: challenges, progress, and promise. NIH publication no. 09-6451. National Institutes of Health, Washington, DC
National Stroke Association (2002) Recovery and rehabilitation. National Stroke Association, Englewood, CO
Nighoghossian N, Wiart M, Cakmak S et al (2007) Inflammatory response after ischemic stroke: a USPIO-enhanced MRI study in patients. Stroke 38:303
Rausch M, Sauter A, Frohlich J (2001) Dynamic patterns of USPIO enhancement can be observed in macrophages after ischemic brain damage. Magn Reson Med 46:1018
Rice HE, Hsu EW, Sheng H et al (2007) Superparamagnetic iron oxide labeling and transplantation of adipose-derived stem cells in middle cerebral artery occlusion–injured mice. AJR Am J Roentgenol 188:1101
Roch A, Muller RN, Gillis P (1999) Theory of proton relaxation induced by superparamagnetic particles. J Chem Phys 110:5403
Rothwell SM (2001) The high cost of not funding stroke research: a comparison with heart disease and cancer. Lancet 357:1612
Saleh A, Schroeter M, Jonkmanns C (2004) In vivo MRI of brain inflammation in human ischaemic stroke. Brain 127:1670

Schroeter M, Franke C, Stoll G et al (2001) Dynamic changes of magnetic resonance imaging abnormalities in relation to inflammation and glial responses after photothrombotic cerebral infarction in the rat brain. Acta Neuropathol (Berl) 101:114
Silva GA, Czeisler C, Niece KL et al (2004) Selective differentiation of neural progenitor cells by high-epitope density nanofibers. Science 303:1352
Simonsen CZ, Ostergaard L, Vestergaard-Poulsen P et al (1999) CBF and CBV measurements by USPIO bolus tracking: reproducibility and comparison with Gd-based values. J Magn Reson Imaging 9:342
Stoll G, Jander S, Schroeter M (1998) Inflammation and glial responses in ischemic brain lesions. Prog Neurobiol 58:233
Thrift AG, Donnan GA, McNeil JJ (1995) Epidemiology of intracerebral hemorrhage. Epidemiol Rev 17:361
Thünemann AF, Schütt D, Kaufner L et al (2006) Maghemite nanoparticles protectively coated with poly(ethylene imine) and poly(ethylene oxide)-block-poly(glutamic acid). Langmuir 22:2351
Wardlaw JM (2008) What is a lacune? Stroke 39:2921
Weissleder R, Kelly K, Sun EY et al (2005) Cell-specific targeting of nanoparticles by multivalent attachment of small molecules. Nat Biotechnol 23:1418
Wiart M, Davoust N, Pialat JB (2007) MRI monitoring of neuroinflammation in mouse focal ischemia. Stroke 38:131
World Health Organization (1978) Cerebrovascular disorders (Offset publications). WHO Press, Geneva
World Health Organization (2008) The global burden of disease: 2004 update. WHO Press, Geneva
Xiao P, Cho SI, Liu R et al (2007) Controlled electrochemical synthesis of conductive polymer nanotube structures. J Am Chem Soc 129:4483
Yadav YR, Mukerji G, Shenoy R et al (2007) Endoscopic management of hypertensive intraventricular haemorrhage with obstructive hydrocephalus. BMC Neurol 7:1
Yang F, Murugan R, Ramakrishna S et al (2004) Fabrication of nano-structured porous PLLA scaffold intended for nerve tissue engineering. Biomaterials 25:1891
Zhang L, Webster TJ (2009) Nanotechnology and nanomaterials: promises for improved tissue regeneration. Nano Today 4:66
Zhang LF, Yang J, Hong Z (2003) Proportion of different subtypes of stroke in China. Stroke 34:2091
Zhang Z, van den Bos EJ, Wielopolski PA et al (2005) In vitro imaging of single living human umbilical vein endothelial cells with a clinical 3.0-T MRI scanner. MAGMA 18:175
Zimmer C, Weissleder R, O'Connor D et al (1995) Cerebral iron oxide distribution: in vivo mapping with MR imaging. Radiology 196:521

Chapter 4
Pneumonia

Pneumonia and other lower respiratory infections are the third leading cause of death worldwide. In 2004, pneumonia and lower respiratory infections were responsible for 4.2 million deaths, or 7.1% of all deaths globally (World Health Organization 2008). Notably, these infections of the lung affect the old as well as the young and account for nearly 10% of all years of life lost globally. Of the 4 million people who die every year from pneumonia, approximately 2 million are children under the age of 5. Lower respiratory infections are the leading cause of death in low-income countries and are the leading cause of death for children under 5 worldwide (World Health Organization 2008). Significant discrepancies exist between developing and developed countries with regard to childhood mortality from pneumonia: for every child that dies of pneumonia in an industrialized country, 2000 children die of pneumonia in developed countries. While there are similarities in adult mortality rates for hospital-treated pneumonia between developing and developed countries, there are important differences in age distributions. The median age at death from hospital-treated pneumonia among Kenyan adults is 33 years; in contrast, the age at death from hospital-treated pneumonia in more developed countries is over 65 years (Scott et al. 2000). Pneumonia is extremely common; each year, there are 429 million episodes of illness worldwide as a result of lower respiratory infections. Of these cases, 131 million illnesses occur in Africa and 134 million illnesses occur in Southeast Asia (World Health Organization 2008). Antibiotics are the main defense against community-acquired and hospital-acquired bacterial pneumonias. However, bacterial organisms form resistant biofilms within the lower respiratory tract, rendering many antibiotics ineffective. If a lower respiratory infection cannot be successfully treated, the infection will eventually overwhelm the system and result in death. New biomaterial formulations of antibiotics are currently being developed to penetrate biofilms in the respiratory tract and destroy pathogenic microbes. These biomaterials may increase the efficacy of antimicrobial regimens, so that fewer adults and children will succumb to lower respiratory disease.

4.1 Historical Perspective on Pneumonia

The clinical syndrome of pneumonia has been recognized since ancient times. In approximately 400 BC, Hippocrates described the symptoms of an acute illness

S.K. Bhatia, *Biomaterials for Clinical Applications*,
DOI 10.1007/978-1-4419-6920-0_4, © Springer Science+Business Media, LLC 2010

called "peripneumonia," which was apparent "if the fever be acute, and if there be pains on either side, or in both. . .and if cough be present, and the sputa expectorated be a blond or livid color, or likewise thin, frothy, and florid" (Hippocrates 1849). The Greek physician characterized severe cases associated with shortness of breath, also known as dyspnea: "it is bad if he has dyspnea, and urine that is thin and acrid, and if sweat come about the neck and head, for such sweats are bad, as proceeding from the suffocation, rales, and violence of the disease" (Hippocrates 1849). This description of lower respiratory infection is remarkably accurate and is consistent with those found in later textbooks. During the Middle Ages, the physician Maimonides distilled the clinical presentation of pneumonia: "The basic symptoms which occur in pneumonia and which are never lacking are as follows: acute fever, sticking [pleuritic] pain in the side, short rapid breaths, serrated pulse and cough, mostly [associated] with sputum" (Rosner 1998).

The pathological basis for pneumonia was first discerned in the eighteenth century by the Italian anatomist Giovanni Morgagni, who related the clinical features of pneumonia with inflammation and solidification within the lungs (Garrison 1921). In the early nineteenth century the French physician Rene Laennec, also known as "the father of pulmonary medicine," invented the stethoscope and demonstrated that lung solidification led to abnormal lung sounds. Pneumonia could thus be diagnosed by listening to the lungs; Laennec distinguished pneumonia, an infection of the lower respiratory tract, from bronchitis, an infection of the upper respiratory tract (Jay 2000). By 1875, the pathologist Edwin Klebs observed bacteria in the airways of individuals who had died from pneumonia (Klebs 1875). Pasteur discovered the *Streptococcus pneumoniae* bacterium in 1880 (Ratner and Weiser 2006). Soon after, Carl Friedlander identified *S. pneumoniae* as the most common causative agent for pneumonia (Friedlander 1882), and Albert Frankel identified *Klebsiella pneumoniae* as another causative agent for pneumonia (Frankel 1884). At the end of the nineteenth century, physicians understood pneumonia to be a pathological disease process in which "the spongy pulmonary tissue is rapidly converted into a solid mass" (Fagge and Pye-Smith 1891). Pneumonia continued to be feared as a source of morbidity and mortality well into twentieth century. Sir William Osler, the "father of modern medicine," called pneumonia "one of the most widespread and fatal of all acute diseases" and coined pneumonia as "the captain of the men of death" (Osler 1901). Pneumonia remains the leading cause of infectious death in both developing and developed countries.

4.2 Pathology of Pneumonia

Pneumonia is an inflammatory disease of the lung tissue, caused by infection and injury within the lower airways. A normal lung contains alveoli, microscopic air-filled sacs responsible for absorbing oxygen from the air into the bloodstream (Fig. 4.1). During an episode of pneumonia, the lung tissue becomes consolidated, and the alveoli become inflamed and abnormally flooded with fluid exudate (Fig. 4.2). The alveolar space undergoes solidification, as the alveoli fill with host

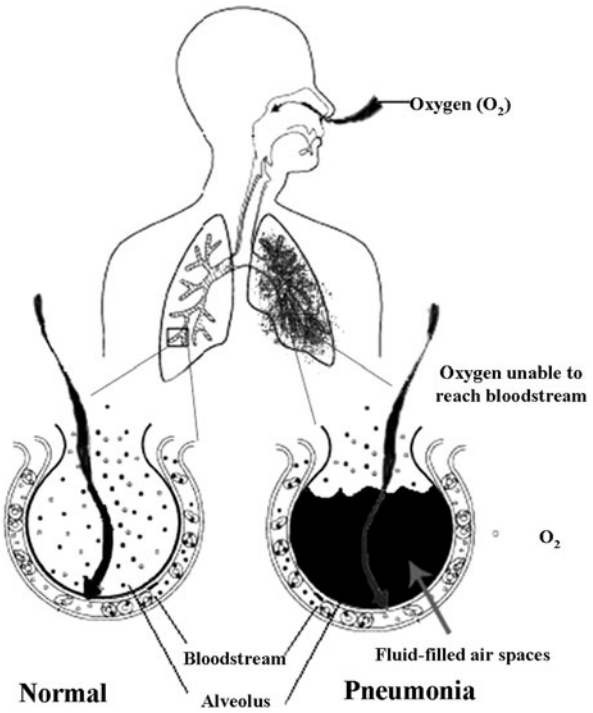

Fig. 4.1 Oxygen transport in the healthy lung versus the lung affected by pneumonia (National Institutes of Health)

cells mucinous material; eventually the alveoli collapse. As a consequence, the ability of the lungs to absorb and transport oxygen is compromised in lower respiratory infections. Pneumonia can result from a variety of infectious agents, including bacteria, viruses, fungi, and parasites. Infectious agents can be introduced into the lower respiratory tract by inhalation of aerosolized material; by aspiration of upper airway flora; or by seeding of bloodborne organisms when there is an infection in another part of the body (Dasaraju and Liu 1996).

Pneumonia occurs when lung defense mechanisms are suppressed or overwhelmed. Risk factors for pneumonia include exposure to infectious agents, environmental contaminants, and autoimmune diseases. Comorbid conditions such as asthma, chronic obstructive pulmonary disease, lung tumors, and diabetes also raise the risk of pneumonia. In addition, cigarette smoking, malnutrition, and low socioeconomic status increase the incidence of pneumonia (Speizer et al. 2006). Individuals with compromised immune defenses, including young children and the elderly, are at particularly high risk. Chronically ill and immunocompromised individuals carry an elevated risk for pneumonia, and lower respiratory infections remain a major concern among adults with HIV/AIDS. In addition, hospitalized patients may have many risk factors for pneumonia, including mechanical ventilation, prolonged malnutrition, underlying heart and lung disease, decreased amounts

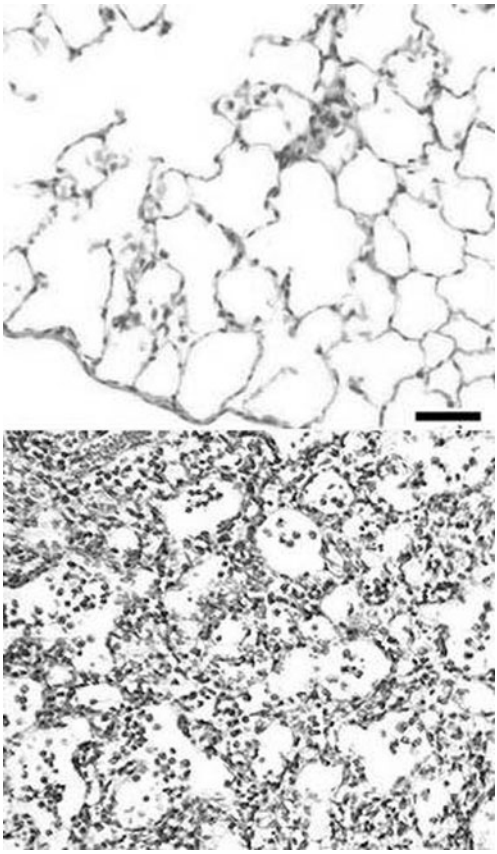

Fig. 4.2 Pathogenesis of pneumonia. The *upper panel* shows a normal lung; the open spaces are air-filled alveolar spaces. The *lower panel* shows a lung affected by pneumonia; the alveoli are filled with inflammatory cells and debris (National Institutes of Health and United States Department of Agriculture)

of stomach acid, and immune disturbance. Moreover, individuals in hospitals are exposed to a different mix of microorganisms, which often include drug-resistant bacteria.

Pneumonia that develops in an individual outside the hospital or institutional setting is classified as community-acquired pneumonia. Pneumonia that arises while an individual is in a nursing home or hospital (72 h or more after admission) is classified as nosocomial or hospital-acquired pneumonia. Up to 5% of patients admitted to a hospital for other causes subsequently develop pneumonia, and up to 25% of patients in intensive care units develop nosocomial pneumonias (Kingston et al. 1991). Community-acquired pneumonias and hospital-acquired pneumonias are associated with distinct pathogenic mechanisms, and the etiologic organisms for community-acquired and hospital-acquired pneumonias are somewhat different.

Typical community-acquired pneumonia occurs when microorganisms residing in the nasopharynx are aerosolized into the lower airway. Common causes of community-acquired pneumonia are gram-positive bacteria, such as *S. pneumoniae* and *Haemophilus influenzae*, as well as respiratory viruses, including

Table 4.1 Infectious causes of community-acquired pneumonia in children

Age	Organisms
Birth to 3 weeks	Group B streptococci, *Listeria monocytogenes*, gram-negative bacilli, cytomegalovirus
3 weeks to 3 months	*S. pneumoniae*, viruses (respiratory syncytial virus, parainfluenza viruses, metapneumovirus), *Bordetella pertussis*, *S. aureus*, *Chlamydia trachomatis* (transnatal exposure)
4 months to 4 years	*S. pneumoniae*, viruses (respiratory syncytial virus, parainfluenza viruses, influenza viruses, adenovirus, rhinovirus, metapneumovirus), *M. pneumoniae* (in older children), group A streptococci
5 years to 15 years	*S. pneumoniae*, *M. pneumoniae*, *C. pneumoniae*

McIntosh (2002)

respiratory syncytial virus, adenovirus, influenza viruses, and parainfluenza viruses. Atypical community-acquired pneumonia can be caused by *Chlamydia pneumoniae*, *Mycoplasma pneumoniae*, *Legionella pneumoniae*, and zoonotic pathogens. Hospital-acquired pneumonia often occurs when pathogenic organisms residing in the oropharynx are aspirated into the lower airway. Frequent causes of hospital-acquired pneumonia are gram-negative bacteria including *Escherichia coli*, *Enterobacter* species, *Proteus* species, *K. pneumoniae*, and *Pseudomonas aeruginosa*, as well as drug-resistant bacteria such as methicillin-resistant *Staphylococcus aureus*. These nosocomial pathogens rarely cause pneumonia in healthy individuals. In neonates, Group B streptococci and cytomegalovirus are important causes of congenital infections. Finally, the fungus *Pneumocystis jiroveci* produces a life-threatening pneumonia among patients immunosuppressed by AIDS; it is the most common pneumonia in patients with AIDS when CD4 counts drop below 200/mm^3 (Dasaraju and Liu 1996). Table 4.1 summarizes the infectious causes of pneumonia in children, and Table 4.2 summarizes the infectious causes of pneumonia in adults.

Overall, *S. pneumoniae* is the most common cause of pneumonia worldwide, across all age groups, settings, and geographic regions. Studies in which sputum specimens from pneumonia patients have been cultured suggest that *S. pneumoniae* is found in between 40 and 50% of cases (Speizer et al. 2006). *S. pneumoniae* is also the most common cause of death from pneumonia; pneumococcal infection accounts for roughly two-thirds of fatal cases of community-acquired pneumonia (Beers et al. 2006). It is therefore worthwhile to focus attention on *S. pneumoniae* pathogenesis. Pneumococcal bacteria are small organisms of approximately 1 μm in diameter (Fig. 4.3). Pneumococci occur in pairs (diplococci) and are surrounded by a polysaccharide capsule, which distinguishes them from other streptococcal species (Fig. 4.4). More than 80 serotypes of pneumococci, as determined by capsular polysaccharides, are known, but just 8–12 of these serotypes cause most cases of pneumonia (Speizer et al. 2006). Many pneumococcal bacteria live in parts of the upper respiratory tract, such as the nose, mouth, and sinuses, and can easily gain

Table 4.2 Infectious causes of pneumonia in adults

Group	Likely organisms
Outpatients – no modifying risk factors	*S. pneumoniae*, *M. pneumoniae*, *C. pneumoniae*, *H. influenzae*, respiratory viruses, miscellaneous (*Legionella* species, *Mycobacterium tuberculosis*, endemic fungi)
Outpatients – modifying risk factors present[a]	*S. pneumoniae*, including drug-resistant forms; *M. pneumoniae*; *C. pneumoniae*; mixed infection (bacteria + atypical pathogen or virus); *H. influenzae*, enteric gram-negative organisms; respiratory viruses; miscellaneous (*Moraxella catarrhalis*, *Legionella* species, anaerobes via aspiration, *M. tuberculosis*, endemic fungi)
Inpatients – not in an intensive care unit	*S. pneumoniae*; *H. influenzae*; *M. pneumoniae*; *C. pneumoniae*; mixed infection (bacteria + atypical pathogen or virus); respiratory viruses; *Legionella* species; miscellaneous (*M. tuberculosis*, endemic fungi, *P. jiroveci*)
Intensive care unit patient –*Pseudomonas* risk factors not present	*S. pneumoniae*, including drug-resistant forms; *Legionella* species; *H. influenzae*; enteric gram-negative organisms; *S. aureus*; *M. pneumoniae*; respiratory viruses; miscellaneous (*C. pneumoniae*, *M. tuberculosis*, endemic fungi)
Intensive care unit patient –*Pseudomonas* risk factors not present	*P. aeruginosa*; *S. pneumoniae*, including drug-resistant forms; *Legionella* species; *H. influenzae*; enteric gram-negative organisms; *S. aureus*; *M. pneumoniae*; respiratory viruses; miscellaneous (*C. pneumoniae*, *M. tuberculosis*, endemic fungi)

[a]Modifying factors:
Increased risk of drug-resistant organisms: Age > 65, alcoholism, antibiotic within 3 months, exposure to child in day care center, multiple co-existing illnesses
Increased risk of enteric gram-negative organisms: Antibiotic use within 3 months, cardiopulmonary disease (including COPD and heart failure), multiple co-existing illnesses
Increased risk of P. aeruginosa: Broad spectrum antibiotics >7 days in past month, corticosteroid use, undernutrition, structural pulmonary disease
Mandell et al. (2007)

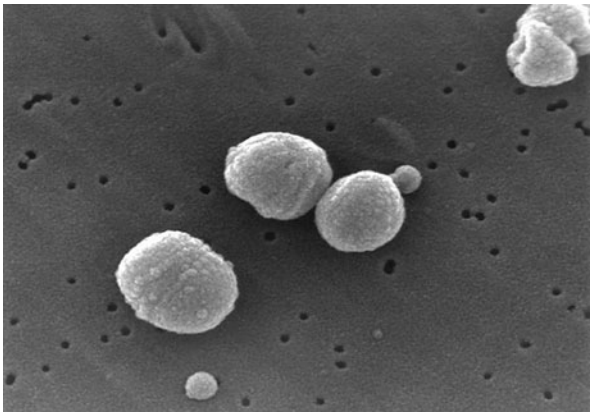

Fig. 4.3 Scanning electron micrograph of *S. pneumoniae* (Centers for Disease Control)

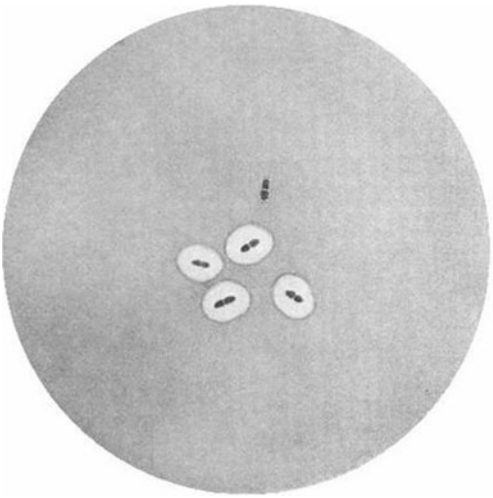

Fig. 4.4 Microscopic image of *S. pneumoniae*, stained to show polysaccharide capsule (Centers for Disease Control)

access to the alveoli in the lung; in fact *S. pneumoniae* is carried asymptomatically in the nasopharynx in 5–10% of healthy adults and 20–40% of healthy children (Orihuela and Tuomanen 2006). The germ is spread between humans via droplets, conveyed through coughing, sneezing, and talking in close proximity. Once inhaled into the lower airway, pneumococci infect alveolar cells. The lesion progresses as pneumococci multiply and invade the alveolar epithelium. Pneumococci spread from alveolus to alveolus through connecting pores and the disease can eventually involve an entire lobe of the lung.

Pneumococcal pneumonia and other typical bacterial pneumonias progress in four clinicopathologic stages, which ultimately result in consolidation of the lung:

1. The recently infected lungs demonstrate congestion and engorgement of alveolar capillaries, along with frothy, serous, and blood-tinged fluid in the alveolar spaces. Grossly, the lung is heavy.
2. The alveoli are filled with copious, clotted, inflammatory exudate, and a fibrin network extends from one alveolus into the next through connecting pores. Vascular congestion persists, with red blood cells in the alveolar spaces. The lung is characterized by a dry, granular, dark-red surface on gross appearance and demonstrates solidification. This stage is also called "red hepatization" as the lung somewhat resembles the liver in appearance. This stage represents a rapid progression from engorgement. Little tissue destruction or necrosis occurs at this stage, and the patient and lung architecture may recover fully.
3. As pneumonia progresses over 2–3 days, white blood cells pack into the alveoli, red blood cells disintegrate, and epithelial cells degenerate. The alveoli remain consolidated, but the lung is paler and drier on gross appearance. This stage is also called "gray hepatization." Dying pneumococci release preformed toxins,

further contributing to damage. The pneumococci are engulfed by white blood cells and begin to be cleared.
4. Resolution results in the formation of a jellylike yellowish-color exudate, which is digested by enzymatic activity and cleared by macrophages or cough mechanisms.

Notably, a pre-existing viral infection such as influenza increases pneumococcal attachment to the respiratory epithelium and a strong association between viral illnesses and pneumococcal pneumonia.

Regardless of the causative organism, time is of the essence with pneumonia. Severe pneumonia can kill victims within hours as they literally drown in the fluids flooding the lungs. Rapid recognition of the signs and symptoms, as well as effective treatment, is essential to saving patients from acute pneumonia. Individuals with pneumonia often present with a cough productive of greenish or yellow sputum, a high fever, and shaking chills. Patients experience shortness of breath and pleuritic chest pain; a sharp and stabbing pain that is worsened by deep breathing or coughing is also common. Additional systemic symptoms include headaches, nausea, vomiting, confusion, loss of appetite, and muscular fatigue and aches. On clinical examination, patients demonstrate a rapid heart rate, rapid respiratory rate, and shallow breathing. In children who are coughing and breathing rapidly, the respiratory rate is a valuable clinical sign for diagnosing acute lower respiratory infection; the presence of lower chest wall indrawing indicates more severe disease (Mulholland et al. 1992). Pneumonia sufferers exhibit dullness to percussion over the area of lung consolidation; decreased breath sounds and rales or crackles may be evident on auscultation of the lungs.

A chest x-ray of a patient with pneumonia may show a focal opacity in the area of lung consolidation (Fig. 4.5) or a diffuse process affecting both lungs (Fig. 4.6). Cultures of blood or sputum may reveal the causative organism. However, in developing countries the diagnosis of pneumonia is often made simply on the basis of cough and fever. For patients with access to a hospital, the likelihood of obtaining a chest x-ray increases; generally the infection is confirmed by microbial culture only in the most advanced medical centers (Speizer et al. 2006). Many patients in developing countries present late in the course of the disease and die before an appropriate diagnostic workup can be completed, leading to an underestimate of pneumonia incidence and fatality rates.

If pneumonia progresses, it can lead to several complications. Microorganisms infecting the lung can cause fluid to accumulate in the pleural space surrounding the lung; this fluid is called a pleural effusion and it can interfere with normal respiration (Fig. 4.7). The microorganisms themselves may migrate to the pleural space, forming an empyema that requires surgery or drainage, as antibiotics do not penetrate well into the pleural cavity. A lung abscess can form, or the pneumonia can develop into a systemic septicemia which poisons the blood and damages the liver, kidneys, and heart. The infection may permanently damage lung tissue or result in necrotizing pneumonia. As more lung tissue is destroyed, pneumonia can lead to respiratory failure, acute respiratory distress syndrome, ventilator dependence, and death.

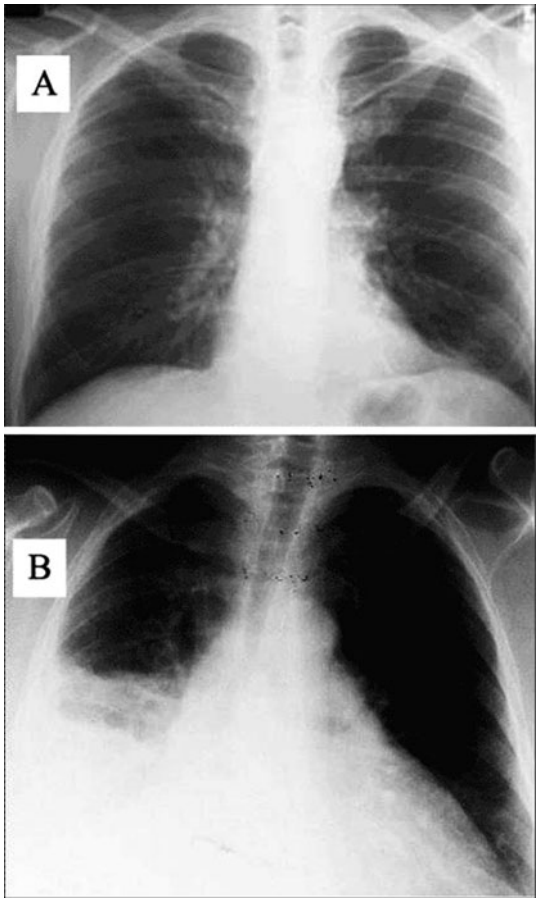

Fig. 4.5 Chest x-ray of a patient with bacterial pneumonia. The *upper panel* shows an x-ray of a normal lung. The *lower panel* shows a lung affected by pneumonia, with shadowing from pneumonia and consolidation in the right lung (Food and Drug Administration)

The prognosis for pneumonia sufferers depends on the causative organism, the age of the patient, and the degree of illness when the patient is diagnosed. The overall mortality rate in hospitalized patients with community-acquired pneumococcal pneumonia is 12%, while the mortality rate for hospitalized patients with hospital-acquired pneumonias is 25–50%, despite the availability of antimicrobial therapies (Beers et al. 2006). For age groups over 60, rates of death from pneumonia more than double for each decade of life (Speizer et al. 2006). Children less than 1 year of age also carry a poor prognosis (Beers et al. 2006).

Treatment of pneumonia is directed at the suspected underlying cause. Patients with bacterial pneumonia are treated with oral or intravenous antibiotics, while patients with viral pneumonia are managed with supportive care and sometimes with antiviral agents. Individuals can completely recover from pneumonia within weeks if treated early with effective antimicrobials. Yet the efficacy of antimicrobial drugs is decreasing as drug-resistant organisms are emerging. For instance, bacteria have

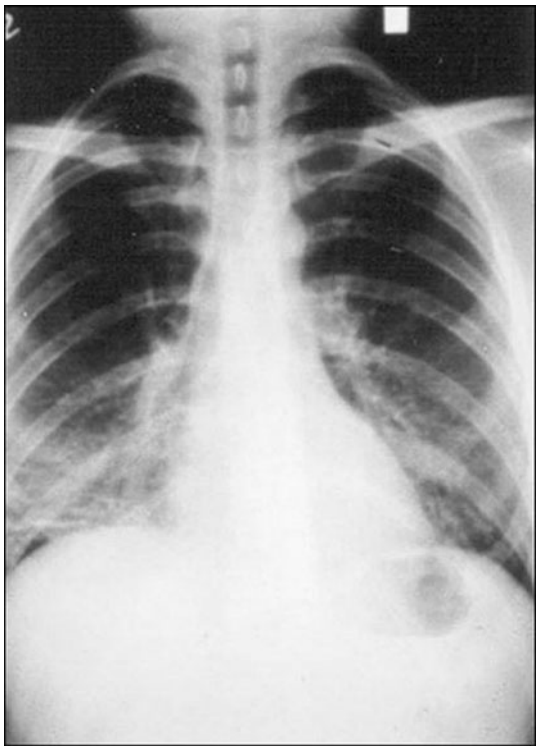

Fig. 4.6 Chest x-ray of a patient with *P. jiroveci* pneumonia (National Institutes of Health)

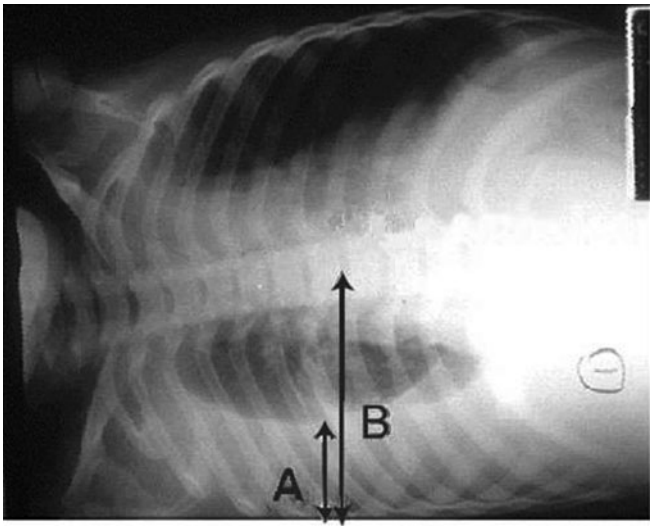

Fig. 4.7 Formation of a pleural effusion. The *A arrow* indicates fluid layering in the *right* chest. The *B arrow* indicates the normal width of the *right* lung. The volume of useful lung is reduced because of the collection of fluid surrounding the lung (Centers for Disease Control)

evolved intrinsic mechanisms for resisting antibiotics; up to one-third of isolates of *S. pneumoniae* in the United States have been found to be multi-drug resistant (Doern et al. 2001). In addition, bacteria such as pneumococci form biofilms during pulmonary infection, which increases the resistance of the bacteria to antibiotics; often treatment fails in spite of antibiotic sensitivity of organisms in laboratory tests. If biomaterial systems can be developed to improve drug delivery into biofilms, these biomaterials could overcome drug resistance and lower mortality from pneumonia. The following section will discuss innovative biomaterial formulations of antibiotics.

4.3 Biomaterials as Novel Antibiotic Carriers

Biomaterials can contribute to improved pneumonia therapies by enabling new antibiotic formulations that infiltrate bacterial biofilms. When bacteria such as *S. pneumoniae* infect tissue surfaces, these pathogens undergo a shift in physiological state from planktonic (suspension) form to a sessile (biofilm) form (Fig. 4.8). The phenotypic switch involves changes in gene expression in pneumococci and may allow the bacteria to morph from colonizing organisms to virulent invaders. Indeed, *S. pneumoniae* cells grown in a biofilm are more effective in inducing pneumonia and meningitis (Oggioni et al. 2006). Many persistent infections are now being

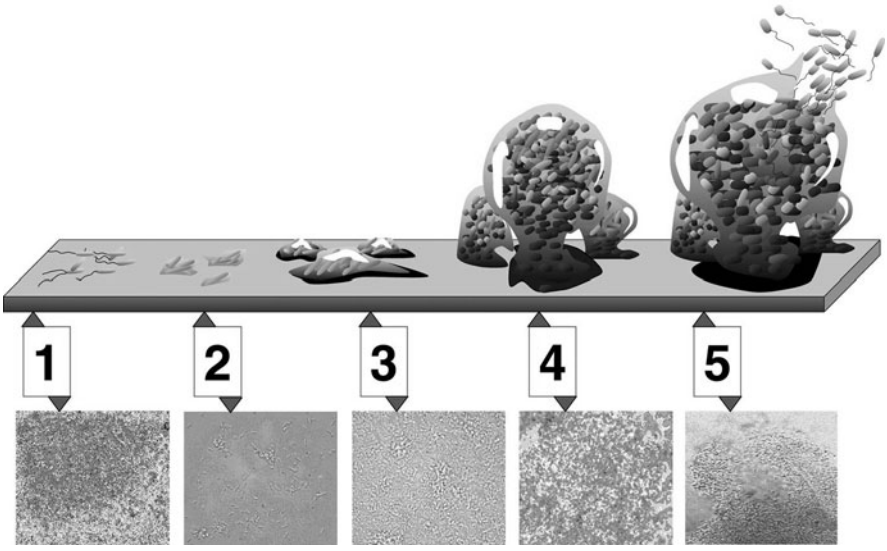

Fig. 4.8 The stages of biofilm development. *Stage 1*, initial attachment; *stage 2*, irreversible attachment; *stage 3*, maturation I; *stage 4*, maturation II; *stage 5*, dispersion. Each stage of development in the diagram is paired with a photomicrograph of a developing *P. aeruginosa* biofilm. All photomicrographs are shown to same scale (Monroe 2007)

attributed to bacterial proliferation as adherent biofilms on tissues. In addition, medical devices such as catheters and endotracheal tubes are notorious for attracting biofilm formation, which greatly raises the risk of nosocomial pneumonias in hospitalized patients. Microbial biofilms are largely responsible for the recalcitrance of many infections to conventional antimicrobial therapy (Stewart and Costerton 2001). Novel biomaterials that successfully eliminate biofilms could therefore aid in treating community-acquired pneumonias from organisms such as *S. pneumoniae*, as well as hospital-acquired pneumonias from organisms such as *K. pneumoniae* and *P. aeruginosa*.

A microbial biofilm is broadly defined as a complex community of adherent microorganisms within a polymeric matrix. Biofilms usually contain stacks of microbes, with aqueous channels in between. The matrix that coats the biofilm, called the glycocalyx, is a polysaccharide secreted by the bacterial cells; the glycocalyx is hydrophilic and typically anionic in nature (Sutherland 2001). The biofilm structure is immobile yet dynamic and may include single or multiple microbial species. Growth within a biofilm protects bacteria from antimicrobial compounds and almost always results in a significant increase in resistance to antimicrobial drugs, compared with microbial cultures grown in suspension. Up to 1,000-fold decreases in antimicrobial susceptibility have been observed for biofilms (Costerton et al. 1999). Biofilm resistance can be determined by the susceptibility of the most resistant cell, and the most resistant members of a biofilm population are typically orders of magnitude more resistant than similar members of a planktonic population.

Eradication of a pulmonary biofilm by antibiotic treatment requires elimination of all the bacteria; even a small fraction of surviving persister cells can re-start biofilm development once antimicrobial therapy is discontinued. Multiple physicochemical mechanisms block the activity of conventional small-molecule antibiotics in biofilms. The antimicrobial agent may react chemically with the anionic glycocalyx polymer surrounding the cells or the drug may adsorb onto the glycocalyx, rendering the antimicrobial ineffective; cationic antibiotics are particularly prone to these interactions. The net effect is that the glycocalyx acts as a penetration barrier. A similar effect occurs when antimicrobials adsorb onto cells, either living or dead, in the outer part of the biofilm. In addition, the bacteria produce drug-inactivating enzymes, such as β-lactamases which inactivate penicillins and cephalosporins; these enzymes accumulate within the glycocalyx and produce concentration gradients that protect underlying cells (Smith 2005). An efficacious biomaterial formulation for pneumonia pharmacotherapy must overcome all of these barriers.

An alternative approach to the classical delivery of antibacterial therapy is to associate the drug with a submicroscopic carrier, which hides and protects the molecule from reaction, degradation, or adsorption. The carrier must also have the ability to deliver the antibiotic to inaccessible target cells in a controlled manner. The ideal biomaterial for this purpose must additionally be biologically, chemically, and physically stable. Liposomes are colloidal biomaterials that have been designed for controlled release of pharmaceuticals. These constructs are ideal structures for

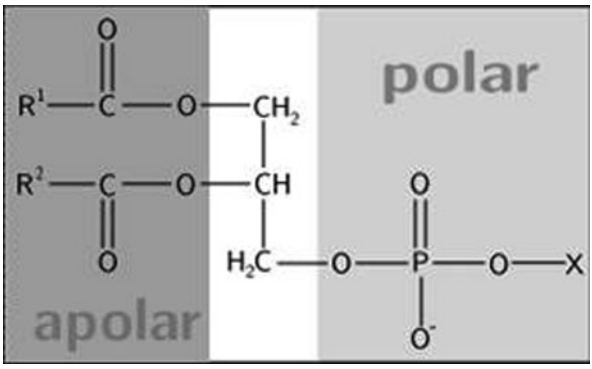

Fig. 4.9 Schematic structure of an amphiphilic phospholipid

targeting biofilms, as liposomes localize preferentially to sites of inflammation and infection following intravenous administration; such site-specific liposomal accumulation occurs as a result of increased capillary permeability and plasma influx at infected tissue sites (Bakker-Woudenberg et al. 1993). Liposomes are biocompatible, biodegradable, and readily cleared by physiological metabolism. Moreover, liposomes are attractive as drug delivery vehicles, due to the range and extent of payloads that they can transport. Liposomes can carry both hydrophobic and hydrophilic drugs over long periods of time and are able to concentrate antimicrobial agents at biofilm interfaces (Jones et al. 1997).

Liposomes were first developed as artificial models for the phospholipid bilayers of biological membranes (Chapman 1984). The word "liposome" is derived from the Greek terms "lipo" referring to the fatty composition, and "soma" referring to the structure. The key ingredients of liposomes are amphiphilic phospholipids which bear hydrophilic phosphate heads and hydrophobic fatty acid tails (Fig. 4.9). In aqueous solutions, the phospholipids align based on their polar and non-polar domains. A fully formed liposome possesses a vesicular structure surrounded by one or more outer protecting shells, consisting of lipids arranged in a bilayer configuration (Fig. 4.10). These phospholipid dispersions in water solutions have been found to exhibit selective permeability to solutes and have been shown to trap and release solutes (Bangham et al. 1965). Based on the ability of liposomes to sequester solutes, the concept of liposomes as drug carriers was proposed (Gregoriadis 1976). The liposome is essentially a double-walled, hollow sphere that encapsulates a drug (Fig. 4.11).

Liposomes can vary widely in size (0.02–10 μm) and in the number of lamellae. Components of liposomes may include cholesterol, phophatidylserine, phophatidylcholine, phosphatidylinositol, phosphatidylglycerol, phosphatidylethanolamine, and derivatives of such molecules (Fig. 4.12). Usually, liposomes are classified into three categories on the basis of size and lamellarity (number of bilayers): small unilamellar vesicles; large unilamellar vesicles; and multilamellar vesicles or oligolamellar vesicles (Fig. 4.13). An active pharmaceutical compound can be enclosed

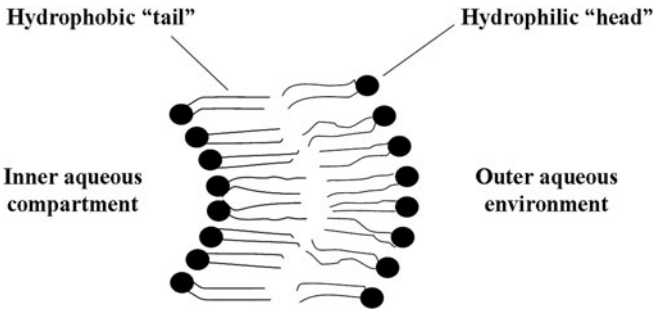

Fig. 4.10 Structure of the lipid bilayer that forms a liposomal membrane. The bilayer consists of amphiphilic phospholipids and encloses an aqueous compartment. One layer of hydrophilic "heads" faces outside the vesicle, attracted to the water in the surrounding environment. Another layer of hydrophilic "heads" faces inside the vesicle, attracted to the water inside the aqueous compartment. Hydrophobic "tails" of one layer face the hydrophobic "tails" of the other layer, arranging to form a lipid membrane

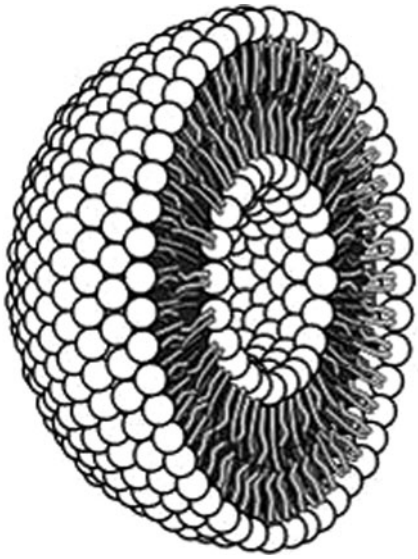

Fig. 4.11 Cross-sectional view of a liposome

in the aqueous spaces if the drug is water soluble or in the lipid membrane if the drug is lipid soluble. The drug entrapment efficiency is determined by the volume of the liposomes and drug solubility. For shelf stability, liposomes can be stably preserved in the dry state in the presence of sugars, particularly trehalose (Crowe and Crowe 1988). Liposomes have been administered via a number of routes, but intravenous injection is the most practical route (Pinto-Alphandary et al. 2000). Liposomes can interact with living cells in one of four ways: adsorption, endocytosis, lipid exchange, and membrane fusion.

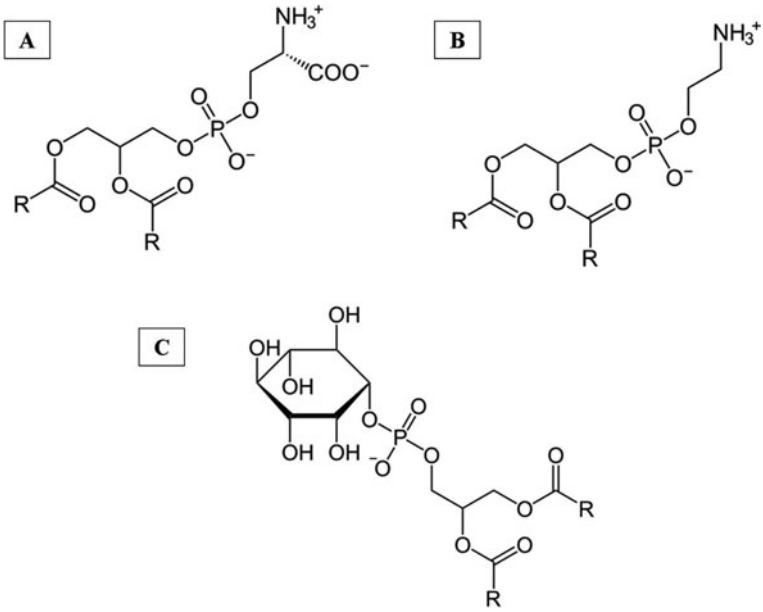

Fig. 4.12 Chemical structures of common phospholipids. **a** Phosphatidylserine. **b** Phosphatidylethanolamine. **c** Phosphatidylinositol

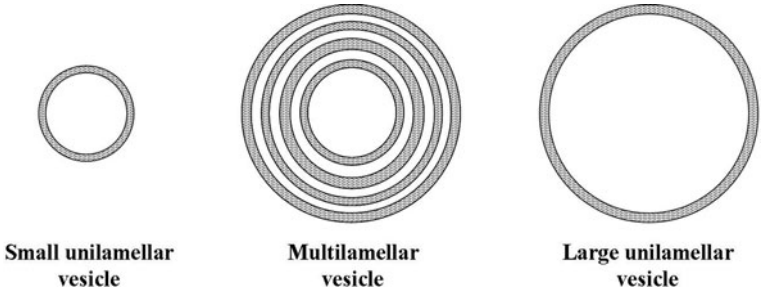

Fig. 4.13 Types of liposomal drug carriers

The half-lives of liposomes in the bloodstream range from a few minutes to several hours, depending on the size and lipid composition of the vesicles. When liposomes are introduced into the blood, many plasma proteins, mainly apolipoproteins, associate with the surface of these carriers. The surface charge, surface coatings, and lipid doses of liposomes can be tuned to influence plasma protein interactions and clearance rates (Cullis et al. 1998). Cationic liposomes exhibit extensive interactions with plasma since the majority of plasma proteins carry a net negative charge at physiological pH. Such liposome formulations demonstrate significant serum turbidity and protein binding (Oku et al. 1996) and induce immediate clot formation at charge concentrations higher than 0.5 mmol/ml (Senior et al. 1991).

Neutral liposomes composed of neutral saturated lipids with acyl chain lengths greater than 16 carbons also bind large quantities of blood proteins and are rapidly cleared from the circulation. This phenomenon may occur because of hydrophobic domains at the surface of the vesicles. For these types of vesicles, the lipid dose can also affect liposome–blood protein interactions. Increased lipid doses result in decreased protein levels on the surface of the liposomes and longer circulation times (Oja et al. 1996). In the case of anionic liposomes, the ability of the liposomes to interact with blood proteins depends on the nature of the anionic lipid, mainly the composition of the acyl chain (Hernandez-Caselles et al. 1993). Liposomal circulation time determines the efficacy and effective dose of the pharmaceutical being delivered, so the charge and composition of liposomes are critical design parameters to consider during development of these biomaterials for antibiotic delivery. Structural stability of liposomes is also important for appropriate targeting of therapeutic drugs, since the osmotic fragility of liposomes can destabilize them leading to leakage of the entrapped drug. In general, multilamellar vesicles containing phospholipids with a long saturated chain and a negative surface charge can achieve satisfactory stability in the plasma.

The most widely used approach for increasing the circulation time of liposomes is to incorporate amphipathic poly(ethyleneglycols) into the lipid bilayer. The typical molecular weights of poly(ethyleneglycols) utilized in liposomes are 2,000–5,000. These polymers confer hydrophilicity to the liposome surface and sterically inhibit the adsorption of plasma proteins. In contrast to other types of long-circulating liposomes, sterically stabilized liposomes are advantageous in that their prolonged blood circulation time is largely independent of liposome characteristics such as liposome particle size, charge, and lipid composition (rigidity) of the bilayer (Bakker-Woudenberg et al. 2005). This affords an opportunity to manipulate antibiotic release from the liposomes at the site of infection, without compromising blood circulation time and degree of target localization of these carriers. This is an important functional property, in view of the differences in pharmacodynamics of different antibiotics. Such “stealth” liposomes repel non-specific cell and protein adhesion and are not readily engulfed by host macrophages. When administered intravenously, stealth liposomes have an enhanced ability to leave the vascular compartment and enter infected tissues. Stealth liposomes with increased half-lives constitute a real therapeutic advance, enabling prolonged antimicrobial therapy for persistent infections.

Liposomal encapsulation significantly changes the pharmacokinetics of antimicrobial agents, increasing the circulation time and reducing the toxic side effects of therapeutic drugs. Liposomes decrease the apparent volume of distribution of the drug within the body, allowing an increase in the maximum tolerated dose. Liposome-encapsulated antibiotic formulations thus demonstrate an improved therapeutic index compared with free antibiotic and reduce the risks of therapeutic failure imposed by impaired host defenses or reduced bacterial susceptibility. In addition, since free antibiotics are commonly associated with side effects of hepatotoxicity and nephrotoxicity, the reduced toxicity of liposomal formulations is a major clinical advantage. The higher efficiency of liposomes could be explained by

the natural targeting of colloidal carriers to infected tissue sites; liposomes have an inherent ability to localize where they are needed most. The biocompatibility of liposomal carriers has been examined in macrophage cells and does not present any contraindications (Pinto-Alphandary et al. 2000).

An added functional benefit of liposomes is their ability to carry two or more drugs simultaneously. In clinical practice, combinations of antimicrobial agents are frequently administered to patients for infectious disease treatment. Co-administration of drugs increases overall therapeutic efficacy by broadening the antimicrobial spectrum of the treatment, preventing the emergence of resistant strains, reducing toxicity, eliminating multidrug-resistant microorganisms, and enhancing bacterial killing by exploiting the synergistic interaction of a specific drug combination. Because various antimicrobial agents have different physicochemical properties, the pharmacokinetics and tissue distributions of the drugs can vary substantially. When combinations of free antibiotic agents are administered, there is no guarantee that the agents will co-localize at the infectious focus and act synergistically. However, the use of a liposomal carrier containing both antibiotics could ensure a parallel tissue distribution of both encapsulated agents (Schiffelers et al. 2001a). Moreover, a liposomal drug carrier can increase the concentrations of both drugs at the site of infection, which further strengthens the synergistic drug interactions. Co-encapsulation of drugs within liposomes could open new therapeutic avenues for pneumonia and other infectious diseases. Since pulmonary biofilms can contain multiple microbial species, the ability to co-deliver multiple antibiotics via liposomes may be particularly valuable in pneumonia.

Antibiotic-loaded liposomes have already demonstrated promise for treating bacterial biofilms in experimental models of pneumonia. For instance, sterically stabilized liposomes containing gentamicin have been examined in a rat model of unilateral pneumonia caused by *K. pneumoniae* (Bakker-Woudenberg et al. 1993), a common cause of hospital-acquired infections. Gentamicin was chosen for encapsulation because it is a commonly used aminoglycoside drug for treating severe nosocomial gram-negative and gram-positive infections, especially in immunocompromised patients. The liposomes were composed of partially hydrogenated egg phosphatidylcholine (PHEPC); cholesterol; and poly(ethylene glycol) -2,000-distearoyl-phosphatidylethanolamine (PEG-DSPE) in molar ratios of 1.95:1.0:0.05, 1.85:1.0:0.15, and 1.70:1.0:0.30. The PEG-DSPE was the stabilizing component in this family of long-circulating liposomes. These PEGylated liposomes were found to preferentially localize to the infected lung, with liposomal accumulation correlating positively with the severity of infection (Schiffelers et al. 2001b). Small-sized liposomes (diameter of 100 nm) localized about 2.3-fold more efficiently in the infected tissues than did large-sized preparations (diameters of 280 and 360 nm). The half-life of liposome-encapsulated gentamicin in the blood was approximately 20 h, while the half-life of free gentamicin was 20 min. In rats with *K. pneumoniae* pneumonia, the administration of free gentamicin resulted in a 47% survival rate, whereas treatment with liposome-encapsulated gentamicin increased the survival rate to 100%. Moreover, liposome-encapsulated gentamicin achieved a 10^4-fold decrease in bacterial counts in the infected lung, when compared to free gentamicin.

The superior therapeutic effect of liposome-encapsulated gentamicin resulted from the accumulation and subsequent degradation of liposomes, followed by release of encapsulated gentamicin at the therapeutic site. Clearly, liposomes have the potential to eradicate biofilms and reduce mortality from pneumonia.

Liposome-encapsulated gentamicin has been further studied in leukopenic rat models with *K. pneumoniae* pneumonia (Schiffelers et al. 2001c). Leukopenia is a state of low white blood cell levels and impaired host defenses, so leukopenic rats are clinically relevant models for immunocompromised patients such as the elderly population and the HIV/AIDS population. In rats with compromised host defenses, treatment with free gentamicin at a low dose of 5 mg/kg/day was ineffective (this dose had been effective in rats with intact host defenses). The free drug had to be administered at the maximum tolerated dose of 40 mg/kg/day to obtain therapeutic efficacy. However, the addition of a single dose of liposome-encapsulated gentamicin (5 mg/kg) to low-dose free gentamicin treatment (5 mg/kg/day) produced a successful therapeutic effect. The combination of liposome-encapsulated gentamicin with standard treatment thus enabled complete survival, with a sevenfold lower cumulative amount of gentamicin compared with free gentamicin alone. The liposomal formulation effectively eliminated the pneumonia while minimizing the overall drug load on the system. Since aminoglycosides are well known for side effects of nephrotoxicity and ototoxicity, liposomal biomaterials that reduce the total required dose will improve patient outcomes and be more cost-effective. In this model of pneumonia in an immunocompromised host, free gentamicin and liposome-encapsulated gentamicin played complementary roles: liposomal gentamicin achieved local bacterial killing, while free gentamicin prevented the occurrence of sepsis.

The efficacy of liposome-encapsulated gentamicin has been investigated in an even more challenging model of nosocomial pneumonia caused by drug-resistant organisms (Schiffelers et al. 2001c). In this study, leukopenic rats were infected with low gentamicin-susceptible strains of *K. pneumoniae*; this model is clinically relevant to difficult-to-treat pneumonias in humans. Free gentamicin was found to be totally ineffective against the low susceptibility strains. Even at the maximum tolerated dose of 40 mg/kg/day of free gentamicin, the survival rate was 0%. When liposome-encapsulated gentamicin in vesicles composed of PEG-DSPE/PHEPC/Cholesterol was added to free gentamicin treatment, the survival rate improved to 50%. The fluidity of the liposome bilayer was then increased by omitting cholesterol from the formulation, to allow greater localized release of gentamicin. When liposome-encapsulated gentamicin in PEG-DSPE/PHEPC was administered along with free gentamicin treatment, a survival rate of 100% was achieved. The tunability and targeting capability of liposome biomaterials therefore has distinct benefits for drug-resistant pneumonias.

Liposomal formulations of other classes of antibiotics have also demonstrated promise for treating biofilms in pneumonia. For instance, the β-lactam antibiotic ceftazidime has been encapsulated in sterically stabilized liposomes composed of PHEPC/Cholesterol/ PEG-DSPE in a molar ratio of 1.85:1.0:0.15 (Bakker-Woudenberg et al. 1995). For β-lactam antibiotics such as ceftazidime, it is known

that continuously maintained plasma concentrations are necessary for successful treatment of severe infections, so these antibiotics are traditionally administered as continuous intravenous infusions. A liposome-encapsulated β-lactam antibiotic could achieve continuous delivery of antibiotic with administration of just a single dose. The therapeutic efficacy of liposome-encapsulated ceftazidime as a single dose has therefore been compared to a continuous 2-day infusion of free ceftazidime at the same total dose. In a rat model of *K. pneumoniae* pneumonia, it was demonstrated that liposome-encapsulated ceftazidime was just as effective as free ceftazidime at a continuous 2-day infusion. This was observed over a dose range varying from 1 mg/kg (not effective) up to 30 mg/kg (fully effective). In a follow-up study, a single dose of liposome-encapsulated ceftazidime (12 mg/kg) given 24 h after bacterial inoculation was found to be as effective as 10 doses of free ceftazidime administered over a period of 5 days at a total dose of 500 mg/kg (Schiffelers et al. 2001a). The effect was even more pronounced when rats with intact host defenses were infected with a low ceftazidime-susceptible strain of *K. pneumoniae*. In this case, liposome-encapsulated ceftazidime administered over a 2-day period was effective at a total dose of 25 mg/kg, which was 80-fold lower than the total dose of 2,000 mg/kg free ceftazidime required to obtain the same therapeutic efficacy. Liposome-encapsulated ceftazidime was thus successful in efficiently treating *K. pneumoniae* pneumonia with a lower antibiotic load and lower dose frequency.

Encouraging results have been observed with liposomal formulations of the fluoroquinolone antibiotic ciprofloxacin as well. For these studies, the lipid composition of the liposomes was PEG-DSPE, hydrogenated soy phosphatidylcholine, and cholesterol in a molar ratio of 5:50:45 (Bakker-Woudenberg et al. 2001). These investigations demonstrated the ability of sterically stabilized liposomes to act as microreservoirs of antibiotic agents in the circulation. For example, when liposome-encapsulated ciprofloxacin was administered by intravenous injection into rats, 77% of the injected dose was still circulating in the bloodstream at 30 min after injection. By contrast, only 1.3% of free ciprofloxacin was circulating in the bloodstream at 30 min after intravenous administration. The liposomal formulation of ciprofloxacin exhibited superior performance to free ciprofloxacin in treating *K. pneumoniae* pneumonia in rat models. A once-daily dose of liposome-encapsulated ciprofloxacin effected a 90% survival rate, which could not be achieved with once-daily administration of free ciprofloxacin. Further, liposomes decreased the occurrence of toxic side effects, including renal toxicity and hepatic toxicity.

Experimental studies have even shown that liposomes can co-encapsulate antibiotics for simultaneous delivery to pneumonia biofilms. Ceftazidime and gentamicin have been co-encapsulated in sterically stabilized liposomes composed of PHEPC/Cholesterol/ PEG-DSPE in a molar ratio of 1.85:1.0:0.15 (Schiffelers et al. 2001a). These dual-delivery liposomes enabled synergistic interactions between the two antibiotics during pneumonia treatment. In rat models of *K. pneumoniae* pneumonia, liposomal encapsulation of gentamicin and ceftazidime together improved survival compared with liposome-encapsulated gentamicin or liposome-encapsulated ceftazidime alone. Specifically, a 5 mg/kg dose

of liposome-encapsulated gentamicin alone or a 3 mg/kg dose of liposome-encapsulated ceftazidime alone each resulted in 60–67% survival. However, co-encapsulation at half these doses (liposome-encapsulated gentamicin and ceftazidime at 2.5 and 1.5 mg/kg, respectively) produced a 100% survival rate. The synergistic effect was also evident when rats with intact host defenses were infected with an antibiotic-resistant strain of *K. pneumoniae*. In this model, a 40 mg/kg/day dose of liposomal gentamicin alone could not produce survival after 2 days, and a 24 mg/kg/day dose of liposomal ceftazidime was required to achieve survival after 2 days. Co-encapsulation at substantially lower doses (liposome-encapsulated gentamicin and ceftazidime at 10 and 12 mg/kg/day, respectively) produced complete survival. Colloidal drug carriers such as liposomes may therefore be applicable for multi-drug therapy of pneumonias.

Overall, studies of liposomal drug carriers for treatment of *K. pneumoniae* pneumonia indicate the versatility of liposomes for delivering a wide variety of antibiotics or combinations of antibiotics. Recent investigations have focused on the ability of liposomes to manage diverse types of pneumonia, including other bacterial pneumonias and fungal pneumonias. For example, a liposomal formulation of the aminoglycoside antibiotic amikacin has been designed specifically for nebulization and inhaled delivery to treat *P. aeruginosa* lung infections (Meers et al. 2008). Nanoscale amikacin-loaded liposomes with a mean diameter of 300 nm were found to readily penetrate both infected human sputum and biofilms of *P. aeruginosa* macro-colonies (larger particles of 1 μm in diameter did not penetrate *Pseudomonas* biofilms). In rat models of chronic *P. aeruginosa* lung infection, inhaled liposomal amikacin was released in a slow sustained manner and was orders of magnitude more efficacious than inhaled free amikacin. In healthy human volunteers, inhaled liposomal amikacin was well tolerated and resulted in prolonged retention of drug-loaded liposomes in the lungs (Weers et al. 2009). A commercial liposomal formulation of amikacin called Arikace™ (Transave, Monmouth, NJ, USA) is currently under development. Arikace™ is now in clinical trials for inhalation therapy of *Pseudomonas* lung infections in cystic fibrosis patients and could potentially find broader patient usage for gram-negative bacterial pneumonias.

For fungal pneumonias, sterically stabilized liposomes have been constructed to carry the antifungal agent amphotericin B (Van Etten et al. 2000). Liposomal formulations of amphotericin B demonstrated impressive results in models of invasive *Aspergillus fumigans* pneumonia in leukopenic rats. A single intravenous dose of liposome-encapsulated amphotericin B at 10 mg/kg was as effective as a 10-day intravenous treatment with 1 mg/kg/day of free amphotericin B, in terms of significantly prolonging the survival rate and reducing fungal dissemination to the liver. Liposomes thus successfully delivered antifungal agents to the lung and reduced the dose frequency required for pneumonia treatment. These results suggest that liposomes could have applicability for other fungal pneumonias caused by endemic species, as well as fungal pneumonias such as *P. jiroveci* in immunocompromised patients.

In summation, liposomal formulations of antimicrobial agents have demonstrated an ability to penetrate biofilms and eradicate pneumonia in animal models and are

undergoing evaluation in human trials. Liposomal carriers have achieved therapeutic efficacy in clinically relevant models of serious, difficult-to-treat infection; liposomes have overcome the challenges of impaired host defense, low antimicrobial susceptibility of the infectious agent, and antibiotic concentration at the site of infection. All liposomes have common features, namely materials that mask the charge and size of the molecules they convey, enabling the transport of small molecules and other therapeutics into sessile bacterial communities. Liposomes modulate the pharmacokinetics of antimicrobial agents, with site-specific delivery and controlled release. The best liposomes combine polyethylene glycol, which creates a steric shell around the particle to lengthen its time in the circulation, with lipids naturally found in biological membranes, such as cholesterol or phosphatidylcholine, which provide structure to the particle. In many cases, antibiotic-loaded liposomal biomaterials can successfully treat serious cases of pneumonia with administration of just a single dose, rather than the continuous dosage of intravenous antibiotics which is traditionally required for pneumonia management. Liposome technology is sufficiently diverse to address the wide range of causative pathogens associated with pneumonia, as well as the variety of antibiotics required to overcome pneumonia. Future work on liposomes must be directed toward liposomal antibiotics to fight *S. pneumoniae*, the most common pathogenic cause of pneumonia. While current studies of liposomal carriers in *K. pneumoniae* models are provocative and suggest the power of liposomes for nosocomial pneumonias, the efficacy of liposome-encapsulated antibiotics against pneumococcal pneumonia has yet to be demonstrated. Ongoing research for liposomal biomaterials must also fully characterize the degradation, metabolism, and elimination of both the liposomes and the entrapped drugs, to ensure non-toxicity. Scalable and inexpensive production methods for liposomes must be established. Finally, research efforts should be focused on moving liposomal antibiotics forward into human clinical trials.

Pneumonia carries the distinction of being the most frequent cause of death in developing countries, the most frequent cause of death in young children worldwide and the third most frequent cause of overall death worldwide. As such, pneumonia demands greater attention from the public health and biomaterials research communities. Unfortunately, pneumonia is one of the truly neglected diseases in terms of research, and pneumonia ranks as the number one cause of morbidity and mortality among all neglected diseases. Only 1.3% of research funding is directed toward bacterial pneumonias and meningitis (Moran et al. 2009a). In 2007, total global spending for research and development on bacterial pneumonias and meningitis was merely $32.5 million (Moran et al. 2009b). Without further research in this field, millions of adults and children will continue to perish; even with early diagnosis and treatment, 5–10% of patients die within 24–48 h of onset of symptoms (Moran et al. 2009b). As Hippocrates stated, “When pneumonia is at its height, the case is beyond remedy if he is not purged” (Hippocrates 1869). Emerging liposomal biomaterials for antibiotic delivery can permit more cost-effective and efficient therapy of pneumonia, not only by lowering the overall drug load but also by simplifying the dosing regimen. Liposome-encapsulated antibiotics could be especially useful in developing countries where healthcare resources and hospital facilities are critically

limited. The prospect of treating pneumonia with a single dose of antibiotic would revolutionize therapy of adults and children. Through innovative biomedical therapies, this "captain of the men of death" can be conquered. The following chapter will discuss another important lung affliction and the fourth leading cause of death worldwide, chronic obstructive pulmonary disease (COPD).

References

Bakker-Woudenberg IA, Lokerse AF, ten Kate MT et al (1993) Liposomes with prolonged blood circulation and selective localization in Klebsiella pneumoniae-infected lung tissue. J Infect Dis 168:164

Bakker-Woudenberg IA, Schiffelers RM, Storm G et al (2005) Long-circulating sterically stabilized liposomes in the treatment of infections. Methods Enzymol 391:228

Bakker-Woudenberg IA, ten Kate MT, Guo L et al (2001) Improved efficacy of ciprofloxacin administered in polyethylene glycol-coated liposomes for treatment of Klebsiella pneumoniae pneumonia in rats. Antimicrob Agents Chemother 45:1487

Bakker-Woudenberg IA, ten Kate MT, Stearne-Cullen LE et al (1995) Efficacy of gentamicin or ceftazidime entrapped in liposomes with prolonged blood circulation and enhanced localization in Klebsiella pneumoniae-infected lung tissue. J Infect Dis 171:938

Bangham AD, Standish MM, Watkins JC (1965) Diffusion of univalent ions across the lamellae of swollen phospholipids. J Mol Biol 13:238

Beers MH, Porter RS, Jones TV et al (2006) Merck manual of diagnosis and therapy, 18th edn. Wiley, New York, NY

Chapman D (1984) Physicochemical properties of phospholipids and lipid-water systems. In: Gregoriadis G (ed) Liposome technology. CRC Press, Boca Raton, FL

Costerton JW, Stewart PS, Greenberg EP (1999) Bacterial biofilms: a common cause of persistent infections. Science 284:1318

Crowe JH, Crowe LM (1988) Factors affecting the stability of dry liposomes. Biochim Biophys Acta 939:327

Cullis PR, Chonn A, Semple SC (1998) Interactions of liposomes and lipid-based carrier systems with blood proteins: relation to clearance behaviour in vivo. Adv Drug Deliv Rev 32:3

Dasaraju PV, Liu C (1996) Infections of the respiratory system. In: Baron S (ed) Medical microbiology, 4th edn. University of Texas Medical Branch, Galveston, TX

Doern GV, Heilmann KP, Huynh HK et al (2001) Antimicrobial resistance among clinical isolates of streptococcus pneumoniae in the United States during 1999–2000, including a comparison of resistance rates since 1994–1995. Antimicrob Agents Chemother 45:1721

Fagge CH, Pye-Smith PH (1891) Textbook of the principles and practice of medicine, 3rd edn. Churchill, London

Frankel A (1884) Über die genuine Pneumonie, Verhandlungen des Congress für innere Medicin. Ditter Congress 3:17

Friedlander C (1882) Über die Schizomyceten bei der acuten fibrösen Pneumonie. Virchow's Arch pathol Anat U Physiol 87:319

Garrison FH (1921) An introduction to the history of medicine, 3rd edn. Saunders, Philadelphia, PA

Gregoriadis G (1976) The carrier potential of liposomes in biology and medicine. N Engl J Med 295:765–770

Hernández-Caselles T, Villalaín J, Gómez-Fernández JC (1993) Influence of liposome charge and composition on their interaction with human blood serum proteins. Mol Cell Biochem 120:119

Hippocrates (1849) The genuine works of Hippocrates (trans: Adams F). Sydenham Society, London

Jay V (2000) The legacy of Laennec. Arch Pathol Lab Med 124:1420

Jones MN, Song YH, Kaszuba M et al (1997) The interaction of phospholipid liposomes with bacteria and their use in the delivery of bactericides. J Drug Target 5:25

Kingston GW, Phang PT, Leathley MJ (1991) Increased incidence of nosocomial pneumonia in mechanically ventilated patients with subclinical aspiration. Am J Surg 161:589
Klebs E (1875) Beiträge zur Kenntniss der pathogenen Schistomyceten. VII Die Monadinen. Arch Exptl Pathol Parmakol 4:40
Mandell LA, Wunderink RG, Anzueto A et al (2007) Infectious diseases society of America/American thoracic society consensus guidelines on the management of community-acquired pneumonia in adults. Clin Infect Dis 44:827
McIntosh K (2002) Community-acquired pneumonia in children. N Engl J Med 346:429
Meers P, Neville M, Malinin V et al (2008) Biofilm penetration, triggered release and in vivo activity of inhaled liposomal amikacin in chronic pseudomonas aeruginosa lung infections. J Antimicrob Chemother 61:859
Monroe D (2007) Looking for chinks in the armor of bacterial biofilms. PLoS Biol 5:e307
Moran M, Guzman J, Ropars AL et al (2009a) Neglected disease research and development: how much are we really spending? PLoS Med 6:e30
Moran M, Guzman J, Ropars AL et al (2009b) Neglected disease research and development: how much are we really spending? The George Institute for International Health, London
Mulholland EK, Simoes EA, Costales MO et al (1992) Standardized diagnosis of pneumonia in developing countries. Pediatr Infect Dis J 11:77
Oggioni MR, Trappetti C, Kadioglu A et al (2006) Switch from planktonic to sessile life: a major event in pneumococcal pathogenesis. Mol Microbiol 61:1196
Oja CD, Semple SC, Chonn A et al (1996) Influence of dose on liposome clearance: critical role of blood proteins. Biochim Biophys Acta 1281:31
Oku N, Tokudome Y, Namba Y et al (1996) Effect of serum protein binding on real-time trafficking of liposomes with different charges analyzed by positron emission tomography. Biochim Biophys Acta 1280:149
Orihuela CJ, Tuomanen E (2006) *Streptococcus pneumoniae*: invasion and inflammation. In: Fischetti V, Novick RP, Ferretti JJ et al (eds) Gram-positive pathogens, 2nd edn. ASM Press, Washington, DC
Osler W (1901) The principles and practice of medicine. Appleton, New York, NY
Pinto-Alphandary H, Andremont A, Couvreur P (2000) Targeted delivery of antibiotics using liposomes and nanoparticles: research and applications. Int J Antimicrob Agents 13:155
Ratner AJ, Weiser JN (2006) Pneumonia before antibiotics: therapeutic evolution and evaluation in twentieth-century America. J Clin Invest 116:2311
Rosner F (1998) The medical legacy of Moses Maimonides. KTAV Publishing House, Jersey City, NJ
Schiffelers RM, Storm G, Bakker-Woudenberg IA (2001b) Host factors influencing the preferential localization of sterically stabilized liposomes in Klebsiella pneumoniae-infected rat lung tissue. Pharm Res 18:780
Schiffelers RM, Storm G, ten Kate MT et al (2001a) In vivo synergistic interaction of liposome-coencapsulated gentamicin and ceftazidime. J Pharmacol Exp Ther 298:369
Schiffelers RM, Storm G, ten Kate MT et al (2001c) Therapeutic efficacy of liposome-encapsulated gentamicin in rat Klebsiella pneumoniae pneumonia in relation to impaired host defense and low bacterial susceptibility to gentamicin. Antimicrob Agents Chemother 45:464
Scott JA, Hall AJ, Muyodi C et al (2000) Aetiology, outcome, and risk factors for mortality among adults with acute pneumonia in Kenya. Lancet 355:1225
Senior JH, Trimble KR, Maskiewicz R (1991) Interaction of positively-charged liposomes with blood: implications for their application in vivo. Biochim Biophys Acta 1070:173
Smith AW (2005) Biofilms and antibiotic therapy: is there a role for combating bacterial resistance by the use of novel drug delivery systems? Adv Drug Deliv Rev 57:1539
Speizer FE, Horton S, Batt J et al (2006) Respiratory diseases of adults. In: Jamison DT, Breman JG, Measham AR et al (eds) Disease control priorities in developing countries, 2nd edn. IBRD/The World Bank and Oxford University Press, Washington, DC
Stewart PS, Costerton JW (2001) Antibiotic resistance of bacteria in biofilms. Lancet 358:135

Sutherland IW (2001) The biofilm matrix – an immobilized but dynamic environment. Trends Microbiol 9:222

Van Etten EW, Stearne-Cullen LE, ten Kate M et al (2000) Efficacy of liposomal amphotericin B with prolonged circulation in blood in treatment of severe pulmonary aspergillosis in leukopenic rats. Antimicrob Agents Chemother 44:540

Weers J, Metzheiser B, Taylor G et al (2009) A gamma scintigraphy study to investigate lung deposition and clearance of inhaled amikacin-loaded liposomes in healthy male volunteers. J Aerosol Med Pulm Drug Deliv 22:131

World Health Organization (2008) The global burden of disease: 2004 update. WHO Press, Geneva

Chapter 5
COPD

Chronic obstructive pulmonary disease (COPD) is the fourth leading cause of death worldwide. In 2004, COPD was responsible for 3.02 million deaths or 5.1% of all deaths globally (World Health Organization 2008). COPD may account for more than 10% of lost disability-adjusted life years on a worldwide basis (Speizer et al. 2006). The global prevalence of COPD is significant: at any given time, 63.6 million individuals worldwide suffer from COPD. Of these COPD sufferers, 26.6 million experience moderate to severe disability as a result of the disease. This makes COPD the tenth most frequent cause of disability in the world (World Health Organization 2008). COPD is mainly a disease of older adults: more than 95% of all COPD-related deaths occur in people older than age 55 (Beers et al. 2006). Much of COPD can be attributed to cigarette smoking, and there is no question that smoking cessation can prevent further decline in pulmonary function. Yet air pollution is also an important trigger for COPD, particularly in developing countries. Both smoking-related COPD and pollution-related COPD are irreversible, and pulmonary function that is already lost cannot be regained. The disease is progressive; patients experience shortness of breath and exercise limitations which gradually and inevitably worsen over time, stressing the cardiopulmonary system. Patients with COPD typically die of respiratory failure, cardiovascular complications, or co-existing cancer. Importantly, COPD is an independent risk factor for cardiovascular disease (Maclay et al. 2007). In fact, COPD often develops together with one or more comorbid conditions and almost never occurs alone (Luppi et al. 2008). Currently available treatments for COPD are primarily symptomatic therapies, including pulmonary rehabilitation; bronchodilators to improve airflow; corticosteroids to reduce inflammation; and supplemental oxygen. These interventions cannot stop the eventual worsening of COPD. However, emerging biomaterials for lung regeneration can potentially replace lung tissue that has been destroyed by COPD, ultimately reducing morbidity and mortality from this relentless disease.

5.1 Historical Perspective on COPD

Over time, the clinical understanding of COPD has evolved and grown, such that the disease is currently understood to encompass both emphysema (alveolar destruction

S.K. Bhatia, *Biomaterials for Clinical Applications*,
DOI 10.1007/978-1-4419-6920-0_5, © Springer Science+Business Media, LLC 2010

with enlargement of air spaces) and chronic bronchitis (inflammation with mucus production). One of the earliest references to emphysema was made in 1679, when the Swiss physician Theophile Bonet described a condition of "voluminous lungs" (Bonet 1679). In 1769, the Italian anatomist Giovanni Morgagni reported 19 cases of emphysema in which the lungs were "turgid," particularly from air (Morgagni 1769). By the early nineteenth century, the chronic bronchitis component of COPD began to be recognized. In 1814, the British doctor Charles Badham used the term "catarrh" to describe chronic cough and mucus hypersecretion, now known as cardinal symptoms of chronic bronchitis (Badham 1814). He described chronic bronchitis as a disabling disorder.

In 1821, the French physician Rene Laennec, known as "the father of pulmonary medicine" for inventing the stethoscope, recognized that emphysematous lungs were hyperinflated and did not empty well and verified the disease using the stethoscope. Laennec described the pathological appearance of emphysematous lungs: "In opening the chest, it is not unusual to find that the lungs do not collapse but they fill up the cavity completely on each side of the heart. When experienced, this will appear full of air" (Laënnec 1821). In addition, he described pathological indications of chronic bronchitis: "The bronchus of the trachea are often at the same time filled with mucus fluid" (Laënnec 1821). By the twentieth century, airflow limitation and shortness of breath were appreciated as central symptoms of COPD. In 1944, the London physician Ronald Christie synthesized the clinical definition of COPD and suggested that the diagnosis should be considered "when dyspnea on exertion, of insidious onset, not due to bronchospasm, or left ventricular failure, appears in a patient who has some physical signs of emphysema together with chronic bronchitis" (Christie 1944). In pathological studies, Christie noted that "the large fluffy lungs strongly suggest that during life there is an increase in the amount of air they contain" (Christie 1944). It was soon recognized that COPD was associated with reductions in forced expiratory volume from the lungs, as measured by spirometry. Patients with the most rapid rate of decline in forced expiratory volume had the worst prognosis, a phenomenon known as the "Horse Racing Effect" (Burrows et al. 1987). This discovery also established the importance of early identification and treatment for COPD.

5.2 Pathology of COPD

COPD is a disease state characterized by persistent obstruction of the airways, occurring with emphysema, chronic bronchitis, or both conditions. In a normal lung, the small airways (bronchioles) contain smooth muscles and are held open by their attachments to alveolar walls. However, a lung affected by COPD bears obstructed airways (Fig. 5.1), so that there is a permanent decrease in the rate of airflow from the lungs when the patient breathes out (exhales). The airflow obstruction of COPD is not fully reversible and typically worsens over time. The poor reversibility of COPD distinguishes it from asthma, in which the airflow obstruction is completely reversible either spontaneously or with treatment. COPD is also known as chronic obstructive lung disease (COLD), chronic obstructive airway disease

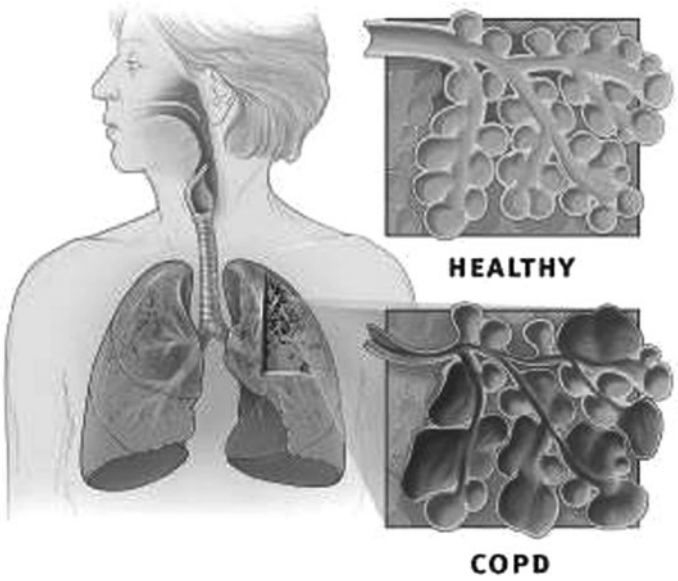

Fig. 5.1 Diagram of normal alveoli in healthy lung versus damaged alveoli in a COPD lung (National Heart, Lung, and Blood Institute)

(COAD), chronic airflow limitation (CAL), and chronic obstructive respiratory disease.

COPD is induced by cigarette smoke and/or other noxious particles and gases which irritate the airways (Fig. 5.2). Cigarette smoking is the most important risk

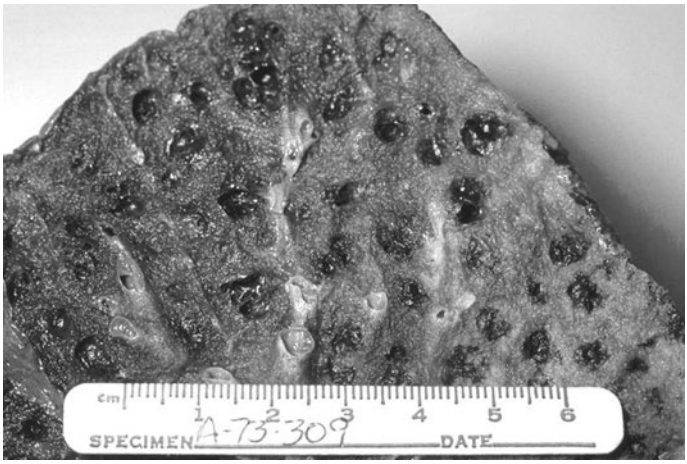

Fig. 5.2 Gross pathology of lung showing COPD characteristic of smoking. This close-up image of the fixed, cut surface of the lung shows multiple cavities lined by heavy *black* carbon deposits (Centers for Disease Control)

factor for COPD; continuous smokers have a 25% risk of developing COPD after 25 years of smoking (Løkke et al. 2006). The likelihood of developing COPD increases with increasing age as the cumulative smoke exposure increases. However, indoor air pollution also raises the risk of disease. COPD is recognized to have the greatest socioeconomic inequality of any common disease and is commonly a disease of the poor, suggesting that environmental factors other than smoking contribute to disease risk (Barnes 2007). In particular, over 10% of patients with a clinical diagnosis of COPD are non-smokers. This proportion is much higher among women in developing countries such as India, where exposure to cooking fire smoke (often using coal or biomass fuels such as wood and animal dung) in an enclosed space is an important cause of COPD (Smith 2000); this exposure begins during childhood and continues into adult life. Outdoor air pollution is an additional risk factor, as evidenced by the higher rate of COPD in urban areas as compared to rural areas (Halbert et al. 2006). Long-term occupational exposures have been implicated in the development of COPD in non-smokers; such intense and prolonged exposures include workplace dusts found in coal mining, gold mining, and the cotton and textile industry, and chemicals such as cadmium, isocyanates, and fumes from welding (Devereux 2006). Finally, genetic susceptibility (especially inherited alpha-1-antitrypsin deficiency), repeated lung infections, and autoimmune mechanisms play a role in the development of COPD.

COPD includes the diagnoses of chronic bronchitis and emphysema, and many patients have both disorders (Beers et al. 2006). Chronic bronchitis and emphysema each have distinct clinical and pathological manifestations, yet both result in airflow obstruction (Fig. 5.3). Chronic bronchitis is diagnosed based on clinical parameters; specifically, chronic bronchitis is defined as a persistent cough with

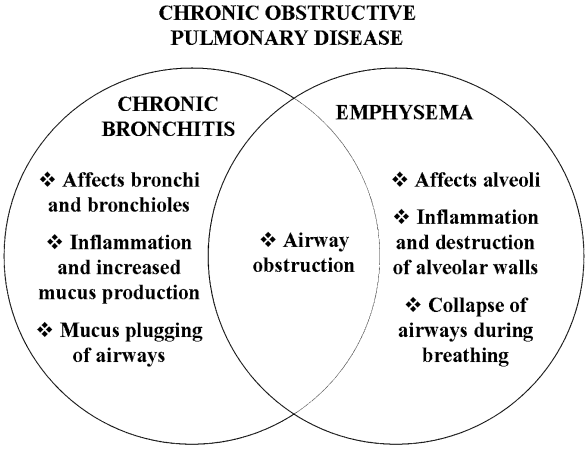

Fig. 5.3 Diagram of the pathologies of chronic bronchitis and emphysema. Both disease processes lead to airflow obstruction. The diagnosis of COPD includes chronic bronchitis and emphysema; many patients have both disorders

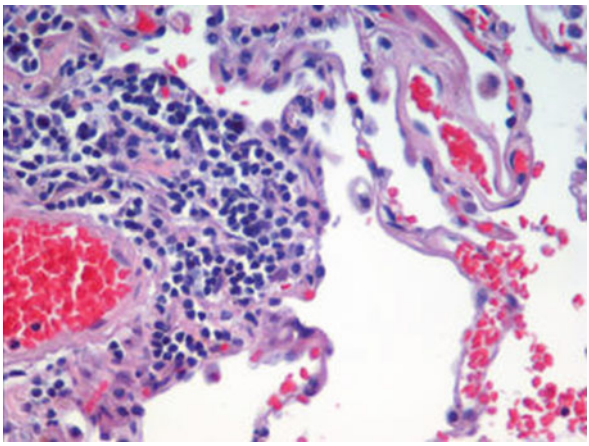

Fig. 5.4 Microscopic image showing infiltration of inflammatory lymphocytes (*stained blue*) into the lung of a patient with severe COPD (Public Library of Science 2004)

sputum production on most days for 3 months a year, for two consecutive years. The pathologic changes of chronic bronchitis are found in the large airways (bronchi) and bronchioles of the lung. During chronic bronchitis, inflammatory cells infiltrate the walls of the bronchi and bronchioles in response to inhaled irritants. The histologic hallmarks of chronic bronchitis are increased numbers (hyperplasia) of mucus-secreting goblet cells and increased volume (hyperplasia) of mucus glands in the airway. As a result, there is an abnormally large amount of mucus in the airways, which blocks airflow. Inflammation causes the smooth muscle surrounding the bronchioles to contract (spasm), further obstructing airflow. Chronic bronchitis eventually leads to scarring, remodeling, and fibrosis, which contribute to narrowing of the airways and limitations in airflow. Emphysema, on the other hand, is diagnosed based on morphologic parameters and is defined as an abnormal permanent enlargement of the airspaces distal to the terminal bronchioles, accompanied by destruction of the alveolar walls in the lung. During emphysema, the inflammatory response occurs within alveoli and results in damage to alveolar surfaces (Fig. 5.4). The obliteration of alveolar walls leads to fewer and larger air sacs instead of many tiny ones. This reduces the surface area available for oxygen exchange during breathing and reduces the elasticity of the lung itself. As a consequence, the small airways are no longer supported by the elastic recoil of alveolar septa; the air sacs lose their shape and integrity and are more likely to collapse during breathing (Fig. 5.5). The collapsing bronchioles ultimately limit airflow. In addition, the dilated airspaces may enlarge to a size greater than 2 cm in dimension. These enlarged airspaces, also called bullae, may be clinically important because of their tendency to rupture.

Symptoms of COPD typically appear in middle age and slowly worsen with time (Beers et al. 2006). One of the most common symptoms of COPD is shortness of breath (dyspnea); patients often first notice dyspnea during vigorous exercise, when the demands on the lungs are greatest, or during a lung infection. Over

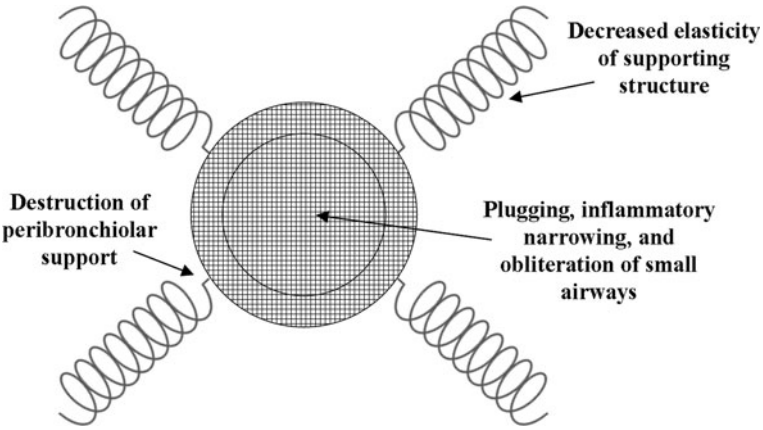

Fig. 5.5 Diagram describing the mechanisms of airflow obstruction in COPD due to the loss of elastic recoil and airway narrowing

time, particularly if patients with COPD continue to smoke, dyspnea becomes more troublesome and occurs during milder everyday activities such as housework. Eventually, dyspnea can become severe, occurring during rest. Patients may also develop a mild cough that produces clear sputum. Cough and sputum production persist, and pneumonia and other lung infections occur more frequently. *(Biomaterials for controlled delivery of antibiotics to pneumonia biofilms could thus find utility for treating lung infections during COPD. These biomaterials include liposomal carriers, which are discussed in Section 4.3 of* Chapter 4.) The color of the sputum changes from clear or white to yellow or green. Other symptoms of COPD include wheezing, chest tightness, and tiredness and headaches due to retention of carbon dioxide. COPD patients experience "flare-ups" or acute worsening of symptoms, triggered by severe air pollution, common allergens, and viral or bacterial infections. During flare-ups, patients exhibit extreme dyspnea (a feeling likened to being drowned), anxiety, sweating, confusion, and bluish discoloration of the skin (cyanosis) due to a lack of oxygen in the blood. People with COPD may intermittently cough up blood (hemoptysis), which is usually induced by inflammation in the bronchi (Beers et al. 2006). Approximately one third of COPD patients also experience severe weight loss, partially because severe dyspnea interferes with eating and partially because of heightened inflammatory factors in the bloodstream (Beers et al. 2006).

Upon clinical examination, patients with COPD may demonstrate a rapid breathing rate, as well as active use of muscles in the neck to aid in breathing. Patients also display unusual breathing patterns, such that expiration takes a longer time than inspiration. Some patients breathe through pursed lips and make an increased effort during exhalation. If airflow is very limited, an individual with COPD may be unable to completely finish breathing out before needing to take another breath. As a result, a portion of the air from the previous breath remains trapped within

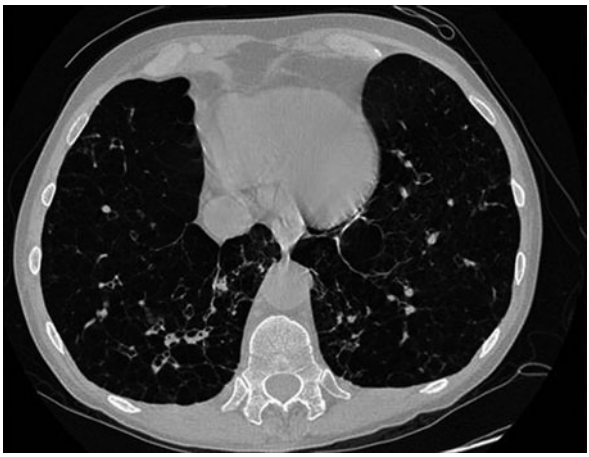

Fig. 5.6 CT scan showing destruction of alveolar walls in the lung of a patient with severe COPD (Public Library of Science 2004)

the lungs when the next breath is started, a physiologic state known as dynamic hyperinflation (Calverley and Koulouris 2005). Individuals affected by COPD may develop a barrel-shaped chest, caused by air trapping and enlargement (hyperinflation) of the lungs. Breathing is uncomfortable for patients with hyperinflated lungs, as it takes more work to move the chest and lungs when they are already stretched by hyperinflation (O'Donnell 2006). Stethoscope examination reveals decreased breath sounds, wheezes, crackles, and prolonged expiration. The chest x-ray may show over-inflation of the lungs, and a CT scan may reveal destruction of alveolar walls with enlargement of airspaces (Fig. 5.6). Moreover, blood gas measurements may show low oxygen levels (hypoxemia) and high carbon dioxide levels (respiratory acidosis) and a high red blood cell count (reactive polycythemia) as a reaction to long-term hypoxemia.

The diagnosis of COPD is confirmed by spirometry (Rabe et al. 2007), a test that measures breathing volumes (Fig. 5.7). Under normal circumstances, the two human lungs hold a combined 6 l of gas, of which 3.7 l is the maximum inspirational capacity and 2.3 l is residual capacity (Freitas 1999). In COPD, the greatest reduction in airflow occurs during expiration, as the pressure in the chest tends to compress rather than expand the airways. Airflow can be increased by breathing more forcefully, thereby increasing the pressure in the chest during expiration. However, COPD patients are limited in their ability to increase airflow with force, a physiologic condition known as expiratory flow limitation (Calverley and Koulouris 2005). A spirometry test measures the forced expiratory volume in 1 s (FEV_1), which is the greatest volume of air that can be exhaled in the first second of a deep breath. In addition, spirometry measures the forced vital capacity (FVC), which is the greatest volume of air that can be exhaled in a complete deep breath. In a normal individual, at least 70% of the FVC is exhaled in the first second (the FEV_1/FVC ratio is >70%). In an individual with COPD, this ratio is less than normal (the FEV_1/FVC ratio is <70%), even after treatment with bronchodilator medications. An FEV_1/FVC ratio

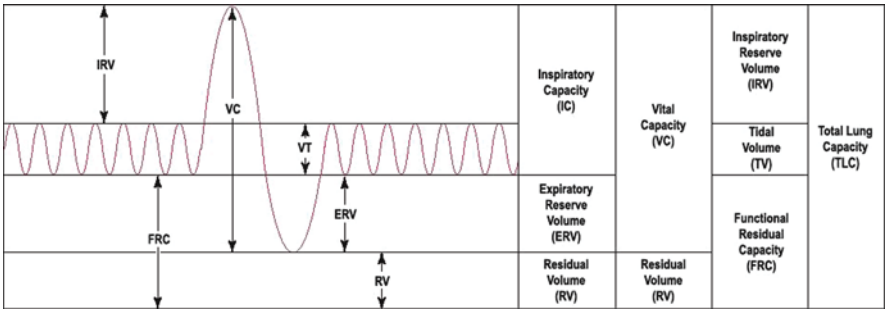

Fig. 5.7 Typical output of a spirometry recording. The *vertical axis* represents the lung volume and the *horizontal axis* represents time. The first small amplitude part of the sinusoid depicts repeated involuntary breathing during the resting state. The amplitude of this small sinusoid corresponds to the "Tidal Volume." The large positive amplitude spike represents voluntary inspiration to maximal volume or "Total Lung Volume." The large negative amplitude spike represents forced expiration to the lowest possible physiological lung volume called "Residual Volume"

of <70% heralds the onset of rapid declines in FEV_1 over the course of a 10-year period (Burrows et al. 1987). Spirometry also determines the severity of COPD, as outlined in Table 5.1. The FEV_1 is measured post-bronchodilator treatment and is expressed as a percentage of a predicted normal value, based on a patient's age, gender, height, and weight. The severity of COPD additionally depends on the severity of dyspnea and exercise limitation. The time course of COPD development is long; 30 or more years of progressive loss in airflow may take place before the threshold to dyspnea on exertion occurs.

As mentioned previously, COPD almost never occurs in isolation and is associated with several comorbid diseases. The most common comorbidities of COPD that are possibly related to the systemic effects of smoking are congestive heart failure, cardiac arrhythmias, hypertension, peripheral and coronary artery diseases, diabetes and metabolic syndrome, osteoporosis, cancer (particularly lung cancer), pulmonary vascular abnormalities, psychiatric disorders (especially depression as a result of activity limitation), and skeletal muscle abnormalities. Arterial wall stiffness and blood pressure are increased in patients with COPD compared with control subjects who smoke (Mills et al. 2008), and it has been suggested that COPD results in systemic vascular dysfunction. This may be the mechanism for enhanced

Table 5.1 Classification of COPD severity based on FEV_1 measurements

Severity of COPD	FEV_1 % predicted
Mild	≥80
Moderate	50–79
Severe	30–49
Very severe	<30 or chronic respiratory failure symptoms

Rabe et al. (2007)

cardiovascular risk in COPD. *(Biomaterials for treatment of coronary artery disease and congestive heart failure could thus find utility for preventing mortality from COPD. These biomaterials include bioactive stents, degradable stents, and tissue-engineered cardiac constructs, which are discussed in Chapter 2.)* The FEV_1 is an independent predictor of all-cause mortality (Schunemann et al. 2000) and a strong risk factor for the development of cardiovascular disease, stroke, and lung cancer (Cook et al. 1994). Other factors that predict a poorer prognosis are severe dyspnea, limited exercise capacity, continued smoking, frequent acute exacerbations, and a significant weight loss or weight gain (Rabe et al. 2007). Progressive respiratory failure accounts for approximately one third of COPD-related deaths; cardiovascular complications and lung cancer are responsible for much of the remainder of COPD-related deaths (Luppi et al. 2008).

Contemporary treatment strategies for COPD, both pharmacologic and non-pharmacologic, are mainly supportive and not curative. The main achievable goals of COPD management include relief from symptoms, improvement of exercise tolerance and quality of life, and prevention and management of exacerbations. Bronchodilators, particularly inhaled bronchodilators, are the chief pharmacologic treatment for COPD. These drugs are used on an as-needed basis to relieve intermittent or worsening symptoms and on a regular basis to suppress persistent symptoms and prevent flare-ups. Inhaled corticosteroids are also utilized to decrease inflammation, but long-term use of these medications leads to serious systemic side effects, such as reduced bone density. Pulmonary rehabilitation, including respiratory therapy techniques, exercise conditioning, and activities of daily living can improve outcomes and alleviate the systemic effects of COPD. Long-term supplemental oxygen therapy is one of the most effective interventions for COPD and reduces mortality from all causes in patients with hypoxemic COPD (Croxton and Bailey 2006). In addition to its effect on mortality, long-term oxygen therapy reduces dyspnea, polycythemia, pulmonary artery pressures, sleep disorders, nocturnal cardiac arrhythmias, and neuropsychiatric abnormalities and improves exercise tolerance. This suggests that improved oxygen delivery has effects far beyond the lungs, so strategies that facilitate oxygenation can have the greatest effect on morbidity and mortality. However, currently available COPD treatments cannot reverse damage to the lungs; the only option for patients with advanced respiratory failure is lung transplantation, and most patients will succumb to disease before a lung transplant becomes available. For these reasons, there is rising interest in biomaterials as scaffolds for lung regeneration, which can restore lung parenchyma that has been lost to COPD. The following section discusses emerging biomaterials for tissue engineering of the lungs.

5.3 Biomaterials for Lung Regeneration

Biomaterial constructs for lung tissue engineering, composed of tissue-specific cells along with polymer matrices, are a promising technology for regenerating and replacing damaged lung. For patients stricken by COPD, such biomaterials could

increase airflow, improve oxygen delivery, reduce systemic side effects of hypoxemia, avoid complications of drug therapy, and ultimately decrease mortality. Unlike existing treatment methods for COPD, the regeneration of native lung tissue offers a permanent solution by restoring lung function. The general strategy for lung tissue engineering is similar to that of cardiac tissue engineering *(discussed in more detail in Chapter 2, Section 2.5)*: lung cells and other progenitor cells are seeded onto a three-dimensional polymeric scaffold to form a precursor tissue structure. The polymer matrix provides support and structure for the cells, while the cells contribute biological functionality. The scaffold may take the form of a mesh, sheet, or tubular structure, and it may be formed from natural or synthetic materials. The construct may also incorporate growth factors to stimulate the expansion of desirable cell populations. Upon implantation, the tissue-engineered construct guides the growth and development of new lung, and the polymer scaffold degrades away to be replaced by healthy functioning lung. An optimal biomaterial for lung regeneration enhances cell attachment, proliferation, and differentiation into desirable cell populations. To initiate tissue renewal, the biomaterial must integrate with the host tissue and promote in vivo angiogenesis to ensure adequate oxygen supply. The implant ultimately must achieve a three-dimensional structure with the potential to connect to the existing airways for ventilation and to blood vessels for gas exchange. At the same time, the implanted biomaterial must safely degrade at a rate similar to that of new lung formation, such that the biomaterial scaffold is eventually removed from the body by natural metabolic processes. The biomaterial is essentially a temporary structure that stimulates re-growth of native lung, and the biomaterial disappears once it has served its therapeutic function and healing is complete.

The development of tissue-engineered lung presents special challenges due to the complex structure of the pulmonary system. The lung itself is composed of both upper and lower respiratory tract; the large and small airways are together affected by COPD, and each must be restored. Structurally, the human airway consists of successive branching segments; and each branch gives rise to two smaller daughter branches. There are more than 20 generations of branchings in the lungs, each resulting in narrower, shorter, and more numerous tubes. Generations 0–16 are the conducting airways, while generations 17–23 constitute the respiratory airways; generation 23 terminates in alveoli.(Frietas 1999) Quantitative measurements of the length and diameter of the pulmonary airways are given in Table 5.2. The cross-sectional area and volumetric capacity of the pulmonary segments are given in Table 5.3. Air speeds and the Reynolds numbers for airflow through each pulmonary branch are shown in Table 5.4.

The anatomy and physiology of the upper and lower airway are different, as are the cell types found there. There are over 40 distinct cell types in the respiratory tract (Nichols and Cortiella 2008). The most important mature cell lineages within functional lung include ciliated epithelial cells, smooth muscle cells, endothelial cells, Clara cells, and specialized pneumocytes (Fig. 5.8). The bronchiole walls are composed of smooth muscle and connective tissue; the smooth muscle normally remains relaxed so that the bronchioles remain open. The bronchioles are lined with ciliated columnar epithelial cells (Fig. 5.9). The cilia wave constantly toward the

Table 5.2 Diameter and length measurements of the human pulmonary system

Pulmonary branch	Generation	Number	Branch diameter (mm)	Branch length (mm)	Cumulative length (mm)
Trachea	0	1	18	120.0	120
Main bronchus	1	2	12.2	47.6	167
Lobar	2	4	8.3	19.0	186
bronchus	3	8	5.6	7.6	194
Segmental	4	16	4.5	12.7	206
bronchus	5	32	3.5	10.7	217
Bronchi	6	64	2.8	9.0	226
with cartilage	7	128	2.3	7.6	234
in wall	8	256	1.86	6.4	240
	9	512	1.54	5.4	246
	10	1,020	1.30	4.6	250
Terminal	11	2,050	1.09	3.9	254
bronchus					
Bronchioles	12	4,100	0.95	3.3	257
with muscle	13	8,190	0.82	2.7	260
in wall	14	16,400	0.74	2.3	262
	15	32,800	0.66	2.0	264
Terminal	16	65,500	0.60	1.65	266
bronchiole					
Respiratory	17	131×10^3	0.54	1.41	267
bronchioles	18	262×10^3	0.50	1.17	269
	19	524×10^3	0.47	0.99	270
Alveolar duct	20	1.05×10^5	0.45	0.83	271
Alveolar duct	21	2.10×10^5	0.43	0.70	271
Alveolar duct	22	4.19×10^5	0.41	0.59	272
Alveolar sac	23	8.39×10^5	0.41	0.50	273
Alveoli, 21 per duct	–	300×10^6	0.28	0.23	273

Measurements are the average of two normal human lungs; includes both lungs
Freitas (1999)

pharynx, moving secreted mucus at a rate of 1.4 cm/min to replace the entire mucoid coating once every 20 min (Freitas 1999). In contrast, the alveolar wall consists of a narrow connective tissue core that contains fibroblasts, myofibroblasts, capillary endothelial cells, and extracellular matrix components such as elastin. The alveolar epithelium is made up of type I and type II epithelial cells also known as pneumocytes. The alveolar type I cells form the actual gas–blood exchange barrier; the moist air-facing surfaces of the alveolar wall are lined by a continuous layer, one cell thick, of squamous type I epithelial cells. The alveolar surface contains smaller numbers of thicker specialized type II epithelial cells that secrete surfactant (a complex of protein with dipalmityl lecithin) in a fluid layer approximately 70 nm thick, which physically stabilizes alveoli during inflation and deflation (Freitas 1999). Because of the intricacy of lung histology and lung architecture, the selection of an appropriate cell source for lung tissue engineering is critical. The selected cell types must

Table 5.3 Area and volume measurements of the human pulmonary system

Pulmonary branch	Generation	Number	Cross-sectional area (cm^2)	Volume (cm^3)	Cumulative volume (cm^3)
Trachea	0	1	2.6	31	21
Main bronchus	1	2	2.3	11	42
Lobar bronchus	2	4	2.2	4	46
	3	8	2.0	2	47
Segmental	4	16	2.6	3	51
bronchus	5	32	3.1	3	54
Bronchi with	6	64	4.0	4	57
cartilage in wall	7	128	5.1	4	61
	8	256	7.0	4	66
	9	512	9.6	5	71
	10	1,020	13	6	77
Terminal bronchus	11	2,050	19	7	85
Bronchioles	12	4,100	29	10	95
with muscle in	13	8,190	44	12	106
wall	14	16,400	70	16	123
	15	32,800	113	22	145
Terminal bronchiole	16	65,500	180	30	175
Respiratory	17	131×10^3	300	42	217
bronchioles	18	262×10^3	534	61	278
	19	524×10^3	944	93	370
Alveolar duct	20	1.05×10^5	1,600	139	510
Alveolar duct	21	2.10×10^5	3,200	224	734
Alveolar duct	22	4.19×10^5	5,900	350	1,085
Alveolar sac	23	8.39×10^5	12,000	591	1,675
Alveoli, 21 per duct	–	300×10^6	–	3,200	4,800

Measurements are the average of two normal human lungs; includes both lungs
Freitas (1999)

reliably differentiate along specific lineages and provide sufficient numbers of cells for tissue growth. An engineered construct can be as simple as replication of the distal alveolar epithelia or as complex as a fully functional replacement tissue that includes both distal lung and branching airways.

With regard to cell sources, two main approaches have been utilized to cultivate lung tissue containing the necessary cellular diversity for proper function. The first method uses mixtures of adult-derived somatic, uni-potent progenitor cells. Adult progenitor cells reside in adult tissues and organs, and they have the capacity to differentiate into a restricted number of cell lineages. In formulations of adult uni-potent progenitor cells, each progenitor gives rise to an array of lung-specific single-cell lineages. For instance, a mixed population of somatic lung progenitor cells has been seeded onto synthetic scaffolds composed of polyglycolic acid or pluronic F127 (Cortiella et al. 2006). When implanted in vivo, the cells expressed

Table 5.4 Air speeds and Reynolds numbers for airflow through the human pulmonary system

Pulmonary branch	Generation	Number	Air speed (cm/s)	Reynolds number
Trachea	0	1	393	4,350
Main bronchus	1	2	427	3,210
Lobar bronchus	2	4	462	2,390
	3	8	507	1,720
Segmental bronchus	4	16	392	1,110
	5	32	325	690
Bronchi with cartilage	6	64	254	434
in wall	7	128	188	277
	8	256	144	164
	9	512	105	99
	10	1,020	73.6	60
Terminal bronchus	11	2,050	52.3	34
Bronchioles with	12	4,100	34.4	20
muscle in wall	13	8,190	23.1	11
	14	16,400	14.1	6.5
	15	32,800	8.92	3.6
Terminal bronchiole	16	65,500	5.40	2.0
Respiratory bronchioles	17	131×10^3	3.33	1.1
	18	262×10^3	1.94	0.57
	19	524×10^3	1.10	0.31
Alveolar duct	20	1.05×10^5	0.60	0.17
Alveolar duct	21	2.10×10^5	0.32	0.08
Alveolar duct	22	4.19×10^5	0.18	0.04
Alveolar sac	23	8.39×10^5	0.09	–
Alveoli, 21 per duct	–	300×10^6	–	–

Measurements are the average of two normal human lungs; includes both lungs; air speed and Reynolds number at 1 l/s flow
Freitas (1999)

lung-specific markers for Clara cells, pneumocytes, and respiratory epithelium and organized into identifiable pulmonary structures (including those similar to alveoli and terminal bronchi), with evidence of smooth muscle development. Other possible sources of somatic progenitor cells for lung tissue engineering include bronchioalveolar duct junction cells, which include bronchioalveolar stem cells (Kim et al. 2005) and variant Clara cells (Giangreco et al. 2002). Bone marrow-derived stem cells have also been shown to engraft in the lung and differentiate into lung cell lineages (Krause et al. 2001). The generation of new lung tissue derived from adult progenitor cells is advantageous, because it offers the possibility of autologous therapy with a patient's own somatic cells. The approach minimizes risks of disease transmission and implant rejection and avoids the use of immunosuppressive drugs with their concomitant side effects.

The second method for generating lung tissue employs multi-potent cells such as embryonic stem cells or fetal lung cells. Embryonic stem cells are formed from early embryos and possess the ability to differentiate into every cell type in the body. Within such formulations, the original cellular population can give rise to

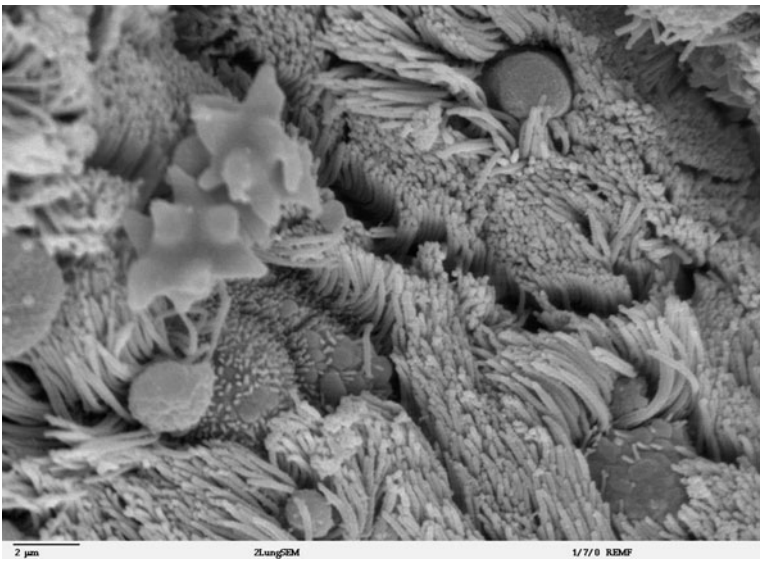

Fig. 5.8 Scanning electron microscope image of lung epithelium, illustrating the structural complexity of pulmonary tissue. The epithelium consists of ciliated and non-ciliated bronchiolar cells. Non-ciliated bronchiolar cells are called Clara cells. There are red blood cells on the surface of the epithelium (Louisa Howard and Charles Daghlian, Dartmouth College)

progeny with multiple cellular phenotypes. Cells derived from fetal lung tissue have been shown to produce mature lung cell lineages (Nichols and Cortiella 2009). Embryonic stem cells have also demonstrated the ability to differentiate into distal lung epithelial lineages such as type II pneumocytes (Rippon et al. 2006). Moreover, embryonic stem cells have been differentiated into upper airway lineages, including ciliated cells and Clara cells (Coraux et al. 2005). Though these multi-potent cells have shown promise for pulmonary regeneration, a major barrier to adoption of fetal tissue or embryonic stem cells is host compatibility. Tissues produced from such sources would need to be human leukocyte antigen (HLA) matched to prevent host rejection of the engineered lung construct. If a perfect HLA or tissue match were not available, immunosuppressive treatment of the patient would be required. Another challenge for lung tissue engineering, both from embryonic and adult-derived stem cells, is that the growth factors which drive lung development are not well understood. Currently, the production of engineered lung tissue requires significant cellular expansion, manipulation, and culture time in vitro, before cell matrices or tissues can form.

In addition to the selection of an appropriate cell source, a further consideration for lung tissue engineering is the choice of scaffold material. Both the elasticity of the scaffold and the adsorption kinetics of the material are critical for lung tissue development. In terms of mechanical properties, the scaffolding must support cell proliferation and initial tissue growth without impeding the elasticity or altering the

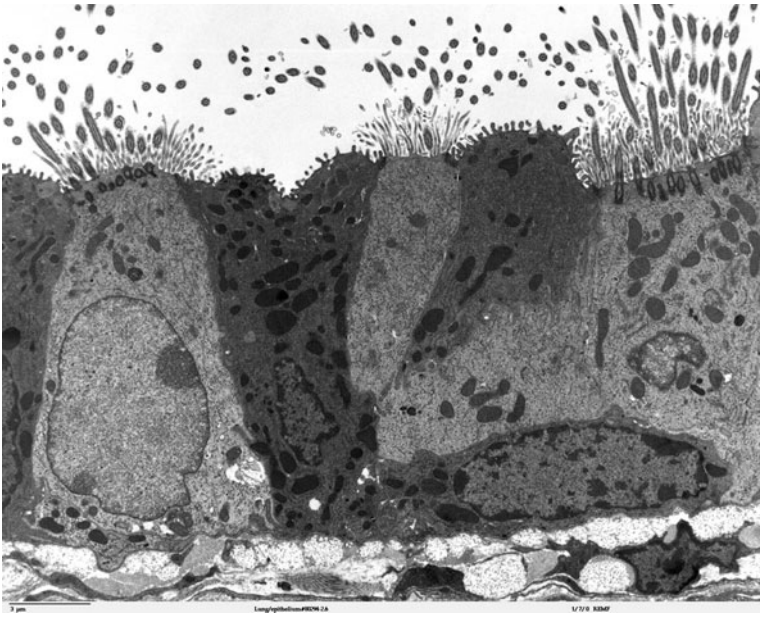

Fig. 5.9 Transmission electron microscope image of lung epithelium, illustrating the variety of cell populations in pulmonary tissue. The bronchiolar epithelium consists of ciliated cells and non-ciliated Clara cells. The image shows the ciliary microtubules in transverse and oblique section. In the cell apex are the basal bodies that are the anchoring sites for the ciliary axonemes. The difference in size and shape between the microvilli and the cilia is notable (Louisa Howard and Michael Binder, Dartmouth College)

elastic recoil of the engineered tissue construct. Tissue-engineered lung implants need to be flexible, stretchable, and compressible during breathing. In addition, the polymer scaffold must not compromise the elasticity of the adjacent lung tissue. If the selected biomaterial does not match the elasticity of native pulmonary structures, the implant can contribute to restrictions in lung expansion and airflow. In terms of adsorption kinetics, the biomaterial scaffold must support movement of nutrients into the tissues and waste removal away from tissues. The porosity of the scaffold influences its adsorption properties; materials with interconnected micropores are desirable for lung tissue engineering (Nichols and Cortiella 2008). The pore size of scaffolds ideally should be similar to that of alveolar units (Andrade et al. 2007). Moreover, the polymer material must provide sufficient surface area to promote cell seeding and cell movement within the scaffold, with subsequent cellular attachment. The construct must simultaneously allow interactions of cells in three dimensions to permit cell-to-cell signaling. A final concern, particularly for regenerating lung for COPD patients, is that the scaffold must not limit the size of the natural airway. Any material that imposes size restrictions on the airway will only add to the existing obstructive problems. It has been proposed that a complex organ such as the lung may eventually require the creation of hybrid scaffolds, formed from more than one material to meet all biological, physical, and mechanical requirements.

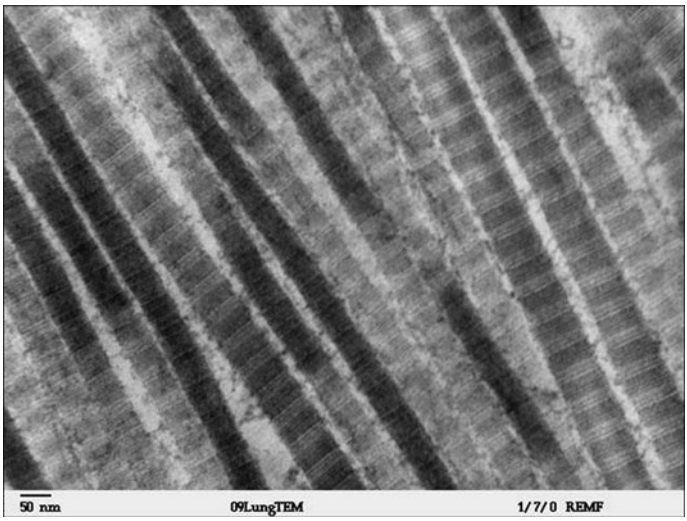

Fig. 5.10 Transmission electron microscope image of a thin section cut through an area of mammalian lung tissue. The high magnification image of connective tissue area shows fibers of Collagen Type I (Louisa Howard, Dartmouth College)

Both natural and synthetic polymers have been evaluated for lung regeneration. Natural materials utilized in lung tissue engineering include collagen, Matrigel, Gelfoam, and Englebreth-Holms tumor basement membrane. For instance, collagen is a component of native lung tissue (Fig. 5.10). A collagen gel matrix seeded with alveolar type II pneumocytes has been shown to reconstruct alveolus-like structures in vitro (Sugihara et al. 1993). Collagen gels incorporating bronchial fibroblasts can also reproduce bronchial mucosa in vitro (Chakir et al. 2001). Human distal lung epithelial cells and human microvascular endothelial cells have been co-cultured on permeable collagen filters to recreate the alveolar–capillary barrier in vitro (Hermanns et al. 2004). Mixed populations of fetal pulmonary cells have additionally been successfully cultured on three-dimensional collagen constructs in vitro (Mondrinos et al. 2007); stimulation of these cells with different forms of fibroblast growth factor resulted in different patterns of lung cell development. The combination of fibroblast growth factors 2, 7, and 10 enhanced cellular proliferation and induced robust budding of the pulmonary epithelial structures in the collagen gels, as well as the formation of a uniform vascular endothelial network parallel to those structures (Mondrinos et al. 2007). The tissues within the collagen constructs produced several markers of distal lung, including cytokeratin, pro- surfactant protein B, pro- surfactant protein C, tropoelastin, and endothelial CD31.

Matrigel, a scaffold composed of basement membrane proteins, has also been employed to culture a wide variety of pulmonary cells. Mixed populations of murine fetal pulmonary cells containing epithelial, mesenchymal, and endothelial cells can be incorporated into Matrigel and can stimulate pulmonary tissue formation when introduced in vivo into mouse models (Mondrinos et al. 2008). The Matrigel

scaffold was shown to support both development of lung epithelia and vascularization of the construct. When Matrigel constructs containing fetal pulmonary cells were supplemented with fibroblast growth factor-2, the tissues developed ductal epithelial structures with pro- surfactant protein C-expressing epithelial cells and patent vasculature. Although the Matrigel implants were highly vascularized, they exhibited few structures reminiscent of alveolar-forming units (Mondrinos et al. 2008), possibly due to the structure of the scaffold itself or the slow degradation of the scaffold material.

Gelfoam, a compressed sponge of porcine skin gelatin which was originally developed as a hemostatic device, is another natural material that supports pulmonary cell proliferation. Gelfoam is a degradable scaffold and is excellent for supporting lung cell attachment. Tissue constructs composed of Gelfoam and fetal rat lung cells have been created; when injected into the lung parenchyma of rat models, such constructs promote the formation of porous, branching, sacculated epithelial structures resembling air sacs (Andrade et al. 2007). The Gelfoam implants were well tolerated, and the pore size of the Gelfoam was similar to alveolar structures in the rat lung. Such Gelfoam-based fetal lung grafts were shown to survive in the adult rat lung for at least 35 days; after long-term in vivo engraftment (40–60 days) the grafts developed into alveolar-like structures at the border between the Gelfoam sponge and the surrounding lung tissue. The new structures expressed pulmonary tissue markers, including pro- surfactant protein C, Clara cell secreted protein, and endothelial von Willebrand factor. Once the Gelfoam sponge degraded after several months, the newly formed "alveoli" were left in place. However, a limitation of the Gelfoam constructs was that most of the newly formed alveolar-like structures were found at the implant border, and few were found within the sponge itself. In addition, there was little evidence to support the development of alveolar–capillary junctions, or even areas of close connection between the lung epithelial cells and the vascular endothelial cells comprising the blood vessels formed in the scaffold.

Finally, reconstituted Englebreth-Holms tumor basement membranes have been shown to support the growth and functional differentiation of adult rat type II pneumocytes in vitro (Shannon et al. 1987). When rabbit fetal lung tissue was cultured on Englebreth-Holms tumor basement membrane, the constructs produced type II pneumocytes (Blau et al. 1988). On thick gels composed of Engelbreth-Holms tumor membrane, the epithelial cells associated into alveolar-like, spherical clusters surrounding a central lumen. The epithelial cells were cuboidal and had lamellar bodies and intercellular tight junctions; they exhibited polarity, with apical microvilli facing the lumen, basally located nuclei, and gel matrix abutting the basal surface. (Blau et al. 1988). Natural biomaterials have therefore demonstrated an ability to promote pulmonary tissue formation in vitro and in vivo, from a variety of cell sources including adult-derived and embryonic stem cells.

The use of natural materials as scaffolds for lung tissue engineering is limited by their mechanical properties and variability in degradation rates. Moreover, there is the possibility that natural scaffolds may be immunogenic and invoke a severe immunologic reaction, leading to inflammation and tissue destruction. Biologically derived natural materials may also harbor bacteria or viruses. Because of these

shortcomings of natural materials, there is interest in using synthetic polymers as matrices for engineered lung tissue. Synthetic polymers offer a much wider range of mechanical and chemical properties, along with the opportunity to tune these properties for specific applications. Degradable synthetic scaffolds that have been applied for lung regeneration include polyglycolic acid (PGA), poly-L-lactic acid (PLLA), poly(lactic-co-glycolic acid) , and PGA combined with Pluronic® F-127 (PF-127).

For example, PGA felt sheets have been seeded with adipose stromal cells to create constructs for lung tissue engineering (Shigemura et al. 2006). PGA is a widely used synthetic polymer in surgical applications and is currently utilized in the suture material Dexon™ (Tyco, Mansfield, MA). PGA degrades by acid hydrolysis, and the degradation rate can be controlled via the molecular weight of the polymer. Within PGA-based matrices, the adipose stromal cells secrete several regenerative and angiogenic factors, including hepatocyte growth factor (Shigemura et al. 2006). The PGA-based scaffolds have been implanted onto remnant lung tissue in rat models of emphysema, after the rats underwent lung volume reduction surgery. One week after implantation of the PGA-based sheets, both alveolar and vascular regeneration were significantly accelerated in the treated rats, as compared with the rats that underwent surgery alone. Gas exchange and exercise tolerance were also significantly restored, and these results persisted for more than 1 month. Scaffolds based on PGA were thus shown not only to regenerate lung tissue, but also to restore functionality and produce meaningful physiologic outcomes. Two additional synthetic polymer scaffolds have been investigated for lung regeneration, the first composed of PLGA fabricated into three-dimensional porous foams, and the second made of PLLA fabricated into three-dimensional nanofibrous matrices (Mondrinos et al. 2006). Each of these scaffolds was seeded with murine fetal pulmonary cells, and each matrix was shown to facilitate ingrowth of fetal pulmonary cells in vitro. However, these matrices did not support the survival of distal lung epithelial cells, despite the presence of tissue-specific growth factors. Still, this investigation demonstrated that pulmonary cells could proliferate within synthetic three-dimensional constructs.

Three-dimensional synthetic scaffolds for lung tissue engineering have been created by combining PGA with the block copolymer surfactant Pluronic® F-127 (Cortiella et al. 2006). Pluronic® polymers (BASF, Mount Olive, New Jersey) are liquids at low temperatures (below 15°C) and gel at higher temperatures such as at body temperature. The firmness or density of the gel increases as the concentration of the polymer is increased. Poloxamer hydrogels such as Pluronic®-based gels are advantageous for cell culture, in that they maintain cells in a three-dimensional structure, enabling cells to secrete extracellular matrix proteins and engage in cell signaling (Cortiella et al. 2006). Hybrid scaffolds composed of Pluronic® F-127 and PGA were seeded with a mixture of sheep somatic lung progenitor cells, and the PGA/ PF-127-based constructs were evaluated both in small animal models (nude mice) and in large animal models (sheep). In the nude mice, the tissue-engineered grafts were implanted onto the backs, to determine whether growth factors alone could be utilized to promote differentiation of somatic lung progenitor cells and

formation of lung tissue at a site distant from the natural microenvironment of the lung. The implanted constructs demonstrated production of smooth muscle, collagen, pro-surfactant protein C, and Clara cell protein, as well as the development of alveolar-like structures. In the sheep, the tissue-engineered biomaterials were implanted directly into the right upper lobe of the lung into a pocket created by a wedge resection. The constructs again developed into structures resembling alveolar tissue. Within both animal models, the implanted PGA/PF-127 grafts were well tolerated, and the synthetic polymer scaffolds facilitated lung tissue assembly. The combination PGA/PF-127 matrix degraded as the development of lung epithelial tissues progressed (Cortiella et al. 2006). In the same study, a PGA/PF-127 matrix seeded with sheep somatic lung progenitor cells was implanted into the thoracic cavity of three adult sheep. The construct was attached to the right main stem bronchus of the lung, after the sheep had undergone a full pneumonectomy. When harvested after 3 months, the constructs formed highly vascularized tissue fragments. However, in this case the implants were not shown to support lung epithelial development, possibly due to the severe inflammatory response following pneumonectomy (Cortiella et al. 2006).

The optimal scaffold material for lung tissue engineering has yet to be formulated. To specifically meet the needs for future production of tissue-engineered lung, it will be essential for biomaterials scientists to develop a biodegradable, highly elastic material with shape and pore size similar to that found in the alveolar structure itself (Nichols and Cortiella 2008). A scaffold that has been proposed to meet these requirements is a novel material bearing an inverted colloidal crystal (ICC) geometry (Kotov et al. 2004). Primary colloidal crystals are hexagonally packed lattices of spheres, with a wide range of diameters from nanometers to micrometers. ICCs are similarly organized structures in which the spheres are replaced with cavities, while the interstitial spaces are filled. When ICC cavity sizes exceed the diameter of cells, the ICC structures can serve as three-dimensional cell scaffolds. ICCs are an attractive structure for supporting the development of alveolus formation, due to the open geometry of the ICC lattice, the high porosity (74% of free space), and the large surface area of the lattice (Shanbhag et al. 2005). ICC structure might allow for tenability of cellular interactions and cell migration by varying the sphere diameter, which is an important consideration for engineered lung tissue. While ICC biomaterials have not yet been evaluated in vivo for lung regeneration, these scaffolds may soon become state of the art for lung tissue engineering.

Clearly, much work remains in the nascent field of biomaterials for lung regeneration. The replacement of lung tissue for COPD patients is wrought with difficult challenges, due to the variety of lung tissues affected by COPD, as well as the complexity and intricacy of lung structures. To produce engineered lung tissue for regenerative therapeutics, biomaterials scientists must

(1) select the cell source with the highest potential for use in transplantation;
(2) determine the best biocompatible and degradable three-dimensional scaffold for lung development, designed to meet the needs for implantation into the lung with consideration of obstructive lung disease;

(3) elucidate the best combinations of growth factors and culture conditions that promote cellular differentiation and increase the efficiency of differentiation of adult-derived, embryonic, and fetal lung-derived cells;
(4) define the best conditions overall that promote three-dimensional production of lung tissue.

Engineered lung tissues will be feasible for clinical application only when the above four research priorities are addressed. Additional biochemical and biophysical stimuli may be needed to enhance cell survival in engineered lung matrices, both in vitro and in vivo. Enriched culture conditions, incorporating biochemical signals including growth factors, matrix molecules, glucocorticoids, and retinoic acids, may be required for tissue formation. Such factors may speed up the maturation of engineered scaffolds into adult lung structures and may enhance the merging of implanted cells, as well as the development of adult lung function. In terms of biophysical signals, applying mechanical stretch to cultured cells to simulate breathing in vitro may facilitate cell-based tissue engineering (Andrade et al. 2007). Optimization of the matrix material will improve cell attachment and ensure cell organization prior to implantation. This will increase the ability of implanted cells to connect to host lung tissues and match the processes of alveolarization and angiogenesis.

COPD is a rising yet neglected global epidemic. It is the only common cause of death in the United States that has increased over the last 40 years, in sharp contrast to the reduction in cardiovascular and infectious diseases (Barnes 2007). More importantly, COPD is a mounting cause of chronic disability and is predicted to become the fifth most common cause of chronic disability worldwide by 2020 (Lopez et al. 2006). Despite growing recognition as a significant international health problem, COPD has been overlooked by clinicians, researchers, and the pharmaceutical industry (Barnes and Kleinert 2004). This neglect occurs largely because COPD is viewed as self-inflicted (by smoking) and because the underlying disease process is perceived to be irreversible. Biomaterials for lung regeneration are absolutely critical, both for reversing COPD and for reversing the widely held perception that COPD is irreparable. Sustained advances in lung tissue engineering will ensure longer and better lives for COPD sufferers and provide hope for this patient population. The following chapter will move from the pulmonary system to the gastrointestinal system, to address the fifth leading cause of mortality worldwide, diarrheal diseases.

References

Andrade CF, Wong AP, Waddell TK et al (2007) Cell-based tissue engineering for lung regeneration. Am J Physiol Lung Cell Mol Physiol 292:L510

Badham C (1814) An essay on bronchitis: with a supplement containing remarks on simple pulmonary abscess, 2nd edn. J Callow, London

Barnes PJ (2007) Chronic obstructive pulmonary disease: a growing but neglected global epidemic. PLoS Med 4:e112

Barnes PJ, Kleinert S (2004) COPD– a neglected disease. Lancet 364:564
Beers MH, Porter RS, Jones TV et al (2006) Merck manual of diagnosis and therapy, 18th edn. Wiley, New York, NY
Blau H, Guzowski DE, Siddiqi ZA et al (1988) Fetal type 2 pneumocytes form alveolar-like structures and maintain long-term differentiation on extracellular matrix. J Cell Physiol 136:203
Bonet T (1679) Sepulchretum sive anatonia pructica ex Cadaveribus Morbo denatis, proponens Histoa's Observations omnium pené humani corporis affectuum, ipsarcomoue Causas recorditas revelans, Geneva
Burrows B, Knudson RJ, Camilli AE et al (1987) The "horse-racing effect" and predicting decline in the forced expiratory volume in one second from screening spirometry. Am Rev Respir Dis 135:788
Calverly PM, Koulouris NG (2005) Flow limitation and dynamic hyperinflation: key concepts in modern respiratory physiology. Eur Respir J 25:186
Chakir J, Pagé N, Hamid Q et al (2001) Bronchial mucosa produced by tissue engineering: a new tool to study cellular interactions in asthma. J Allergy Clin Immunol 107:36
Christie RV (1944) Emphysema of the lungs (part II). BMJ 1–145
Cook NR, Hebert PR, Satterfield S et al (1994) Height, lung function, and mortality from cardiovascular disease among the elderly. Am J Epidemiol 139:1066
Coraux C, Nawrocki-Raby B, Hinnrasky J et al (2005) Embryonic stem cells generate airway epithelial tissue. Am J Respir Cell Mol Biol 32:87
Cortiella J, Nichols JE, Kojima K et al (2006) Tissue-engineered lung: an in vivo and in vitro comparison of polyglycolic acid and pluronic F-127 hydrogel/somatic lung progenitor cell constructs to support tissue growth. Tissue Eng 12:1213
Croxton TL, Bailey WC (2006) Long-term oxygen treatment in chronic obstructive pulmonary disease: recommendations for future research: an NHLBI workshop report. Am J Respir Crit Care Med 174:373
Devereux G (2006) ABC of chronic obstructive pulmonary disease. Definition, epidemiology, and risk factors. BMJ 332:1142
Freitas RA Jr (1999) Nanomedicine, volume I: basic capabilities. Landes Bioscience, Georgetown, TX
Giangreco A, Reynolds SD, Stripp BR (2002) Terminal bronchioles harbor a unique airway stem cell population that localizes to the bronchoalveolar duct junction. Am J Pathol 161:173
Halbert RJ, Natoli JL, Gano A et al (2006) Global burden of COPD: systematic review and meta-analysis. Eur Respir J 28:523
Hermanns MI, Unger RE, Kehe K et al (2004) Lung epithelial cell lines in coculture with human pulmonary microvascular endothelial cells: development of an alveolo-capillary barrier in vitro. Lab Invest 84:736
Kim CF, Jackson EL, Woolfenden AE et al (2005) Identification of bronchioalveolar stem cells in normal lung and lung cancer. Cell 121:823
Kotov NA, Liu Y, Wang S et al (2004) Inverted colloidal crystals as three-dimensional cell scaffolds. Langmuir 20:7887
Krause DS, Theise ND, Collector MI et al (2001) Multi-organ, multi-lineage engraftment by a single bone marrow-derived stem cell. Cell 105:369
Laënnec RTH (1821) In: Forbes J (ed) A treatise on the diseases of the chest (English translation from the French). T and G Underwood; London
Løkke A, Lange P, Scharling H et al (2006) Developing COPD: a 25 year follow up study of the general population. Thorax 61:935
Lopez AD, Shibuya K, Rao C et al (2006) Chronic obstructive pulmonary disease: current burden and future projections. Eur Respir J 27:397
Luppi F, Franco F, Beghé B et al (2008) Treatment of chronic obstructive pulmonary disease and its comorbidities. Proc Am Thorac Soc 5:848
Maclay JD, McAllister DA, Macnee W (2007) Cardiovascular risk in chronic obstructive pulmonary disease. Respirology 12:834

Mills NL, Miller JJ, Anand A et al (2008) Increased arterial stiffness in patients with chronic obstructive pulmonary disease: a mechanism for increased cardiovascular risk. Thorax 63:306
Mondrinos MJ, Koutzaki S, Jiwanmall E et al (2006) Engineering three-dimensional pulmonary tissue constructs. Tissue Eng 12:717
Mondrinos MJ, Koutzaki S, Lelkes PI et al (2007) A tissue-engineered model of fetal distal lung tissue. Am J Physiol Lung Cell Mol Physiol 293:L639
Mondrinos MJ, Koutzaki SH, Poblete HM et al (2008) In vivo pulmonary tissue engineering: contribution of donor-derived endothelial cells to construct vascularization. Tissue Eng A 14:361
Morgagni GB (1769) The seats and causes of disease. In: Investigated by anatomy; in five books, containing a great variety of dissections, with remarks (trans: Alexander B, Miller A, Caldwell T). Johnson and Payne, London
Nichols JE, Cortiella J (2008) Engineering of a complex organ: progress toward development of a tissue-engineered lung. Proc Am Thorac Soc 5:723
O'Donnell DE (2006) Hyperinflation, dyspnea, and exercise intolerance in chronic obstructive pulmonary disease. Proc Am Thorac Soc 3:180
Public Library of Science (2004) T cells cause lung damage in emphysema. PLoS Med 1:e25
Rabe KF, Hurd S, Anzueto A et al (2007) Global strategy for the diagnosis, management, and prevention of chronic obstructive pulmonary disease: GOLD executive summary. Am J Respir Crit Care Med 176:532
Rippon HJ, Polak JM, Qin M et al (2006) Derivation of distal lung epithelial progenitors from murine embryonic stem cells using a novel three-step differentiation protocol. Stem Cells 24:1389
Schunemann HJ, Dorn J, Grant BJ et al (2000) Pulmonary function is a long-term predictor of mortality in the general population: 29-year follow-up of the Buffalo health study. Chest 118:656
Shanbhag S, Wang S, Kotov NA (2005) Cell distribution profiles in three-dimensional scaffolds with inverted-colloidal-crystal geometry: modeling and experimental investigations. Small 1:1208
Shannon JM, Mason RJ, Jennings SD et al (1987) Functional differentiation of alveolar type II epithelial cells in vitro: effects of cell shape, cell-matrix interactions and cell-cell interactions. Biochim Biophys Acta 931:143
Shigemura N, Okumura M, Mizuno S et al (2006) Lung tissue engineering technique with adipose stromal cells improves surgical outcome for pulmonary emphysema. Am J Respir Crit Care Med 174:1199
Smith KR (2000) Inaugural article: national burden of disease in India from indoor air pollution. Proc Natl Acad Sci USA 97:13286
Speizer FE, Horton S, Batt J et al (2006) Respiratory diseases of adults. In: Jamison DT, Breman JG, Measham AR et al (eds) Disease control priorities in developing countries, 2nd edn. IBRD/The World Bank and Oxford University Press, Washington, DC
Sugihara H, Toda S, Miyabara S et al (1993) Reconstruction of alveolus-like structure from alveolar type II epithelial cells in three-dimensional collagen gel matrix culture. Am J Pathol 142:783
World Health Organization (2008) The global burden of disease: 2004 update. WHO Press, Geneva

Chapter 6
Diarrheal Diseases

Diarrheal diseases are the fifth leading killer worldwide. In 2004, diarrheal disease was responsible for 2.16 million deaths or 3.7% of all deaths globally (World Health Organization 2008). Diarrhea disproportionately affects the young; over 90% of cases in the developing world occur in children under the age of 5 (Keusch et al. 2006). Because diarrheal infections strike within the first few years of life, they account for 7% of all years of life lost globally (World Health Organization 2008). Worldwide, diarrheal diseases are a leading cause of pediatric morbidity and mortality, with 1.5 billion episodes of diarrhea annually in children under 5. Diarrhea contributes to 20% of childhood deaths, resulting in approximately 2 million childhood deaths each year (Black et al. 2003). Particularly in developing countries, the young suffer from a seemingly never-ending sequence of infections, rarely receive appropriate preventive care, and encounter the healthcare system when they are already severely ill. A strong relationship exists between poverty, an unhygienic environment, and the number and severity of diarrheal episodes, especially for children under 5 years old (Keusch et al. 2006). However, diarrheal disease can occur at any age, in both rich and poor. When an individual is suffering from diarrhea, the underlying pathogen can be difficult to identify based on clinical symptoms alone, as a variety of microorganisms can cause similar diarrheal syndromes. A range of microorganisms may infect the human gastrointestinal tract and induce diarrhea, including viruses, bacteria, and parasites. Mixed infections of bacteria and viruses are not uncommon, further complicating the diagnostic process. Yet accurate diagnosis of the causative pathogen is often essential, not only for appropriate treatment of diarrhea, but also for epidemiological tracking of outbreaks as well as prevention of future infections. Many developing countries lack the sophisticated laboratory facilities, microscopy equipment, and resources required for accurate microbiologic diagnosis of diarrheal infection. To solve this dilemma, biomaterial scientists are creating new low-cost diagnostic devices, to permit cost-effective identification of gastrointestinal pathogens. Such devices will allow rapid and reliable diagnosis of patients suffering from diarrhea and will lower mortality from these diseases.

S.K. Bhatia, *Biomaterials for Clinical Applications*,
DOI 10.1007/978-1-4419-6920-0_6, © Springer Science+Business Media, LLC 2010

6.1 Pathology of Diarrhea

The intestinal tract regulates the absorption and secretion of water and electrolytes to meet physiological needs and maintain hydration. Approximately 10 l of fluid enters the adult intestine per day, and more than 98% of this fluid is reabsorbed by healthy human intestines (Keusch 2001). During diarrhea, the normal net absorption of water and electrolyte reverses to secretion. A diarrheal episode can develop when microorganisms infect intestinal cells and colonize the intestinal wall; etiologic organisms include viruses, bacteria, protozoa, and helminths. Microbes associated with infectious diarrhea are given in Table 6.1.

Such pathogens are transmitted from the stool of one individual to the mouth of another, a process known as fecal–oral transmission. Some enteric pathogens are well known, such as rotavirus (Fig. 6.1), *Salmonella* (Fig. 6.2), *Shigella*, and *Escherichia coli* (Fig. 6.3); others are recently discovered or emerging new agents, and many remain to be identified. Worldwide, rotavirus is the single most common cause of infectious diarrhea. Rotavirus and adenovirus are particularly prevalent in children younger than 2 years. Astrovirus and norovirus (Fig. 6.4) usually infect children younger than 5 years. Among the bacterial pathogens, *Yersinia enterocolitica* typically infects children younger than 1 year, and the *Aeromonas* organism is a significant cause of diarrhea in young children.

Microbial pathogens differ in the route from the stool to the mouth and in the number of organisms needed to initiate infection and illness. Among viral species, norovirus is one of the most highly infectious and requires as few as 10–100 particles for transmission. Among bacterial species, the ability to survive gastric acid is an important determinant of the inoculum size required to cause illness (Keusch et al. 2006). For instance, *Shigella* bacteria are resistant to low pH, and a few thousand organisms are sufficient to provoke infection. This amount is readily transferred by person-to-person contact or through contamination of everyday objects such as a cup. By contrast, bacteria which are readily killed by acid, such as *Vibrio cholerae* (Fig. 6.5), require millions of organisms to cause illness and must first multiply in food or water to an infectious dose. Diarrheal pathogens must be adapted to humans and possess essential virulence factors. Pathogenic microbes may elicit diarrhea via several mechanisms:

- Microbial attachment to intestinal epithelium
- Microbial invasion into intestinal epithelium
- Microbial production of enterotoxins which induce fluid secretion
- Microbial release of cytotoxins which damage intestinal cells
- Infiltration of inflammatory cells which contribute to activated secretion

Most enterotoxins block Na^+–H^+ exchange, which is an important driving force for fluid absorption in the small bowel and colon (Beers et al. 2006). These pathological factors combine to push the intestine into a state of active secretion and net fluid loss.

Diarrhea is conventionally defined based on clinical symptoms and is present when three or more stools are passed in 24 h that are sufficiently liquid to take the

Table 6.1 Microbial pathogens associated with infectious diarrhea

Group	Organisms	Pathogenesis
Viruses	Rotavirus	Infects villus epithelial cells in small intestine; may also produce a toxin
	Norovirus	Infects epithelium of small intestine
	Caliciviruses	Infects epithelium of small intestine
	Adenoviruses • serotypes 40 and 41	Infects duodenal mucosa
	Astroviruses	Infects the duodenal epithelium in the lower third of the villi
Bacteria	*Escherichia coli* • enteropathogenic *E. coli* (EPEC) • enterotoxigenic *E. coli* (ETEC) • enterohemorrhagic *E. coli* (EHEC) • enteroinvasive *E. coli* (EIEC)	EPEC infects both small intestine and colon; ETEC colonizes the small intestine and produces enterotoxin; EIEC invades epithelial cells and damages them through intracellular multiplication; EHEC including O157:H7 is associated with foodborne (ground beef) infection and colonizes distal ileum and colon – it is non-invasive but produces a verotoxin which induces hemolytic–uremic syndrome
	Shigella species • *S. dysenteriae* • *S. flexneri* • *S. boydii* • *S. sonnei*	Infects colonic epithelial cells and produces a toxin
	Salmonella species • over 2,500 serotypes	Binds to and penetrates the small intestinal wall and produces toxins
	Vibrio cholerae	Colonizes small intestine; associated with waterborne and foodborne infection; pathogenesis assisted by toxins
	Campylobacter species • includes *C. jejuni*	Principally infects the colon, but may also involve small intestine; bacterial toxin production may facilitate cell damage
Bacteria	*Aeromonas* species	Produces toxin in the host gut
	Yersinia enterocolitica	Bind to and penetrate the small intestinal mucosa; they then colonize Peyer's patches and spread to other organs; pathogenesis partly related to toxin production
	Clostridium species • *C. difficile* • *C. perfringens* • *C. botulinum*	*C. difficile* is the most serious cause of antibiotic-associated diarrhea – it colonizes colon and induces diarrhea following the production of toxins; *C. perfringens* is a common cause of food poisoning and secretes a toxin during the process of sporulation within the intestine; *C. botulinum* is also an important cause of food poisoning and produces neurotoxin
	Bacillus species • includes *B. cereus*	Associated with outbreaks of foodborne illness; infection can involve either small intestine or colon; produces a number of toxins
Parasites	*Giardia* species	Infects the small intestine and interferes with the absorption of fat in the intestine (malabsorption)
	Cryptosporidium species	Infects the small intestine; an opportunistic pathogen that affects immunocompromised (HIV/AIDS) and immunosuppressed individuals
	Entamoeba histolytica	Infects the colon and cecum; can bore into the intestinal wall and reach the bloodstream; may spread to other vital organs including liver, lungs, brain, and spleen

Beers et al. (2006), Marshall (2002)

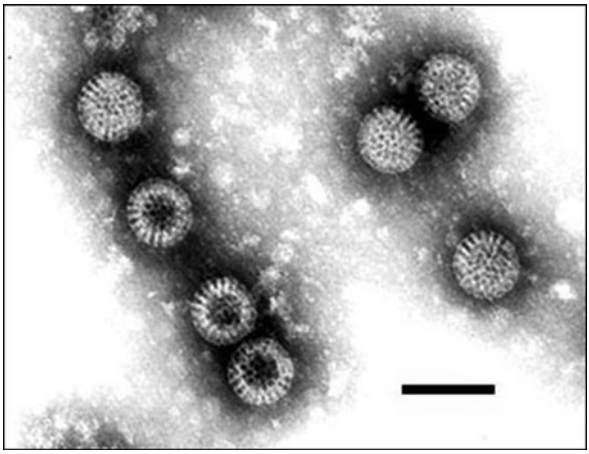

Fig. 6.1 Transmission electron micrograph of rotavirus particles (bar = 100 nm). The rotavirus particle derives its name from its wheel-like appearance (US Environmental Protection Agency)

Fig. 6.2 Color-enhanced scanning electron micrograph showing *Salmonella typhimurium* (*red*) invading human cells (National Institute of Allergy and Infectious Diseases)

shape of the container in which they are placed (Keusch et al. 2006). The interval between two separate episodes of diarrhea is additionally defined as at least 48 h of normal stool. Three major diarrhea syndromes exist: acute watery diarrhea, which results in varying degrees of dehydration; bloody diarrhea, which is a manifestation of the intestinal damage caused by inflammation; and persistent diarrhea, which lasts 14 days or longer. The three are physiologically distinct, require specific management strategies, and are linked to different organisms. Table 6.2 summarizes the clinical diarrhea syndromes and systemic effects associated with selected pathogens.

Acute watery diarrhea is characterized by stool water losses of 250 ml/kg/day or more and can be rapidly dehydrating (Keusch et al. 2006). The quantity of fluid

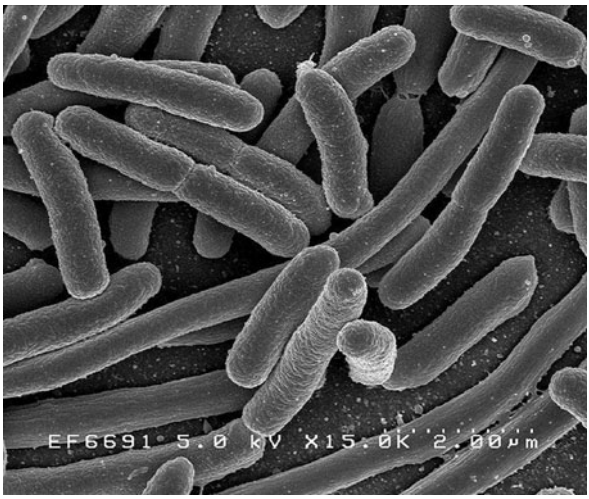

Fig. 6.3 Scanning electron micrograph of *Escherichia coli* bacteria (National Institute of Allergy and Infectious Diseases)

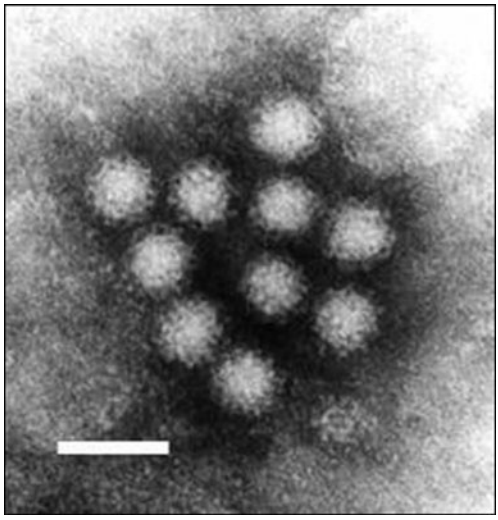

Fig. 6.4 Transmission electron micrograph of norovirus particles (bar = 50 nm). Individual virus particles have a lace-like appearance (US Environmental Protection Agency)

loss quickly exceeds total plasma and interstitial volumes and is incompatible with life unless fluid therapy can be initiated to keep up with losses. Dehydration is the principal cause of morbidity and mortality from diarrhea. Important clinical signs of dehydration are sunken eyes, dry mucous membranes, lack of tears, poor skin turgor, lethargy, and depressed consciousness. This dramatic dehydration is usually due to rotavirus, enterotoxigenic *E. coli*, or *V. cholerae* (the cause of cholera), and it is most dangerous in the very young. Other viral causes of watery diarrhea include adenovirus, calicivirus (Fig. 6.6), astrovirus, and norovirus. Additional enterotoxigenic

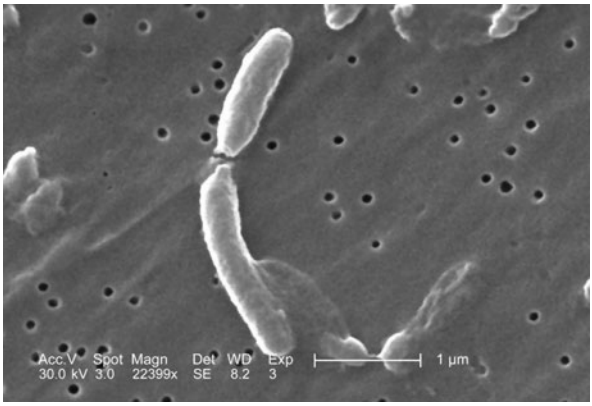

Fig. 6.5 Scanning electron micrograph of *Vibrio cholerae* bacteria of the serogroup 01 (Centers for Disease Control)

Table 6.2 Clinical features of selected diarrheal diseases

Etiologic agents	Clinical manifestations
Salmonella, other than *S. typhi* and *S. paratyphi*	Abdominal pain, diarrhea, nausea, vomiting, fever, septicemia
Shigella species	Diarrhea with blood, mucus, pus, cramping, tenesmus, fever
V. cholerae	Profuse watery stools, vomiting, dehydration, acidosis, collapse
Vibrio parahemolyticus	Watery diarrhea, abdominal cramps, vomiting, dysentery-like illness
Enteropathogenic *E. coli* (EPEC)	Watery diarrhea; 17 specific serotypes
Enterotoxigenic *E. coli* (ETEC)	Watery diarrhea, abdominal pain, dehydration, acidosis, occasional fever, Traveler's diarrhea
Enteroinvasive *E. coli* (EIEC)	Shigellosis-like diarrhea, fever, abdominal cramps
Campylobacter species	Febrile dysentery, diarrhea (3–5 days or weeks)
Staphylococcus aureus	Severe nausea, vomiting, abdominal pain, diarrhea
Bacillus cereus	Diarrhea, abdominal pain, nausea, vomiting
Y. enterocolitica	Diarrhea, abdominal pain, septicemia, low-grade fever; mimics appendicitis
C. difficile	Pseudomembranous colitis
C. perfringens	Abdominal pain, diarrhea, nausea
C. botulinum	Weakness, dryness of mouth, vomiting, diarrhea, visual difficulty, eyelid drooping

Santiago (1983)

bacteria that induce watery diarrhea include *Klebsiella* species and *Clostridium perfringens*. The parasites *Giardia* (Fig. 6.7) and *Cryptosporidium* (Fig. 6.8) can also initiate watery diarrhea.

Bloody diarrhea is defined as diarrhea with visible or microscopic blood in the stools and is characterized by intestinal damage and nutritional deterioration.

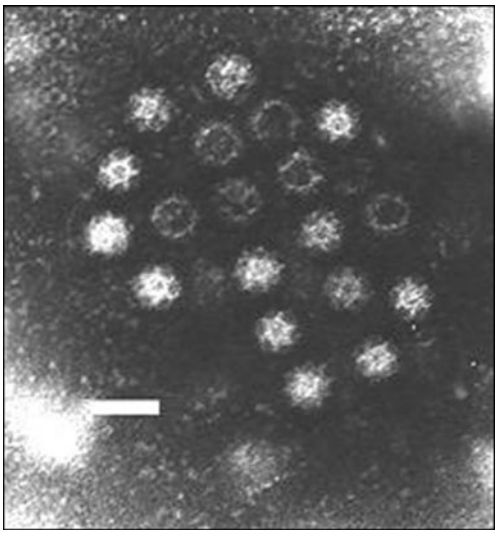

Fig. 6.6 Transmission electron micrograph of calicivirus particles (bar = 50 nm). Individual virus particles exhibit a "Star of David" appearance (US Environmental Protection Agency)

Fig. 6.7 Scanning electron micrograph of the flagellated *Giardia lamblia* protozoan parasite (Centers for Disease Control)

Because bloody diarrhea is associated with disruption of the intestinal wall, it often progresses to secondary sepsis, as microbes penetrate through the intestines and enter the bloodstream. Some dehydration is common, though it is rarely severe. Fever is also typically observed during bloody diarrhea. A related condition is

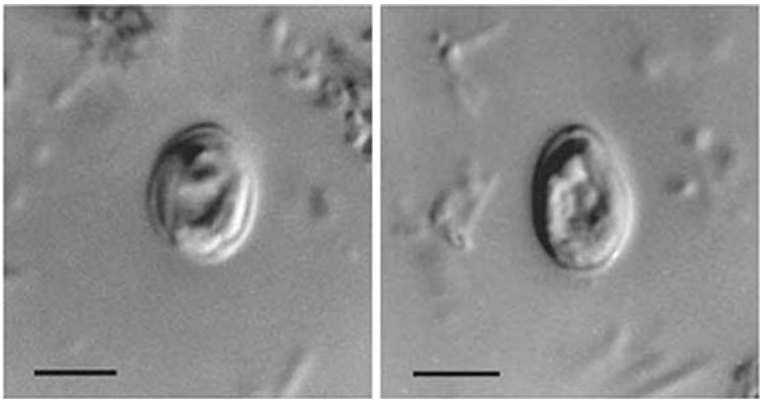

Fig. 6.8 Nomarski interference contrast photomicrographs of *Cryptosporidium muris* parasites (bars = 5 μm). These parasites were isolated from the stool of an HIV-positive patient (Centers for Disease Control)

dysentery, which is a syndrome consisting of the frequent passage of characteristic, small volume, bloody mucoid stools, abdominal cramps, and tenesmus, a severe pain that accompanies straining to pass stool (Keusch et al. 2006). These clinical features indicate the severity of intestinal injury. Agents that cause bloody diarrhea or dysentery provoke mucosal damage and an inflammatory response; fecal blood and white blood cells are usually detectable by microscopy. The intense inflammation leads to the release of host-derived cytokines, resulting in fever and altered host metabolism. This leads to a breakdown in body stores of protein, carbohydrate, and fat, as well as the loss of nitrogen and other nutrients. Reduced muscle and fat mass or peripheral swelling (edema) may indicate the presence of carbohydrate, fat, or protein losses. Because these losses must be replenished, recovery from bloody diarrhea takes much longer than the illness does to develop. The management strategies for bloody diarrhea are thus markedly different than those for watery diarrhea: while fluid replenishment and rehydration are critical for patients suffering from watery diarrhea, nutrient replenishment is a priority for patients with bloody diarrhea. New bouts of infection that occur before complete restoration of nutrient stores can initiate a downward spiral of nutritional status, terminating in fatal protein–energy malnutrition (Keusch 2003). Bloody diarrhea is usually caused by invasive bacteria such as enteroinvasive *E. coli*, *Shigella* species, *Salmonella* species, *Campylobacter* species (Fig. 6.9), *Yersinia* species, *Aeromonas* species, and *Plesiomonas* species. Globally, almost a quarter of all diarrhea deaths are associated with dysentery, a large proportion caused by *Shigella* organisms (Bhutta 2006). Enterohemorrhagic *E. coli* and the toxin-producing *Clostridium difficile* (Fig. 6.10) bacteria can also produce bloody diarrhea. Finally, the parasite *Entamoeba histolytica* (Fig. 6.11) can instigate a severe bloody diarrhea with systemic disease.

Persistent diarrhea is defined as a diarrheal episode that began acutely but lasts for at least 14 days (World Health Organization 1988). Such episodes may account

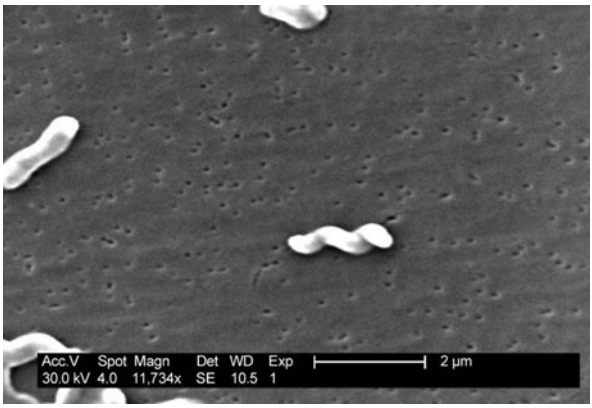

Fig. 6.9 Scanning electron micrograph of *Campylobacter jejuni* bacteria. The bacteria are *slender, curved, motile* rods (Centers for Disease Control)

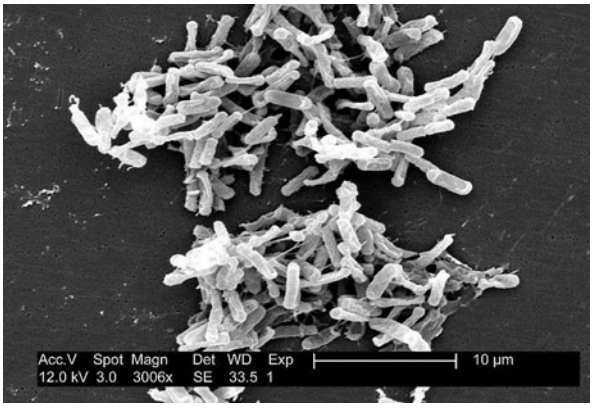

Fig. 6.10 Scanning electron micrograph of *Clostridium difficile* bacteria (Centers for Disease Control)

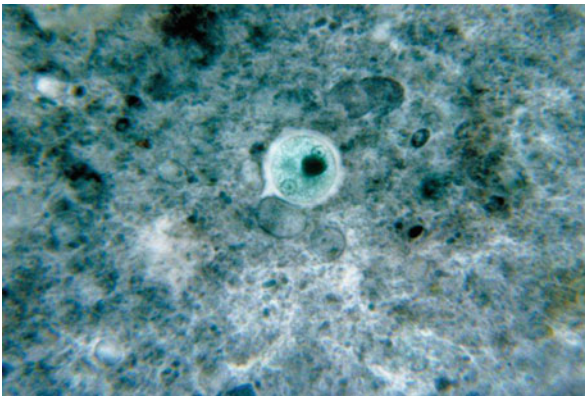

Fig. 6.11 Micrograph of an *Entamoeba histolytica* cyst (Centers for Disease Control)

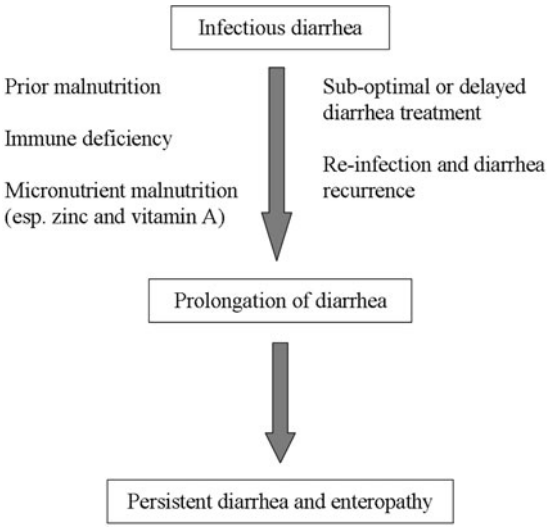

Fig. 6.12 Physiological factors contributing to the development of prolonged and persistent diarrhea

for 3–20% of all diarrheal episodes in children under 5 years of age (World Health Organization 1996). Even though persistent diarrhea accounts for a small percentage of the total number of diarrheal episodes, it is associated with a disproportionately increased risk of death. In several large community-based studies of diarrhea in South America and Southeast Asia, it has been shown that persistent diarrhea is directly responsible for between 36 and 54% of all diarrhea-related deaths (Schorling et al. 1990; Faveau et al. 1992; Khan et al. 1993). Persistent diarrhea is typically associated with malnutrition, which can either precede the diarrheal illness or result from the illness itself (Ochoa et al. 2004). The relative risk of death among infants with persistent diarrhea and severe malnutrition is 17 times greater than for those with mild malnutrition (Faveau et al. 1992). Persistent diarrhea occurs more often during an episode of bloody diarrhea than an episode of watery diarrhea, and the mortality rate when bloody diarrhea progresses to persistent diarrhea is 10 times greater than for bloody diarrhea without persistent diarrhea (Keusch et al. 2006). Several physiological factors contribute to diarrheal persistence, including general undernutrition, micronutrient malnutrition, and immune deficiencies (Fig. 6.12). Such nutritional and systemic deficiencies may delay intestinal healing and repair following initial injury to the intestine and predispose patients to a prolonged diarrheal episode. Table 6.3 lists a number of pathogens associated with prolonged and persistent diarrhea. In particular, *Shigella* infections are significantly associated with an increased risk of persistent diarrhea. In a study from Bangladesh, persistent diarrhea was observed in 23% of children with shigellosis (Ahmed et al. 2001). HIV infection is another risk factor for persistent diarrhea in both adults and children (Keusch et al. 1992). Importantly, persistent post-enteritis diarrhea has a strong inverse correlation with age, especially in developing countries.

Table 6.3 Microbial pathogens associated with prolonged and persistent diarrhea

Group	Organisms
Bacteria	Enteroaggregative *E. coli*
	Enteropathogenic *E. coli*
	Campylobacter species
	Salmonella enteritides
	Shigella species
	C. difficile
	Arcobacter butzleri
	Klebsiella species
Parasites	*Giardia lamblia*
	Blastocystis hominis[a]
	Cryptosporidium species[a]
	E. histolytica
	Cyclospora cayetanensis[a]
Viruses	Human astrovirus 3
	Enterovirus
	Picobernaviruses

[a]Especially associated with HIV infections and AIDS
Bhutta (2006)

The three types of diarrhea share common risk factors, including poverty, environment, young age, malnutrition, and HIV infection. Poverty is linked to poor housing, dirt floors, crowding, lack of access to sufficient clean water or to sanitary disposal of fecal waste, cohabitation with domestic animals that may carry human pathogens, and a lack of refrigerated storage for food – all of which increase the incidence of diarrhea (Keusch et al. 2006). Families living in poverty are often unable to provide age-appropriate, nutritionally balanced diets for children. Once diarrhea develops in poverty-stricken areas, it is difficult to modify diets to mitigate and repair nutrient losses. Nutritional status and age are the most critical factors in determining the frequency, severity, and duration of diarrhea. In developing nations, children experience an average of 3.2 diarrheal episodes per child per year (Black et al. 2003). Finally, the HIV/AIDS epidemic in Africa has resulted in a change to the usual etiological patterns of diarrhea. In HIV endemic areas, chronic diarrhea is increasingly recognized as a common manifestation of advancing HIV infection and AIDS (Adejuyigbe et al. 2003). Prolonged diarrheal episodes caused by relatively rare pathogens such as *Cryptosporidium* are now more common. In HIV-infected persons with low CD4 cell counts, the probability of developing diarrhea within 1, 2, and 3 years is 48.5, 74.5, and 95.6%, respectively (Weber et al. 1999); diarrhea is an independent negative predictor of survival in this population.

Treatment of diarrhea consists of oral rehydration, nutrient replenishment, and antimicrobial therapy directed at the underlying organism when appropriate. In developed countries, the prognosis is very good with proper management; diarrhea is typically a benign, self-limited condition that subsides within a few days. However, in developing countries, the prognosis is more guarded. Poverty is exacerbated by a lack of adequate, available, and affordable medical care. Even

patients showing danger signals, such as blood in the stools, are not treated early or receive poor medical care. Once severe dehydration and malnutrition set in, the prognosis turns grim. Very young children are particularly susceptible to dehydration and nutrient malabsorption; the younger the child, the higher the risk for life-threatening dehydration as a result of the high body-water turnover and limited renal compensatory capacity of young children. Early and accurate diagnosis, as well as rapid intervention, is therefore essential for preventing deaths from infectious diarrhea. In addition, several organisms can induce asymptomatic carrier states, including *Salmonella*, *C. difficile*, and rotavirus. If such carrier states persist undetected, carrier individuals can unknowingly facilitate disease spread; timely detection thus becomes critical for stopping further infections and decreasing mortality.

Even in cases where individuals survive an initial episode of diarrheal illness, both acute and chronic complications can develop if the underlying infection is not sufficiently identified and eliminated. Table 6.4 summarizes common medical complications of specific infections. Moreover, there are long-term consequences of diarrheal disease for physical, motor, and cognitive development in young children.

Table 6.4 Complications of selected diarrheal diseases

Etiologic agents	Complications
Aeromonas caviae	Intussusception (telescoping or prolapse of bowel), gram-negative sepsis, hemolytic–uremic syndrome (anemia, thrombocytopenia, acute renal failure)
Campylobacter species	Bacteremia, meningitis, cholecystitis (gall bladder inflammation), urinary tract infection, pancreatitis
C. difficile	Chronic diarrhea
C. perfringens serotype C	Enteritis necroticans (segmental, necrotizing gangrene of the small intestinal wall)
Enterohemorrhagic *E. coli* (EHEC)	Hemorrhagic colitis
Enterohemorrhagic *E. coli* (EHEC) O157:H7	Hemolytic–uremic syndrome (anemia, thrombocytopenia, acute renal failure)
Plesiomonas species	Septicemia
Salmonella species	Seizures, hemolytic–uremic syndrome (anemia, thrombocytopenia, acute renal failure), intestinal perforation
S. typhi	Enteric fever (fever, abdominal pain, diarrhea, rash, decreased heart rate, hepatitis, myocarditis, cholecystitis, and GI bleeding)
Vibrio species	Rapid dehydration
Y. enterocolitica	Appendicitis, intestinal perforation, intussusception (telescoping of bowel), peritonitis, toxic megacolon, bacteremia, cholangitis (infection of bile duct)
Rotavirus	Dehydration, carbohydrate intolerance
Giardia species	Chronic fat malabsorption
Cryptosporidium species	Chronic diarrhea
Entamoeba species	Colonic perforation, liver abscesses

There is a significant inverse correlation between episodes of early diarrheal disease and overall intellectual capacity and concentration (Dobbing 1990). In a cohort study in Brazil, children with an early history of persistent diarrhea scored 25–65% lower on tests of cognitive function. Recurrent episodes of diarrhea with malnutrition lead to growth faltering in children and reduce their physical fitness and work productivity when they become adults. Prompt diagnosis and management of diarrheal disease are needed to allay these adverse effects, and preserve the overall health of populations.

6.2 Complexity and Cost of Current Diagnostic Methods

For diarrheal diseases, accurate identification of the causative pathogen is a prerequisite for determining a suitable treatment strategy, predicting the course of disease, preventing short-term and long-term complications, and halting disease spread. Yet many organisms can cause diarrhea as listed in Table 6.1; there are 2,500 serotypes of *Salmonella* alone. The symptoms of initial infection with various enteric pathogens can overlap as shown in Table 6.2, though the chronic consequences and health implications can be very different as exhibited in Table 6.4. The infectious pathogen responsible for a diarrheal episode can only be reliably determined through laboratory analysis. The laboratory diagnosis of infectious diarrhea is additionally complicated by the multitude of methods required for organism identification. Currently, there is no single diagnostic test which can detect all of the myriad organisms that are implicated in infectious diarrhea. Numerous diagnostic tests may be necessary to obtain the correct epidemiological information on the nature and extent of the diarrheal problem in a region.

The typical laboratory workup for a patient with infectious diarrhea involves several stool tests, including microbiological culture, microscopic examination, pH measurement, toxin assays, fecal leukocyte testing, enzyme immunoassay, latex agglutination, electrolytes, and fat. Routine stool cultures identify only *Campylobacter*, *Shigella*, *Salmonella*, *Aeromonas*, and *Yersinia* (Fig. 6.13). Special

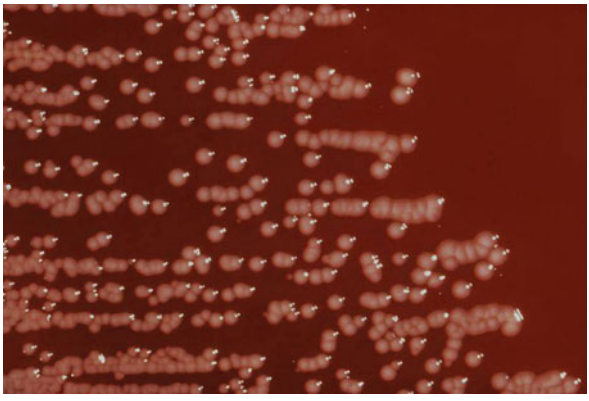

Fig. 6.13 Growth of *Yersinia enterocolitica* bacterial colonies on a blood agar plate (Centers for Disease Control)

Table 6.5 Culture media required for isolation of bacterial species

Detection method	Microbiologic characteristics
Blood agar	All aerobic bacteria and yeast; detects cytochrome oxidase production
MacConkey eosin-methylene blue (EMB) agar	Inhibits gram-positive organisms; permits lactose fermentation
Xylose-lysine-deoxycholate (XLD); Hektoen enteric (HE) agar	Inhibits gram-positive organisms and nonpathogenic GNB; permits lactose fermentation and H_2S production
Skirrow agar	Selective for *Campylobacter* species
Sorbitol-MacConkey (SM) agar	Selective for enterohemorrhagic *E. coli*
Cefsulodin-ingrasan-novobiocin (CIN) agar	Selective for *Y. enterocolitica*
Blood or thiosulfate-citrate-bile-salts-sucrose (TCBS) agar	Selective for *Vibrio* species
Cycloserine-cefoxitin-fructose-egg (CCFE) agar	Selective for *C. difficile*

culture methods are required for other bacterial pathogens, such as *Vibrio* species, enterohemorrhagic *E. coli* O157:H7, and other Shigatoxin-producing bacteria. Table 6.5 lists the various culture media that are currently used to isolate bacteria for diagnosis of diarrhea. Table 6.6 summarizes the optimal growth conditions and microbiologic characteristics of selected pathogens. As indicated by these lists, stool culture alone can encompass several tests, and a large investment of equipment and time. A high index of suspicion is needed to choose the appropriate medium.

In addition to stool culture for isolation of bacterial organisms, the following laboratory strategies are utilized to distinguish enteric pathogens:

- The presence of fecal leukocytes raises suspicion for *Salmonella*, *Shigella*, *Campylobacter*, and *Y. enterocolitica* (Fig. 6.14). It eliminates consideration of enterotoxigenic *E. coli*, *Vibrio*, and viruses.
- A stool pH level of less than 6.0 in the presence of reducing substances indicates carbohydrate intolerance, which is usually secondary to viral illness.
- Microscopic examination of stools for ova and parasites is used for finding parasites.
- Rotavirus antigen can be identified by enzyme immunoassay and latex agglutination assay of the stool.
- Adenovirus antigens can be detected by enzyme immunoassay.
- Immunofluorescent antibody and enzyme immunoassays are also available for *Giardia* and *Cryptosporidium* organisms.
- *C. difficile* can be identified by a specific toxin assay.
- Intestinal biopsy may be indicated for chronic diarrhea, as well as cases in which the search for a cause is mandatory (HIV/AIDS or immunosuppressed patients).

Even if all of these tests are performed, an infectious cause for diarrhea may not be discovered, or the testing may be too slow to permit immediate intervention. Stool cultures typically take several days to complete, and culture methods lack

Table 6.6 Optimum culture media and microbiologic characteristics of bacteria commonly associated with infectious diarrhea

Organism	Detection method	Microbiologic characteristics
Aeromonas species	Blood agar	Oxidase-positive flagellated gram-negative bacillus
Campylobacter species	Skirrow agar	Rapidly motile curved gram-negative rod
C. difficile	Cycloserine-cefoxitin-fructose-egg (CCFE) agar; enzyme immunoassay (EIA) for toxin; latex agglutination (LA) for protein	Anaerobic spore-forming gram-positive rod
C. perfringens	None available	Anaerobic spore-forming gram-positive rod
E. coli	MacConkey eosin-methylene blue (EMB) or Sorbitol-MacConkey (SM) agar	Lactose-producing gram-negative rod
Plesiomonas species	Blood agar	Oxidase-positive gram-negative rod
Salmonella species	Blood, MacConkey eosin-methylene blue (EMB), xylose-lysine-deoxycholate (XLD), or Hektoen enteric (HE) agar	Non-lactose producing, non-hydrogen sulfide producing gram-negative rod
Shigella species	Blood, MacConkey eosin-methylene blue (EMB), xylose-lysine-deoxycholate (XLD), or Hektoen enteric (HE) agar	Non-lactose-producing, hydrogen sulfide producing gram-negative rod
Vibrio species	Blood or thiosulfate-citrate-bile-salts-sucrose (TCBS) agar	Oxidase-positive motile curved gram-negative bacillus
Y. enterocolitica	Cefsulodin-ingrasan-novobiocin (CIN) agar	Non-lactose-producing oval gram-negative rod

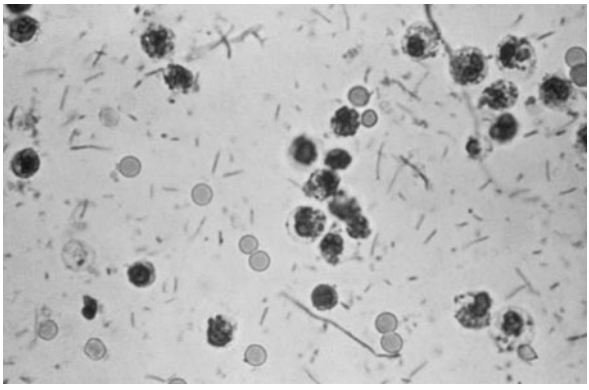

Fig. 6.14 Microscopic examination of stool from a patient with shigellosis revealing fecal leukocytes (Centers for Disease Control)

specificity. For instance, the culture method used to detect *E. coli* O157:H7 generally utilizes selective media based upon the observation that the majority of *E. coli* O157:H7 isolates do not ferment sorbitol. However, other enteric bacteria can share this phenotype, and there are reports of sorbitol-fermenting O157:H7

phenotypes. Screening based on selective culture can therefore result in false-positive and false-negative results (Weigl et al. 2006). Enzyme immunoassays are faster (2–6 h), but are still too slow for a point-of-care response; such immunoassays often lack sensitivity, specificity, and the ability to identify or differentiate organisms. Toxin assays and antigen assays are limited by the fact that bacterial organisms share virulence factors: a *Shigella* toxin originally associated with *Shigella dysenteriae* is also found in enterohemorrhagic *E. coli*. Individual antigen detection tests do not have complete correlation with diagnosis of the cause of disease. As a result, diagnostic tests that are highly specific to the etiologic agent are difficult to design. Protracted diagnosis can lead to improper treatment or uncontrolled spread of the organism.

In developing countries, where diarrhea imposes the greatest disease burden, diagnosis is further limited by financial and capital resources, as well as a lack of skilled laboratory personnel and laboratory facilities. Diagnostic testing for diarrhea is expensive: a thorough laboratory workup including stool culture costs hundreds of dollars per patient. Scientists at the Program for Appropriate Technology in Health (PATH) have summarized the current state of diarrheal diagnosis: "Diagnosing the pathogen that causes diarrhea is a non-trivial undertaking under the best conditions and essentially not feasible when resources are extremely stressed as in developing countries" (Weigl et al. 2006). Novel diagnostic platforms are needed to enable low-cost, accurate, point-of-care diagnosis of infectious diarrhea; such biomaterial devices incorporate biological molecules for pathogen capture and precise identification.

6.3 Biomaterials as Low-Cost Diagnostic Devices

There is clearly room for innovation, adaptation, and cost reduction in the diagnosis of infectious diarrhea. A major challenge for the biomaterials community is to develop diagnostic tests to meet the needs of diarrhea patients, the majority of whom are in the developing world. The goal of biomaterials research into new diagnostics is to create portable, lab-on-a-chip devices to enable immediate point-of-care diagnosis. Portable diagnostic capabilities could empower healthcare workers and patients with important information in even the most remote settings. Emerging biomaterial devices utilize microfluidics to allow miniaturization of laboratory procedures, along with multiplexing to detect the multitude of causative pathogens implicated in diarrhea. Lab-on-a-chip research can fulfill public health priorities by automating complex diagnostic procedures into a handheld microfluidic chip, bypassing the requirement of a central laboratory.

Biomaterial devices intended for diagnostic use in the developing world must meet a number of design constraints, as described in Table 6.7. Few centralized diagnostic laboratories exist in developing nations, so diagnostic tests must be able to function independently of laboratory facilities. Healthcare centers in rural areas commonly have only basic equipment; healthcare workers may have little training; and the resources to maintain complex equipment and handle fragile reagents

Table 6.7 Critical attributes of a diagnostic technology in the developing world

Factors affecting the introduction, acceptance, and sustained use of a diagnostic technology in developing countries	Key attributes of a diagnostic technology for use in developing countries
Cost of the technology	Low cost
Degree of accuracy	High degree of accuracy; low rate of false positives and false negatives
Quality control	Reproducible performance
Level of training of users	User interface that requires little training
Length of time to obtain test results	Short time to test results
Performance in a variety of settings	Stable ambient temperature storage and low power consumption
Performance under variable operating conditions (such as temperature and humidity) over time	Reproducible operation in variable environments and ruggedness
Local education on health issues	A high perceived need for the test
Availability of successful therapies	Potential for significant health improvements

Yager et al. (2006)

are often limited (Yager et al. 2006). For optimal function in low-resource settings, diagnostic assays must be rapid, low cost or cost-effective, easily interpretable, and stable when transported and stored under extreme conditions. Point-of-care diagnostics for enteric infections must return same-day test results so that patients can receive appropriate therapy while still at the clinic. Assays must be completely self-contained, since power, running water, and refrigeration are intermittent or absent in villages at the periphery of the medical care system. Devices must be battery operated, dust proof, and functional at a wide range of ambient temperatures; the devices must also be easily secured and require no maintenance or calibration.

Most importantly, diagnostic devices must be simple to use. The United States Food and Drug Administration defines a "simple test" as fulfilling the following criteria (Food and Drug Administration 2008):

- Fully automated instrument or unitized self-contained test
- Uses direct unprocessed specimens/capillary blood (fingerstick), nasal swabs, or urine
- Needs only basic, non-technique-dependent specimen manipulation, including any for decontamination
- Needs only basic, non-technique-dependent reagent manipulation, such as "mix reagent A and reagent B"
- Needs no operator intervention during the analysis steps
- Needs no technical or specialized training
- Needs no electronic or mechanical maintenance
- Produces results that require no operator calibration, interpretation, or calculations

- Produces results that are clear to read, such as positive or negative, a direct read-out of numerical values, the clear presence or absence of a line, or obvious color gradations
- Has test performance comparable to a traceable reference method, as demonstrated by studies in which intended operators perform the test
- Contains a quick reference instruction sheet written at the educational level of the user

These definitions provide an excellent goal for the ideal near-patient diagnostic.

Microfluidic systems, which operate with tiny volumes of fluid and low energy consumption, are ideal platforms for diagnostic biomaterials. Such systems manipulate fluids that are geometrically constrained to a small, typically sub-millimeter scale (Fig. 6.15). Microfluidic diagnostics can be designed to acquire and process measurements from minute samples of complex fluids, without the need for an expert operator. Complicated assays can be automated, integrated, and miniaturized into a chip of only millimeters to a few square centimeters in size. The lab-on-a-chip format has several advantages, including faster analysis and response times due to short diffusion distances, fast heating, high surface area to volume ratios, and small heat capacities. The chip consumes low amounts of sample and reagents, generating less waste and enabling lower reagent costs and smaller required sample volumes. The technology facilitates more precise process control and finer process tuning, because of faster response times and shorter dead times within the system; for instance, a microfluidic system can permit better thermal control for exothermic chemical reactions. The system is compact due to functional integration, which enables massive parallelization and high-throughput analysis. A lab-on-a-chip has low fabrication costs, allowing cost-effective mass production of disposable chips. Moreover, a microfluidic device is a safer platform for chemical or biological studies, especially with pathogens, because of smaller fluid volumes and stored energies.

There are technical hurdles associated with development of a lab-on-a-chip device. First, in order to minimize the cost of the microfluidic platform, it is essential to reduce the usage of expensive components such as glass, quartz, and silicon.

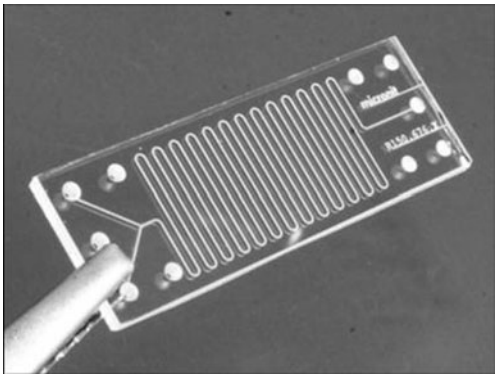

Fig. 6.15 Example of a microfluidic microreactor (Micronit Microfluidics)

Plastics are an inexpensive alternative; plastic-based microfabricated devices can be manufactured via injection molding, allowing production of large numbers at very low per-part cost. Further, within the device itself, both wet reagents and dry reagents must be stabilized. Sample pre-treatment steps, including sampling, extraction, filtration, pre-concentration, and dilution must be integrated into the device (de Mello and Beard 2003); this is especially important for complex biological specimens such as blood and stool. The device should be capable of actuating the flow of fluids with reliable flow rates using inexpensive and compact instrumentation; pneumatic actuation and capillary force are both practical for portable applications (Sia et al. 2004; Juncker et al. 2002). For complicated assays, a series of different reagents must be delivered into the microfluidic chip; passive delivery of reagents is an attractive option for portable automated devices (Juncker et al. 2002). Physical and chemical effects, such as capillary forces, surface roughness, and chemical interactions of construction materials with reaction processes, become more dominant on a small scale. This can make processes in a microfluidic device more complex than in conventional laboratory equipment. In addition, detection principles may not always scale down in a positive way, leading to low signal-to-noise ratios. An intrinsic challenge in microfluidics is detection of a signal emanating from a small physical region; appropriate detection methods for a portable device include electrical conductance and optical detection (Chin et al. 2007). Finally, it is necessary to contain the chemical reagents and biological samples in the device for disposal; environmentally friendly chemicals are preferred. Given these engineering considerations, microfluidic systems are challenging to develop and implement; however, their unique set of capabilities are precisely what is needed to create point-of-care medical diagnostics (Toner and Irimia 2005).

In terms of analytical methodology within the diagnostic device, a multiplex panel that detects multiple pathogens is advantageous for addressing infectious diarrhea. Multiplexing refers to the simultaneous detection of more than one pathogen from a single specimen. From the clinical perspective, multiplexing provides differential diagnosis capability, because the same clinical symptoms generally occur due to infections from many enteric pathogens. (*Biomaterials for multiplexed diagnostics could thus find utility for any infectious disease that has multiple causative agents, such as pneumonia and lower respiratory infections. Pneumonia and its etiologic pathogens are discussed in* Chapter 4.) There is a solid clinical rationale for a multiplex panel in diagnosing diarrhea, though there are technical risks inherent in this engineering strategy that can impact the cost, sensitivity, and specificity of the assay. Table 6.8 summarizes the advantages and disadvantages of a multiplexed assay format. A significant problem in the development of diagnostic panels for diarrhea is that the relevant pathogen combinations will vary depending on geographical disease patterns. This will not only vary from country to country, but could also shift from year to year. Such variation necessitates either a totally comprehensive diagnostic platform that can identify all potential pathogens, or an extremely flexible platform that can be readily changed for different settings.

One approach to multiplex detection is to engineer the diagnostic device so that the specimen is split or aliquoted into separate reaction compartments. As an

Table 6.8 Advantages and disadvantages of a multiplex point-of-care platform

Advantages	Disadvantages
Panel of pathogens simultaneously detected	Panel varies by geographic location
Multiple pathogen detection at reduced cost per pathogen	Increase in per-assay cost
Reagent mixture reduces cost	Reduced assay sensitivity and specificity
Single specimen mixture detection	Lower copy target may not be detected
Single assay versus multiple	Increased assay complexity – method must detect RNA, DNA, and protein (antibodies, antigens) from bacteria, viruses, parasites
Multiplex can incorporate redundancy, controls, subtyping, and drug resistance	Increased cost and assay complexity

Yager et al. (2008)

example, immunoassays for pathogen detection can be multiplexed by incorporating multiple antibodies or antigens into the device and fluidically splitting the sample specimen into different antigen or antibody assays. Similarly, nucleic acid amplification can be multiplexed in a molecular assay by incorporating multiple polymerase chain reaction (PCR) primers into the device and splitting the sample into different PCR assays. Multiplexed assay approaches that split the initial specimen into separate simplex reactions do not decrease the per-analyte cost (i.e., the reagent cost for a panel that detects six pathogens from one specimen split into six immunoassays will be equivalent to the cost of six individual assays).

An alternative approach to multiplex detection, which can save on reagent costs, is the combined detection of multiple pathogens within one reaction. For instance, the multiplexed reaction strategy for PCR is to carefully select and optimize specific primers that can function when combined into a single reaction (Markoulatos et al. 2002). The multiplexed reaction method for immunoassays is to combine antigens or antibodies into a reaction mixture. While multiplexed reactions with reagent mixtures reduce costs, frequent artifacts can result from cross-reactivity or non-specific binding when antibody, antigen, or nucleic acid primer detection reagents are combined. This results in false-positive or background signals; in general, multiplexed reactions are less sensitive and less specific than the corresponding simplex reactions. Thus, in the design of multiplex diagnostic platforms, there is a trade-off between cost and assay sensitivity and specificity. Any novel multiplexed diagnostic test must be rigorously evaluated and validated in the intended target population, particularly given the complexities of disease pathogenesis and population variations.

A lab-on-a-card assay, incorporating both microfluidic circuits and multiplex detection, is now under development for diagnosis of infectious diarrhea (Weigl et al. 2006). This “diagnostic enteric card” has been created by a consortium that includes the Program for Appropriate Technology in Health (PATH) and Micronics, Inc. The system simultaneously detects multiple enteric pathogens and rapidly recognizes and differentiates *S. dysenteriae* serotype 1; *Shigella* toxin-producing

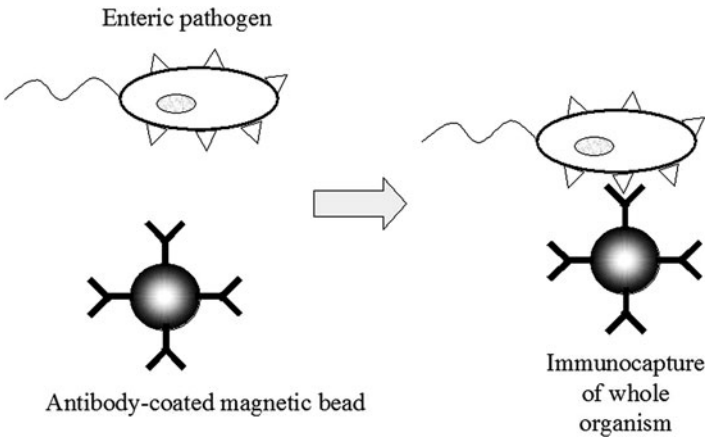

Fig. 6.16 Schematic of whole organism immunocapture with antibody-coated magnetic beads

E. coli; *Camplyobacter jejuni*; *E. coli* O157:H7; and *Salmonella* and *Shigella* species. The user injects a stool sample at one end of the card and then places the card in a processor. A combination of capillary action and positive-displacement pumping draws the sample via microchannels through a series of stations on the card. The card consists of four microfluidic subcircuits, each of which contains biomolecules for diagnosis:

(1) Immunocapture and lysing of enteric pathogens
(2) Nucleic acid extraction
(3) On-card rapid PCR for nucleic acid amplification
(4) Lateral flow detection of amplified nucleic acids

The system first identifies the bacterial agent via specific antigen capture (Fig. 6.16). The capture method utilizes antibodies coupled to magnetic beads of 1 μm diameter; the ability of such immunomagnetic beads to capture organisms has been validated for spiked stools and freshly shed stools (Weigl et al. 2006). The system then performs nucleic acid amplification to enable identification of specific virulence genes (Weigl et al. 2006). In the final step, the assay employs lateral flow strips to detect amplified nucleic acids.

The diagnostic enteric card has already demonstrated its ability to selectively isolate pathogenic organisms from stool. The immunocapture subcircuit has been tested against 14 non-pathogenic confounder organisms, and the system captures only pathogenic strains of bacteria (Weigl et al. 2006). Even in a microbially complex milieu such as the stool, the antibody-coupled magnetic beads are sufficiently selective for organism identification; for instance, antibody capture can be used to enrich for *E. coli* O157:H7 away from generic *E. coli* and other flora. The microfluidic immunocapture methodology was compared against traditional microbial culture

and enzyme immunoassay for organism identification, and the results were concordant in all cases (Weigl et al. 2006). Therefore, a microfluidic immunocapture platform can achieve point-of-care diagnosis for infectious diarrhea, independently of laboratory-based culture or enzyme immunoassay.

Another significant technical accomplishment for the diagnostic enteric card has been the validation of PCR primer sequences for on-card nucleic acid amplification. Primers have been designed for *Shigella*, *Salmonella*, *Campylobacter*, and *E. coli* that are sufficiently specific to amplify each pathogen's target sequence in the presence of other organisms (Weigl et al. 2006). The system also provides timely results: PCR at the required sensitivity levels can be accomplished in 8 min, and the total time for organism identification is approximately 10 min. All of the biochemical reagents needed for pathogen immunocapture, lysis, and DNA amplification by PCR can be stored in dry form on the diagnostic card; the dried reagents are stabilized in a trehalose matrix and retain their activity upon reconstitution. The assay card is self-contained and disposable, so that there is no risk of sample contamination, even when testing is carried out under less than ideal conditions. Because no manual intervention is required other than connecting the card to the reader, the user needs little training; almost no risk of user error exists. With only minimal equipment, such as the swab needed for sample collection, the card can be used outside the clinical setting. The projected assay cost for the entire biomolecular detection card is $1–5 in US dollars. As of 2009, PATH and Micronics Inc were recruiting patients for a clinical trial of the diagnostic enteric card in Brazil; the observational study will evaluate the performance of the assays and the platform in clinical conditions with non-expert users. If successful, such a system could soon displace current methods for diagnosis of infectious diarrhea.

Many clinical problems remain to be addressed with biomaterial diagnostics for diarrheal illness. Several other bacterial organisms are important causes of diarrhea, including *V. cholerae* and *Clostridium* species, and these microbes must be considered in the design of diagnostics for enteric pathogens. In addition, viral pathogens and parasitic pathogens contribute significantly to the overall incidence of diarrhea. An ideal point-of-care platform would distinguish viral, bacterial, and parasitic organisms and identify any and all pathogenic organisms present during a diarrheal episode. This capability would be especially helpful for mixed enteric infections caused by both bacteria and viruses. More flexible diagnostics for diarrhea, which can be adapted according to the geographic region and the patient's symptoms, must also be created. One could envision a diagnostic card for watery diarrhea, another card for bloody diarrhea, and yet another card for persistent diarrhea. These diagnostics will be enabled by biomolecules in combination with microfluidics and multiplex design.

Diarrheal disease is recognized as the most common illness in the world; diarrheal episodes cause more morbidity than any other ailment (World Health Organization 2008). Diarrhea is the third leading killer in low-income countries and is second only to pneumonia as a leading killer of children worldwide. The journalist Rose George has asserted, "Diarrhea is the world's most effective weapon of mass destruction" (George 2009). The disease has short-term and long-term effects

on the health of populations, as early malnutrition from diarrhea adversely affects growth and development of children. Diarrheal disease is not just a health issue, but an economic one as well. In sub-Saharan Africa, the treatment of waterborne diseases like diarrhea costs governments at least 12% of their total health budgets each year (United Nations Development Program 2006). The World Bank estimates the environmental health problems such as diarrhea and associated malnutrition cost low-income governments up to 9% of their annual gross domestic product (World Bank 2008). Yet diarrhea is one of the truly neglected diseases in terms of research and development efforts. Only 4.4% of research funding is directed toward diarrheal disease (Moran et al. 2009a). In 2007, total global spending for research and development to address diarrhea was merely $113.9 million (Moran et al. 2009b). In the absence of more effective diagnostics and treatments for diarrhea, millions of adults and children will continue to perish, particularly in developing nations. New biomaterials for rapid, low-cost, point-of-care diagnosis of enteric pathogens can empower caregivers to provide timely and appropriate treatment for patients, as well as enable public health officials to stem the spread of infectious diarrhea. Diagnostics are increasingly being appreciated as a global health priority: in one survey of international scientists familiar with the public health programs of developing countries, the top ranking overall priority was "modified molecular technologies for affordable, simple diagnosis of infectious diseases" (Daar et al. 2002). Similarly, in a study by the National Institutes of Health and the Bill and Melinda Gates Foundation to identify "Grand Challenges in Global Health," two of the 14 priorities involved diagnosis and measurement of patients' health statuses: "develop technologies that allow assessment of individuals for multiple conditions or pathogens at point-of-care" and "develop technologies that permit quantitative assessment of population health status" (Varmus et al. 2003). The need for improved diagnostic technologies is heightened by the emergence of antibiotic-resistant microbes; the growing HIV pandemic; and the increased threat of an accelerated epidemic-to-pandemic transition of a communicable disease owing to globalization. With improved diagnostic devices, the diarrheal "weapon of mass destruction" can be overcome. The next chapter will turn to another devastating infectious disease and the sixth leading global killer, the HIV/AIDS epidemic.

References

Adejuyigbe EA, Oyelami O, Onayemi O et al (2003) Paediatric HIV/AIDS in Ile-Ife, Nigeria. Cent Afr J Med 49:74

Ahmed F, Ansaruzzaman M, Haque E et al (2001) Epidemiology of postshigellosis persistent diarrhea in young children. Pediatr Infect Dis J 20:525

Beers MH, Porter RS, Jones TV et al (2006) Merck manual of diagnosis and therapy, 18th edn. Wiley, New York, NY

Bhutta ZA (2006) Persistent diarrhea in developing countries. Ann Nestle 64:39

Black RE, Morris SS, Bryce J (2003) Where and why are 10 million children dying every year? Lancet 361:2226

Chin CD, Linder V, Sia SK (2007) Lab-on-a-chip devices for global health: past studies and future opportunities. Lab Chip 7:41

Daar AS, Thorsteinsdottir H, Martin DK et al (2002) Top ten biotechnologies for improving health in developing countries. Nat Genet 32:229

de Mello AJ, Beard N (2003) Dealing with real samples: sample pre-treatment in microfluidic systems. Lab Chip 3:11 N

Dobbing J (1990) Early nutrition and later achievement. Proc Nutr Soc 49:103

Faveau V, Henry FJ, Breind A et al (1992) Persistent diarrhoea as a cause of childhood mortality in rural Bangladesh. Acta Paediatr 381(suppl):12

Food and Drug Administration (2008) Guidance for industry and FDA staff: recommendations for clinical laboratory improvement amendments of 1988 (CLIA) waiver applications for manufacturers of in vitro diagnostic devices. U.S. Department of Health and Human Services, Washington, DC

George R (2009) The politics of toilets. FrontLines June 2009. U. S. Agency for International Development, Washington, DC

Juncker D, Schmid H, Drechsler U et al (2002) Autonomous microfluidic capillary system. Anal Chem 74:6139

Keusch GT (2001) Toxin-associated gastrointestinal disease: a clinical overview. In: Sussman M (ed) Molecular medical microbiology. Academic Press, New York, NY

Keusch GT (2003) The history of nutrition, malnutrition, infection, and immunity. J Nutr 133:336S

Keusch GT, Fontaine O, Bhargava A et al (2006) Diarrheal diseases. In: Jamison DT, Breman JG, Measham AR et al (eds) Disease control priorities in developing countries, 2nd edn. IBRD/The World Bank and Oxford University Press, Washington, DC

Keusch GT, Thea DM, Kamenga M et al (1992) Persistent diarrhea associated with AIDS. Acta Paediatr 381(suppl):45

Khan SR, Jalil F, Zaman S et al (1993) Early child health in Lahore, Pakistan: X. Mortality. Acta Paediatr 390(suppl):109

Markoulatos P, Siafakas N, Moncany M (2002) Multiplex polymerase chain reaction: a practical approach. J Clin Lab Anal 16:47

Marshall JA (2002) Mixed infections of intestinal viruses and bacteria in humans. In: Sussman Brogden, KA; Guthmiller JM (eds) Polymicrobial diseases. ASM Press, Washington, DC

Moran M, Guzman J, Ropars AL et al (2009a) Neglected disease research and development: how much are we really spending? PLos Med 6:e30

Moran M, Guzman J, Ropars AL et al (2009b) Neglected disease research and development: how much are we really spending? The George Institute for International Health, London

Ochoa TJ, Salazar-Lindo E, Cleary TG (2004) Management of children with infection-associated persistent diarrhea. Semin Pediatr Infect Dis 15:229

Santiago LT (1983) Laboratory methods in the diagnosis of diarrheal diseases. Phil J Microbiol Infect Dis 12:130

Schorling JB, Wanke CA, Schorling SK et al (1990) Persistent diarrhea in Northeast Brazil: etiologies and interactions with malnutrition. Am J Epidemiol 132:144

Sia SK, Linder V, Parviz BA et al (2004) An integrated approach to a portable and low-cost immunoassay for resource-poor settings. Angew Chem Int Ed Engl 43:498

Toner M, Irimia D (2005) Blood-on-a-chip. Annu Rev Biomed Eng 7:77

United Nations Development Program (2006) Human development report 2006, beyond scarcity: poverty, power and the global water crisis. UNDP, New York, NY

Varmus H, Klausner R, Zerhouni E et al (2003) Public health: grand challenges in global health. Science 302:398

Weber R, Ledergerber B, Zbinden R et al (1999) Enteric infections and diarrhea in human immunodeficiency virus-infected persons: prospective community-based cohort study. Swiss HIV cohort study. Arch Intern Med 159:1473

Weigl BH, Gerdes J, Tarr P et al (2006) Fully integrated multiplex lab-on-a-card assay for enteric pathogens. Proc SPIE 6112:1

World Bank (2008) Environmental health and child survival: epidemiology, economics, experiences. World Bank, Washington, DC
World Health Organization (1988) Persistent diarrhoea in children in developing countries: memorandum from a WHO meeting. Bull World Health Organ 66:709
World Health Organization (1996) Evaluation of an algorithm for the treatment of persistent diarrhoea: a multi-centre study. International Working Group on Persistent Diarrhoea. Bull World Health Organ 74:479
World Health Organization (2008) The global burden of disease: 2004 update. WHO Press, Geneva
Yager P, Domingo GJ, Gerdes J (2008) Point-of-care diagnostics for global health. Annu Rev Biomed Eng 10:107
Yager P, Edwards T, Fu E et al (2006) Microfluidic diagnostic technologies for global public health. Nature 442:412

Chapter 7
HIV/AIDS

Infections with human immunodeficiency virus (HIV), and the resulting epidemic of acquired immune deficiency syndrome (AIDS), are the sixth leading cause of death worldwide. In 2004, HIV/AIDS was responsible for 2 million deaths, or 3.5% of all deaths globally (World Health Organization 2008). Because HIV/AIDS affects children as well as adults, the disease accounts for 5.6% of all years of life lost globally, a disproportionately high amount (World Health Organization 2008). The number of people living with HIV worldwide continues to grow. In 2008, an estimated 2.7 million new HIV infections occurred, including 430,000 new infections in children under 15 years of age, and the total population of HIV infected individuals reached approximately 33.4 million (Joint United Nations Programme on HIV/AIDS 2009a). The total number of people living with the virus in 2008 was more than 20% higher than the number in 2000, and the prevalence was roughly threefold higher than in 1990. HIV-related mortality also remains high: an estimated 2 million deaths due to AIDS-related illness occurred worldwide in 2008, including roughly 300,000 deaths in children under the age of 15 (Joint United Nations Programme on HIV/AIDS 2009a). Sub-Saharan Africa is the region most affected and is home to two-thirds of all people living with HIV worldwide, as well as over 90% of all new infections among children (Joint United Nations Programme on HIV/AIDS 2009b). Although significant advances have been made in antiretroviral therapy, HIV infection can only be managed and not cured. Once HIV infects an individual, the virus overcomes every challenge presented by the immune system. An infected person must remain on treatment medications for life, and such medications are not universally available in developing countries; only 42% of those in need had access to treatment in 2008 (Joint United Nations Programme on HIV/AIDS 2009b). An effective HIV vaccine is urgently needed to protect individuals from contracting the virus. The vaccine must be inexpensive; simple to administer; effective against all HIV subtypes; and capable of inducing long-lasting immunity. Unfortunately, efforts at developing a HIV vaccine have been unsuccessful, as the virus presents two major obstacles to vaccine research. First, HIV is characterized by enormous genetic diversity. Second, HIV establishes a chronic infection in the context of an unprimed immune system (Surman et al. 2009). Polymeric biomaterials have a potential role to play in HIV vaccines, because synthetic polymers can function as immunomodulators and vaccine adjuvants. Such adjuvants can be

S.K. Bhatia, *Biomaterials for Clinical Applications*,
DOI 10.1007/978-1-4419-6920-0_7, © Springer Science+Business Media, LLC 2010

administered with either peptide-based vaccines on DNA-based vaccines and may potentiate the immune response to HIV vaccines. Biomaterial adjuvants could be utilized to deliver and enhance HIV vaccines, thereby stopping the spread of the virus, and ultimately preventing morbidity and mortality from HIV/AIDS.

7.1 Pathogenesis of HIV/AIDS

HIV is a member of the *Lentivirus* genus, part of the Retroviridae family (Fig. 7.1). The retroviruses all contain a single-stranded RNA genome, along with the reverse transcriptase enzyme; all retroviruses are enveloped in an icosahedral protein shell known as the capsid. Retroviruses are associated with malignancies, neurological deficiencies, and immunodeficiencies (Coffin et al. 1997). In particular, the lentiviruses (also called the "slow" viruses) are characteristically responsible for long-duration illnesses with an extended incubation period. Lentiviruses are the causative agents of a variety of diseases, including immunodeficiencies, neurological degeneration, and arthritis (Coffin et al. 1997). The lentiviruses are unique among retroviruses, in that lentiviruses can infect dividing as well as non-dividing cells. In addition, lentiviruses possess a unique cone-shaped capsid (Fig. 7.2). Lentiviruses are transmitted as single-stranded, positive-sense, enveloped RNA viruses; each lentivirus is diploid, possessing two strands of single-stranded RNA in the genome. When a lentivirus enters a target cell, the viral RNA genome is converted to double-stranded DNA by the virally encoded reverse transcriptase enzyme. The viral DNA is then integrated into the host cell chromosome by a virally encoded integrase enzyme, so that the viral genome can be transcribed.

HIV primarily infects vital cells of the human immune system. Specifically, HIV targets human cells bearing the CD4 surface receptor (so-called CD4+ cells); susceptible cellular populations include CD4+ T lymphocytes, macrophages, and dendritic cells. Two distinct subtypes of HIV exist: HIV-1 and HIV-2. HIV-1 is

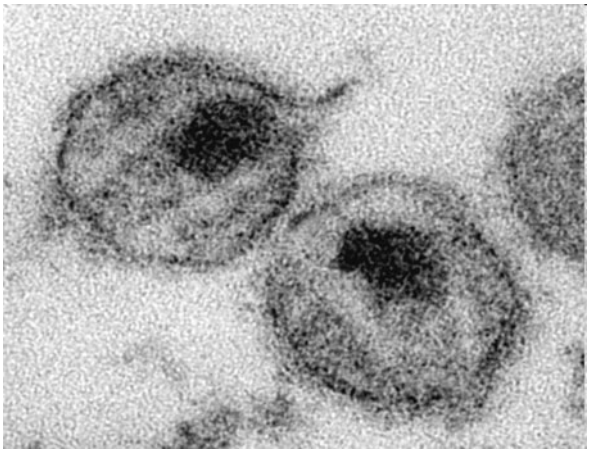

Fig. 7.1 Transmission electron micrograph of several HIV particles, depicting the ultrastructural details of the viruses. HIV is the causative agent for AIDS (Centers for Disease Control)

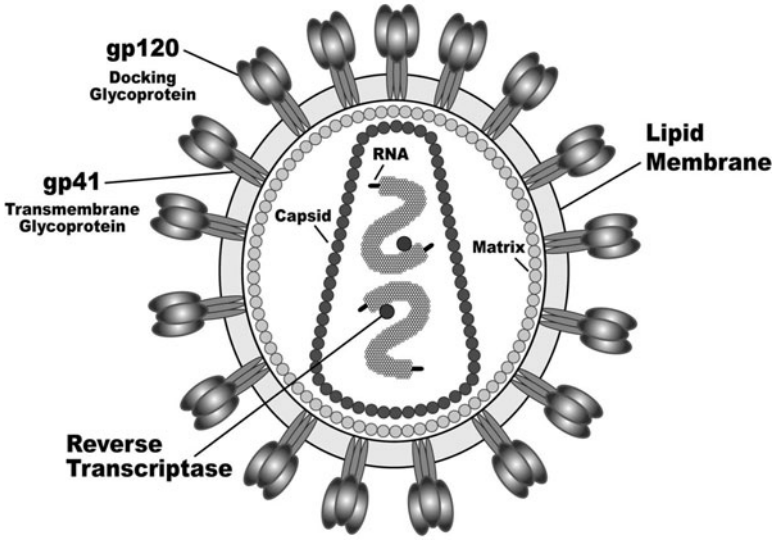

Fig. 7.2 Schematic diagram of a HIV virion (National Institute of Allergy and Infectious Diseases)

predominant and found throughout the world, while HIV-2 has been isolated primarily in West African countries such as Guinea Bissau, Ivory Coast, and Senegal, with some cases also identified in the Americas and Western Europe (Coffin et al. 1997). Both agents can cause progressive immunologic deterioration, and both have the capacity to persist and replicate in the face of humoral and cellular immune responses. HIV-1 has been used as the prototype in the majority of studies on HIV pathogenesis, and HIV-1 is the major cause of AIDS.

In terms of structure, HIV is a roughly spherical particle, approximately 100 nm in diameter (Kindt et al. 2006). The interior of the HIV particle contains two copies of single-stranded RNA, two molecules of p64 (reverse transcriptase), and an integrase and a protease. The viral genome is enclosed by a conical capsid composed of the viral protein p24. A matrix composed of the viral protein p17 surrounds the capsid, to ensure the integrity of the virion particle. The matrix is further surrounded by a viral envelope, consisting of a phospholipid bilayer. Two glycoproteins are present on the outer envelope of HIV: gp120 and gp41. The gp120 surface protein binds to the CD4 receptor on human T lymphocytes, monocytes, and macrophages; the gp120 molecule is critical for HIV attachment onto host cells during the infectious cycle. The gp41 molecule associates with gp120 and crosses the viral lipid bilayer, thereby anchoring gp120 to the viral envelope. During infection, gp41 enables fusion to occur between the lipid membranes of the virus and the target cell. Both gp120 and gp41 have been considered as targets for vaccines against HIV.

The RNA genome of HIV contains nine genes: *gag, pol, env, tat, rev, nef, vif, vpr,* and *vpu* (Kuiken et al. 2009). Three of these genes (*gag, pol,* and *env*) encode the structural proteins of HIV virions. The *gag* gene codes for building blocks of the virus particle core; the *pol* gene codes for several enzymes including reverse

transcriptase and integrase; and the *env* gene codes for the gp120 and gp41 surface proteins. The remaining six genes of HIV (*tat, rev, nef, vif, vpr,* and *vpu*) play auxiliary roles; these regulatory genes encode proteins that control HIV's ability to infect cells, replicate, and induce disease. For instance, the *tat* gene codes for viral transcriptional transactivators. The nine genes of HIV are targets for DNA-based vaccines against HIV.

When HIV infects a cell, two pathways are possible: either the virus becomes latent and the infected cell continues to function or the virus becomes active and replicates. Like all viruses, HIV replicates using the genetic machinery of the host cell, typically a CD4+ lymphocyte (Fig. 7.3). The replication cycle of HIV consists of the following steps (Beers et al. 2006):

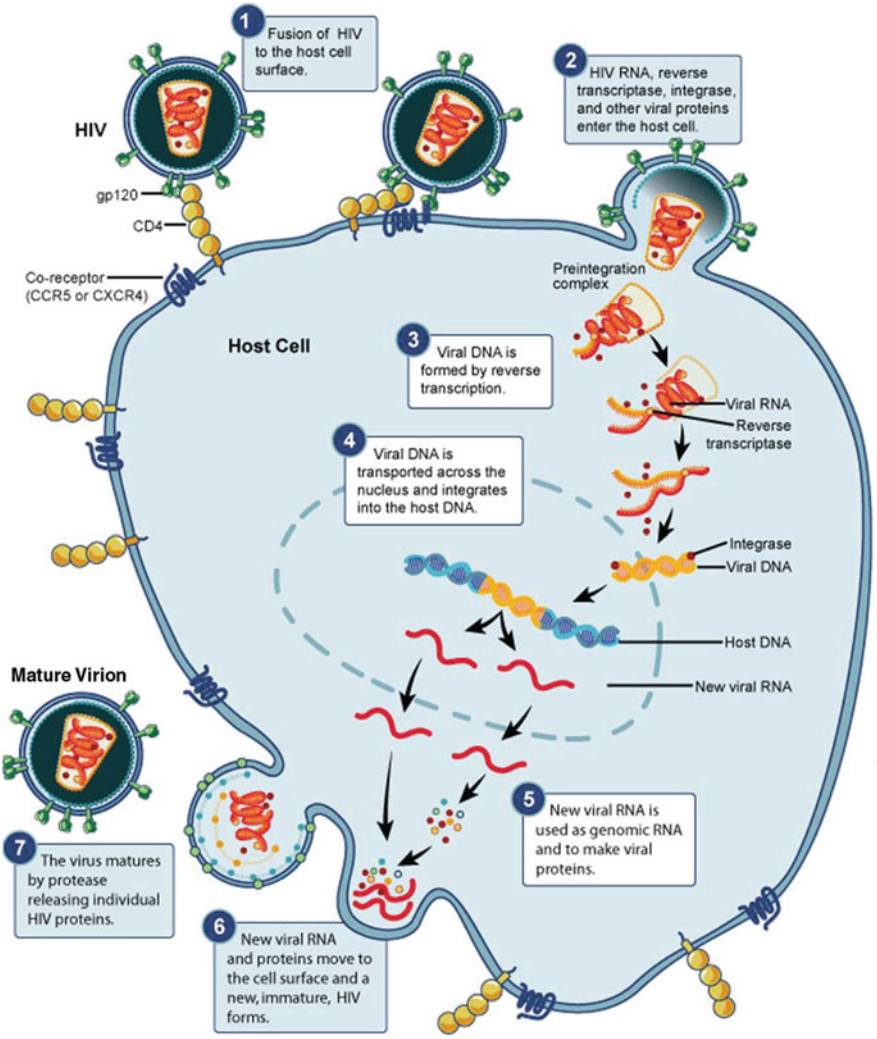

Fig. 7.3 Replication cycle of HIV (National Institute of Allergy and Infectious Diseases)

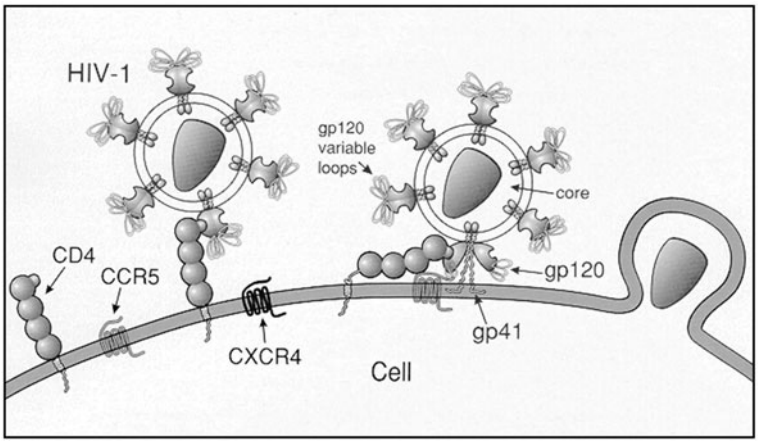

Fig. 7.4 Schematic of HIV attachment to a CD4+ lymphocyte. During HIV entry into the host cell, the surface glycoproteins (gp120 and gp41) of HIV bind to a CD4 receptor and a chemokine receptor (CCR5 or CXCR4) on the host cell surface (National Institute of Allergy and Infectious Diseases)

(1) HIV first attaches to and penetrates its target cell. To enable HIV entry into the host cell, the surface glycoproteins (gp120 and gp41) of HIV must bind to a CD4 receptor and a chemokine receptor (CCR5 or CXCR4) on the host cell surface (Fig. 7.4). CCR5 is the major co-receptor for viral entry of HIV into macrophages. CXCR4 is the entry co-receptor for those HIV strains that have an affinity for T cells (Kindt et al. 2006).
(2) HIV releases its enzymes and RNA genome into the infected cell.
(3) The viral RNA is converted to DNA, using the viral reverse transcriptase enzyme. HIV mutates easily at this point, because reverse transcriptase is prone to errors during the conversion of viral RNA to DNA.
(4) The viral DNA enters the nucleus of the host cell. The viral DNA becomes integrated into the host cell's DNA using the viral integrase enzyme.
(5) The DNA of the infected cell now produces RNA as well as proteins that are required to assemble a new HIV virion. New viral RNA is used both as genomic RNA and as a template for the production of viral proteins.
(6) A new virus is assembled from RNA and short pieces of viral protein. The immature virus particle buds through the membrane of the host cell, enveloping itself in a fragment of the cell membrane and pinching off from the infected cell (Fig. 7.5). A large number of virus particles can be liberated from an infected cell (Fig. 7.6).
(7) The virus must mature before it can infect other cells. HIV matures when a viral enzyme (HIV protease) cleaves and releases structural proteins within the virus.

Each time an HIV-infected cell divides, it creates a new copy of the integrated HIV DNA, as well as its own genes.

HIV presents a formidable challenge to immune defenses, as the virus evades the immune system, destroys the immune system, and hides from the immune system.

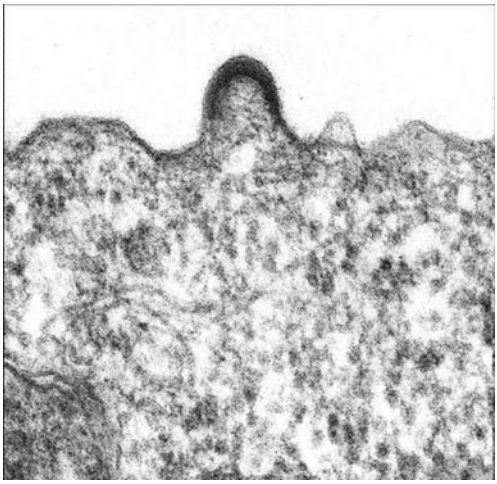

Fig. 7.5 Transmission electron micrograph of HIV budding from a cultured lymphocyte cell (Centers for Disease Control)

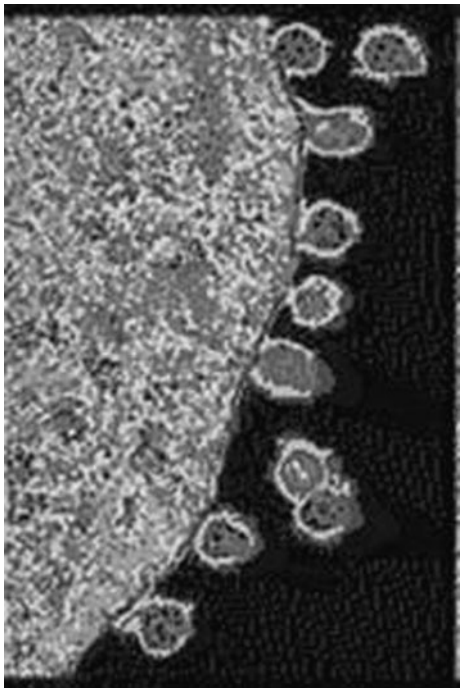

Fig. 7.6 HIV daughter particles being shed from an infected T cell (National Institute of Allergy and Infectious Diseases)

HIV evades the immune response because the virus exhibits high genetic variability; this characteristic distinguishes HIV from many other viruses. This diversity results from the fast replication cycle of HIV, along with the high HIV mutation rate and the recombinogenic properties of reverse transcriptase (Robertson et al. 1995).

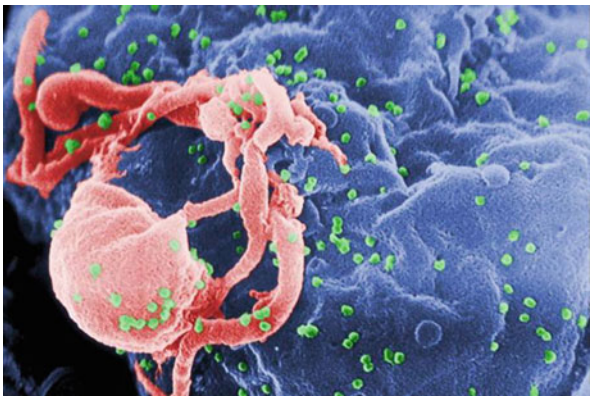

Fig. 7.7 Scanning electron micrograph of several HIV virions budding from a cultured lymphocyte cell. Multiple round bumps on the cell surface represent sites of assembly and budding of virions (Centers for Disease Control)

The HIV replication cycle generates 1,010–1,012 virions every day (Perelson et al. 1996), and reverse transcriptase makes approximately 0.2 errors per HIV genome during each replication cycle (Preston et al. 1988). This scenario leads to the generation of many variants of HIV in a single infected patient over the course of 1 day. Variability is compounded when a single cell is simultaneously infected by two or more different strains of HIV. When simultaneous infection occurs, the reverse transcriptase enzyme may recombine two genomes to synthesize a new retroviral sequence (Robertson et al. 1995). The extensive genetic variation of HIV makes the virus one of the fastest evolving of all organisms (Rambaut et al. 2004); the host immune system struggles to keep up with such a rapidly changing invader.

HIV further confounds immune defenses by destroying the cells of the immune response. HIV induces cell death via several mechanisms (Kindt et al. 2006). The virus directly kills infected host cells during active viral replication. Infected CD4+ T cells perish as a large amount of virus is produced and buds out from the cell surface (Fig. 7.7). The budding process disrupts the cell membrane and causes cytotoxicity. The host cell may also expire when the virus excessively utilizes cellular machinery for viral replication, compromising normal cellular metabolism. Beyond direct cell killing, HIV can also provoke apoptosis (cell suicide) of both infected cells and uninfected "bystander" cells. Eventually, HIV overwhelms and decimates the immune response. The immune system loses its ability to regenerate or fight infections, either from HIV or other pathogens.

Finally, HIV frustrates the efforts of the immune system, as well as antiretroviral therapies, by hiding in latent reservoirs. The formation of reservoirs allows HIV to escape the immune response; the virus can persist for long periods of time and establish a chronic infection. Latently infected resting memory CD4+ T cells are the best characterized reservoir for HIV (Richman et al. 2009). Memory T cells can survive for years or even decades, and integrated HIV can remain dormant for the duration

of an infected cell's lifetime. Antiretroviral drugs are capable of suppressing HIV to undetectable levels in the blood, yet 1 in 10^6 $CD4^+$ T cells remain latently infected with HIV in patients on antiretroviral therapy. The virus can relapse from latent reservoirs upon discontinuation of therapy. Even patients receiving antiretroviral therapy for 10 years exhibit no appreciable decrease in the size of the latent reservoir (Richman et al. 2009). Other drug-insensitive reservoirs for HIV include the brain, macrophages, and hematopoietic stem cells. Latent reservoirs of HIV represent a major obstacle to eradication of the virus.

HIV is transmitted sexually, perinatally, and via exposure to contaminated blood or body fluids. In general, the initial infection is not associated with any symptoms. However, a mononucleosis-like illness may develop 14–28 days after the infection (Kindt et al. 2006). This illness can persist from 14 days to 6 weeks. The symptoms include fever, rash, arthralgia (joint pain), malaise (generalized weakness or discomfort), hepatosplenomegaly (enlargement of the liver and spleen), and lymphadenopathy (swollen lymph nodes). During this period following primary infection, HIV disseminates widely throughout the body, and an abrupt decrease in CD4+ T cells is observed. An immune response to HIV ensues, causing a drop in blood levels of virus. The initial symptoms of primary infection eventually disappear, though lymph nodes often remain enlarged. The initial infection is followed by a long period of clinical latency. During this time, the CD4+ T-cell population continues to decline. Individuals can be infected with HIV for years, even a decade or longer, before developing any further symptoms. Once the CD4+ T-cell count falls below a critical level, the immune system is unable to fight certain infections, and the symptoms of AIDS appear (Fig. 7.8).

AIDS is diagnosed when the CD4+ T-cell count falls below 200 cells/μl of blood or when extreme wasting or certain serious opportunistic infections or cancers develop (Beers et al. 2006). Opportunistic infections take advantage of the weakened immune system and do not typically appear in individuals with a healthy immune system. Table 7.1 lists opportunistic infections that are commonly associated with AIDS. A CD4+ T-cell count below 50 cells/μl of blood is particularly dangerous, because additional opportunistic infections that rapidly cause severe weight loss, blindness, or death commonly occur. Because patients with AIDS are at increased risk of viral infection, these patients are additionally vulnerable to virally induced malignancies. Patients with AIDS may develop cancers of the immune system such as lymphomas, usually caused by Epstein–Barr virus. These patients are also susceptible to Kaposi's sarcoma, a cancer caused by a herpesvirus, as well as anogenital carcinomas caused by human papillomavirus.

The symptoms of AIDS are usually those of the specific opportunistic infections and cancers that develop. However, HIV can cause symptoms when it directly infects organ systems (Beers et al. 2006):

- Brain – memory loss or difficulty thinking and concentrating, eventually resulting in dementia as well as weakness, tremor, or difficulty walking
- Kidneys – swelling in the legs and face, fatigue, and changes in urination
- Heart – shortness of breath, cough, wheezing, and fatigue

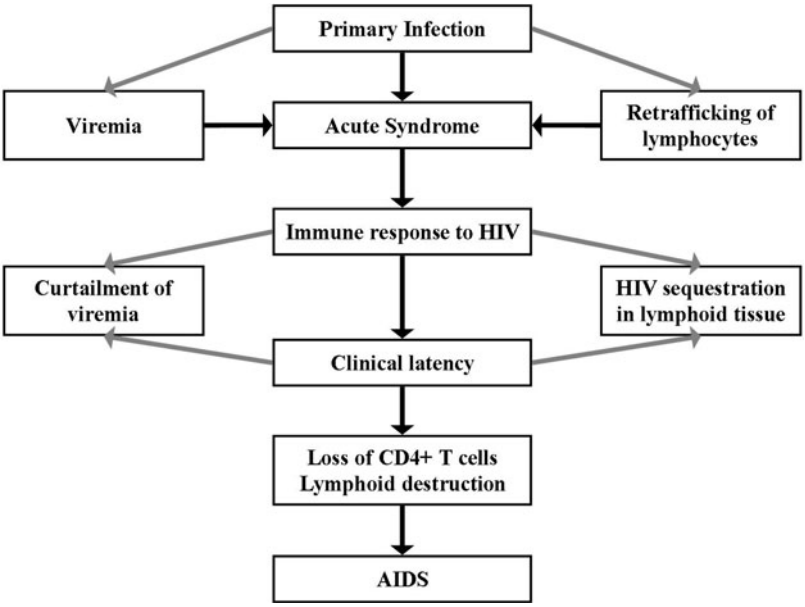

Fig. 7.8 Schematic diagram of the pathogenic events that occur from initial HIV infection to the development of clinical disease

Table 7.1 Common opportunistic infections associated with AIDS

Infection	Description	Symptoms
Candidal esophagitis	A yeast infection of the esophagus	Painful swallowing and burning in the chest
Pneumocystis jiroveci pneumonia	An infection of the lungs with the fungus *Pneumocystis jiroveci*	Difficulty breathing, cough, and fever
Toxoplasmosis	Infection with the parasite *Toxoplasma gondii* usually in the brain	Headache, confusion, lethargy, and seizures
Tuberculosis	Infection of the lungs and sometimes other organs with tuberculosis bacteria	Cough, fever, night sweats, weight loss, and chest pain
Mycobacterium avium complex infection	Infection of the intestine or lungs with a bacterium that resembles tuberculosis bacteria	Fever, weight loss, diarrhea, and cough
Cryptosporidial infection	Infection of the intestine with the parasite *Cryptosporidium*	Diarrhea, abdominal pain, and weight loss
Cryptococcal meningitis	Infection of the lining of the brain with the yeast *Cryptococcus*	Headache, fever, and confusion
Cytomegalo-virus infection	Infection of the eyes or intestinal tract with cytomegalovirus	Eye: clouding of vision or blindness Intestinal tract: diarrhea and weight loss

Beers et al. (2006)

HIV may be directly responsible for substantial weight loss (known as AIDS wasting) in infected individuals. Death is usually caused by the cumulative effects of opportunistic infections or cancers, wasting, and dementia.

HIV infection is diagnosed by testing the blood or oral mucus for the presence of anti-HIV antibodies. Current treatment for HIV consists of antiretroviral drugs, including reverse transcriptase inhibitors, protease inhibitors, fusion inhibitors, integrase inhibitors, and chemokine co-receptor inhibitors. If the CD4+ T-cell count is low, antimicrobial therapies are routinely administered to prevent opportunistic infections. While antiretroviral drugs are extremely effective in decreasing the viral load, these drugs must be taken consistently and continued for life. The drugs are expensive, with side effects which reduce quality of life. Moreover, such therapies are not always available in resource-limited settings. Without treatment, the net median survival time after initial HIV infection is approximately 10 years (Morgan et al. 2002). Once an individual progresses to AIDS, death normally occurs within a year, if antiretroviral therapy is not initiated (Morgan et al. 2002). Existing treatment regimens cannot eradicate the virus, and cure is not yet possible. For these reasons, intensive research efforts are underway to develop both prophylactic HIV vaccines and therapeutic HIV vaccines. A successful HIV vaccine must address the enormous variability of HIV isolates, stimulating a broad and potent immune response. For this reason, polymeric biomaterials are being examined as vaccine adjuvants, to create more powerful HIV vaccines.

7.2 Biomaterials as Vaccine Adjuvants

Vaccines have historically been one of the most successful interventions for infectious diseases and hold promise for halting the spread of HIV. Typical vaccines are made of either whole pathogens (killed or attenuated) or parts of pathogens and are used to induce an immune response against the targeted pathogen. Two types of vaccines can be developed: prophylactic vaccines (administered before infection occurs) and therapeutic vaccines (administered after infection has occurred). Prophylactic vaccines introduce microbial antigens into the bloodstream, thereby provoking the immune system to create antibodies, a memory record of the pathogen to fight off future infection. In contrast, therapeutic vaccines carry antigens specific to an already-present disease, attempting to stimulate the immune system against a present condition.

Both types of vaccines often include an agent to stimulate the immune system and strengthen the immune response; this additive is called an adjuvant. An adjuvant amplifies the response to a vaccine, while not having any specific antigenic effect. Adjuvants perform one or more of three main functions (Mallapragada and Narasimhan 2008): (i) adjuvants provide a delivery system or "depot" for the antigen to enable slow release; (ii) adjuvants facilitate targeting of the antigen to immune cells and enhance phagocytosis; and (iii) adjuvants modulate and enhance the type of immune response induced by the antigen alone. In addition, adjuvants may provide the "danger signal" the immune system needs to respond as vigorously to the

vaccine antigen as it would to an active infection (Janeway et al. 2001). Adjuvants thus play a significant role in every aspect of the immune response and have recently been a major target of research. Better adjuvants can enable single-dose vaccination with no boosting (Jones 2008). This would be a significant boon to developing countries, in terms of both cost-effectiveness and healthcare delivery. Improved adjuvants that are both non-toxic and strongly immunogenic are required for new vaccine technology.

In current clinical practice, the only adjuvants which are widely used in vaccines are insoluble aluminum salts, generically known as "alum." Alum is a suboptimal adjuvant for inducing antibody responses with recombinant proteins, and alum is not an effective adjuvant for inducing cytotoxic T-lymphocyte responses (Gupta and Siber 1995). This is an important consideration for the development of HIV vaccines, since cytotoxic T-lymphocyte activity is thought to be an important component of a protective vaccine against HIV infection. Further, a therapeutic vaccine to treat HIV infection is also likely to require a cytotoxic T-lymphocyte behavior (Kazzaz et al. 2000). Better adjuvants are needed to boost both the humoral immune response and the cellular immune response to HIV antigens.

Certain polymeric biomaterials, particularly polymers that contain hydrophobic domains, can exhibit natural adjuvant behavior. For example, the adjuvant activity of block copolymers of hydrophilic poly(ethylene glycol) (PEG) and hydrophobic poly(propylene glycol) (PPG) has been investigated, and the adjuvant activity increased in proportion to the size of the hydrophobic block within the copolymer (Hunter 2002). It is also well known that hydrophobic polymers increase the inflammatory response; hydrophobic bacteria are more readily phagocytosed by macrophages; and many immunostimulatory microbial products have large hydrophobic portions (Mallapragada and Narasimhan 2008). There is evidence to suggest that the toll-like surface receptors on dendritic cells have evolved to recognize and react to hydrophobic portions of molecules, should they suddenly become exposed (Seong and Matzinger 2005). In vitro studies have shown that exposure of dendritic cells to hydrophobic polymers such as poly(lactide-co-glycolide) (PLGA) and poly(β-amino ester) results in dendritic cell maturation (Little et al. 2004; Yoshida and Babensee 2004). Hydrophobic and amphiphilic polymers can therefore be exploited as vaccine adjuvants to magnify the immune response. Further, polymer particles are suitable for conjugation or loading with antigens and can simultaneously serve as delivery devices for the antigens. Polymeric particles can protect the antigen from degradation, allowing alternate routes of antigen delivery, as well as enabling sustained release of antigen.

The most popular biomaterial in adjuvant research has been the hydrophobic, biodegradable polyester PLGA (Fig. 7.9). The delivery and degradation properties of PLGA are well characterized, and the polymer has been approved for a variety of clinical uses. The PLGA copolymer is biocompatible and biodegrades by random non-enzymatic hydrolysis of ester bonds, to form lactic and glycolic acids. PLGA particles can incorporate purified native or recombinant antigens, serving as potent and safe adjuvants. It has been demonstrated that immunization with antigens entrapped in PLGA microparticles is an efficient method for boosting the

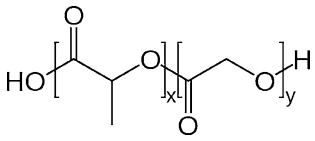

Fig. 7.9 Chemical structure of poly(lactide-co-glycolide) (PLGA). In this structure, *x* represents the number of units of lactic acid and *y* represents the number of units of glycolic acid. PLGA biodegrades by random non-enzymatic hydrolysis of ester bonds, to form lactic and glycolic acids

systemic antibody response to a soluble protein (O'Hagan et al. 1989; Eldridge et al. 1991). Antigens entrapped in PLGA microparticles can also induce a cytotoxic T-lymphocyte response (Maloy et al. 1994). Antigen-loaded PLGA particles have considerable potential as a controlled-release vaccine delivery system, providing an effective means of overcoming the need for repeated immunizations. PLGA microparticles have been utilized as vaccine delivery systems for both systemic and mucosal vaccines (O'Hagan 1997).

PLGA microparticles containing the HIV envelope protein gp120 have been examined as antigen delivery systems (Moore et al. 1995). In this investigation, the particles had a mean diameter in the range 368–501 nm, and the particles contained 0.5 wt% recombinant HIV-1 gp120. The gp120-loaded microparticles were evaluated for their ability to induce HIV-specific T-cell responses in mice. Systemic immunization (via the subcutaneous and intraperitoneal routes) of mice with gp120-loaded PLGA microparticles induced a CD4+ T-cell response. A single systemic immunization with gp120-loaded PLGA microparticles also generated a cytotoxic T-lymphocyte response, as well as proliferative T-cell responses. The proliferative response following systemic immunization with gp120-loaded microparticles was consistently stronger than that observed following immunization with soluble gp120 alone. A single intranasal administration of the gp120-loaded microparticles induced HIV-specific CD8+ cytotoxic T lymphocytes. Significant T-cell proliferation was also detected after a single intranasal immunization with the gp120-loaded particles, and this response was boosted after a second immunization. In contrast, intranasal immunization with soluble gp120 resulted in weak or undetectable proliferative T-cell responses. Entrapment of HIV gp120 in biodegradable PLGA microspheres thus enhanced the immunogenicity of the viral protein, indicating that PLGA particles can function as an effective adjuvant for HIV antigens. The HIV gp120 protein has also been encapsulated into nanoparticles composed of self-assembled amphiphilic polymers (Akaji et al. 2007). In this case, the particles were composed of poly(γ-glutamic acid) as the hydrophilic biodegradable polymer, with hydrophobic amino acids as the hydrophobic side chain. The poly(γ-glutamic acid) was hydrophobically modified by L- phenylalanine ethylester, L- tryptophan methylester, or L- tyrosine ethylester. Mice immunized with these gp120-loaded nanoparticles exhibited strong cytotoxic T-lymphocyte responses.

Polymer microparticles have shown adjuvant capabilities not only for recombinant HIV proteins but also for HIV-derived peptides. A branched octameric peptide,

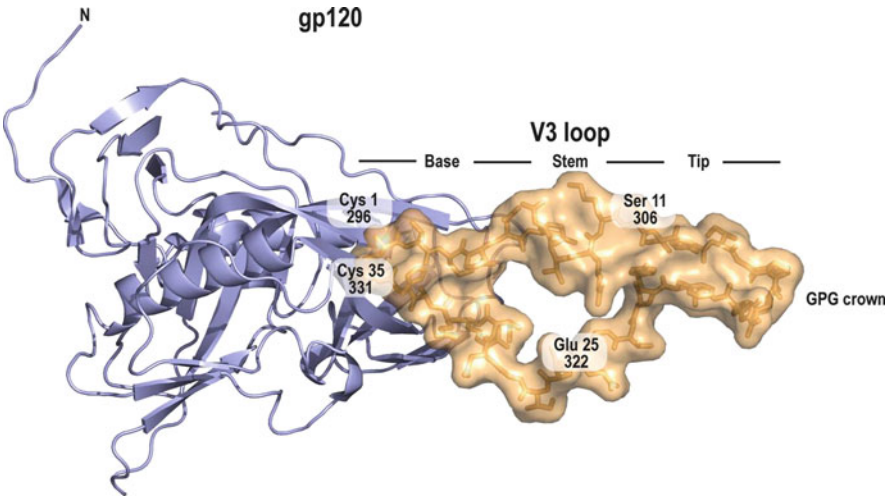

Fig. 7.10 Crystal structure of the HIV gp120 envelope protein. The V3 loop of the protein is colored in *amber* (Sander et al. 2007). The V3 region is the principal neutralizing determinant of HIV and is an important target for vaccination. HIV gp120 proteins, as well as peptides representing the gp120 V3 region, have been encapsulated in polymers to create slow-release vaccines

consisting of a sequence of 30 amino acids from the V3 loop of the HIV gp120 protein (Fig. 7.10), has been incorporated into PLGA microparticles to create a controlled-release HIV vaccine (Singh et al. 1997). The branched octameric peptide, known as p200M, represented the gp120 V3 sequence (amino acids 295–325) which is an important target for vaccination (Fig. 7.11). The V3 loop of gp120 is

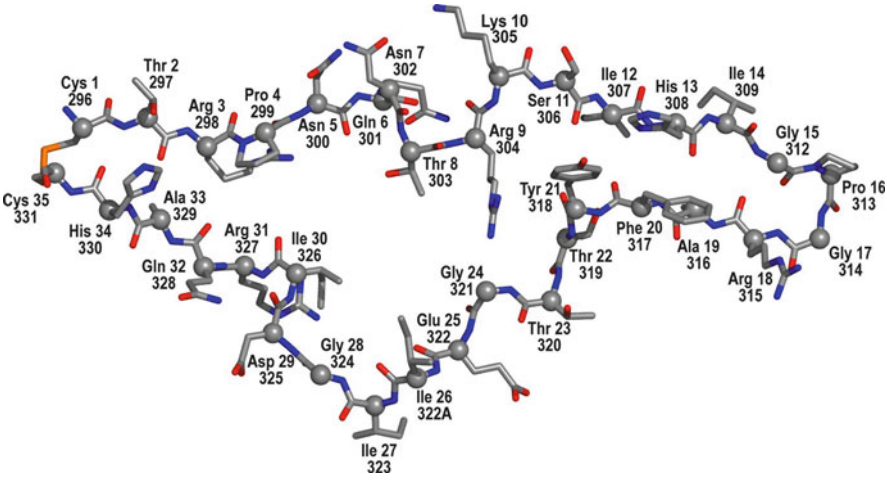

Fig. 7.11 Structure of the V3 loop of HIV gp120 envelope protein, with amino acid identifiers (Sander et al. 2007). The V3 region is the principal neutralizing determinant of HIV and is an important target for vaccination. HIV gp120 proteins, as well as peptides representing the gp120 V3 region, have been encapsulated in polymers to create slow-release vaccines

the principal neutralizing determinant of HIV: prior studies have demonstrated that neutralizing antibodies directed to the V3 region of gp120 can protect chimpanzees from virus challenge (Emini et al. 1992). The p200M peptide was encapsulated within both small and large PLGA microparticles at a 2 wt% loading level (Singh et al. 1997). The mean size of the small microparticles was approximately 500 nm and that of the large microparticles was approximately 28 μm. Both the small and large p200M-loaded microparticles exhibited a good loading efficiency of the p200M immunogen, ranging from 78 to 94%. The p200M-loaded microparticles were evaluated for their ability to induce antibody responses in mice. A single systemic immunization with the p200-loaded PLGA microparticles induced a sustained antibody response. Following the single immunization, an antibody response to the HIV immunogen was observed for 48 weeks. The antibody response was comparable to the same dose of p200M peptide administered alone on three occasions at 0, 4, and 18 weeks. This result suggested that the p200M-loaded microparticles slowly released the entrapped antigen over several months. A single-dose microparticle vaccine for HIV, which includes polymeric biomaterials, could achieve the same results as a multiple-dose vaccine schedule.

One potential issue with entrapment of antigens within polymeric particles is instability, or degradation of the encapsulated antigen. During encapsulation, antigens may be exposed to a variety of potentially damaging conditions, including high shear, aqueous–organic interfaces, organic solvents, and freeze drying. To overcome this issue, charged microparticles have been developed which allow antigen adsorption to the particle surface. PLGA microparticles can be modified to display a positively charged surface by inclusion of a cationic surfactant, such as cetyltrimethylammonium bromide (CTAB). Alternatively, PLGA microparticles may be modified to display a negatively charged surface by inclusion of an anionic detergent, such as sodium dodecyl sulfate (SDS).

Anionic microparticles have been constructed from PLGA and SDS and have shown success in efficiently and reproducibly adsorbing the recombinant p55 Gag protein from HIV (Kazzaz et al. 2000). The microparticles were used with a loading level of approximately 0.7 wt% p55 Gag, which demonstrated an adsorption efficiency of 80%. The p55-coated PLGA particles were evaluated for their ability to induce cytotoxic T-lymphocyte responses in mice. A single intramuscular immunization with the p55-coated particles, at a 10 μg dose of protein, was effective for cytotoxic T-lymphocyte induction. In contrast, the p55 Gag protein alone was ineffective for cytotoxic T-lymphocyte induction at doses of 10, 25, and 50 μg. The microparticles also exhibited a potent adjuvant effect for antibody induction against p55 Gag protein. Anionic nanoparticles have also been constructed for surface adsorption of the HIV Tat protein (Cui et al. 2004). In this case, the particle size of the nanoparticles prior to protein binding was 105 nm. At a Tat protein concentration of 25 μg/ml, the adsorption efficiency of Tat to the anionic nanoparticles was close to 100%. Approximately 6–7 Tat molecules were adsorbed on each nanoparticle. The Tat-coated nanoparticles elicited good antibody titers, as well as a CD4+

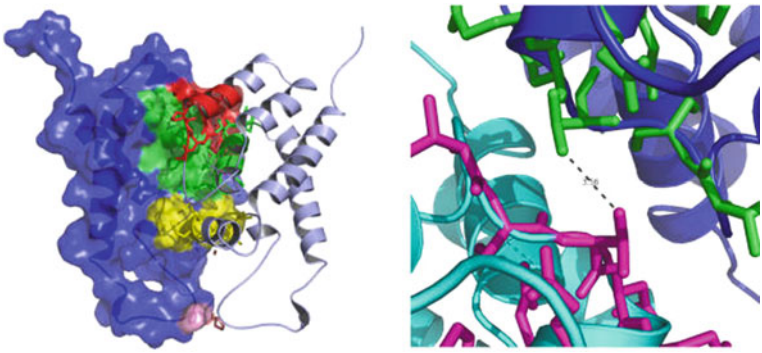

Fig. 7.12 Crystal structure of a dimer of the HIV p24 protein. One monomer is shown in combined cartoon and surface representation to show the extent of the surface-exposed part of the epitopes. For clarity, the other monomer is shown only in cartoon representation (Borghans et al. 2007). HIV p24 proteins have been adsorbed onto polymeric particles to create HIV vaccines

T helper cell type-1 immune response in mice. These results indicate that surface-modified polymeric particles can serve as adjuvants, stimulating both the humoral immune response and the cellular immune response.

Anionic nanoparticles have been further investigated for surface adsorption of HIV p24 protein (Ataman-Onal et al. 2006). Surfactant-free anionic nanoparticles were prepared from poly(D,L-lactide) (PLA) and were coated with recombinant HIV p24 protein (Fig. 7.12). The p24-coated PLA particles had a mean diameter of 500–800 nm. The particles contained approximately 21 mg of adsorbed p24 protein per gram of PLA, which corresponds to a surface density of 2.0 mg of adsorbed p24 per m^2. The p24-coated PLA particles were evaluated for their capacity to induce immune responses in mice, rabbits, and macaque monkeys. In mice, the p24-displaying PLA nanoparticles effectively induced a cytotoxic T-lymphocyte response. By contrast, p24 protein alone or p24 adjuvanted with alum were ineffective for cytotoxic T-lymphocyte induction. The p24-coated PLA nanoparticles elicited high antibody titers ($>10^6$) in mice, rabbits, and macaques. The ability of the nanoparticles to elicit a CD4+ T helper cell type-1 immune response was also confirmed in the macaque model. These outcomes again confirm that protein-coated polymeric particles can stimulate both arms of the immune system, cellular and humoral.

Because many vaccines under development are based on combined delivery of multiple antigens, the feasibility of combining multiple antigens on nanoparticle surfaces has been explored. Two HIV vaccine antigens, p24 and gp120 proteins, have been adsorbed to the surface of surfactant-free anionic PLA nanoparticles (Lamalle-Bernard et al. 2006). Nanoparticles were prepared with a 1:1 mass ratio of p24/gp120 and a 1:5 mass ratio of p24/gp120; in both cases, the mass ratio of proteins was identical in the feed and on the particle surface. The 1:1 p24/gp120

nanoparticles were 250 nm in diameter and contained 14.5 mg of total adsorbed protein per gram of PLA. The 1:5 p24/gp120 nanoparticles were 299 nm in diameter and contained 5 mg of total adsorbed protein per gram of PLA. The antigenicity of both proteins on the nanoparticle surface was preserved, and both antigens maintained their immunogenicity in the particle formulations. Monovalent and divalent PLA formulations elicited high antibody titers in mice (10^6 for p24 and 10^5 for gp120). The p24/gp120-coated particles demonstrate that anionic nanoparticles can be used for the delivery of multivalent HIV vaccines.

While anionic particles are promising vehicles for protein-based and peptide-based vaccine delivery, cationic particles can be used for DNA-based vaccine delivery. Although traditional vaccines have comprised proteins, much attention has recently been focused toward DNA vaccination. Immunization with DNA has several advantages over immunization with proteins, including the induction of cytotoxic T-lymphocyte responses (Singh et al. 2002). DNA is relatively rugged with a straightforward structure, offering the potential for improved vaccine stability and reduced costs for vaccine production. Compared to attenuated viruses as delivery vehicles for HIV genes, DNA offers a much safer alternative. Toward the creation of a DNA-based HIV vaccine, HIV gag DNA has been adsorbed onto the surface of positively-charged PLGA/CTAB microparticles (Singh et al. 2002). Intranasal immunization of mice with the PLGA–DNA microparticles produced local and systemic immune responses: gag-specific antibody-secreting cells and gag-specific cytotoxic T lymphocytes were detected in local as well as systemic lymphoid tissues. These effects were not observed in mice receiving naked gag DNA alone, indicating that the PLGA–DNA constructs were necessary to produce an immune response. Cationic PLGA/CTAB microparticles have also been created to efficiently adsorb more than one type of DNA molecule. For instance, HIV gag DNA and HIV env DNA have been simultaneously adsorbed to cationic PLGA/CTAB microparticles (Briones et al. 2001). These microparticles induced both gag-specific and env-specific antibody responses in mice, and the responses were significantly better than those elicited by naked DNA alone. The most effective vaccination regimen may turn out to be a combination of DNA-based vaccines and protein-based vaccines: in rhesus macaque monkeys, a priming vaccine of HIV gag DNA followed by a booster vaccine of p55 Gag-coated PLGA particles elicited strong antibodies, helper T cells, and cytotoxic T lymphocytes (Otten et al. 2003).

While there are several promising HIV vaccination schemes that may incorporate polymeric biomaterials, HIV vaccines still face daunting technical hurdles. There must be greater translation of HIV vaccines from animal models to clinical trials: no studies have been reported on PLGA-based vaccine formulations that attest to protective immunity in humans. Moreover, a more robust understanding of the immune response to specific polymeric biomaterials, as well as the immune response to vaccine candidates, must be established. As vaccine adjuvants, biomaterials must activate the desired adaptive immune response without overstimulating innate immune function (Mallapragada and Narasimhan 2008). From a practical perspective, HIV vaccines must be easily manufactured under good manufacturing

practice (GMP) conditions; this may be challenging for microparticles and nanoparticles, which are often fabricated in solvent-intensive processes. Most importantly, HIV vaccines must be cost-effective and stable for use in resource-limited areas, where vaccines are needed most urgently.

The HIV/AIDS epidemic has exacted a heavy toll on global health. Since the beginning of the epidemic, almost 60 million people have been infected with HIV, and 25 million people have died of HIV-related causes (Joint United Nations Programme on HIV/AIDS 2009b). In sub-Saharan Africa, the epidemic has orphaned more than 14 million children. Although treatments are available for HIV-infected individuals, the number of new HIV infections continues to outstrip the numbers on treatment. For every two people starting treatment, a further five become infected with the virus (Joint United Nations Programme on HIV/AIDS 2009b). The development of an HIV vaccine remains one of the most desirable objectives of research aimed at halting the spread of AIDS. Further research is absolutely critical to design biomaterials as HIV vaccine adjuvants and delivery systems. A controlled-release vaccine for HIV could increase patient compliance, reduce the number of drop-outs, and reduce overall vaccine immunization costs by providing savings on delivery, storage, and number of administrations (Singh et al. 1997). Unfortunately, those infected with HIV confront multiple diseases at once. One-third of people living with HIV are co-infected with tuberculosis, and tuberculosis is a leading cause of death among HIV-infected individuals (Joint United Nations Programme on HIV/AIDS 2009b). The next chapter will directly address tuberculosis, the seventh leading killer worldwide.

References

Akaji T, Wing X, Uto T et al (2007) Protein direct delivery to dendritic cells using nanoparticles based on amphiphilic poly(amino acid) derivatives. Biomaterials 28:1427

Ataman-Onal Y, Munier S, Ganee A et al (2006) Surfactant-free anionic PLA nanoparticles coated with HIV-1 p24 protein induced enhanced cellular and humoral immune responses in various animal models. J Control Release 112:175

Beers MH, Porter RS, Jones TV et al (2006) Merck manual of diagnosis and therapy, 18th edn. Wiley, New York, NY

Borghans JAM, Malgaard A, de Boer RJ et al (2007) HLA alleles associated with slow progression to AIDS truly prefer to present HIV-1 p24. PLoS One 19:e920

Briones M, Singh M, Ugozzoli M et al (2001) The preparation, characterization, and evaluation of cationic microparticles for DNA vaccine delivery. Pharm Res 18:709

Coffin JM, Hughes SH, Varmus H (1997) Retroviruses. Cold Spring Harbor Laboratory Press, Cold Spring Harbor, NY

Cui Z, Patel J, Tuzova M et al (2004) Strong T cell type-1 immune responses to HIV-1 Tat(1–72) protein-coated nanoparticles. Vaccine 22:2631

Eldridge JH, Staas JK, Meulbroek JA et al (1991) Biodegradable microspheres as a vaccine delivery system. Mol Immunol 28:287

Emini EA, Schleif WA, Nunberg JH et al (1992) Prevention of HIV-1 infection in chimpanzees by gp120 V3 domain-specific monoclonal antibody. Nature 355:728

Gupta RK, Siber GR (1995) Adjuvants for human vaccines – current status, problems and future prospects. Vaccine 13:1263

Hunter RL (2002) Overview of vaccine adjuvants: present and future. Vaccine 20:S7
Janeway CA, Travers P, Walport M et al (2001) Immunobiology: the immune system in health and disease, 5th edn. Garland Publishing, New York, NY
Joint United Nations Programme on HIV/AIDS (2009a) 2009 AIDS epidemic update. UNAIDS, Geneva
Joint United Nations Programme on HIV/AIDS (2009b) Global facts and figures. UNAIDS, Geneva
Jones KS (2008) Biomaterials as vaccine adjuvants. Biotechnol Prog 24:807
Kazzaz J, Neidleman J, Singh M et al (2000) Novel anionic microparticles are a potent adjuvant for the induction of cytotoxic T lymphocytes against recombinant p55 gag from HIV-1. J Control Release 67:347
Kindt TJ, Osborne BA, Goldsby RA (2006) Kuby immunology, 6th edn. W.H. Freeman, New York, NY
Kuiken C, Leitner T, Foley B et al (2009) HIV sequence compendium 2009. Los Alamos National Laboratory, Los Alamos, NM
Lamalle-Bernard D, Munier S, Compagnon C et al (2006) Coadsorption of HIV-1 p24 and gp120 proteins to surfactant-free anionic PLA nanoparticles preserves antigenicity and immunogenicity. J Control Release 115:57
Little SR, Lynn DM, Ge Q et al (2004) Poly-beta amino ester-containing microparticles enhance the activity of nonviral genetic vaccines. Proc Natl Acad Sci USA 101:9534
Mallapragada SK, Narasimhan B (2008) Immunomodulatory biomaterials. Int J Pharm 364:265
Maloy KJ, Donachie AM, O'Hagan DT et al (1994) Induction of mucosal and systemic immune responses by immunization with ovalbumin entrapped in poly(lactide-co-glycolide) microparticles. Immunology 81:661
Moore A, McGuirk P, Adams S et al (1995) Immunization with a soluble recombinant HIV protein entrapped in biodegradable microparticles induces HIV-specific CD8+ cytotoxic T lymphocytes and CD4+ Th1 cells. Vaccine 13:1741
Morgan D, Mahe C, Mayanja B et al (2002) HIV-1 infection in rural Africa: is there a difference in median time to AIDS and survival compared with that in industrialized countries? AIDS 16:597
O'Hagan DT (1997) Prospects for the development of new and improved vaccines through the use of microencapsulation technology. In: Levine MM, Woodrow GC, Kaper JB et al (eds) New generation vaccines, 2nd edn. Marcel Dekker, New York, NY
O'Hagan DT, Palin K, Davis SS et al (1989) Microparticles as potentially orally active immunological adjuvants. Vaccine 7:421
Otten G, Schaefer M, Greer C et al (2003) Induction of broad and potent anti-human immunodeficiency virus immune response in rhesus macaques by priming with a DNA vaccine and boosting with protein-adsorbed polylactide coglycolide microparticles. J Virol 77:6087
Perelson AS, Neumann AU, Markowitz M et al (1996) HIV-1 dynamics in vivo: virion clearance rate, infected cell life-span, and viral generation time. Science 271:1582
Preston BD, Poiesz BJ, Loeb LA (1988) Fidelity of HIV-1 reverse transcriptase. Science 242:1168
Rambaut A, Posada D, Crandall KA et al (2004) The causes and consequences of HIV evolution. Nat Rev Genet 5:52
Richman DD, Margolis DM, Delaney M et al (2009) The challenge of finding a cure for HIV infection. Science 323:1304
Robertson DL, Hahn BH, Sharp PM (1995) Recombination in AIDS viruses. J Mol Evol 40:249
Sander O, Sing T, Sommer I et al (2007) Structural descriptors of gp120 V3 loop for the prediction of HIV-1 coreceptor usage. PLoS Comput Biol 3:e58
Seong S-Y, Matzinger P (2005) Hydrophobicity: an ancient damage associated molecular pattern that initiates innate immune responses. Nat Rev Immunol 4:469
Singh M, McGee JP, Li X-M et al (1997) Biodegradable microparticles with an entrapped branched octameric peptide as a controlled-release HIV-1 vaccine. J Pharm Sci 86:1229

Singh M, Vajdy M, Gardner J et al (2002) Mucosal immunization with HIV-1 gag DNA on cationic microparticles prolongs gene expression and enhances local and systemic immunity. Vaccine 20:594

Surman SL, Sealy R, Jones BG et al (2009) HIV-1 vaccine design: harnessing diverse lymphocytes to conquer a diverse pathogen. Hum Vaccin 5:268

World Health Organization (2008) The global burden of disease: 2004 update. WHO Press, Geneva

Yoshida M, Babensee JE (2004) Poly(lactic-co-glycolic acid) enhances maturation of human monocyte-derived dendritic cells. J Biomed Mater Res A 71:45

Chapter 8
Tuberculosis

Infections with tuberculosis are the seventh leading cause of death worldwide. In 2004, tuberculosis was responsible for 1.5 million deaths or 2.5% of all deaths globally (World Health Organization 2008). The tuberculosis epidemic affects a staggering number of people: at any given time, 13.7 million individuals worldwide suffer from tuberculosis (World Health Organization 2009a). The global incidence of tuberculosis is equally significant, with new infections occurring at an alarming rate. The WHO estimates that 9.27 million new cases of tuberculosis occurred in 2007, compared to 9.24 million new cases in 2006. The disease is predominantly concentrated in developing countries: 55% of global cases occur in Asia and 31% of global cases occur in the African region. In addition, HIV co-infection plays an important role in the epidemiology of tuberculosis. Among the 9.27 million incident cases of tuberculosis that occurred in 2007, approximately 1.37 million (14.8%) were HIV positive. Among the 15 countries with the highest tuberculosis incidence rates, 13 are in Africa, a phenomenon linked to HIV co-infection (World Health Organization 2009a). While tuberculosis can be treated with antimicrobial therapies, the disease has a propensity to recur: on top of the 9.27 million "first episodes" of tuberculosis in 2007, an estimated 1.16 million "subsequent episodes" of tuberculosis occurred in 2007. Such subsequent episodes are defined as episodes occurring in patients who had already experienced at least one previous episode of tuberculosis in the past and who had received at least 1 month of anti-tuberculosis treatment (World Health Organization 2009a). Moreover, tuberculosis pathogens may be either drug susceptible or multidrug resistant; the therapeutic arsenal for both types of pathogens needs improvement. For drug-susceptible tuberculosis, the current four-drug treatment regimen (isoniazid, rifampin, ethambutol, and pyrazinamide) is effective in most cases, but the treatment takes 6–9 months because the bacteria in the infected host range from rapidly dividing to fully dormant (Webb 2009). Faster treatment protocols, as well as drugs that target both dormant and active tuberculosis bacteria, are required. The length of current treatment regimens has also contributed to the emergence of multidrug-resistant tuberculosis, a major challenge of this disease. If patients initiate treatment but cannot complete the treatment course, there is an increased risk that drug resistance will develop. The absence of effective treatments for multidrug-resistant tuberculosis is a pressing problem. Of all episodes of tuberculosis (first and subsequent), approximately

S.K. Bhatia, *Biomaterials for Clinical Applications*,
DOI 10.1007/978-1-4419-6920-0_8, © Springer Science+Business Media, LLC 2010

4.9% are multidrug resistant (World Health Organization 2009a). Therefore, novel therapeutics with different mechanisms of action are also urgently needed to counter drug-resistant strains. Biomaterials can contribute to new therapeutic regimens for tuberculosis, as new drug delivery systems can target the intracellular tuberculosis pathogen and eliminate infectious reservoirs. Nanoparticle-based drug delivery systems are under development for tuberculosis chemotherapy and may enable more directed, cost-effective cures for tuberculosis.

8.1 Pathology of Tuberculosis

Tuberculosis is a chronic, progressive infection with a period of latency following initial infection; it occurs most commonly in the lungs. Tuberculosis is caused by pathogenic mycobacteria, principally *Mycobacterium tuberculosis* (Fig. 8.1). Similar disease can also result from the closely related organisms *Mycobacterium bovis, Mycobacterium africanum,* and *Mycobacterium microti* (Beers et al. 2006). The *M. tuberculosis* pathogen is a small, aerobic non-motile bacillus. As an obligate aerobe, *M. tuberculosis* can only survive in an environment containing oxygen. The bacterium has a cell wall but lacks a phospholipid outer membrane and can be visualized by acid-fast staining (Fig. 8.2). Under physiological conditions, the bacterium can only grow within the cells of a host organism, although *M. tuberculosis* can be cultured in vitro (Fig. 8.3). *M. tuberculosis* is characterized by its extremely slow growth rate: the doubling time for *M. tuberculosis* is approximately 16–24 h (Cox 2004). By comparison, the doubling time for most bacteria is typically less than 1 h, and *Escherichia coli* divide roughly every 20 min. The extremely long generation time of *M. tuberculosis* likely contributes to the chronic nature of the disease.

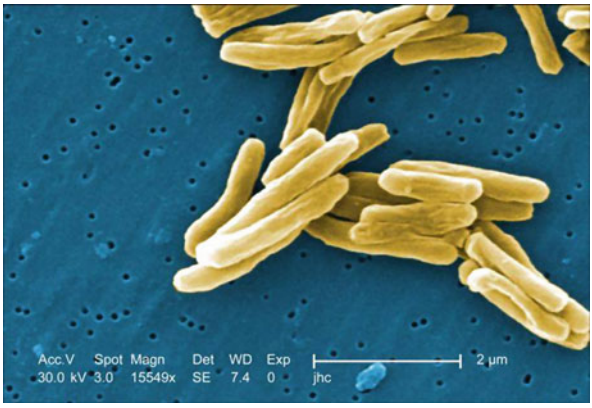

Fig. 8.1 Scanning electron micrograph of *Mycobacteria tuberculosis* organisms displaying the ultrastructural features of the bacterial cell wall. The bacterium ranges in length between 2 and 4 μm, with a width of 0.2–0.5 μm (Centers for Disease Control)

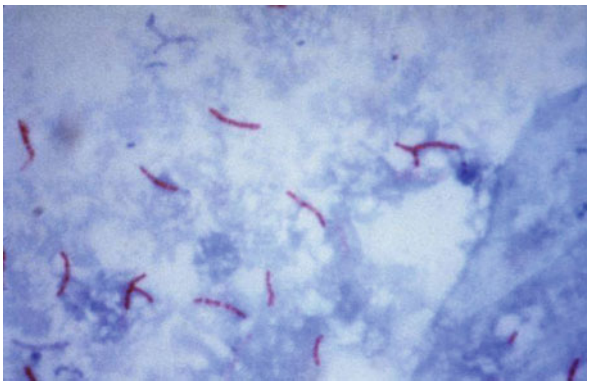

Fig. 8.2 Photomicrograph of *M. tuberculosis* bacteria stained using acid-fast Ziehl–Neelsen stain. This technique imparts a *bright red* stain to acid-fast bacilli, which are clearly visible against a *blue background* (Centers for Disease Control)

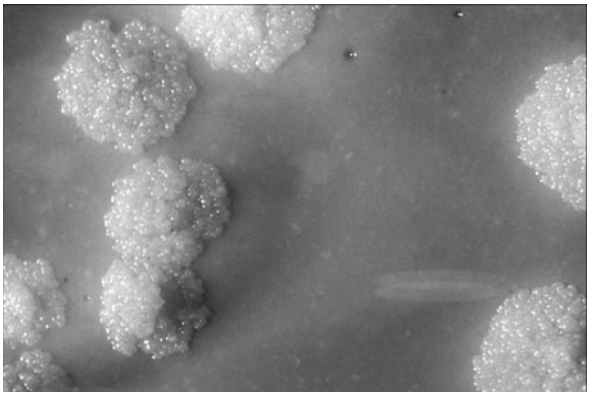

Fig. 8.3 Culture of *M. tuberculosis* bacteria revealing the colonial morphology of these organisms. Colonies exhibit a colorless rough surface with a distinct growth pattern (Centers for Disease Control)

Tuberculosis results from inspiration of airborne particles (droplet nuclei) containing *M. tuberculosis*. Individuals with active pulmonary or laryngeal tuberculosis produce airborne droplets while coughing, sneezing, or talking. The sputum of individuals with active pulmonary infection often contains a significant number of organisms, enough to render a sputum smear positive (Fig. 8.4). Although there is wide variation, patients with pulmonary tuberculosis infect an average of seven close contacts (Beers et al. 2006). Transmission is enhanced by frequent or prolonged exposure to a contagious individual in overcrowded, enclosed, poorly ventilated spaces; individuals living in poverty or in institutions are particularly at risk. Although 14–15 million individuals around the globe have active tuberculosis at any given time, it is estimated that about onethird of the world's population harbors an infection (Beers et al. 2006).

For tuberculosis infection to become established in the lung, inhaled particles must be small enough to traverse the upper respiratory defenses and deposit deep within the lung. Infection typically is initiated in the pulmonary alveoli, and the infection usually begins from a single primary focus. Once infectious droplets lodge in the alveoli, the bacteria are non-specifically phagocytosed by alveolar

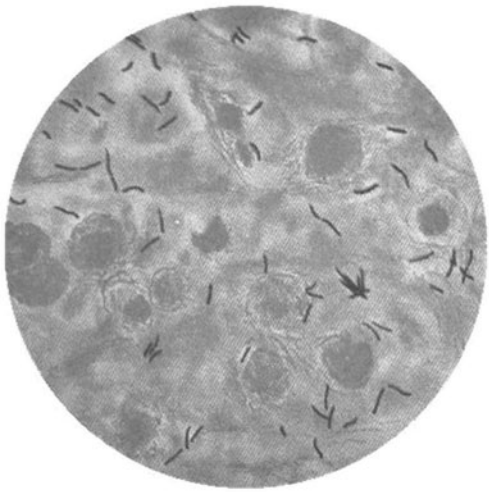

Fig. 8.4 Photomicrograph of a sputum sample containing *M. tuberculosis* bacteria (Centers for Disease Control)

macrophages (Fig. 8.5). Instead of being destroyed by the host macrophages, the bacteria survive and replicate intracellularly within the endosomes of the macrophages (Houben et al. 2006). Pathogenic mycobacteria thus have the rare ability to evade destruction within one of the most hostile cells of the host immune system, the macrophage. The mycobacteria thereby persist and maintain a niche inside the macrophages; this begins a series of events that result in either the containment of infection or the progression to active disease (Frieden et al. 2003). Bacterial replication proceeds slowly but continuously and can eventually kill host macrophages. Inflammatory cells, including activated T lymphocytes and B lymphocytes, are recruited to the site of infection. Lymphocytes surround the infected macrophages, and the cells aggregate to form a granuloma (Fig. 8.6). In the

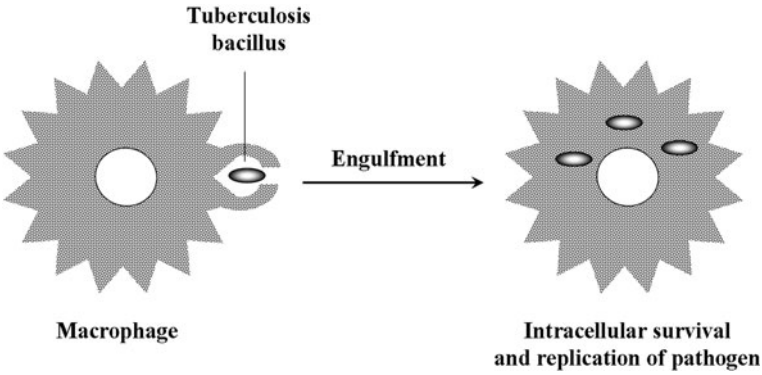

Fig. 8.5 Schematic diagram of macrophage engulfment of tuberculosis bacilli. Rather than being destroyed by the host macrophages, the bacteria survive and replicate intracellularly within the macrophages

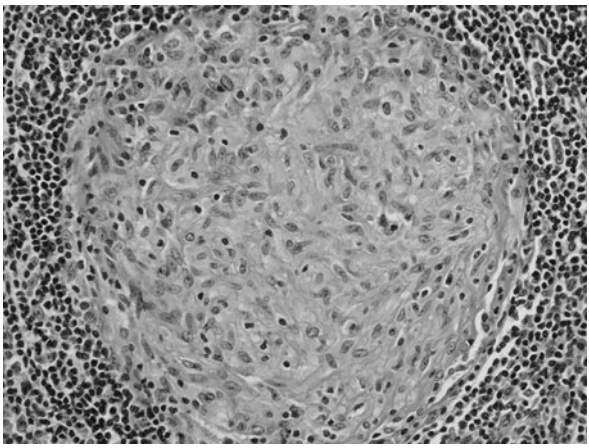

Fig. 8.6 Microscopic image of a granuloma from the lymph node of a patient with *Mycobacterium avium* infection (Sanjay Mukhopadhyay, State University of New York, Upstate Medical University)

early weeks of infection, some infected macrophages may migrate to regional lymph nodes (hilar lymph nodes of the lungs, as well as mediastinal lymph nodes between the lungs). From the lymph nodes, macrophages can access the bloodstream and spread hematogenously to any part of the body, especially the apices of the lungs, long bones, vertebrae, kidneys, and meninges. As pathogens spread through the body, the bacteria may set up additional foci of infection.

Tuberculosis infection only rarely causes acute illness; such exceptional cases are more common among young children and immunosuppressed patients and are characterized by immediate progression of the infection. However, in 95% of cases, the immune system suppresses bacillary replication within a few weeks of the infection (Beers et al. 2006). In most infected people, cell-mediated immunity develops 2–8 weeks after infection (Dye and Floyd 2006). Consequently, foci of infection within the lung or other sites resolve into epithelioid cell granulomas, which may have necrotic or caseous centers as a result of tissue destruction (Fig. 8.7). Bacteria are not always eliminated within the granuloma, but can become dormant, resulting in a latent infection. Tubercle bacilli can survive within the granuloma for years. The balance between the host's resistance and the microbial virulence determines whether the infection ultimately resolves without treatment, remains dormant, or becomes active (Beers et al. 2006). Tissue destruction and necrosis are offset by healing and fibrosis, as affected tissue is replaced by scarring and cavities (Grosset 2003). Infectious foci may leave fibronodular scars in one or both lungs, calcified scars from the primary infection, or calcified hilar lymph nodes. Unless a later defect occurs in cell-mediated immunity, the infection remains contained within the granulomas (Dye and Floyd 2006).

The cell-mediated immunity generated in tuberculosis is so potent that on average, 90% of the immunocompetent humans infected with *M. tuberculosis* are able to contain the infection and avoid progression to clinical disease during their lifetimes (Enarson and Rouillon 1994). Unfortunately, in approximately 10% of immunocompetent patients, latent infection develops into active disease. Any organ

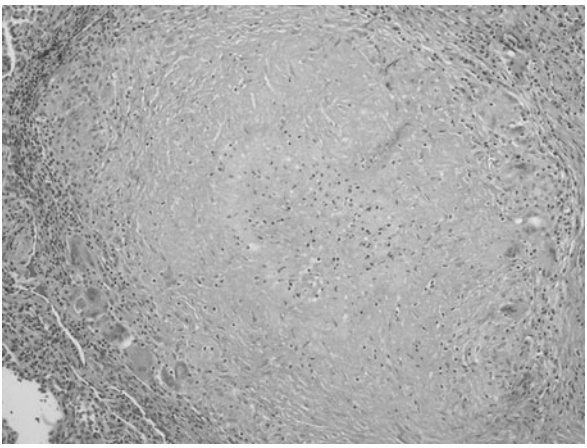

Fig. 8.7 Microscopic image of a necrotizing granuloma from a patient with tuberculosis infection. The *center* of the granuloma contains dead cells and appears as a mass of formless debris with no nuclei present. Langhans-type giant cells surround the periphery of the granuloma; each giant cell contains many nuclei arranged in a horseshoe-like pattern at the edge of the cell. Langhans giant cells are formed by the fusion of epithelioid cells (macrophages)

initially seeded with bacilli may become a site of reactivation, but reactivation occurs most often in the apices of the lungs (Beers et al. 2006). Tuberculosis usually reactivates within 2 years following the primary infection, though reactivation can occur decades later. Medical conditions that increase the risk of reactivation include impaired immunity (particularly HIV infection), immunosuppressant medications, stress, diabetes, significant weight loss, adolescence, advanced age (particularly >70 years), renal insufficiency, head or neck cancer, silicosis, renal insufficiency, and certain gastrointestinal surgeries (Beers et al. 2006). HIV-infected individuals with tuberculosis infection have a 50–60% chance of reactivation during a lifetime (Schluger 2005). During reactivation, pathogenic bacteria continue to destroy tissue and create tissue cavities. In active pulmonary disease, some of these cavities extend to the bronchi, and infectious material can be present in sputum.

A prominent symptom of active pulmonary tuberculosis is a prolonged, productive cough for more than 3 weeks. Chest pain and hemoptysis (coughing up blood) may be present, especially with cavitary tuberculosis. Systemic symptoms include low-grade fever, chills, drenching night sweats, anorexia, pallor, and weight loss. Affected individuals have a tendency to fatigue very easily. Dyspnea (shortness of breath) can result from damage to the lung parenchyma. A chest x-ray may show a multinodular infiltrate in the apical lungs; calcifications and cavitation are also evident on chest x-ray (Fig. 8.8).

Active tuberculosis infection can also extend outside the lungs via hematogenous dissemination or direct extension from an adjacent organ. This causes other types of tuberculosis, collectively denoted as extrapulmonary tuberculosis. Manifestations of extrapulmonary tuberculosis include the following:

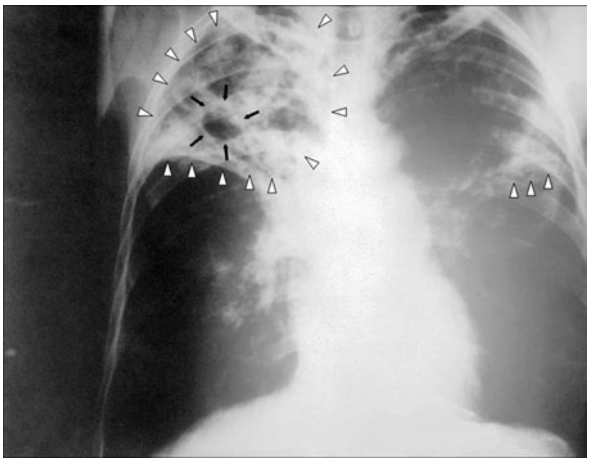

Fig. 8.8 An anteroposterior chest x-ray of a patient diagnosed with advanced bilateral pulmonary tuberculosis (Centers for Disease Control). This x-ray of the chest reveals the presence of bilateral pulmonary infiltrate (*white triangles*) and "caving formation" (*black arrows*) present in the *right* apical lung region

- *Miliary tuberculosis* – Miliary tuberculosis occurs when a tuberculous lesion erodes into a blood vessel, disseminating millions of bacteria into the blood-stream and throughout the body. The lungs and bone marrow are most often affected.
- *Genitourinary tuberculosis* – Infection in the kidneys may cause fever, back pain, and pyuria. Infection commonly spreads to the bladder. The infection can also spread to the prostate in men and the fallopian tubes in women. In pregnant women, tuberculosis infection can extend to the placenta (Fig. 8.9).
- *Tuberculous meningitis* – Meningitis results in unremitting headache, nausea, and drowsiness, which may progress to stupor and coma. It often occurs in the absence of infection at other extrapulmonary sites and has high morbidity and mortality.

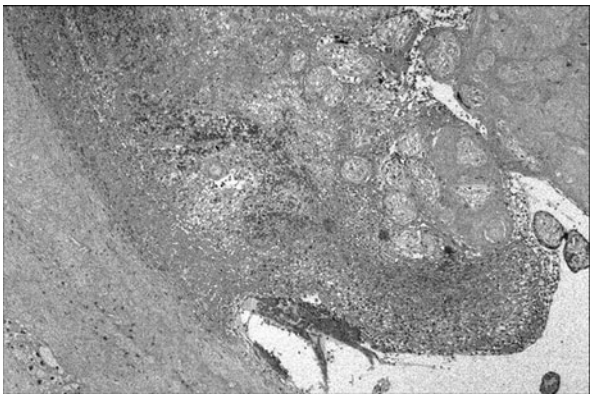

Fig. 8.9 Photomicrograph of tuberculosis of the placenta (Centers for Disease Control)

- *Tuberculous peritonitis* – Peritoneal infection may cause abdominal pain and tenderness.
- *Tuberculous pericarditis* – Pericardial infection can result in chest pain and fever. Tuberculous pericarditis is a common cause of heart failure.
- *Tuberculosis of bones and joints* – Weight-bearing joints are most commonly involved. Pott's disease is a spinal tuberculosis infection and may cause vertebral collapse and spinal cord compression.
- *Gastrointestinal tuberculosis* – Intestinal invasion causes an inflammatory bowel syndrome with pain, diarrhea, obstruction, and ulceration.

Clearly, active tuberculosis has the capacity to affect virtually every organ system in the body.

Treatment for tuberculosis consists of a multi-drug treatment regimen, which optimally includes four antimicrobial agents: isoniazid, rifampin, ethambutol, and pyrazinamide. An initial intensive phase of therapy must be continued for 2 months, followed by a continuation phase of therapy for 4–7 months. The long therapeutic course for tuberculosis is distinct from that of other bacterial infections, which are often cured following a short course of antibiotics. The lengthy treatment for tuberculosis stems from the presence of (i) non-metabolizing pathogens that are not killed by the antibiotics; and (ii) pathogens in stationary phase or proliferating at extremely low rates in old lesions or within fibrotic or calcified sites (Rook and Hernandez-Pando 1996). Tuberculosis-infected patients must take multiple drugs and comply with therapeutic regimens; treatment with any single antibiotic always results in survival of a very few (approximately 1 in a million) bacterial organisms that have acquired spontaneous resistance mutations (Beers et al. 2006). Incomplete or irregular therapy selects for these resistant pathogens; treatment compliance is therefore critical for prevention of resistance. Yet treatment adherence for tuberculosis is typically quite poor: the prolonged pharmacotherapy and the burden of multiple pills can be a hindrance to patients, particularly those in resource-limited settings with inconsistent healthcare access. As a result of non-compliance, multidrug-resistant tuberculosis (MDR-TB) strains have emerged that are resistant to both isoniazid and rifampin. Even more worrisome, extremely drug-resistant tuberculosis (XDR-TB) strains have emerged that are additionally resistant to fluoroquinolone antibiotics and injectable antibiotics (Beers et al. 2006); XDR-TB carriers dire therapeutic implications.

The importance of tuberculosis among infectious diseases is attributable not so much to the number of cases, as to the high case-fatality rate among untreated or improperly treated patients (Dye and Floyd 2006). Low adherence to treatment regimens is the main reason for therapeutic failure. In immunocompetent patients with drug-susceptible pulmonary tuberculosis, even severe disease and large cavities can heal if appropriate therapy is completed. Still, the case-fatality rate can exceed 10% if adherence to treatment is low. Tuberculosis is even more deadly in immunocompromised patients and may be fatal in as little as 2 months, especially with MDR-TB, in which mortality can approach 90% (Beers et al. 2006). Treatment adherence and clinical outcomes could be improved with long-duration drug formulations, which

release the antimicrobial agents in a slow and sustained manner. Nanoparticle-based drug delivery systems could facilitate controlled release, reducing frequency and dosing numbers. Further, nanoparticles could increase the intracellular accumulation of antimicrobial agents to target mycobacterial reservoirs within infected macrophages. These emerging biomaterials may both simplify treatment regimens and advance therapeutic efficacy, decreasing the fatality of tuberculosis.

8.2 Biomaterials for Sustained Drug Release

Currently available tuberculosis treatments involve continuous, frequent, multiple-drug dosing; this approach imposes a burden on tuberculosis patients and compromises efforts to control the tuberculosis epidemic. Biomaterials can enable long-duration drug formulations, thereby boosting patient compliance, and allowing more patients to complete a curative therapeutic course. Nanoparticles are an ideal platform for sustained release of anti-tuberculosis drugs. For the purposes of drug delivery, nanoparticles are defined as submicron (<1 μm) colloidal particles. The particles may be monolithic nanoparticles (nanospheres), in which the drug is absorbed, dissolved, or dispersed throughout the matrix. Alternatively, nanoparticles may be formulated as nanocapsules, in which the drug is contained in an aqueous or oily core, which is surrounded by a shell-like wall. Finally, drug-conjugated nanoparticles can be created; in such particles, the drug is covalently attached to the surface or within the matrix (Gelperina et al. 2005).

Drug delivery nanoparticles are typically constructed from biocompatible and biodegradable materials. These systems may be composed of natural polymers (gelatin, albumin); synthetic polymers (polylactides, polyalkylcyanoacrylates); or solid lipids. Under physiological conditions, drug-loaded nanoparticles typically release their therapeutic drugs via diffusion, swelling, erosion, or degradation. Nanoparticles possess several technical advantages as drug carriers: high stability (long shelf life); high carrier capacity (many drug molecules can be incorporated into the delivery vehicle); the ability to incorporate both hydrophobic and hydrophilic drugs; and the feasibility of various routes of administration (oral, pulmonary, subcutaneous, and intravenous). Because of the versatility of particle technologies, nanoparticle-based drug delivery systems can be tailored to the targeted tissue, the desired pharmacokinetic profile, and the route of administration (Gelperina et al. 2005).

Nanoparticle systems have been designed for sustained release of first-line anti-tuberculosis drugs and have already shown promise in vivo. Table 8.1 summarizes the properties of several nanoparticle formulations of anti-tuberculosis drugs. Polymeric nanoparticles composed of poly(lactide-co-glycolide) (PLGA) have been formulated to co-encapsulate three anti-tuberculosis drugs: isoniazid, pyrazinamide, and rifampin (Fig. 8.10). For instance, an oral formulation of PLGA (50:50) nanoparticles was created to provide controlled release of all three agents (Pandey et al. 2003a). In this case, the PLGA nanoparticles were in the size range of 186–290 nm. The encapsulation efficiency was 66% for isoniazid, 68% for pyrazinamide,

Table 8.1 Nanoparticle-based formulations of first-line anti-tuberculosis drugs (rifampin, isoniazid, and pyrazinamide)

Delivery system	In vivo model	Administration route	Duration of drug release		Regimen producing sterilizing effect
			Plasma (days)	Organs (days)	
PLGA nanoparticles	Mice	Oral	6–9	9–11	5 doses every 10 days
	Mice	Subcutaneous	32	36	Single injection
	Guinea pigs	Aerosol	4–9	10 (each drug)	5 doses every 10 days
	Guinea pigs	Oral	4–9	10 (each drug)	5 doses every 10 days
Lectin-coated PLGA nanoparticles	Guinea pigs	Oral	7–13	15 (each drug)	3 doses every 15 days
	Guinea pigs	Aerosol	6–14	15 (each drug)	3 doses every 15 days
Solid-lipid nanoparticles	Guinea pigs	Aerosol	5	7	7 doses weekly

All nanoparticle formulations were loaded with three anti- tuberculosis drugs: rifampin, isoniazid, and pyrazinamide. The drug-to-polymer ratio is 1:1 for each drug
Gelperina et al. (2005)

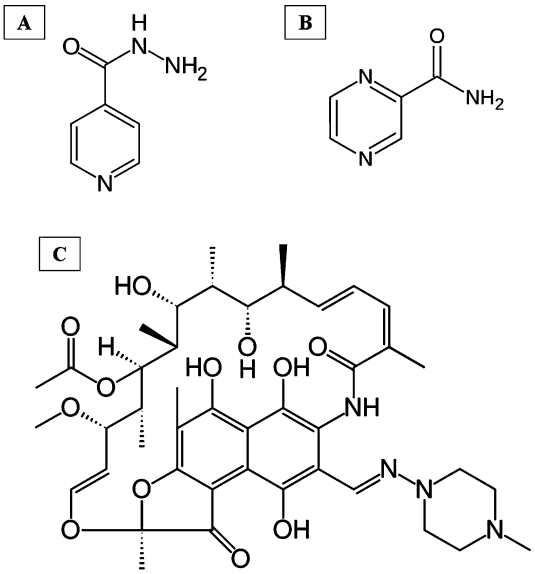

Fig. 8.10 Chemical structures of anti-tuberculosis drugs: **a** isoniazid, **b** pyrazinamide, and **c** rifampin. All three of these agents have been incorporated into nanoparticles for intracellular drug targeting

and 57% for rifampin. The drug-loaded nanoparticles contained 663 mg isoniazid per gram of polymer; 680 mg pyrazinamide per gram of polymer; and 570 mg rifampin per gram of polymer. After a single oral administration of this formulation to mice, rifampin could be detected in the circulation for 6 days, and both isoniazid

and pyrazinamide could be detected in the circulation for 9 days. Therapeutic concentrations of anti-tuberculosis drugs were maintained in the tissues for 9–11 days. In contrast, when mice received oral dosing of free (unbound) anti-tuberculosis agents, the drugs were cleared from the plasma within 12–24 h following administration. Studies in *M. tuberculosis*-infected mice revealed that five oral doses of drug-loaded PLGA nanoparticles effectively eliminated the pathogen from the lungs and spleen; each dose was administered every 10 days over a total of 50 days. Free anti-tuberculosis drugs were only able to produce bacterial clearance after daily administration for 46 days (Pandey et al. 2003a). Similar results have also been achieved in larger in vivo models: when *M. tuberculosis*-infected guinea pigs received five oral doses of drug-loaded PLGA nanoparticles every 10 days over a total of 50 days, the tuberculosis bacilli were completely cleared from the organs (Sharma et al. 2004a).

PLGA nanoparticles have additionally been functionalized with lectin molecules, to improve the bioavailability of anti-tuberculosis agents. Lectins are bioadhesive molecules that allow nanoparticles to attach to mucosal surfaces. Lectin coatings increase the adhesion of drug-loaded nanoparticles to the gastrointestinal mucosa, thereby enhancing intestinal uptake of the associated drugs. Specifically, PLGA nanoparticles have been coated with wheat germ agglutinin (Fig. 8.11). Wheat germ agglutinin is one of the least immunogenic lectins and has been widely utilized in drug delivery research. This agglutinin has affinity for receptors on intestinal epithelium and can amplify the absorption of oral drug formulations. Wheat germ agglutinin-functionalized PLGA nanoparticles have been created to provide controlled release of isoniazid, pyrazinamide, and rifampin (Sharma et al. 2004b). The functionalized nanoparticles were in the size range of 350–400 nm, with binding of 3–3.5 μg of agglutinin per mg of polymer. The encapsulation efficiency was 64% for

Fig. 8.11 Three-dimensional structure of wheat germ agglutinin, a member of the lectin family of proteins (Jawahar Swaminathan and Macromolecular Structure Database staff at the European Bioinformatics Institute). This agglutinin is one of the least immunogenic lectins and has been widely utilized in drug delivery research. Wheat germ agglutinin binds to receptors on intestinal epithelium and can enhance the absorption of oral drug formulations. The agglutinin also binds to receptors on alveolar epithelium and can enhance aerosol delivery of drug formulations

isoniazid, 67% for pyrazinamide, and 54% for rifampin. After a single oral administration of this lectin-functionalized formulation to guinea pigs, rifampin could be detected in the circulation for 7 days, and both isoniazid and pyrazinamide could be detected in the circulation for 13 days. All three drugs were present in the lungs, liver, and spleen for 15 days. (By contrast, when guinea pigs received a single oral dose of uncoated PLGA nanoparticles, rifampin could be detected in the circulation for only 4 days, and both isoniazid and pyrazinamide could be detected in the circulation for 9 days.) Because the lectin-functionalized PLGA nanoparticles extended the plasma half-life of anti-tuberculosis drugs, the nanoparticles required less frequent dosing. Studies in *M. tuberculosis*-infected guinea pigs revealed that three oral doses of drug-loaded PLGA nanoparticles effectively eliminated the pathogen from the lungs and spleen; each dose was administered every 15 days over a total of 45 days. Free anti-tuberculosis drugs were only able to produce bacterial clearance after daily administration for 45 days (Sharma et al. 2004b). Lectin-coated PLGA nanoparticles might achieve prolonged circulation of anti-tuberculosis agents by allowing (1) an increase in the time interval available for gastrointestinal absorption and (2) a localized increase in the concentration gradient between the luminal and serosal membranes of intestinal cells.

Aside from oral drug delivery, PLGA nanoparticles have also been evaluated for pulmonary drug delivery of anti- tuberculosis drugs. Direct release of anti-tuberculosis agents to the lungs can enable higher drug concentrations at the main site of infection, while reducing systemic toxicity of drugs. PLGA nanoparticles co-loaded with isoniazid, pyrazinamide, and rifampin were administered via the respiratory route to guinea pigs, and the pharmacokinetics and antibacterial effect were investigated (Pandey et al. 2003b). The aerosolized particles exhibited a mass median aerodynamic diameter of 1.88 μm, favorable for bronchoalveolar lung delivery. Following a single nebulization of the drug-loaded PLGA nanoparticles to guinea pigs, rifampin could be detected in the circulation for 6 days, and both isoniazid and pyrazinamide could be detected in the circulation for 8 days. All three drugs were present at therapeutic concentrations in the lungs for 11 days. The therapeutic effect was similar to that obtained after oral administration of the nanoparticle formulation of anti-tuberculosis drugs. Studies in *M. tuberculosis*-infected guinea pigs revealed that five nebulization doses of drug-loaded PLGA nanoparticles effectively eliminated the pathogen from the lungs; each dose was administered every 10 days over a total of 50 days. The respiratory route of administration has also been explored for wheat germ agglutinin-functionalized PLGA nanoparticles carrying isoniazid, pyrazinamide, and rifampin (Sharma et al. 2004b). In *M. tuberculosis*-infected guinea pigs, administration of three inhalation doses of lectin-functionalized PLGA nanoparticles effectively eliminated the pathogen from the lungs and spleen; each dose was administered every 15 days over a total of 45 days.

The feasibility of the aerosol route of administration has additionally been demonstrated for solid lipid nanoparticles incorporating isoniazid, pyrazinamide, and rifampin (Pandey and Khuller 2005). An advantage of solid lipid nanoparticles is that they are composed of physiological compounds, which may aid in

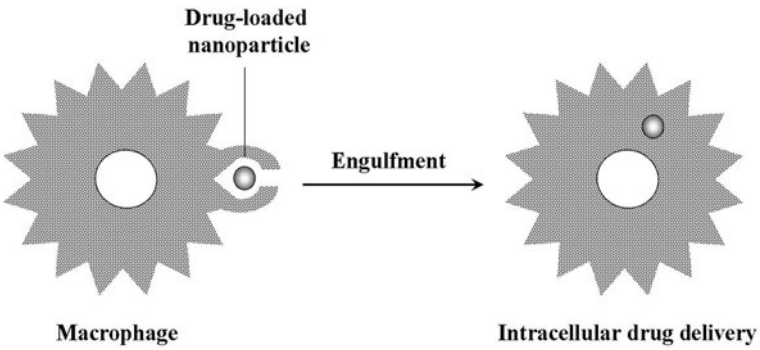

Fig. 8.12 Schematic diagram of macrophage engulfment of drug-loaded nanoparticles. The nanoparticles can be loaded with antimicrobial drugs, and the engulfment process enables intracellular delivery of the antimicrobial therapies

biocompatibility. Within the solid lipid nanoparticle formulation, the encapsulation efficiency was 45% for isoniazid, 41% for pyrazinamide, and 51% for rifampin. In *M. tuberculosis*-infected guinea pigs, administration of seven inhalation doses of drug-loaded solid lipid nanoparticles effectively eliminated the pathogen from the lungs and spleen. Taken together, these data suggest that the respiratory route is viable for controlled delivery of anti- tuberculosis agents.

Nanoparticles are sufficiently flexible to allow other dosing methods, including subcutaneous and intravenous routes of administration. For instance, a single subcutaneous dose of PLGA nanoparticles co-loaded with isoniazid, pyrazinamide, and rifampin to mice produced therapeutic drug levels in plasma for 32 days, as well as therapeutic drug concentrations in the lungs for 36 days (Pandey and Khuller 2004). A single subcutaneous injection of this formulation was sufficient to treat *M. tuberculosis*-infected mice and produced a sterilizing effect in the lungs and spleen. As an alternative, intravenous administration of drug-loaded nanoparticles is currently being pursued; this strategy could facilitate intracellular targeting of tuberculosis pathogens. In the vascular system, nanoparticles are small enough to allow intracapillary passage followed by efficient cellular uptake. When administered intravenously, nanoparticles follow the same route as other foreign particulates, including intracellular pathogens such as *Mycobacterium*. The drug-loaded nanoparticles are preferentially engulfed by macrophages (Fig. 8.12). This phenomenon results in improved drug delivery to macrophages, increasing the amount of drug at the target site and decreasing adverse effects. Clofaziminie, an agent considered for treating patients with *Mycobacterium avium* infection, has been formulated as a nanosuspension (Peters et al. 2000). Intravenous injection of this nanocrystalline formulation resulted in considerable reduction of bacterial loads in the liver, spleen, and lungs of mice infected with *M. avium*.

Overall, nanoparticle-based delivery systems for anti- tuberculosis drugs may represent a cost-effective and promising approach, particularly for treatment of patients in developing countries. Nanoparticles have shown the potential to improve

drug bioavailability and reduce dosing frequency through versatile routes of administration, including oral, inhalation, subcutaneous, and intravenous. Nanoparticle-based drug delivery systems may be a sound technology platform for better management of tuberculosis, making treatment more practical and affordable. If such technologies reach clinical usage, more patients may successfully complete tuberculosis treatment. In turn, fewer patients would develop drug-resistant tuberculosis. Future research on nanoparticle-based drug delivery systems should focus on the fate of nanoparticles in the body, as well as any toxicologic issues associated with nanoparticles. Moreover, future work must translate the experimental success of nanoparticles into clinical trials.

In 2008, WHO reported that the highest rates of MDR-TB ever recorded, with peaks of up to 22% of new tuberculosis cases, were in some settings of the former Soviet Union. In the same region, 1 in 10 cases of MDR-TB was XDR-TB (World Health Organization 2009b). In 2009, a World Health Assembly resolution regarding MDR-TB and XDR-TB was endorsed by 192 WHO Member States and included recommended priority actions to combat drug-resistant tuberculosis. To minimize the emergence of drug resistance, patients with tuberculosis must receive efficacious and complete treatment. Biomaterials for drug delivery can be integral to successful treatment regimens, preventing not only drug resistance but also morbidity and mortality from tuberculosis. Millions of tuberculosis-infected patients are in need of sensible treatment strategies, especially in light of the parallel epidemics of HIV and tuberculosis. While tuberculosis often begins in the lungs, the infection can extend to the bloodstream and virtually every organ in the body. The next chapter will discuss yet another disease that originates in the lungs, but can spread to affect the entire body: lung cancer, the eighth leading killer in the world.

References

Beers MH, Porter RS, Jones TV et al (2006) Merck manual of diagnosis and therapy, 18th edn. Wiley, New York, NY

Cox RA (2004) Quantitative relationships for specific growth rates and macromolecular compositions of *Mycobacterium tuberculosis*, *Streptomyces coelicolor* A3(2) and *Escherichia coli* B/r: an integrative theoretical approach. Microbiology 150:1413

Dye C, Floyd K (2006) Tuberculosis. In: Jamison DT, Breman JG, Measham AR et al (eds) Disease control priorities in developing countries, 2nd edn. IBRD/The World Bank and Oxford University Press, Washington, DC

Enarson DA, Rouillon A (1994) The epidemiological basis of tuberculosis control. In: Davis PDO (ed) Clinical tuberculosis. Chapman & Hall, London, UK

Frieden TR, Sterling TR, Munsiff SS et al (2003) Tuberculosis. Lancet 362:887

Gelperina S, Kisich K, Iseman MD et al (2005) The potential advantages of nanoparticle drug delivery systems in chemotherapy of tuberculosis. Am J Respir Crit Care Med 172:1487

Grosset J (2003) *Mycobacterium tuberculosis* in the extracellular compartment: an underestimated adversary. Antimicrob Agents Chemother 47:833

Houben ENG, Nguyen L, Pieters J (2006) Interaction of pathogenic mycobacteria within the host immune system. Curr Opin Microbiol 9:76

Pandey R, Khuller GK (2004) Subcutaneous nanoparticle-based antitubercular chemotherapy in an experimental model. J Antimicrob Chemother 54:266

Pandey R, Khuller GK (2005) Solid lipid particle-based inhalable sustained drug delivery system against experimental tuberculosis. Tuberculosis 85:227

Pandey R, Sharma S, Zahoor A et al (2003b) Poly (DL-lactide-co-glycolide) nanoparticle-based inhalable sustained drug delivery system for experimental tuberculosis. J Antimicrob Chemother 52:981

Pandey R, Zahoor A, Sharma S et al (2003a) Nanoparticle encapsulated antitubercular drugs as a potential oral drug delivery system against murine tuberculosis. Tuberculosis 83:373

Peters K, Leitzke S, Diederichs JE et al (2000) Preparation of a clofazimine nanosuspension for intravenous use and evaluation of its therapeutic efficacy in murine Mycobacterium avium infection. J Antimicrob Chemother 45:77

Rook GAW, Hernandez-Pando R (1996) The pathogenesis of tuberculosis. Annu Rev Microbiol 50:259

Schluger NW (2005) The pathogenesis of tuberculosis. The first one hundred (and twenty-three) years. Am J Respir Cell Mol Biol 32:251

Sharma A, Pandey R, Sharma S et al (2004a) Chemotherapeutic efficacy of poly (DL-lactide-co-glycolide) nanoparticle encapsulated antitubercular drugs at sub-therapeutic dose against experimental tuberculosis. Int J Antimicrob Agents 24:599

Sharma A, Sharma S, Khuller GK (2004b) Lectin-functionalized poly(lactide-co-glycolide) nanoparticles as oral/aerosolized antitubercular drug carriers for treatment of tuberculosis. J Antimicrob Chemother 54:761

Webb S (2009) Public-private partnership tackles TB challenges in parallel. Nat Rev Drug Discov 8:599

World Health Organization (2008) The global burden of disease: 2004 update. WHO Press, Geneva

World Health Organization (2009a) Global tuberculosis control: WHO report 2009. WHO Press, Geneva

World Health Organization (2009b) Tuberculosis facts 2009. WHO Press, Geneva

Chapter 9
Lung Cancer

Lung cancers, including tracheal and bronchial cancers, are the eighth leading cause of death worldwide. Globally, lung cancers are the most frequent cause of cancer death among men and the second most frequent cause of cancer death among women. In 2004, lung cancer was responsible for 1.3 million deaths or 2.3% of all deaths globally and 1.2% of all years of life lost (World Health Organization 2008). Lung cancer is predominantly a twentieth century phenomenon, whose rising incidence has been closely linked to the rise of cigarette smoking. Already, lung cancer has established itself as the third leading cause of death overall in high-income countries (World Health Organization 2008). With increased smoking in developing countries, the incidence of lung cancer is expected to rise in coming years, particularly in China (Liu et al. 1998) and India (Behera and Balamugesh 2004). Moreover, smokers are not the only people at increased risk for lung cancer; non-smokers can develop lung cancer as a result of genetic predisposition, radon gas exposure, occupational carcinogens, and environmental air pollution including secondhand smoke. Several treatment modalities for lung cancer are currently available, such as surgery, radiation, and chemotherapy. Yet these treatment options have limited efficacy, and the prognosis for those afflicted by lung cancer is grim: The 5-year survival rate with treatment is only 14% (Minna and Schiller 2008). Fortunately, rapid progress has been made in defining the pathophysiological characteristics and molecular basis of cancerous lung tumors. Biomaterials are now being developed that specifically target the vasculature and cellular architecture of cancerous lung masses. Such materials can carry anti-cancer agents directly to cancer cells and have the promise to decrease mortality from lung cancer.

9.1 Pathology of Lung Cancer

Lung cancer, like all cancers, is a disease of uncontrolled cellular proliferation and unchecked tissue growth. Tumor growth may lead to compression and disruption of local anatomical structures of the lung, as well as invasion of adjacent tissue, and infiltration beyond the lungs in a process known as metastasis. Cancerous lung tumors are caused by chronic exposure to inhaled irritants and carcinogens; noxious

S.K. Bhatia, *Biomaterials for Clinical Applications*,
DOI 10.1007/978-1-4419-6920-0_9, © Springer Science+Business Media, LLC 2010

agents such as tobacco smoke inflict repeated injury on lung tissues. This exposure triggers a reactive and inflammatory process, eventually resulting in alterations to the DNA of pulmonary cells. As genetic alterations accumulate, lung cells transform from a normal phenotype into a malignant phenotype. When the process involves the full thickness of the lung mucosa, carcinoma in situ is present. Infiltration of malignant cells into the underlying stromal tissue signals the first sign of invasive cancer. The process of carcinogenesis may take 10–20 years to evolve (Kufe et al. 2003). The long time period between the initial exposure to a carcinogen and the development of clinical lung cancer suggests that multiple molecular events are required for the expression of the malignant phenotype.

Lung cancer is one of the few human cancers for which the carcinogen is known. Cigarette smoke contains over 60 carcinogens (Hecht 2003), including polycyclic aromatic hydrocarbons from tars produced during tobacco combustion. Tobacco also contains specific carcinogens related to nicotine, including nitrosamines such as 4-(*N*-methyl-*N*-nitrosamino)-1-(3-pyridyl)-1-butanone (NNK) (Hecht et al. 1998). In addition, nicotine suppresses the immune response to malignant growths in exposed tissue (Sopori 2002). Across the developed world, almost 90% of cancer deaths are caused by smoking (Peto et al. 2006). The risks of dying of lung cancer are 22 times higher for male smokers and 12 times higher for female smokers than for those who have never smoked (Kufe et al. 2003). An individual's risk of developing lung cancer increases with the length of time that the individual has smoked, as well as the rate of smoking.

However, smoking is not the only cause of lung cancer; approximately 10–15% of lung cancer patients have never smoked (Thun et al. 2008). Lung cancer occurs in association with occupational and environmental exposure to carcinogenic agents other than tobacco smoke, such as arsenic, asbestos, beryllium, chloromethyl ethers, chromium, hydrocarbons, mustard gas, nickel, and radiation (Frank 1989). Several viruses, including human papillomavirus and cytomegalovirus, have also been implicated as potential causes of lung cancer (Giuliani et al. 2007). Genetic factors and prior respiratory disease can additionally predispose individuals to lung cancer. Finally, the incidence of lung cancer increases with age, and the percentage of patients with advanced-stage disease increases with age (O'Rourke et al. 1987).

Lung cancer can arise in a number of cellular types. The World Health Organization has developed a classification system for lung tumors according to cellular origin, as detailed in Table 9.1. The histological classification of lung cancer has important implications for the prognosis and management of disease. The vast majority of lung cancers are malignancies that arise from epithelial cells; such malignancies are termed carcinomas. Lung carcinomas are clinically grouped into two main categories based on the size and histological appearance of the malignant cells: non-small cell lung carcinoma and small cell lung carcinoma. Table 9.2 summarizes the frequencies of histological types of lung cancers. The non-small cell lung carcinomas are the most common and are grouped together because their prognosis and management are similar.

There are three major subtypes of non-small cell lung carcinoma: squamous cell lung carcinoma, adenocarcinoma, and large cell lung carcinoma. Squamous cell carcinomas account for approximately one-third of all lung cancers (Kufe et al.

Table 9.1 World Health Organization classification of lung tumors

I. Epithelial tumors
  A. Benign
    1. Papillomas
    2. Adenomas
  B. Dysplasia/carcinoma in situ
  C. Malignant
    1. Squamous cell carcinoma
      a. Spindle cell variant
    2. Small cell carcinoma
      a. Oat cell carcinoma
      b. Intermediate cell type
      c. Combined oat cell carcinoma
    3. Adenocarcinoma
      a. Acinar
      b. Papillary
      c. Bronchioalveolar
      d. Solid carcinoma with mucin formation
    4. Large-cell carcinoma
      a. Giant cell carcinoma
      b. Clear cell carcinoma
    5. Adenosquamous carcinoma
    6. Carcinoid tumor
    7. Bronchial gland carcinoma
    8. Others
II. Soft tissue tumors
III. Mesothelial tumors
  A. Benign
  B. Malignant
IV. Miscellaneous tumors
  A. Benign
  B. Malignant
V. Secondary tumors
VI. Unclassified tumors
VII. Tumor-like lesions

World Health Organization (1981)

Table 9.2 Frequency of histological types of lung cancer

Histological type	Frequency (%)
Non-small cell lung carcinoma	80.4
Small cell lung carcinoma	16.8
Carcinoid	0.8
Sarcoma	0.1
Unspecified lung cancer	1.9

Etienne-Mastroianni et al. (2002), Morandi et al. (2006), Travis et al. (1995)

2003). They usually originate within a central bronchus (Fig. 9.1); tissue necrosis and a hollow cavity are typically found at the center of the tumor. Histologically, these tumors exhibit keratin formation, keratin pearl formation, and intercellular bridging between adjacent cells (Fig. 9.2). Adenocarcinomas account for 30–45%

Fig. 9.1 Gross appearance of squamous cell carcinoma from a surgical specimen. The tumor is on the *left* and is obstructing the bronchus

of all lung cancers (Kufe et al. 2003) and usually originate within the periphery of the lung. On histological examination, these tumors demonstrate glandular formation or the presence of mucus production in a solid tumor (Fig. 9.3). Large cell carcinoma accounts for approximately 9% of all lung cancers (Kufe et al. 2003). These tumors are characterized histologically by large cells with large nuclei and prominent nucleoli (Fig. 9.4).

In general, the non-small cell lung carcinomas may be amenable to surgical therapy in their initial stages, although poorly differentiated tumors of the non-small cell type can grow quickly and spread to distant sites. In contrast to the non-small cell lung cancers, small cell lung cancer has a very aggressive clinical course, and

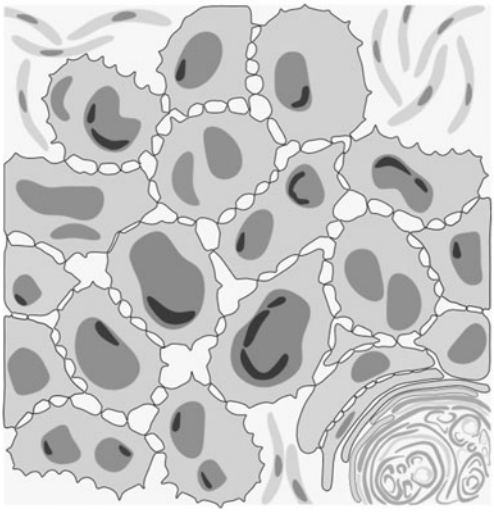

Fig. 9.2 Diagram of histological appearance of squamous cell carcinoma. These tumors demonstrate intercellular bridging, keratin formation, and keratin pearl formation

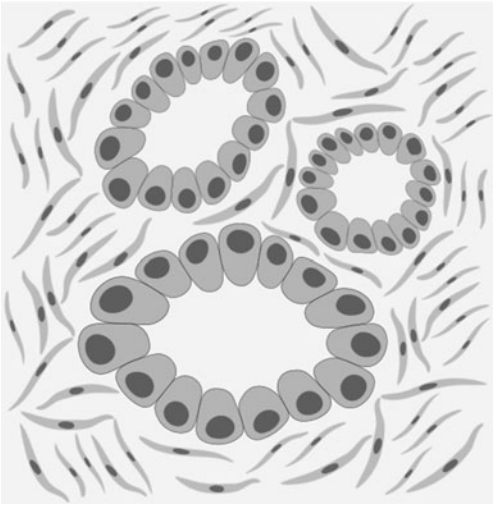

Fig. 9.3 Diagram of histological appearance of adenocarcinoma. These tumors exhibit glandular formation

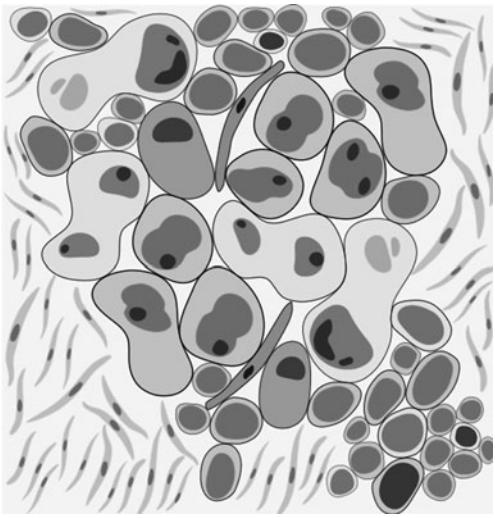

Fig. 9.4 Diagram of histological appearance of large cell carcinoma. These tumors contain large cells with large nuclei and prominent nucleoli

frequent widespread metastases occur regularly. Small cell lung cancer is considered a distinct clinical pathological entity due to its characteristic aggressive biology and propensity for diffuse disease; less than 5% of cases are localized peripheral parenchymal lesions upon clinical presentation (Kufe et al. 2003). Small cell lung carcinomas typically originate in a peribronchial location and invade the bronchial submucosa and peribronchial parenchymal tissues. The cells of the tumor contain a paucity of cytoplasm and exhibit a high nuclear:cytoplasmic ratio; these cells are sometimes called "oat cells" (Fig. 9.5). Cell division rates are high, and the tumor

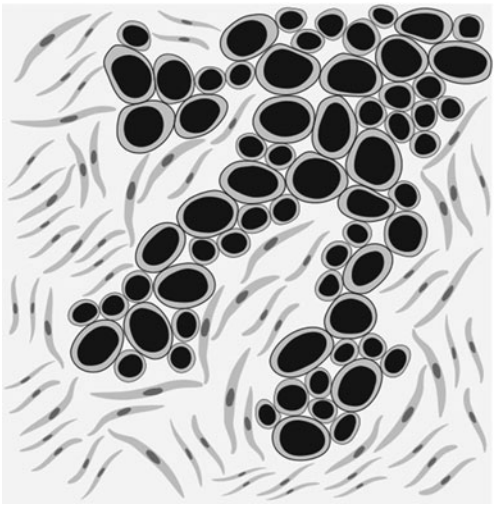

Fig. 9.5 Diagram of histological appearance of small cell lung carcinoma. These tumors contain cells with a high nuclear:cytoplasmic ratio

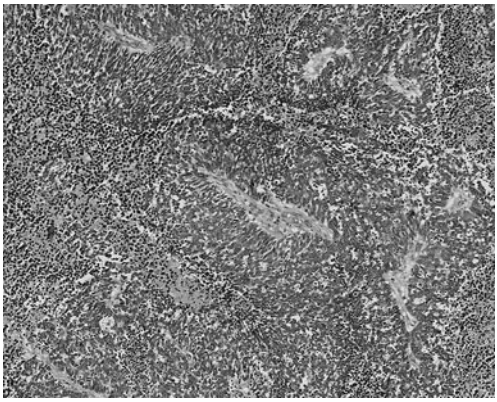

Fig. 9.6 Microscopic appearance of small cell lung carcinoma, also known as "oat cell carcinoma" (Department of Clinical Pathomorphology and Cytology, Medical University, Lodz, Poland)

often grows in sheets (Fig. 9.6). While small cell lung cancers are initially sensitive to chemotherapy, these tumors carry a poor prognosis.

The clinical manifestations of lung cancer depend on the location and size of the tumor; many signs and symptoms are attributable to local tumor growth and intrathoracic spread (Kufe et al. 2003). Centrally located tumors that affect the airways can produce cough, a localized wheeze, and hemoptysis (a cough productive of blood). If the cancer obstructs airflow, it may cause dyspnea (shortness of breath) and post-obstructive pneumonia. Peripheral lung tumors can be asymptomatic when they are small and confined to the lung; cough and chest pain may be present. Lung cancer additionally causes systemic symptoms, including weight loss, anorexia, fatigue, fever, and anemia. Metastatic spread of lung cancer can also lead to clinical symptoms; typical sites of metastasis include the brain, bones, adrenal glands, liver,

Fig. 9.7 Chest x-ray for diagnosis of lung cancer showing a growth on the *left* side of the lung (National Cancer Institute)

kidneys, pericardium, and opposite lung (Greene 2002). Bone pain and abdominal pain commonly result from metastatic lung cancer. Patients with lung cancer often show an obvious mass on chest x-ray (Fig. 9.7); the tumor type can be confirmed by CT-guided biopsy or bronchoscopy. Unfortunately, about 10% of individuals with lung cancer are asymptomatic at diagnosis; these cancers are incidentally found on a routine chest x-ray (Minna and Schiller 2008).

Treatment for lung cancer depends on the histological type, the tumor location, the extent of spread, the patient's overall condition, and the stage of the cancer. Non-small lung carcinoma is staged from IA (best prognosis) to IV (worst prognosis), based on the anatomic extent of disease (Mountain et al. 2003). Small cell lung carcinoma is staged according to a two-stage system (Collins et al. 2007); this cancer is categorized as either limited stage (disease confined to one half of the chest and within the scope of a single radiotherapy field), or extensive stage (disease reaching beyond the confines of limited disease). Available treatments for lung cancers include surgery, chemotherapy, and radiotherapy. Surgery is typically only an option for non-small cell lung carcinoma limited to one lung, up to stage IIIA (Collins et al. 2007). A limitation of surgery is that it cannot be performed if the patient has poor respiratory function or is not well enough to undergo an operation. Moreover, surgery itself has an operative death rate of approximately 4.4% within 30 days (Strand et al. 2007). Chemotherapy is the mainstay of treatment for small cell lung carcinoma and is also used for treating metastatic non-small cell lung carcinoma. A disadvantage of chemotherapy is that it induces severe systemic adverse effects, including immunosuppression, fatigue, nausea, vomiting, diarrhea, ulcers, and hair loss; these side effects limit the dosage of chemotherapy that can be administered. Although over 90 chemotherapeutic drugs have been approved by the FDA for clinical use, their efficacy has been hindered by dose-limiting toxicity and patient morbidity (Blanco et al. 2009). Radiotherapy is often given in combination

with chemotherapy for both non-small cell lung carcinoma and small cell lung carcinoma; it may also be used with curative intent in patients with non-small cell lung carcinoma who are not eligible for surgery. Radiotherapy does cause side effects, including fatigue, chest pain, cough, and fever.

Existing treatments for lung cancer are not only uncomfortable for patients, they are ineffective. In cases of non-small cell lung carcinoma, the prognosis is not especially good. Following complete surgical resection of stage IA disease, the 5-year survival is 67%. For stage IB disease, the 5-year survival is 57% (Mountain 1997). For patients with stage IV non-small cell lung carcinoma, the 5-year survival rate is only 1% (Beers et al. 2006). In cases of small cell lung carcinoma, the prognosis is even poorer. Patients with limited-stage disease have a median survival time of 20 months, with a 5-year survival rate of 20%. Patients with extensive-stage disease have a 5-year survival rate of 1% (Beers et al. 2006). The overall 5-year survival rate for patients with small cell lung carcinoma is approximately 5% (Minna and Schiller 2008). Undoubtedly there is ample room for improvement in lung cancer therapy.

9.2 Biomaterials for Passive Targeted Drug Delivery

Nanoscale biomaterials have recently emerged as novel systems for targeted drug delivery to cancerous tumors. In particular, polymeric micelles in the diameter range of 10–100 nm have the ability to solubilize hydrophobic chemotherapeutic molecules and carry the therapeutics specifically to solid tumors. Such nanoscale carriers take advantage of the "enhanced permeability and retention" effect (Maeda et al. 2000). This effect is based on the unique pathophysiological characteristics of solid tumor tissues. Cancerous tumors are hypervascular with incomplete, leaky vascular tissue (Fig. 9.8). In addition, tumors secrete vascular permeability factors that stimulate extravasation within cancer tissue. The enhanced permeability

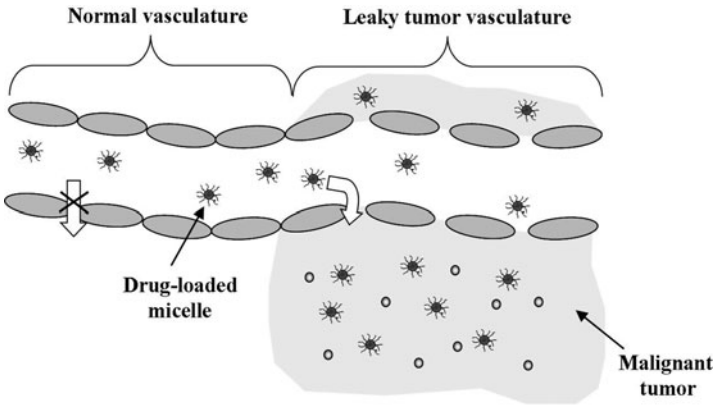

Fig. 9.8 The enhanced permeability and retention effect. Nanoscale polymeric micelles are loaded with chemotherapeutic drugs. The micelles cannot penetrate normal vasculature, but are able to permeate leaky tumor vasculature. The drug-loaded micelles enter the tumor interstitium and accumulate in the tumor, releasing the chemotherapeutic drug. This system achieves selective targeting of tumor tissues, along with a high local concentration of chemotherapeutic drugs within the tumor

of the tumor vasculature allows bloodborne nanoscale drug carriers to penetrate into the tumor mass. Malignant tumors are characterized not only by increased permeability, but also by increased retention; tumors lack an effective lymphatic drainage system and cannot rapidly clear macromolecules from the tissues. As a result, nanosized polymeric micelles are retained within the tumor mass and release the chemotherapeutic drug. As micelles accumulate within the tumor mass, a high local concentration of chemotherapeutic drug is achieved. In contrast to tumor blood vessels, normal blood vessels are not leaky; micelles within the diameter range 10–100 nm cannot permeate normal vessel walls. Thus, micelles preferentially migrate to tumor tissue and accumulate within the target tissue by virtue of the micelle size and the tumor architecture; this phenomenon is also known as "passive targeting" of cancerous tissue. Because nanosized micelles exploit the enhanced permeability and retention of tumors, they have several advantages compared to conventional chemotherapy. Advantages of nanotherapeutics for cancer therapy include improved anti-tumor efficacy, reduced toxicity to healthy tissues, reduced side effects, prolonged blood circulation times, and higher capacity to deliver a drug payload.

Polymeric micelles are spherical supramolecular constructs, formed from the self-assembly of amphiphilic block copolymers in aqueous environments (Jones and Leroux 1999). The block copolymer is biocompatible and contains a hydrophobic block and a hydrophilic block (Fig. 9.9). In aqueous solutions, the hydrophobic portions of the block copolymers self-associate into a semi-solid core, while the hydrophobic segments of the copolymers form a coronal layer. The resulting core–shell architecture has significant functionality for drug delivery. The hydrophobic core can act as a reservoir for water-insoluble chemotherapeutic drugs and enables biodegradability for drug release (Sutton et al. 2007). The hydrophilic corona

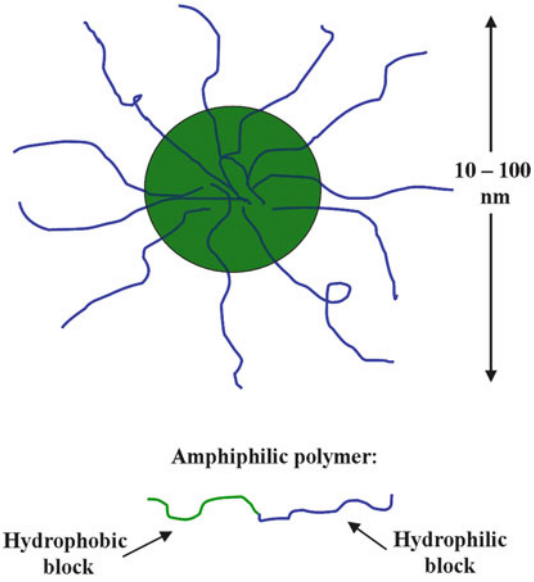

Fig. 9.9 Schematic diagram of the core–shell architecture of a polymer micelle

Table 9.3 Commonly used polymers for micellar drug delivery systems

Copolymers	Abbreviations
Corona segment	
Poly(ethylene glycol)	PEG, PEO
Poly(*N*-vinyl pyrrolidone)	PVP
Poly(*N*-isopropyl acrylamide)	pNIPAM, NIPAM
Core segment	
Polyethers	
Poly(propylene oxide)	PPO
Polyesters	
Poly(L-lactide)	PLA
Poly(D,L-lactide)	PDLLA
Poly(lactide-co-glycolide)	PLGA
Poly(ε-caprolactone)	PCL
Poly(β-amino ester)	
Polyamides	
Poly(L-histidine)	pHis
Poly(L-aspartic acid) derivatives	pAsp
Poly(L-glutamic acid) derivatives	pGlu

Sutton et al. (2007)

enables water solubility of the complex, prevents aggregation, and prevents protein adhesion; the outer shell also protects the micelle from rapid clearance in the bloodstream (Torchilin 2001).

The most important criteria in selecting polymers for micellar drug carriers are biocompatibility and biodegradability. Table 9.3 lists polymers that are commonly utilized in micellar drug delivery systems. For the hydrophilic corona-forming segment, the most frequently used polymer is polyethylene glycol (PEG) in a molecular weight range of 2,000–15,000. PEG is completely water soluble, non-toxic, and uncharged; this last property lessens the possibility of undesired electrostatic interactions with plasma proteins. Micelle formulations that incorporate PEG coronas are resistant to opsonization and have long blood circulation times; such micelles are often called "stealth" micelles. For the hydrophobic core-forming segments, the most common materials are hydrophobic polyesters, but other materials such polyethers, polyamides, and poly(β-amino ester) are also employed. Polyesters undergo hydrolytic degradation, while polyamides undergo enzyme-catalyzed degradation; both are considered biodegradable.

The properties of polymeric micelles are particular well suited for cancer therapy. Most anti-cancer drugs are inherently water insoluble, as a result of their lipophilic nature. When a lipophilic drug is encapsulated within the hydrophobic core of a micelle, there is a significant increase in the apparent solubility of the drug in aqueous environments. For example, the water solubility of the anti-cancer agent paclitaxel can be increased by several orders of magnitude, from 0.0015 to 2 mg/ml through micelle incorporation (Soga et al. 2005). Micellar carriers therefore permit the clinical use of drugs that would otherwise be too hydrophobic or

Table 9.4 Comparison of nanotherapeutic biomaterials for cancer drug delivery

Nano systems	Polymer–drug conjugates	Dendrimers	Polymer micelles	Liposomes
Size (nm)	<10	2–10	10–100	100–200
Structural characteristics	Macro-molecular structure	Macro-molecular tree-like structure	Spherical, supramolecular, core–shell structure	Spherical, bilayer vesicle structure
Carrier composition	Water-soluble polymer	Hyper-branched polymer chains	Amphiphilic di- and tri block copolymers>	Phospholipid, cholesterol membrane lipids
Drug incorporation strategy	Covalent conjugation requiring functional groups on drug and polymer	Covalent conjugation requiring functional groups on drug and polymer	Non-covalent encapsulation, compatible with hydrophobic drugs	Non-covalent encapsulation, compatible with hydrophobic drugs
Clinical status	Clinical use	Preclinical trials	Phase I/II clinical trials	Clinical use

Blanco et al. (2009)

toxic. Further, micellar encapsulation does not require manipulation of the chemical structure of the therapeutic drug, as shown in Table 9.4. The polymer core of the micelle also increases drug stability, by shielding the drug from enzymatic degradation and inactivation (Blanco et al. 2009). The critical micelle concentration (CMC, the concentration threshold of polymers at which micelles are formed) is very low for polymeric micelles, typically on the order of 10^{-6} to 10^{-7} M; polymeric micelles are stable constructs that do not readily dissociate in physiological environments (Liu et al. 2007).

Table 9.4 compares the physical properties of polymeric micelles to those of other nanotherapeutic systems for drug delivery, including polymer–drug conjugates, dendrimers, and liposomes. Both polymer–drug conjugates and dendrimeric systems incorporate therapeutic drugs via covalent conjugation of the drug molecule to the polymer carrier. These systems require the presence of functionalizable chemical groups on the drug molecules as well as the carriers, which limits the generalizability of these approaches (Gillies and Frechet 2005). Because covalent bonds are highly stable, polymer–drug conjugates and dendrimers also require specific chemical strategies (such as acid-catalyzed hydrolysis or enzymatic activation) to release the drug molecule at tumor sites. Importantly, the small size of these systems (<10 nm) permits very rapid kidney filtration and clearance from the blood stream, resulting in much shorter blood half-lives (Peer et al. 2007). Liposomal particles have the opposite problem: most liposomal particles are over 90 nm in diameter, which considerably limits their transport in tumor tissues. Liposomal formulations of anti-cancer drugs have a lower volume of distribution than micellar formulations, suggesting that liposomal carriers may not extravasate into tumor tissue as widely

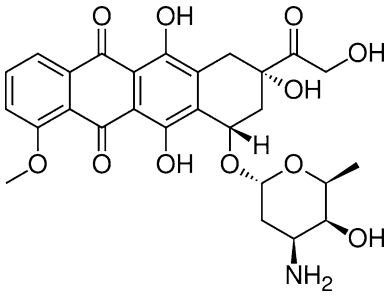

Fig. 9.10 Chemical structure of doxorubicin, a hydrophobic drug for the treatment of non-small cell lung cancer and small cell lung cancer. This chemotherapeutic has been successfully encapsulated in both PEG-polyaspartate micelles and Pluronic® micelles

as comparable micelles (Sutton et al. 2007). (*However, liposomal biomaterials have shown promise as novel antibiotic carriers for the treatment of pneumonia and other infectious diseases. These biomaterials are discussed in Chapter 4.*). Micelles have been shown to accumulate more readily inside lung carcinoma tumors compared to liposomes, primarily due to the smaller micellar size (Weissig et al. 1998). Overall, polymeric micelles are uniquely well matched for cancer drug delivery applications, providing a natural carrier environment for anti-cancer drugs. The size range of polymer micelles, 10–100 nm, allows for evasion of kidney filtration, while permitting increased tumor penetration of micelles compared to liposomes (Torchilin 2007). The size of polymeric micelles can be readily controlled within this desirable range, by varying the length of the hydrophobic block of the amphiphilic copolymer (Shuai et al. 2004).

Micellar carriers have been developed for at least four major chemotherapeutic drugs: doxorubicin, paclitaxel, cisplatin, and SN-38. All four of these chemotherapeutics have significant activity against lung cancer, and all could potentially be enhanced by encapsulation within polymer micelles. Doxorubicin (Fig. 9.10) is a hydrophobic anti-cancer agent and is currently an important part of treatment regimens for both non-small cell lung cancer and small cell lung cancer (Kufe et al. 2003). Two different polymer micelle formulations have been created for doxorubicin delivery. The first system utilizes Pluronic® copolymer, a tertiary copolymer of PEG and poly(propylene oxide) (PPO) oriented in a PEG-PPO-PEG configuration. During micelle formation, the hydrophobic PPO segments form the core while the PEG segments form the corona. The doxorubicin-loaded Pluronic® micelles are also known as the SP1049C formulation (Danson et al. 2004). The second system for doxorubicin encapsulation is constructed from a copolymer of PEG and doxorubicin-conjugated poly(aspartic acid). This system is also known as the NK911 formulation (Matsumura et al. 2004).

Table 9.5 compares the clinical pharmacokinetics of free doxorubicin to those of both micellar doxorubicin delivery systems. This comparison reveals several important advantages of micellar formulations. Free doxorubicin has an elimination phase half-life ($t_{1/2,\beta}$), or physiological excretion half-life, of 48 min. In contrast, both polymer micelle formulations roughly triple the half-life to a range of 2.3–2.8 h. The drug clearance rates (C_L) further highlight important pharmacological differences.

Table 9.5 Comparison of clinical pharmacokinetics for free doxorubicin and micellar doxorubicin delivery systems

Formulation	Free doxorubicin[a]	SP1094C[b]	NK911[c]
Carrier	Doxorubicin-hydrochloride in 0.9% NaCl	Pluronic® micelles, mixture of L61 and F127	PEG (5,000 MW)-pAsp (30 units) conjugated with doxorubicin
Diameter (nm)	–	22–27	40
Number of patients	8	26	23
$t_{1/2,\alpha}$ (min), distributional half-life	2.4 ± 0.9	6.0 ± 2.7	7.5 ± 0.7
$t_{1/2,\beta}$ (h), apparent elimination half-life	0.8 ± 1.1	2.4 ± 2.1	2.8 ± 0.3
$t_{1/2,\gamma}$ (h), apparent elimination half-life	25.8 ± 11.4	50.2 ± 29.2	64.2 ± 8.9
V_{ss} (l/kg), volume of distribution	24 ± 12	–	14.9 ± 3.6
C_L (ml/(min kg)), clearance rate	14.4 ± 5.6	12.6 ± 0.6	6.7 ± 1.1
MTD (mg/m^2), maximum tolerated dose	50	70	67
AUC (μg h/ml), area under the plasma concentration curve	1.6 ± 1.1	1.8 ± 0.3	3.3 ± 0.4

Pharmacokinetic data are reported for a dose of 50 mg/m^2
[a]Mross et al. (1988)
[b]Danson et al. (2004)
[c]Matsumura et al. (2004)

The clearance rate of free doxorubicin is 14.4 ± 5.6 ml/(min kg). Doxorubicin encapsulation within PEG-polyaspartate micelles reduces the clearance rate to 6.7 ± 1.1 ml/(min kg), almost half that of free doxorubicin. Pluronic® micelles have a less marked effect on the clearance rate, possibly due to the low stability of Pluronic® micelles (Sutton et al. 2007). Both micellar systems increase the maximum tolerated dose (MTD) of doxorubicin in patients. Taken together, these clinical data indicate the distinct benefits of micelle-delivered drugs over free chemotherapeutic drugs. Each of the doxorubicin-loaded micelle systems exhibit improved half-lives, slower clearance rates, higher maximum tolerated doses, and increased area under plasma concentration (AUC) values over non-encapsulated doxorubicin.

Paclitaxel (Fig. 9.11) is another potent anti-cancer drug that is utilized in treatment regimens for both non-small cell lung cancer and small cell lung cancer (Kufe et al. 2003); it is also a useful agent for breast cancer, ovarian cancer, and head and neck cancers. However, paclitaxel is hydrophobic with a very low water solubility (1.5 μg/ml), and the drug already requires administration with a surfactant called Cremophor® EL, which is a PEG-modified castor oil (Soga et al. 2005). Moreover, paclitaxel causes serious adverse effects, including neurotoxicity and neutropenia. There are no effective methods for preventing or reducing the nerve damage associated with paclitaxel, so that neurotoxicity constitutes a significant dose-limiting toxicity of the drug (Wasserheit et al. 1996). In addition, paclitaxel is associated with severe hypersensistive reactions and anaphylaxis in 2–4% of patients receiving

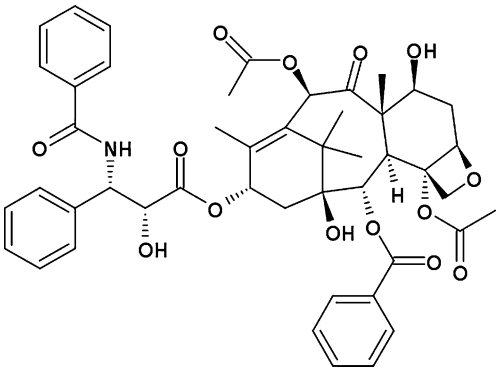

Fig. 9.11 Chemical structure of paclitaxel, a hydrophobic drug for the treatment of non-small cell lung cancer and small cell lung cancer. This chemotherapeutic has been successfully encapsulated in PEG-PLA micellar carriers

the drug, even when patients are pre-medicated with anti-allergic agents (Weiss et al. 1990). These adverse reactions have been attributed to the mixture of Cremophor® EL surfactant and ethanol currently used for solubilizing paclitaxel.

To overcome the limitations of conventional paclitaxel, a polymeric micelle formulation known as Genexol®-PM (Samyang Pharmaceuticals, Korea) has been created for paclitaxel delivery. Genexol®-PM employs PEG-PLA copolymers for micelle formation (Kim et al. 2004). Table 9.6 details the clinical pharmacokinetics of the traditional Cremophor®-EL formulation and the Genexol®-PM micelle system for paclitaxel delivery.

Both traditional paclitaxel and Genexol®-PM have similar half-lives and clearance rates. However, the Genexol®-PM micelle formulation demonstrated a marked improvement in patient morbidity in a Phase I clinical trial (Kim et al. 2004). None of the patients in the trial exhibited hypersensitivity reactions, and a lower degree

Table 9.6 Comparison of clinical pharmacokinetics for traditional paclitaxel and micellar paclitaxel delivery systems

Formulation	Taxol®[a]	Genexol®-PM[b]
Carrier	Cremophor® EL PEG-modified castor oil	PEG-PLA micelles
Diameter (nm)	–	20–50
Number of patients	34	21
$t_{1/2,\alpha}$ (min), distributional half-life	21.8 ± 13.9	–
$t_{1/2,\beta}$ (h), apparent elimination half-life	8.9 ± 1.8	11.0 ± 1.9
C_L (ml/(min kg)), clearance rate	3.9 ± 1.1	4.8 ± 1.0
MTD (mg/m^2), maximum tolerated dose	230	390
AUC (μg h/ml), area under the plasma concentration curve	25 ± 6.5	27.5 ± 8.2

Pharmacokinetic data are reported for a dose of 230 mg/m^2.
[a]Wiernik et al. (1987)
[b]Kim et al. (2004)

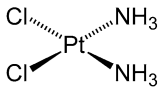

Fig. 9.12 Chemical structure of cisplatin, a powerful drug for the treatment of non-small cell lung cancer and small cell lung cancer. This chemotherapeutic has been successfully encapsulated in PEG-poly(glutamic acid) micellar carriers

of neutropenia was observed for the Genexol®-PM formulation than for the conventional paclitaxel formulation. As a result, the micellar paclitaxel formulation achieved a considerable increase in the maximum tolerated dose (MTD), with an MTD of 390 mg/m^2, compared to 230 mg/m^2 for Cremophor® EL. Interestingly, in the Phase I clinical trial, one patient with non-small cell lung cancer experienced a 77% decrease in the size of lung metastasis following Genexol®-PM administration; this patient had not shown a response to previous chemotherapy with a traditional paclitaxel formulation (Kim et al. 2004). This raises the possibility that paclitaxel-loaded polymer micelles may succeed where conventional chemotherapeutics have failed. Another patient with refractory small cell lung cancer experienced an 84% decrease in the size of the lung mass and mediastinal lymph nodes following Genexol®-PM administration. As of late 2009, Genexol®-PM entered Phase III clinical trials for patients with advanced non-small cell lung cancers.

Cisplatin (*cis*-dichlorodiammineplatinum[II]: CDDP) is a key drug in the chemotherapy of various cancers, including lung, gastrointestinal, and genitourinary cancers. Regimens including cisplatin (Fig. 9.12) constitute the standard treatment for non-small cell lung cancer and small cell lung cancer (Kufe et al. 2003), as well as gastric, testicular, and urothelial cancers. Despite the efficacy of cisplatin against malignant solid tumors, the chemotherapeutic must often be discontinued because of adverse effects, particularly neurotoxicity and nephrotoxicity. A micellar formulation of cisplatin has been constructed to enable more selective accumulation of cisplatin in solid tumors, while lessening its distribution in normal tissue. In this formulation, PEG constitutes the outer shell, and a coordinate complex of poly(glutamic acid) and cisplatin constitutes the inner core. These cisplatin-loaded micelles are also called the NC-6004 formulation (Nishiyama et al. 2003). The polymeric micelles are 20 nm in diameter, with a narrow size distribution. Cisplatin-loaded micelles show no dissociation upon dilution, and the critical micelle concentration (CMC) is $<5 \times 10^{-7}$ M, indicating remarkable stability compared with typical micelles from amphiphilic block copolymers.

The NC-6004 micelle delivery system for cisplatin has been evaluated in animal models (Uchino et al. 2005). Table 9.7 compares the in vivo pharmacokinetics of the traditional cisplatin (CDDP) formulation and the NC-6004 cisplatin-loaded micelles. The PEG-poly(glutamic acid) micelles demonstrated a very long blood retention profile compared with CDDP. The AUC value for the polymer micelles was 65-fold higher than that of CDDP, and the polymer micelles achieved an 8-fold higher maximum concentration (C_{max}) than CDDP. Within tumors, the C_{max}

Table 9.7 Comparison of in vivo pharmacokinetics for traditional cisplatin and micellar cisplatin delivery systems

Formulation	Cisplatin (CDDP)	NC-6004
Carrier	Aqueous solution	PEG-pGlu micelles
Diameter (nm)	–	20
AUC (μg h/ml), area under the plasma concentration curve	20.47 ± 2.25	1,325.90 ± 77.85
C_{max} (μg/ml), maximum plasma concentration	11.67 ± 0.57	89.90 ± 4.29
C_L (ml/(h kg)), clearance rate	70.67 ± 20.34	3.77 ± 0.21
MRT (h), mean residence time	46.57 ± 22.38	10.67 ± 0.15
V_{ss} (L/kg), volume of distribution	3.00 ± 0.61	0.04 ± 0.0023

Pharmacokinetic data are reported for a dose of 5 mg/kg.
Uchino et al. (2005)

was 2.5-fold higher for the micelles than for CDDP and the tumor AUC was 3.6-fold higher for the cisplatin-loaded micelles than for CDDP (Uchino et al. 2005). The polymer micelles not only achieved an improved pharmacokinetic profile, but also an improved toxicity profile for cisplatin. Notably, the cisplatin-loaded micelles induced significantly less neurotoxicity and nephrotoxicity in vivo than CDDP. Phase I clinical trials of the cisplatin-loaded NC-6004 micelles have been completed, and Phase II clinical trials may soon be initiated.

Another chemotherapeutic agent that may benefit from micellar encapsulation is SN-38 (Fig. 9.13). This compound is the active metabolite of irinotecan, and demonstrates activity against extensive small cell lung cancer (Noda et al. 2002) and advanced non-small lung cancer (Negoro et al. 2003), as well as colorectal and ovarian cancers. SN-38 exhibits up to 1,000-fold more potent cytotoxic activity against cancer cells in vitro than irinotecan (Takimoto and Arbuck 2001). Due

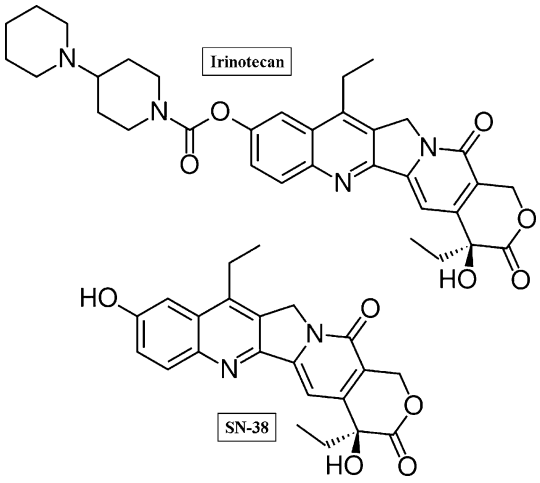

Fig. 9.13 Chemical structures of irinotecan and SN-38. Irinotecan is a prodrug and is metabolized to SN-38 by hydrolysis. The SN-38 chemotherapeutic is a powerful drug for the treatment of non-small cell lung cancer and small cell lung cancer. The SN-38 compound has been successfully encapsulated in PEG-poly(glutamic acid) micellar carriers

to its toxicity and poor solubility, SN-38 cannot be administered directly to cancer patients and must be administered as the prodrug irinotecan. Within the liver and tumors, irinotecan is converted to SN-38 by carboxylesterase enzymes. This therapeutic approach is problematic for two reasons. First, the metabolic conversion rate of irinotecan to SN-38 is less than 10% the original volume of irinotecan (Slatter et al. 2000). Second, the metabolic conversion of irinotecan to SN-38 depends on the genetic inter-individual variability of carboxylesterase activity (Guichard et al. 1999), so it is difficult to achieve consistent dosing regimens. A delivery system that makes more efficient use of SN-38 is desirable for lung cancer treatment.

To enable systemic administration of the active SN-38 agent, polymeric micelles for SN-38 delivery have been developed (Koizumi et al. 2006). The micellar particles are constructed from a copolymer of PEG and SN-38-conjugated poly(glutamic acid). In an aqueous environment, the PEG-PGlu(SN-38) amphiphilic block copolymer self-assembles into an SN-38-loaded micelle. This system is also known as the NK012 formulation. In freeze-dried form, the micelles contain approximately 20% SN-38 by weight. The mean particle size of the drug-loaded micelles is 20 nm in diameter, with a relatively narrow size distribution. The release profile of SN-38 from PEG-PGlu(SN-38) micelles has been measured in phosphate-buffered saline at 37°C: the micelles release 57% of the SN-38 load by 24 h and 74% by 48 h. These data suggest that the micelles can deliver SN-38 under neutral conditions, without requiring a hydrolytic enzyme. Yet the micelles are stable in 5% glucose solution: the micelles release only 1% of the SN-38 load at 24 h and 3% at 48 h when suspended in a 5% glucose solution. The PEG-PGlu(SN-38) micelles can therefore be prepared and administered in stable form in 5% glucose. The micellar carriers begin to release SN-38 following administration, once exposed to physiological conditions.

The NK012 micellar system for SN-38 chemotherapy has been further evaluated in animal models (Koizumi et al. 2006; Saito et al. 2008). The SN-38-loaded micelles exhibited slower plasma clearance compared with the traditional irinotecan formulation (6 ml/h/kg for NK012 versus 3,010 ml/h/kg for irinotecan). A 14-fold higher AUC of free SN-38 was achieved in mice given NK012, compared with mice given irinotecan (Koizumi et al. 2006). Within tumors, micellar clearance was significantly slower than that of irinotecan (mean residence time of 60 h for NK012 versus approximately 5 h for irinotecan). The maximum concentration of free SN-38 in tumors was achieved at 6 h following micelle administration versus 1 h after irinotecan administration. The micelles also maintained the free SN-38 concentration in tumors for a longer time following injection, with high concentrations persisting for 168 h. In very large experimental tumors (>1.5 cm) in mice, the NK012 micelles showed a much higher cytotoxic effect against small cell lung cancer cell lines than did irinotecan (Koizumi et al. 2006). Phase I clinical trials of the SN-38-loaded NK012 micelles have been completed in patients with advanced solid tumors; one patient with small cell lung cancer demonstrated a partial response (Matsumura and Kataoka 2009). Phase II clinical trials may soon be initiated.

Micellar delivery systems for doxorubicin, paclitaxel, cisplatin, and SN-38 demonstrate the therapeutic potential of polymer micelles for cancer chemotherapy.

By delivering anti-cancer agents directly to cancerous tumors, micelles minimize the toxicity associated with traditional delivery systems and increase the maximum tolerated dose of chemotherapeutics. In addition, micelles enhance the pharmacokinetics of chemotherapeutic agents, allowing longer blood circulation times and slower clearance rates. These micellar carriers are typically "stealth" delivery vehicles, which are passively targeted toward the vasculature of malignant tumors. Further enhancements in therapeutic activity may be achieved by actively targeting micelles toward malignant cells; such actively targeted biomaterials are described in the following section.

9.3 Biomaterials for Active Targeted Drug Delivery

Although polymeric "stealth" micelles can passively accumulate inside cancerous tumors with leaky vasculature, the majority of these nanoparticles are still cleared by the reticulo-endothelial system. This results in shorter micelle half-lives, as well as unwanted micelle deposition in the liver and spleen (Sutton et al. 2007). While passively targeted micelles are a major advance for cancer treatment, and such systems are now having a positive impact on lung cancer patients, work is already underway to create actively targeted micelles for cancer chemotherapy. Actively targeted carriers are functionalized to allow specific interactions with tumor cells, as well as specific control of drug release (Fig. 9.14). These formulations can increase the exposure of tumor cells to chemotherapeutics, enabling greater anti-tumor efficacy.

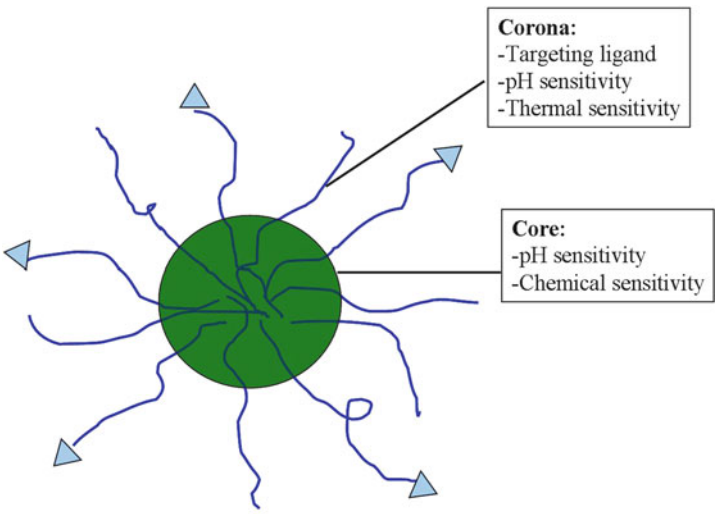

Fig. 9.14 Schematic diagram of strategies for functionalizing polymer micelles. Micellar structures can be functionalized with ligands for active targeting to tumor cells. Micelles can also be functionalized with stimuli-responsive polymers for specific drug release properties

Table 9.8 Ligand-functionalized micellar systems for active tumor targeting

Ligand type	Ligand	Polymer composition	Micelle size (nm)	Therapeutic drug
Small organic molecule[a]	Folic acid	PEG- PLGA	105	Doxorubicin
Small organic molecule[b]	Folic acid	PEG-PCL	50–130	Paclitaxel
Peptide[c]	cRGD peptide	PEG-PCL	20–40	Doxorubicin
Antibody[d]	Anti-cancer mAb 2C5	PEG-PE	20	Paclitaxel

[a]Yoo and Park (2004)
[b]Park et al. (2005)
[c]Nasongkla et al. (2004)
[d]Torchilin et al. (2003)

A main strategy for creating functionalized polymer micelles is to introduce targeting ligands into the micellar structure. Such ligands selectively bind to surface receptors expressed by tumor cells. Targeting ligands are conjugated to the corona of the micelle and enable specific targeting and uptake of the micelle by tumor cells. Ligands for targeted binding of lung cancer cells may include small organic molecules, peptides, and antibodies. Table 9.8 provides an overview of ligand-functionalized micelle formulations that have been constructed.

Micelles bearing small organic molecules have been designed to target the receptor for folic acid. The folate receptor is a cell proliferation protein that is overexpressed in lung cancer cells, as well as ovarian, breast, and brain cancer cells (Goren et al. 2000). The receptor is a glycosyl- phosphatidyl-inositol-anchored glycoprotein that has high binding affinity to folic acid (K_d 10^{-10} M). The expression levels of the folate receptor in tumors have been reported to be 100–300 times higher than those observed in normal tissue (Ross et al. 1994). To enable binding to the folate receptor, functionalized micelles have incorporated the folic acid ligand (Fig. 9.15). For instance, the folic acid ligand has been covalently conjugated, via its γ-carboxyl group, onto the hydrophilic corona of doxorubicin-loaded PEG- PLGA micelles (Yoo and Park 2004). In vitro, the doxorubicin-loaded folate micelles demonstrate greater cellular uptake and higher cytotoxicity than

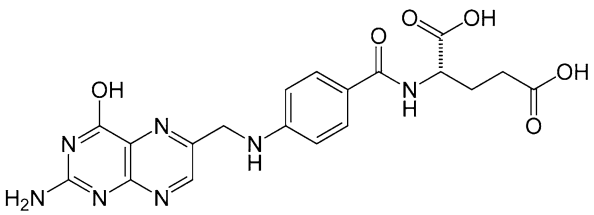

Fig. 9.15 Chemical structure of folic acid (vitamin B9). This molecule has been incorporated into polymer micelles to allow active targeting of tumor cells

non-targeted micelles. In experimental in vivo tumor models, the doxorubicin-loaded targeted micelles achieved a marked improvement in anti-tumor efficacy and decreased the tumor growth rate by twice as much as non-targeted micelles (Yoo and Park 2004). Another folate-targeted micelle for chemotherapeutic delivery has been constructed using a unique conjugation strategy. In this system, folic acid is attached to the hydrophobic end of PEG-PCL block copolymers, and paclitaxel is then encapsulated in the micelle (Park et al. 2005). Although the folate molecule is conjugated to the hydrophobic portion of the micelle, the targeting ligand can be detected on the surface of the micelles via x-ray photoelectron spectroscopy. The folate-bearing paclitaxel-loaded micelles exhibited significant cytotoxicity toward cancer cells with folate receptor expression, while non-targeted micelles did not show significant toxicities in these cell lines (Park et al. 2005). These examples illustrate the potential of actively targeted micelles to enhance cancer chemotherapy, beyond the advances already made by traditional polymer micelles.

Micelles have also been functionalized with small, tightly binding peptides for cancer-targeted drug delivery. An advantage of this strategy is that ligand behavior can be optimized via adjustment of the peptide sequence or conformation. As a case in point, the cyclic RGD (cRGD) peptide has been integrated into micelle structures, to target the $\alpha_v\beta_3$ integrin receptor. This integrin is a cellular transmembrane protein, which is over-expressed on both tumor cells and sprouting tumor vasculature. The membrane receptor has been shown to greatly affect tumor growth, local invasiveness, and metastatic spread; over-expression of $\alpha_v\beta_3$ integrin correlates positively with tumor metastatic potential (Tucker 2003). The receptor is highly expressed in angiogenic vessels, but is not readily detectable in quiescent vessels. This makes $\alpha_v\beta_3$ integrin an appropriate target for treating tumors, which are in a constant state of new vasculature growth. In particular, $\alpha_v\beta_3$ integrin is an excellent target for anti-angiogenic interventions. Cyclic(Arg-Gly-Asp-D-Phe-Lys), also known as cyclic RGD, peptides have been developed to provide specific binding to $\alpha_v\beta_3$ integrins (Kessler et al. 1995).

Polymer micelles bearing cRGD peptides have been created to specifically bind tumor endothelial cells which over-express $\alpha_v\beta_3$ integrin (Nasongkla et al. 2004). In these micellar constructs, micelles are formed from maleimide-terminated PEG-poly(ϵ-caprolactone) copolymer, with doxorubicin encapsulated inside the micelle core. The polymer is conjugated to cRGD after micelle formation. The uptake of cRGD-labeled micelles by tumor endothelial cells has been studied using flow cytometry: the degree of cellular uptake increased with increasing cRGD density on the micelle surface. With 5% cRGD occupancy on the micelle surface, the cRGD-labeled micelles achieved a threefold increase in cellular uptake, compared to non-targeted micelles. With 76% cRGD occupancy on the micelle surface, the cRGD-labeled micelles demonstrated an impressive 30-fold increase in cellular uptake, compared to non-targeted micelles (Nasongkla et al. 2004). Peptide-labeled micelles can therefore be readily internalized by tumor cells, allowing direct exposure of tumor cells to chemotherapeutic drugs.

Cancer-specific monoclonal antibodies are another class of targeting ligands for micelles. Antibodies are large molecules (approximately 150 kD) with a high

affinity for their antigenic targets (K_d 0.1 nM). An advantage of these ligands is that they can be customized to bind specifically to a wide variety of targets, such as cancer cell-specific antigens. Another advantage of antibodies is that few ligands are required to improve micelle behavior, due to the high binding affinity of antibodies for their targets; as few as 10 antibody ligands per micelle can enhance micelle efficacy. Since excessive levels of surface modification can lead to unintended nonspecific uptake of micelles, it is highly desirable to create targeted micelles with small levels of surface modifications. Micelles functionalized with antibodies have also been termed "immunomicelles" (Torchilin et al. 2003).

Antibody-linked immunomicelles have been developed to actively target lung cancer cells (Torchilin et al. 2003). These micelles utilize PEG-PE copolymers, with the free PEG terminus activated with *p*-nitrophenylcarbonyl (pNP) to enable antibody conjugation. The cancer-targeting micelles are prepared from PEG-PE, with the addition of a small fraction of pNP-PEG-PE polymers. The PE residues form the micelle core, while the PEG forms the corona. The pNP groups allow for fast attachment of amino group-containing antibody ligands via the formation of a carbamate bond. The micelles are functionalized with anticancer monoclonal antibody 2C5, which targets the nucleosome of cancerous cells. The antibody-bearing micelles were assessed for their ability to bind nucleosome substrates: the 2C5 antibody retained its ability to bind substrates following conjugation to micelles (Torchilin et al. 2003). The immunomicelles were also loaded with paclitaxel and evaluated in mouse models of lung cancer. Paclitaxel-loaded immunomicelles induced a fourfold increase in drug accumulation in the tumor at 2 h following administration, as compared to non-targeted micelles. The immunomicelles also demonstrated greater anti-tumor efficacy, inhibiting tumor growth to a greater extent than non-targeted micelles. Importantly, antibody conjugation to immunomicelles did not significantly change the blood clearance rate from that of non-targeted control micelles. Immunomicelles can thus effect improvements in chemotherapy of lung tumors, without adversely affecting pharmacokinetics.

Overall, micelles bearing small organic molecules, peptides, and antibodies have shown early success for actively targeting tumors. In all of these constructs, ligand presentation on the micelle surface is a critical design factor. Ligand presentation can make the difference between a successful and an unsuccessful therapeutic formulation: while some ligand-functionalized micelles have shown efficacy in binding tumor cells, other formulations have suffered from a lack of ligand binding to targets (Kunath et al. 2003). Problems with ligand binding have been attributed to the dynamic nature of the micellar PEG corona, which can assume conformations that bury the ligand within the hydrophilic chains. The polydispersity of PEG chains may also contribute to the problem, as ligands that attach to shorter PEG chains are shielded by longer PEG chains. Ligand optimization strategies have been explored, with the goal of optimizing the binding efficiency of actively targeted micelles to tumor cells (Sutton et al. 2007). The focus of these efforts is to minimize the shielding effects of the PEG corona and maximize the chemical availability of the targeting ligand.

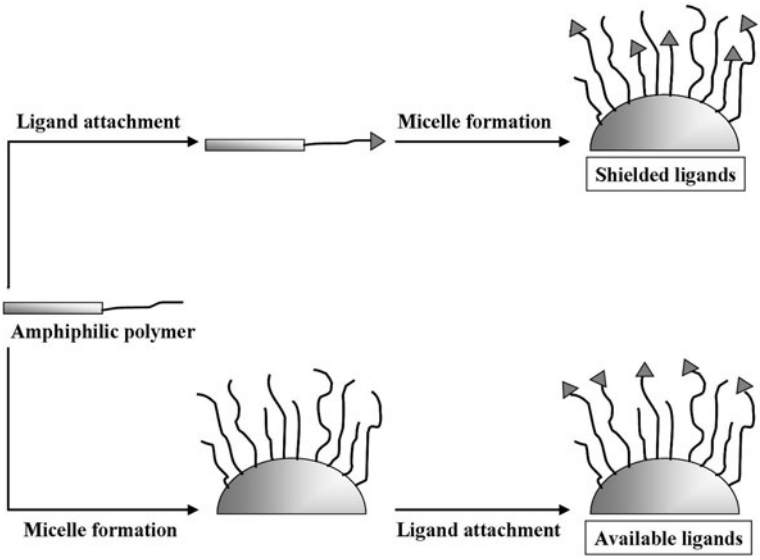

Fig. 9.16 Two different methods for ligand attachment to micelles. In the first case, the ligand is attached to the copolymer before micelle formation. The first method can result in shielded ligands, because ligands can attach to shorter polymer chains and be shielded by longer chains. In the second case, the micelle is assembled first and the ligand is attached afterward. The second method ensures that the ligand is attached to available sites on the micelle surface, which aids in ligand presentation for subsequent targeting of tumor cells

Two different ligand attachment methods have been evaluated and compared (Fig. 9.16), using the cRGD ligand and the PEG-PLA copolymer (Sutton et al. 2007). In the first case, the ligand was attached to the copolymer before micelle self-assembly. In the second case, the micelles were assembled from the copolymer first and the ligand attached afterward; this method would ensure that the ligand was attached to chemically available sites on the micelle surface. The uptake of the two functionalized micelle preparations was compared in tumor cell lines, and the micelles prepared by the second method (i.e., ligand attachment to an already-formed micelle) demonstrated a marked increase in cellular uptake. This result suggests that ligand attachment to a formed micelle does indeed promote ligand availability. Although the two methods appear to be similar, they are different upon consideration of the polydisperse nature of the PEG corona. When ligands are attached to the copolymer before micelle formation, they are more likely to conjugate to shorter PEG chains within the population and suffer from shielding effects. This problem may be exacerbated by higher chemical reactivity of shorter polymer chains. In contrast, the method of post-micelle ligand addition selects for ligands attaching to longer PEG chains, which aids in ligand presentation to targeted tumor cells. This analysis reveals the importance of synthetic strategy in the formulation of micellar biomaterials for cancer treatment.

Table 9.9 Environmentally responsive micelle formulations for site-specific drug release to tumors

Polymer composition	Release mechanism	Micelle size (nm)	Therapeutic drug
pH sensitivity acid-labile bonds (*covalent*)			
PEG-PLA-DOX	Acid-labile bond	89	Doxorubicin
PEG-p(Asp-Hyd-DOX)	Acid-labile bond	65	Doxorubicin
PEG-acetal linked dendritic polyester/ polylysine	Acid-labile bond	35	Doxorubicin
Non-covalent pH sensitivity			
Hydrophobic core			
PLA- PEG PHis-PEG	Histidine protonation	50–114	Doxorubicin
Pluronic–β amino ester	β amino ester protonation	130	Paclitaxel
pNIPAM copolymer	Undecanoate protonation	160	Doxorubicin
Hydrophilic core			
PEG-PMA	Nanogel swelling	130	Cisplatin
Temperature sensitivity			
pNIPAM	LCST transition	12–31	Doxorubicin
pNIPAM-PLA	LCST transition	40–65	Doxorubicin
pNIPAM-copol- PLGA	LCST transition	85–120	Paclitaxel
Ultrasound activation			
Pluronic, PEG-lipid	Ultrasound	13	Doxorubicin
NNDEA pluronic	Ultrasound	50–100	Doxorubicin

Sutton et al. (2007)

Beyond ligand attachment, micelles can also be functionalized to enable site-specific drug release to tumor tissues. When micelles reach the tumor site, efficient drug release from micelle carriers is essential for drug bioavailability and the desired cytotoxic effect. Micelle structures may be designed as environmentally responsive systems, so that drug release is triggered specifically at the tumor site. Such functionality is typically incorporated into micelles by introducing pH-sensitive, temperature-sensitive, or ultrasound-activated polymers. Micelles that dynamically change their physical properties in response to environmental triggers such as pH, temperature, and chemical species are also known as "smart micelles." Table 9.9 provides a summary of reported "smart micelle" formulations that allow site-specific drug release.

Smart micelles with pH-sensitive drug release take advantage of the acidic nature of tumor tissues. While the normal tissue environment maintains a physiological pH of 7.4, tumors tend to have lower pH values, as low as 5.7 (Engin et al. 1995). This acidification results from the general tendency of cancer cells to rely on glycolysis for metabolism. This phenomenon provides a therapeutic opportunity for pH-responsive micelles that release their contents upon exposure to acidic environments. Two methods are generally used to impart pH sensitivity to micellar biomaterials. The first strategy utilizes covalent acid-labile bonds between the drug

and the micelle copolymer. Covalent modification of the polymer with the anticancer drug allows for extremely high drug loading, though it requires functional groups on the drug molecule. An example of this technique is the direct conjugation of doxorubicin to micelle-forming block copolymers via acid-labile bonds. In one demonstration of this method, doxorubicin was conjugated to the aspartic acid residues of a PEG-poly(aspartic acid) (PEG-pAsp) copolymer via a hydrazone linkage (Bae et al. 2003). Although the precursor block copolymer is fully hydrophilic, the binding of doxorubicin to the poly(aspartic acid) segment introduces hydrophobicity in this block. The doxorubicin-loaded PEG-pAsp micelles exhibited almost no drug release at pH 7.4, with less than 3% of the drug released after 48 h. However, the micelles readily released drug in solutions at pH 5.5, with 25% of the drug released after 48 h. In vivo biodistribution studies revealed the ability of this micellar system to target tumors: while only 2% of free doxorubicin deposits in tumors, micellar encapsulation of doxorubicin improves this value to 10%. Accordingly, the PEG-pAsp micelles significantly increased the maximum tolerated dose of drug (40 mg/kg for micelle-encapsulated doxorubicin versus 15 mg/kg for free doxorubicin). In mouse models, the pH-sensitive doxorubicin-loaded micelles inhibited tumor growth to a greater extent than free doxorubicin. The highest tolerated dose of free doxorubicin resulted in complete tumor regression in only 17% of treated mice, but the doxorubicin-loaded micelles induced a complete cure in 50% of the mice (Bae et al. 2005). These studies confirm that pH-sensitive micelles containing acid-labile bonds can achieve site-specific drug release to tumors.

The second strategy for imparting pH sensitivity to micelles is a non-covalent method. In this technique, the micelle copolymer incorporates an ionizable component, which alters its conformation upon protonation. The resulting micelle has a pH-dependent stability. When the micelle encounters an acidic environment, it destabilizes and releases its drug payload. For example, pH-sensitive micelles have been created from poly(β amino esters), a class of polymers with pH-dependent stability. These biodegradable polymers are hydrophobic at neutral pH, but can become fully soluble at pH below 6.1. Micelles have been constructed by surrounding a hydrophobic poly(β amino ester) core with a PEG corona from the pluronic copolymer F108 (Potineni et al. 2003); the resulting micellar particles were loaded with paclitaxel. In animal models, the pH-sensitive micelles demonstrated the long residence time and improved half-life typical of micellar nanoparticles. Moreover, the pH-responsive β-amino ester micelles achieved a 23-fold improvement in paclitaxel deposition within tumors, as compared to free paclitaxel administration. The pH-sensitive micelles also achieved a threefold improvement in paclitaxel deposition in tumors, as compared to non-pH sensitive micelles (Shenoy et al. 2005). This case reveals the potential of pH-sensitive micelles to increase drug delivery to cancerous tumors.

An alternative method for constructing environmentally responsive micelles is to build temperature sensitivity into the micelle structure. Local temperatures inside the body can be readily raised, making temperature-triggered drug release a viable strategy for site-specific drug delivery. In addition, localized hyperthermia is sometimes used clinically to treat tumors, since the chaotic vasculature of tumors is more

vulnerable to hyperthermia than normal tissue (van der Zee 2002). Temperature-sensitive micelles could therefore be part of a synergistic treatment regimen, in which elevated temperature not only induces local drug release, but also directly destroys tumor cells. The most common technique for designing temperature-responsive micelles is to utilize a thermosensitive coronal polymer with lower critical solution temperature (LCST) behavior. The LCST is the critical temperature below which a mixture is miscible. The resulting micelles are stable below the LCST, but a temperature increase above the LCST induces the entire system to be hydrophobic and precipitate out of solution.

The most extensively used polymer for temperature-responsive biomaterials is poly(*N*-isopropylacrylamide) , or pNIPAM. Pure pNIPAM homopolymer has an LCST of 32°C, which can be adjusted by random copolymerization with monomers such as dimethylacrylamide to obtain LCST values within a desired range. For instance, temperature-responsive micelles have been created using pNIPAM as the corona and poly(butyl methacrylate) (PBMA) as the core-forming segment (Chung et al. 1999). The pNIPAM-PBMA micelles were loaded with doxorubicin and exhibited significant sensitivity to temperature: the micelles released only 15% of the loaded drug after 15 h at 30°C, but released 90% of the loaded drug after 15 h at 37°C. Drug release could also be switched on and off using temperature cycling. Importantly, the micelles showed temperature-sensitive cytotoxicity: at a 0.1 μg/ml dose, the micelles destroyed less than 5% of cells at 29°C, but killed 65% of cells when the temperature was increased to 37°C. Another temperature-sensitive micelle system has been constructed from pNIPAM- PLGA copolymers. In this case, pNIPAM was copolymerized with dimethylacrylamide (DMMAAm) to develop materials with a desirable LCST of 39°C (Liu et al. 2005). The micelles were loaded with paclitaxel and showed temperature sensitivity over a very tight range, with a fourfold increase in paclitaxel release at 39.5°C versus 37°C and an eightfold increase in cytotoxicity toward tumor cells at 39.5°C versus 37°C. Temperature can thus serve as a tunable trigger for chemotherapeutic delivery to tumors.

A final major strategy for site-specific drug release from smart micelles is ultrasound activation. Ultrasound facilitates drug delivery through numerous mechanisms, including a local temperature increase in exposed tissues; cavitation which increases the permeability of cell membranes; and the production of highly reactive free radical species which can accelerate polymer degradation (Mitragotri 2005). The most frequently used polymer in ultrasound-triggered micelles is Pluronic® copolymer (PEG-PPO-PEG). This polymer also appears to have a synergistic effect with some chemotherapeutic agents and has been proposed to inhibit the *p*-glycoprotein that causes multi-drug resistance in many cancer cells (Kabanov et al. 2002). Ultrasound-sensitive pluronic micelles have been designed, which incorporate PEG-phospholipids (PEG-DSPE) for micellar stabilization (Gao et al. 2005). These micelles were loaded with doxorubicin and evaluated in vivo. Ultrasound was able to improve the anti-tumor efficacy of both free doxorubicin and micelle-encapsulated doxorubicin; in the latter case, micelles with ultrasound delayed tumor growth an additional 2.6 days over micelles without ultrasound. Biodistribution

studies revealed that ultrasound not only increased the level of drug accumulation in the tumor, but also lowered the level of drug accumulation in the kidneys and heart. This last result is particularly relevant, as cardiotoxicity is a major side effect of traditional doxorubicin administration. Overall, ultrasound-sensitive micelles may have the capacity to both increase chemotherapeutic effectiveness and decrease adverse effects during tumor treatment.

In conclusion, functionalized micelles are becoming a powerful therapeutic platform for cancer-targeted drug delivery. Functionalized micelles can actively target tumor cells, either through receptor-ligand interactions or through environmental triggers, and effect site-specific drug release. As a result, these micelles can deliver chemotherapeutics with higher efficiency and greater safety. Before functionalized micelles can achieve clinical success, several research goals must still be met: the long-term stability of micelles must be confirmed; the accumulation of micelles at tumor sites must be evaluated; and the anti-tumor efficacy of functional micelles must be established in the clinical setting. While passively targeted micelles are already entering clinical trials, actively targeted micelles and smart micelles have not yet reached the clinic. Well-designed micellar biomaterials for drug delivery could decrease mortality not only from lung cancer, but other cancers as well.

Although lung cancer kills more individuals than any other cancer, it has received insufficient attention from the research community. Lung cancer research is dramatically underfunded, when compared to the number of people affected by the disease (Gritz et al. 2007). Unfortunately, there are relatively few survivors of lung cancer, and these individuals are underrepresented in advocacy efforts for greater research support. Smoking and lung cancer also carry a stigma (despite the fact that 15% of lung cancers are not associated with smoking), which contributes to the underfunding of lung cancer research. Micellar biomaterials can play a central role in advancing chemotherapy for lung cancer, as well as improving the bleak prognosis for lung cancer patients. Such biomaterials can strengthen current chemotherapeutics and make new chemotherapeutics possible, which may halt the spread of lung cancer. The ideal targeted micelle could fulfill the vision of a "magic bullet," where an agent introduced into the bloodstream has the capacity to selectively target diseased tissue, while leaving healthy tissue untouched. The following chapter will focus on a different type of diseased tissue, that caused by traumatic injury.

References

Bae Y, Fukushima S, Harada A et al (2003) Design of environment-sensitive supramolecular assemblies for intracellular drug delivery: polymeric micelles that are responsive to intracellular pH change. Angew Chem Int Ed Engl 42:4640

Bae Y, Nishiyama N, Fukushima S et al (2005) Preparation and biological characterization of polymeric micelle drug carriers with intracellular pH-triggered drug release property: tumor permeability, controlled subcellular drug distribution, and enhanced in vivo antitumor efficacy. Bioconjug Chem 16:122

Beers MH, Porter RS, Jones TV et al (2006) Merck manual of diagnosis and therapy, 18th edn. Wiley, New York, NY

Behera D, Balamugesh T (2004) Lung cancer in India. Indian J Chest Dis Allied Sci 46:269
Blanco E, Kessinger CW, Sumer BD et al (2009) Multifunctional micellar nanomedicine for cancer therapy. Exp Biol Med 234:123
Chung JE, Yokoyama M, Yamato M et al (1999) Thermo-responsive drug delivery from polymeric micelles constructed using block copolymers of poly(N-isopropylacrylamide) and poly(butylmethacrylate). J Control Release 62:115
Collins LG, Haines C, Perkel R et al (2007) Lung cancer: diagnosis and management. Am Fam Physician 75:56
Danson S, Ferry D, Alakhov V et al (2004) Phase I dose escalation and pharmacokinetic study of pluronic polymer-bound doxorubicin (SP1049C) in patients with advanced cancer. Br J Cancer 90:2085
Engin K, Leeper DB, Cater JR et al (1995) Extracellular pH distribution in human tumours. Int J Hyperthermia 11:211
Etienne-Mastroianni B, Falchero L, Chalabreysse L et al (2002) Primary sarcomas of the lung: a clinicopathologic study of 12 cases. Lung Cancer 38:283
Frank AL (1989) Epidemiology of lung cancer. In: Roth JA, Weisenburger T (eds) Thoracic oncology. WB Saunders, Philadelphia, PA
Gao ZG, Fain HD, Rapoport N (2005) Controlled and targeted tumor chemotherapy by micellar-encapsulated drug and ultrasound. J Control Release 102:203
Gillies ER, Fréchet JM (2005) Dendrimers and dendritic polymers in drug delivery. Drug Discov Today 10:35
Giuliani L, Jaxmar T, Casadio C et al (2007) Detection of oncogenic viruses SV40, BKV, JCV, HCMV, HPV and p53 codon 72 polymorphism in lung carcinoma. Lung Cancer 57:273
Goren D, Horowitz AT, Tzemach D et al (2000) Nuclear delivery of doxorubicin via folate-targeted liposomes with bypass of multidrug-resistance efflux pump. Clin Cancer Res 6:1949
Greene FL (2002) AJCC cancer staging manual, 6th edn. Springer, New York, NY
Gritz ER, Sarna L, Dresler C et al (2007) Building a united front: aligning the agendas for tobacco control, lung cancer research, and policy. Cancer Epidemiol Biomarkers Prev 16:859
Guichard S, Terret C, Hennebelle I et al (1999) CPT-11 converting carboxylesterase and topoisomerase activities in tumour and normal colon and liver tissues. Br J Cancer 80:364
Hecht SS (2003) Tobacco carcinogens, their biomarkers and tobacco-induced cancer. Nat Rev Cancer 3:733
Hecht SS, Abbaspour A, Hoffman D (1998) A study of tobacco carcinogenesis. XLII. Bioassay in A/J mice of some structural analogues of tobacco-specific nitrosamines. Cancer Lett 42:141
Jones M, Leroux J (1999) Polymeric micelles – a new generation of colloidal drug carriers. Eur J Pharm Biopharm 48:101
Kabanov AV, Batrakova EV, Alakhov VY (2002) Pluronic block copolymers for overcoming drug resistance in cancer. Adv Drug Deliv Rev 54:759
Kessler H, Diefenbach B, Finsinger D et al (1995) Design of superactive and selective integrin receptor antagonists containing the RGD sequence. Lett Pept Sci 2:155
Kim TY, Kim DW, Chung JY et al (2004) Phase I and pharmacokinetic study of Genexol-PM, a cremophor-free, polymeric micelle-formulated paclitaxel, in patients with advanced malignancies. Clin Cancer Res 10:3708
Koizumi F, Kitagawa M, Negishi T et al (2006) Novel SN-38-incorporating polymeric micelles, NK012, eradicate vascular endothelial growth factor-secreting bulky tumors. Cancer Res 66:10048
Kufe DW, Pollock RE, Weichselbaum RE et al (2003) Cancer medicine, 6th edn. BC Decker, Hamilton, Canada.
Kunath K, Merdan T, Hegener O et al (2003) Integrin targeting using RGD-PEI conjugates for in vitro gene transfer. J Gene Med 5:588
Liu BQ, Peto R, Chen ZM et al (1998) Emerging tobacco hazards in China: 1. Retrospective proportional mortality study of one million deaths. BMJ 317:1411

Liu SQ, Tong YW, Yang YY (2005) Thermally sensitive micelles self-assembled from poly(N-isopropylacrylamide-co-N,N- dimethylacrylamide)-b-poly(D,L-lactide-co-glycolide) for controlled delivery of paclitaxel. Mol Biosyst 1:158

Liu J, Zeng F, Allen C (2007) In vivo fate of unimers and micelles of a poly(ethylene glycol)-block-poly(caprolactone) copolymer in mice following intravenous administration. Eur J Pharm Biopharm 65:309

Maeda H, Wu J, Sawa T et al (2000) Tumor vascular permeability and the EPR effect in macromolecular therapeutics: a review. J Control Release 65:271

Matsumura Y, Hamaguchi T, Ura T et al (2004) Phase I clinical trial and pharmacokinetic evaluation of NK911, a micelle-encapsulated doxorubicin. Br J Cancer 91:1775

Matsumura Y, Kataoka K (2009) Preclinical and clinical studies of anticancer agent-incorporating polymer micelles. Cancer Sci 100:572

Minna JD, Schiller JH (2008) Neoplasms of the lung. In: Fauci AS, Braunwald E, Kasper DL et al (eds) Harrison's principles of internal medicine, 17th edn. McGraw Hill, New York, NY

Mitragotri S (2005) Healing sound: the use of ultrasound in drug delivery and other therapeutic applications. Nat Rev Drug Discov 4:255

Morandi U, Casali C, Rossi G (2006) Bronchial typical carcinoid tumors. Semin Thor Cardiovasc Surg 18:191

Mountain CF (1997) Revisions in the international system for staging lung cancer. Chest 111:1710

Mountain CF, Libshitz HI, Hermes KE (2003) Lung cancer: A handbook for staging, imaging, and lymph node classification. Charles P. Young, Houston, TX

Mross K, Maessen P, van der Vijgh WJF et al (1988) Pharmacokinetics and metabolism of epidoxorubicin and doxorubicin in humans. J Clin Oncol 6:517

Nasongkla N, Shuai X, Ai H et al (2004) cRGD-functionalized polymer micelles for targeted doxorubicin delivery. Angew Chem Int Ed Engl 43:6323

Negoro S, Masuda N, Takada Y et al (2003) Randomised phase III trial of irinotecan combined with cisplatin for advanced non-small-cell lung cancer. Br J Cancer 88:335

Nishiyama N, Okazaki S, Cabral H et al (2003) Novel cisplatin-incorporated polymeric micelles can eradicate solid tumors in mice. Cancer Res 63:8977

Noda K, Nishiwaki Y, Kawahara M et al (2002) Irinotecan plus cisplatin compared with etoposide plus cisplatin for extensive small-cell lung cancer. N Engl J Med 346:85

O′Rourke MA, Feussner JR, Feigl P et al (1987) Age trends of lung cancer stage at diagnosis: implications for lung cancer screening in the elderly. JAMA 258:921

Park EK, Lee SB, Lee YM (2005) Preparation and characterization of methoxy poly(ethylene glycol)/poly(epsilon-caprolactone) amphiphilic block copolymeric nanospheres for tumor-specific folate-mediated targeting of anticancer drugs. Biomaterials 26:1053

Peer D, Karp JM, Hong S et al (2007) Nanocarriers as an emerging platform for cancer therapy. Nat Nanotechnol 2:751

Peto R, Lopez AD, Boreham J et al (2006) Mortality from smoking in developed countries 1950–2000: indirect estimates from national vital statistics. Oxford University Press, Oxford, UK

Potineni A, Lynn DM, Langer R et al (2003) Poly(ethylene oxide)-modified poly(beta-amino ester) nanoparticles as a pH-sensitive biodegradable system for paclitaxel delivery. J Control Release 86:223

Ross JF, Chaudhuri PK, Ratnam M et al (1994) Differential regulation of folate receptor isoforms in normal and malignant tissues in vivo and in established cell lines. Physiologic and clinical implications. Cancer 73:2432

Saito Y, Yasunaga M, Kuroda J et al (2008) Enhanced distribution of NK012, a polymeric micelle-encapsulated SN-38, and sustained release of SN-38 within tumors can beat a hypovascular tumor. Cancer Sci 99:1258

Shenoy D, Little S, Langer R et al (2005) Poly(ethylene oxide)-modified poly(beta-amino ester) nanoparticles as a pH-sensitive system for tumor-targeted delivery of hydrophobic drugs: part 2. In vivo distribution and tumor localization studies. Pharm Res 22:2107

Shuai X, Ai H, Nasongkla N et al (2004) Micellar carriers based on block copolymers of poly(epsilon-caprolactone) and poly(ethylene glycol) for doxorubicin delivery. J Control Release 98:415

Slatter JG, Schaaf LJ, Sams JP et al (2000) Pharmacokinetics, metabolism, and excretion of irinotecan (CPT-11) following I.V. infusion of [(14)C]CPT-11 in cancer patients. Drug Metab Dispos 28:423

Soga O, van Nostrum CF, Fens M et al (2005) Thermosensitive and biodegradable polymeric micelles for paclitaxel delivery. J Control Release 103:341

Sopori M (2002) Effects of cigarette smoke on the immune system. Nat Rev Immunol 2:372

Strand TE, Rostad H, Damhuis RA et al (2007) Risk factors for 30-day mortality after resection of lung cancer and prediction of their magnitude. Thorax 62:991

Sutton D, Nasongkla N, Blanco E et al (2007) Functionalized micellar systems for cancer targeted drug delivery. Pharm Res 24:1029

Takimoto CH, Arbuck SG (2001) Topoisomerase I targeting agents: the camptothecins. In: Chabner BA, Lango DL (eds) Cancer chemotherapy and biotherapy: principles and practice, 3rd edn. Lippincott Williams & Wilkins, Philadelphia, PA

Thun MJ, Hannan LM, Adams-Campbell LL et al (2008) Lung cancer occurrence in never-smokers: an analysis of 13 cohorts and 22 cancer registry studies. PLoS Med 5:e185

Torchilin VP (2001) Structure and design of polymeric surfactant-based drug delivery systems. J Control Release 73:137

Torchilin VP (2007) Micellar nanocarriers: pharmaceutical perspectives. Pharm Res 24:1

Torchilin VP, Lukyanov AN, Gao Z et al (2003) Immunomicelles: targeted pharmaceutical carriers for poorly soluble drugs. Proc Natl Acad Sci USA 100:6039

Travis WD, Travis LB, Devesa SS (1995) Lung cancer. Cancer 75(1 suppl):191

Tucker GC (2003) Alpha v integrin inhibitors and cancer therapy. Curr Opin Investig Drugs 4:722

Uchino H, Matsumura Y, Negishi T et al (2005) Cisplatin-incorporating polymeric micelles (NC-6004) can reduce nephrotoxicity and neurotoxicity of cisplatin in rats. Br J Cancer 93:678

van der Zee J (2002) Heating the patient: a promising approach? Ann Oncol 13:1173

Wasserheit C, Frazein A, Oratz R et al (1996) Phase II trial of paclitaxel and cisplatin in women with advanced breast cancer: an active regimen with limiting neurotoxicity. J Clin Oncol 14:1993

Weiss RB, Donehower RC, Wiernik PH et al (1990) Hypersensitivity reactions from taxol. J Clin Oncol 8:1263

Weissig V, Whiteman KR, Torchilin VP (1998) Accumulation of protein-loaded long-circulating micelles and liposomes in subcutaneous Lewis lung carcinoma in mice. Pharm Res 15:1552

Wiernik PH, Schwartz EL, Strauman JJ et al (1987) Phase I clinical and pharmacokinetic study of taxol. Cancer Res 47:2486

World Health Organization (1981) Histological typing of lung tumors, 2nd edn. WHO Press, Geneva

World Health Organization (2008) The global burden of disease: 2004 update. WHO Press, Geneva

Yoo HS, Park TG (2004) Folate receptor targeted biodegradable polymeric doxorubicin micelles. J Control Release 96:273

Chapter 10
Traumatic Injuries

Road traffic accidents are the ninth leading killer worldwide. In 2004, road traffic accidents were responsible for 1.3 million deaths or 2.2% of all deaths globally and 3.3% of all years of life lost (World Health Organization 2008). Traumatic injuries resulting from traffic accidents are extremely common. Each year, 24.3 million individuals worldwide suffer injuries severe enough to require medical attention, as a result of road traffic accidents (World Health Organization 2008). Other catastrophes add further to the annual toll of traumatic injuries worldwide. For instance, 37.3 million individuals around the globe experience traumatic injuries from falls, 10.9 million individuals suffer injuries from fires, and 17.2 million individuals experience injuries from violence every year. Despite refinements in suturing and stapling techniques for tissue reattachment and wound closure, surgeons continue to struggle with difficult tissue repairs. Reliable closure of tissues and organs remains one of the great unsolved challenges of clinical medicine, and physicians are constantly seeking better methods for achieving efficient and secure closure of both surgical and traumatic wounds. There is great demand for tissue adhesives to replace or augment sutures and staples for wound repair, as well as adhesive materials for hemorrhage control. An effective tissue adhesive has the potential to reduce operating times, lessen the bleeding and leakage from wounds, lower the incidence of complications, and reduce hospital stays. Such an adhesive will save time and money, as well as lessen morbidity and mortality in surgical patients. Extensive progress has been made in the development of adhesive biomaterials, with several platforms available for clinical use. Continued innovation in this field is essential for patient safety. This chapter reviews the current status of adhesive biomaterials for tissue reconstruction and highlights new developments in bioadhesive platforms. The chapter will begin with a discussion of the clinical necessity for adhesive biomaterials, as well as recommended properties of novel tissue adhesives. The chapter will then describe existing commercial adhesives for wound closure, including fibrin-based adhesives, cyanoacrylate-based adhesives, crosslinked protein-based adhesives, and PEG-based adhesives. The chapter will subsequently describe novel bioadhesives under development, including bio-inspired adhesives, polysaccharide-based adhesives, and dendrimer-based adhesives.

S.K. Bhatia, *Biomaterials for Clinical Applications*,
DOI 10.1007/978-1-4419-6920-0_10, © Springer Science+Business Media, LLC 2010

10.1 Clinical Necessity for Wound Closure Technologies

Novel wound closure techniques are required to address a multitude of traumatic and surgical wounds. The limitations of traditional approaches for wound closure are best illustrated by current rates of adverse events following common surgical procedures. For example, gastrointestinal anastomotic closures demonstrate a leakage rate of 3–15%, resulting in dire clinical consequences (infection, hemorrhage) and a 2–3% mortality rate for patients undergoing abdominal surgeries (Bruce et al. 2001; Pickleman et al. 1999). Leaking fluids can escape between suture or staple lines; fluids can also leak through needle holes and staple punctures created by the placement of sutures and staples. A slight seepage of intestinal contents can lead to local contamination and infection, abscess formation, and fulminant bacterial peritonitis. Likewise, a small oozing blood vessel can permit significant blood loss. Moreover, in patients undergoing a potentially curative surgery for colorectal cancer, the presence of gastrointestinal anastomotic leakage is associated with a lower 5-year survival rate (44.3% in patients with leakage versus 64.0% in patients without leakage), even when there are no immediate clinical consequences of wound leakage (Walker et al. 2004). Failure to achieve robust tissue closure thus carries both short-term and long-term risks.

Even tiny surgical incisions present significant challenges with regard to wound closure. As a case in point, the optimal sealing of corneal incisions during cataract surgery is a complex issue for ophthalmic surgeons. Sutures have traditionally been utilized for closure of corneal wounds, but the use of sutures is associated with several disadvantages. Suture placement requires fine technical skill and a prolonged operative time, and sutures inflict trauma to corneal tissue. In addition, suture materials can activate infection, inflammation, and neovascularization with resultant corneal scarring and defects in vision (Varley and Meisler 1991). In addition, uneven tension on sutures can lead to asymmetric healing and astigmatism (Binder 1985). Postoperative integrity of sutures can also be compromised. There has recently been a progressive increase in the use of sutureless clear corneal incisions by cataract surgeons; however, sutureless corneal incisions have been associated with an increased incidence of acute endophthalmitis (Nagaki et al. 2003; Powe et al. 1994), likely due to bacterial contamination of the unsutured open wound.

The above clinical cases reveal a pressing need in medicine for adhesive biomaterials for tissue reconstruction. Tissue adhesives are an attractive method for ensuring strong, leak-free repairs that preserve tissue and organ function and subsequently improve patient quality of life and patient survival. An adhesive biomaterial for tissue reconstruction may function in multiple capacities (Fig. 10.1): a hemostatic agent to limit blood loss, an adjunct to sutures and staples to limit leakage, or a primary closure agent to avoid the use of sutures or staples. In fact, polymeric adhesives can be applied to virtually every organ system in the body (Fig. 10.2). Adhesive biomaterials have numerous potential clinical uses, ranging from cardiovascular medicine to orthopedics to neurosurgery; a detailed list of possible surgical applications for bioadhesives is given in Table 10.1.

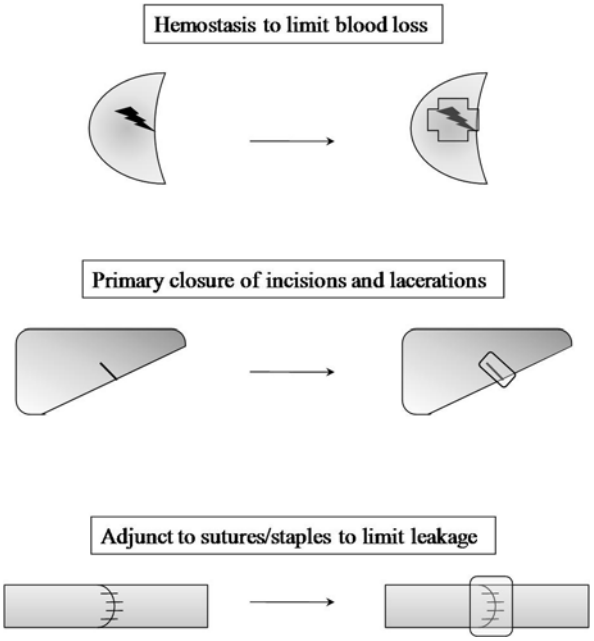

Fig. 10.1 Clinical usage of adhesive biomaterials for wound closure; bioadhesives may function as hemostats, primary closure agents, and adjuncts to sutures and staples

The concept of using an adhesive to join or rejoin tissues dates back to at least 1,787, when it was noted "that many workmen glue their wounds with solid glue dissolved in water" (Haring 1972). The use of hide glue (similar to gelatin, which is itself derived from collagen protein) was most common, but other biological adhesives such as blood and egg white (albumin) have also been used for centuries. However, the search for the perfect operative sealant continues, as an ideal tissue adhesive must overcome difficult performance challenges.

A number of technical factors must be considered in the selection and development of novel adhesive polymers for tissue reconstruction. First, tissue adhesives must demonstrate adequate physical and mechanical properties. A useful tissue adhesive must exhibit strong adhesion to the target tissue, as well as sufficient cohesion to bind tissue sites together. The tissue adhesive should cure rapidly, preferably without requiring extra equipment to induce curing, and the material should have the ability to cure in a wet physiological environment. Second, in addition to meeting mechanical specifications, novel adhesive polymers must meet biocompatibility specifications. The tissue adhesive must be biocompatible to the target site, performing in its desired application without causing adverse effect. Both the polymer construct and its degradation products must be non-cytotoxic, non-hemolytic, and non-inflammatory; undesirable responses such as irritation and sensitization must be avoided. The polymer adhesive must not interfere with wound healing or induce fibrosis or a foreign body response; it is also necessary that the adhesive does

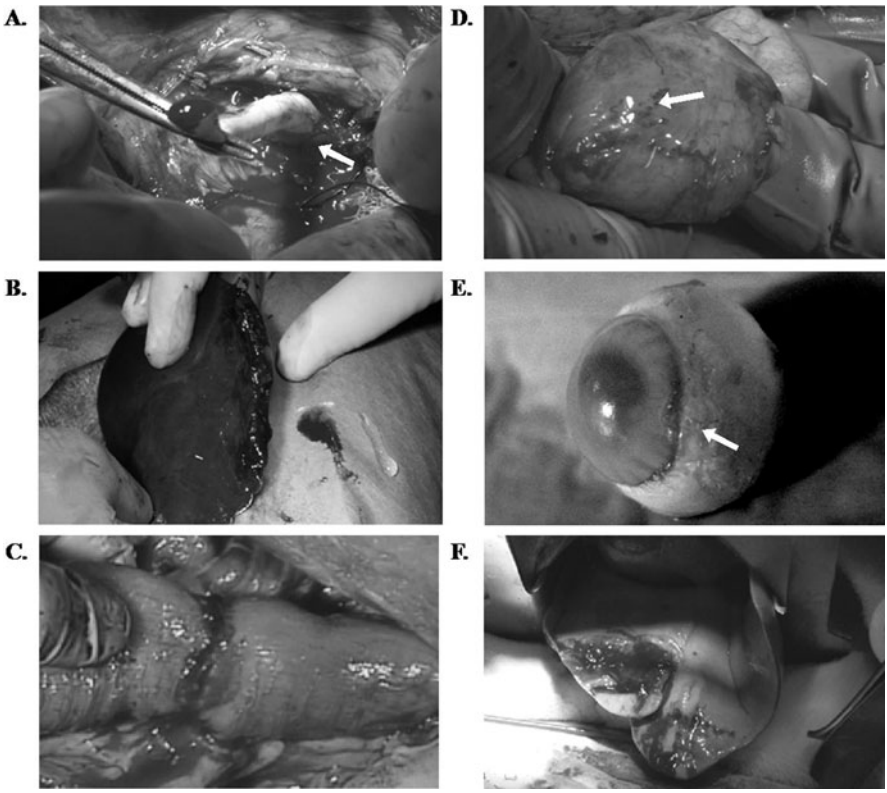

Fig. 10.2 Application of polymeric bioadhesive to a variety of organs and tissue surfaces. A polysaccharide-based adhesive is shown applied to **a** vascular tissue; **b** liver; **c** large intestine; **d** bladder; **e** cornea; and **f** lung

not act as a hospitable environment for bacteria, so that it does not propagate an infection.

Third, adhesive polymers must meet the requirements of physiological metabolism. It is essential that the adhesive be biodegradable, with degradation achieved via either hydrolysis or enzymatic cleavage. The degradation time should be tuned such that the adhesive remains on the target site until physiological wound healing has taken place and degrades soon afterward to avoid polymer encapsulation by immune cells. Indeed, the success of the adhesive joint can be judged by the how well the tissue is replaced. The degradation products must be readily excreted via renal clearance, which generally imposes an upper limit of 70,000 for the molecular weight of degradation products. Finally, tissue adhesives must be easily usable in surgical and trauma situations. The ideal adhesive for clinical usage should be rapidly and reproducibly delivered through a reliable device. An optimal system would require minimal advance preparation time, so that the sealant is available at a moment's notice for emergency care. The system should be shelf-stable for several

Table 10.1 Potential clinical applications for polymeric tissue adhesives and sealants

Neurosurgery
Repair of dural defects
Repair of central nervous system tissue
Spinal cord repair
Nerve grafting
Intervertebral disc surgery
Treatment of cerebrospinal fluid (CSF) leaks
Ophthalmic surgery
Clear corneal cataract surgery
Laser in situ keratomileusis (LASIK) surgery
Corneal ulcer treatment
Corneal transplantation
Conjunctival repair
Retinal attachment
Punctal plugging for treatment of dry eyes
Oculoplastics and blepharoplasty (eyelid lifts)
Vitrectomy closure
Attachment of extraocular muscles
Ear, nose, and throat (ENT) surgery
Control of epistaxis (nosebleeds)
Repair of vocal cord defects
Tympanoplasty for repair of perforated eardrum
Myringotomy (eardrum incision for drainage) with tube insertion
Sinus surgery
Nasal reconstructive surgery
Tonsillectomy surgery
Adenoidectomy surgery
Head and neck surgery
Salivary gland removal
Lymph node dissection
Treatment of chylous leakage after neck dissection
Interventional radiology
Therapeutic embolization
Femoral artery closure during interventional procedures
Vascular surgery
Arteriovenous fistula repair
Aortic aneurysm repair
Vascular anastomois
Cardiovascular surgery
Cardiac valve repair
Repair of ventricular wall rupture
Coronary artery anastomosis during bypass surgery
Pacemaker and lead placement
Defibrillator and lead placement
Aortic anastomosis
Treatment of aortic dissection
Thoracic surgery
Lung lobectomy
Lung biopsy
Pneumothorax treatment

Table 10.1 (continued)

Gastrointestinal surgery
Gastrointestinal anastomosis
Peptic ulcer treatment
Treatment of esophageal rupture
Gallbladder or bile duct anastomosis
Gastric bypass surgery
Appendectomy
Cholecystectomy (gallbladder removal)
Pancreatic surgery
Gastrointestinal fistula repair
Sealing of peritoneal dialysis catheter leakage
Prevention of intra-abdominal adhesions
Colorectal surgery
Colonic anastomosis
Rectal fistula repair
Treatment of diverticular bleeding
Hernia patch placement
Hemorrhoidectomy
Liver surgery
Liver resection
Liver transplantation
Gynecologic surgery
Hysterectomy
Myomectomy for uterine fibroid removal
Fallopian tube anastomosis
Vaginal fistula repair
Cervical surgery
Ovarian cyst removal
Breast biopsy
Mastectomy and lumpectomy
Management of preterm premature rupture of membranes
Urologic surgery
Nephrectomy
Kidney transplantation
Ureteral fistula repair
Ureteral anastomosis
Repair for stress urinary incontinence
Bladder closure
Radical prostatectomy
Vasectomy reversal surgery
Pediatric surgery
Congenital cleft lip repair
Orthopedic surgery
Hip replacement surgery
Knee replacement surgery
Tendon reattachment
Cartilage repair
Fracture repair
Bone grafting

Table 10.1 (continued)

Plastic and reconstructive surgery
Face lift surgery
Closure of skin incisions
Soft tissue augmentation
Trauma surgery
Closure of splenic lacerations and other solid organs
Closure of skin lacerations
Bleeding control during burn debridement
Skin grafting for burn victims

Table 10.2 Methods for characterizing novel polymeric tissue adhesives

Mechanical characterization	*Biological characterization*
Adhesive strength	Sterility properties
• Tensile strength	• Bioburden
• Overlap shear strength	• Bacterial endotoxin assay
• Peel adhesion strength	Tissue compatibility
• Impact strength	• Cytotoxicity
Cohesive tissue sealing ability	• Cellular inflammation
• Leak pressure test	• Cell and protein attachment
• Burst pressure test	• Tissue irritation
Physical/chemical characterization	• Tissue implantation response
Curing and reaction properties	• Wound healing
• Tack-free time	Hemolysis testing
• Total setting time	Systemic effects
• Extent of reaction	• Pyrogenicity
• Residual monomer content	• Sensitization
• Heat of polymerization	Toxicokinetic evaluation
Degradation properties	• Metabolic fate
• Degradation rate	Antimicrobial effects
• Degradation products	Encapsulated live cell viability
Swelling determination	*Clinical characterization*
Viscosity determination	Ease of use
Device characterization	Patient and clinician acceptance
Accelerated shelf stability test	Clinical efficacy
Physical integrity	Cost-effectiveness
Applicator functionality	Time to hemostasis
Device preparation time	Total amount of blood lost
	Long-term aesthetic outcome

months and permit storage at room temperature. A versatile adhesive system should require little instrumentation or equipment, so that the sealant can be used in field situations.

Throughout the development process, novel tissue adhesives must be assessed to ensure their suitability for clinical targets; characterization should include mechanical properties, physical/chemical properties, biological properties, shelf stability, and usability. A listing of recommended tests for adhesive biomaterials is presented in Table 10.2. Standardized testing protocols are available specifically for

tissue adhesives; in particular, the American Society for Testing and Materials has developed several guidelines for measuring the strength of bioadhesives (American Society for Testing and Materials 2008). These include:

- ASTM F2255-05 Standard Test Method for Strength Properties of Tissue Adhesives in Lap-Shear by Tension Loading
- ASTM F2256-05 Standard Test Method for Strength Properties of Tissue Adhesives in T-Peel by Tension Loading
- ASTM F2258-05 Standard Test Method for Strength Properties of Tissue Adhesives in Tension
- ASTM F2458-05 Standard Test Method for Wound Closure Strength in Tissue Adhesives and Sealants

These methods can provide a consistent means for comparing the performance of surgical adhesives on soft tissue.

The precise mechanical and chemical properties required of each adhesive biomaterial are determined to a large extent by the surgical target. Clinician input is an essential component of the design process, so that surgeon needs and patient needs can be translated into technical specifications. For example, an adhesive biomaterial for emergency hemostasis should demonstrate a very fast cure time and must be delivered over a wide surgical field; a hemostat may also exhibit a high degree of fluid absorption to stanch blood flow. In contrast, an adhesive for fine ophthalmic surgery or neurosurgery may need a slower cure time to allow adjustments of tissues and must be delivered through a smaller delivery device; such an adhesive might require low fluid absorption and low swell to avoid pressure on anatomical structures. The clinical target should continually guide the creation of a polymeric tissue adhesive.

10.2 Fibrin-Based Biomaterials for Wound Closure

Fibrin-based tissue adhesives are currently the principal biological sealant systems in clinical use. Fibrin glues take advantage of a physiological clotting cascade to form a synthetic fibrin clot on the surface of wounded tissue. As early as 1909, surgeons reported the hemostatic properties of fibrin powder applied in the operative field (Bergel 1909). In 1915, the use of fibrin as a hemostatic agent during cerebral surgery was described (Grey 1915). Purified thrombin became available in 1938, and combinations of thrombin with fibrinogen were first utilized in World War II to enhance adhesion of skin grafts to burned soldiers (Cronkite et al. 1944); the use of fibrin sealants for peripheral nerve attachment was also first demonstrated in the 1940s (Young and Medawar 1940). The Cohn process for blood fractionation was developed during World War II, and cryoprecipitation of fibrinogen was achieved in the 1960s, which led to the development of fibrin sealants in the 1970s. Commercially prepared fibrin sealants have been widely used in Europe since the 1970s. In 1972, a fibrin sealant containing concentrated fibrinogen was demonstrated to have utility for neural anastomoses (Matras et al. 1972); by 1977, a

two-suture microvascular anastomosis with fibrin glue was described (Matras et al. 1977). However, these products were not available in the United States until more recently, due to concerns by the Food and Drug Administration (FDA) regarding viral transmission of HIV, hepatitis B, or hepatitis C from fibrin sealants prepared using pooled blood. Indeed, an increased risk of hepatitis B transmission had been previously demonstrated with fibrinogen prepared from pooled human plasma (Bove 1978). Since that time, viral elimination protocols have been implemented. On May 1, 1998, Tisseel® (Baxter Healthcare, Deerfield, IL) became the first fibrin sealant approved by the Food and Drug Administration (FDA) for use in the United States.

Fibrin-based tissue adhesives mimic the final steps of the physiological coagulation cascade (Fig. 10.3) and produce a synthetic fibrin clot on the surface of wounded tissue. The key plasma proteins involved in the cascade are thrombin and fibrinogen. During physiological clotting, thrombin activates fibrinogen by cleaving fibrinopeptides A & B from fibrinogen. This cleavage step produces fibrin monomers, which then polymerize by hydrogen bonding and electrostatic

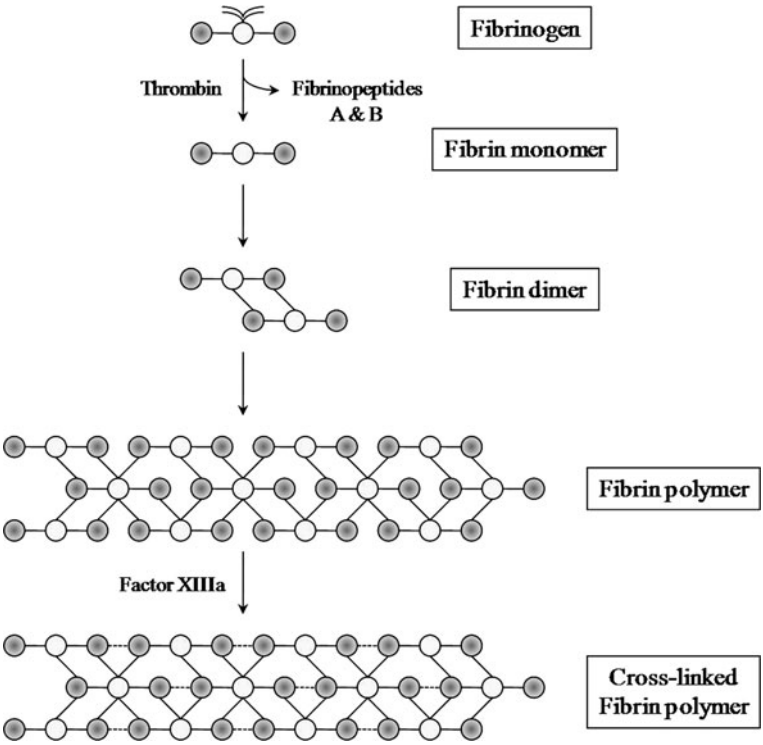

Fig. 10.3 Mechanism of action of fibrin-based tissue adhesive. Thrombin cleaves fibrinopeptides A and B from fibrinogen to produce fibrin monomers. The monomers then polymerize to form fibrin polymer, an unstable soft clot. Thrombin-catalyzed fibrin polymerization is followed by factor XIIIa-catalyzed fibrin crosslinking, resulting in formation of a stable fibrin clot

interactions to form fibrin polymer, an unstable soft clot. Thrombin also activates clotting factor XIII to form factor XIIIa in the presence of calcium ions. Factor XIIIa catalyzes crosslinking of fibrin polymer to form a stable clot at the site of injury. Crosslinking occurs via the formation of amide links between glutamine and lysine residues in proteins (Martinowitz et al. 1996; Martinowitz and Saltz 1996; Martinowitz and Spotnitz 1997). Additional crosslinking occurs between fibrin and adhesive glycoproteins of the extracellular matrix, including collagen, fibronectin, and von Willebrand factor; fibrin also crosslinks with cellular glycoproteins (Radosevich et al. 1997). This covalent crosslinking helps to anchor the fibrin clot to the injury site.

Commercial fibrin-based adhesives are typically comprised of a two-component system, in which two solutions are mixed immediately before application to wounded tissue, to provide a controlled fibrin deposition. During mixing of the fibrin adhesive, a solution of thrombin and calcium is combined with a solution of fibrinogen and factor XIII to form a coagulum. The fibrinogen is at a much higher concentration than that in human plasma. On combining the two solutions, a reaction similar to that of the final stages of the blood clotting cascade occurs. In some preparations of fibrin glue, the anti-fibrinolytic agent aprotinin is included in the tissue adhesive, presumably to prevent premature lysis of the clot. The exact composition of various commercial products differs, and this alters the properties of the resulting fibrin clot (Buchta et al. 2005). Fibrinogen concentration contributes to the tensile strength of the fibrin glue, while thrombin concentration determines the curing time to achieve maximum adhesive strength. Tissue adhesives with high fibrinogen concentrations tend to produce stronger, but more slowly forming clots. On the other hand, those containing high thrombin concentrations clot rapidly, but the resulting clot is not as strong (Busuttil 2003). For example, a sealant formulation containing 4 IU/ml thrombin sets in approximately 30–60 s, while a sealant formulation containing 500 IU/ml thrombin sets in 10 s (Detweiler et al. 1999). All fibrin glues produce clots that are biodegradable and bioabsorbable; the adherent fibrin clot on the tissue surface degrades naturally, within several days to weeks, by thrombolysis.

Fibrin-based tissue adhesives have been clinically utilized in a variety of organ systems and have been applied as hemostats, primary wound closure agents, and adjuncts to sutures and staples. A listing of commercially available fibrin tissue adhesives, along with their approved indications, is given in Table 10.3. Approved indications for fibrin adhesives include hemostasis in operations involving cardiopulmonary bypass, splenic trauma, and liver resection, as well as sealing of colonic anastomoses during the time of colostomy closure; in addition, one commercial fibrin sealant has gained approval for general hemostasis during surgery. However, fibrin sealants have found numerous uses in virtually every surgical discipline and have additionally been used off-label for drug delivery and tissue regeneration applications.

In vascular surgery, fibrin-based adhesives are an effective adjunct to sutures; fibrin adhesives prevent blood leakage from sewn vascular anastomoses and facilitate hemostasis in arteriovenous polytetrafluoroethylene (PTFE) vascular grafts (Schenk

Table 10.3 Commercially available fibrin-based tissue adhesives

Commercial product	Approved indications	Constituents
Tisseel® (Baxter Healthcare)	• Hemostasis during cardiopulmonary bypass surgery • Treatment of splenic injuries • Adjunct in colostomy closure	Human fibrinogen Human thrombin Human factor XIII Bovine aprotinin
Evicel® (J&J/Ethicon)	• General hemostasis in surgery	Human fibrinogen Human thrombin
CryoSeal® (Thermogenesis) Autologous fibrin sealant	• Hemostasis in liver resection surgery	Human fibrinogen Human fibronectin Human factor XIII Human factor VIII Human vWF Human thrombin

et al. 2002, 2003). In cardiac surgery, fibrin-based adhesives induce hemostasis during cardiopulmonary bypass procedures (Rousou et al. 1989); fibrin sealant is effective as a hemostatic agent to stop bleeding from adhesions at the time of reoperative cardiac surgery and from diffuse surfaces with capillary bleeding. Fibrin adhesives may also be used to seal sutured large vessel anastomoses, as well as woven Dacron cardiac prostheses (Koveker et al. 1981). Fibrin sealant additionally improves surgical results during acute aortic dissection (Seguin et al. 1991). The sealant is useful in both adult cardiac and pediatric cardiac surgical operations, including congenital heart surgery (Kjaergard and Fairbrother 1996). A fibrin sealant patch was reported to stop bleeding in the dramatic case of a free wall rupture of the left ventricle (Hvass et al. 1995). For thoracic surgery, there are reports of using fibrin glues to seal parenchymal air leaks to achieve pneumostasis and to close leaks of the bronchial tree (Bayfield and Spotnitz 1996).

In trauma settings, fibrin sealant has been used to control hemorrhage following solid organ injury in patients sustaining severe abdominal trauma (Ochsner 1998) and is FDA approved for repair of the liver and spleen. For gynecologic surgery, fibrin adhesives have been utilized to seal premature rupture of the membranes (Sciscione et al. 2001), and fibrin sealant has been used to enhance embryo transfer to improve adherence to enhance at the time of in vitro fertilization (Bar-Hava et al. 1999). In gastrointestinal surgery, beyond its FDA approved use for colonic anastomoses, fibrin adhesive has been applied to control bleeding from peptic ulcers (Lau et al. 1995) and for repair of anal fistulae (Sentovitch 2003). Fibrin sealants have also been injected endoscopically in the GI tract to control bleeding from gastric varices (Heneghan et al. 2002). In orthopedic procedures, fibrin-based adhesives reduce bleeding during both hip replacement (Wang et al. 2003a) and knee replacement (Wang et al. 2003b).

Fibrin-based adhesives have found utility in plastic and reconstructive surgery, as hemostatic agents following burn debridement; adhesives for attachment of skin grafts; and hemostatics to reduce hematomas and bruising following facelift

procedures (Currie et al. 2001; Marchac and Sandor 1994). In neurosurgery, fibrin sealants have been used for dural closure to prevent and treat cerebrospinal fluid leaks (Shaffrey et al. 1990). In the head and neck, fibrin-based adhesives reduce bleeding following tonsillectomy (Moralee et al. 1994) and serve as a replacement for nasal packing to provide hemostasis in endonasal operations (Vaiman et al. 2002). In ophthalmic surgery, fibrin-based adhesives have been employed for primary closure of conjunctival wounds to avoid suturing (Biedner and Rosenthal 1996), as well as closure of corneal perforations and deep corneal ulcers (Sharma et al. 2003).

Beyond their use in a variety of surgical applications, fibrin-based tissue adhesives have been demonstrated as carrier matrices for the controlled delivery of therapeutic drugs and biologics. One of the first drug delivery applications of fibrin glues was for antibiotics, to provide a local antimicrobial effect during wound healing (Thompson and Davis 1997; van der Ham et al. 1992). Antibiotics that have been successfully delivered from fibrin glues include tetracycline (Woolverton et al. 2001), erythromycin, ciprofloxacin, vancomycin, gentamicin, cefazolin (Tredwell et al. 2006), ampicillin, carbenicillin, dibekacin, clindamycin, and cefotaxime. In addition, fibrin has been used for the delivery of chemotherapeutic agents such as doxorubicin (Kitazawa et al. 1997) and cisplatin (Miura et al. 1995); bone growth inducers such as bone morphogenetic protein and transforming growth factor-beta (Kim et al. 2007); and nerve growth factors such as neurotrophin-4 to promote nerve regeneration (Yin et al. 2001).

Despite the versatility of fibrin-based tissue adhesives in surgical procedures, these adhesives are associated with important limitations. Although stringent precautionary measures are employed, fibrin glues containing blood components from pooled human plasma still pose a risk of viral transmission. There have been no known cases of hepatitis or HIV transmission with the use of commercial fibrin sealants. However, there are reports of transmission of symptomatic parvovirus B19 transmission by fibrin sealant used during surgery (Hino et al. 2000; Kawamura et al. 2002).

An additional risk is raised by the formulation of fibrin glues containing bovine proteins; such foreign proteins can stimulate an immune response, with the resultant formation of antibodies to physiologic clotting factors. Sensitization to bovine thrombin in fibrin sealants has been reported (Enzmann 1982), and there are several cases of surgical patients developing antibodies to factor V and thrombin (Berruyer et al. 1993), following the application of fibrin glue containing bovine thrombin. The formation of inhibitor antibodies has been observed in peptic ulcer surgery (Caers et al. 2003), as well as adult and pediatric cardiac surgery (Muntean et al. 1994); this complication carries a bleeding risk and often requires plasmapheresis treatment. Serious clinical complications have also resulted from the use of currently approved fibrin glues containing bovine aprotinin. Patients who have been exposed to bovine aprotinin in fibrin sealant may develop antibodies to aprotinin and may exhibit an allergic or anaphylactic reaction upon re-exposure to aprotinin. Cases of immediate allergic skin response (Beierlein et al. 2000) and severe anaphylaxis (Kober et al. 2008) have been reported as a result of bovine aprotinin

in fibrin tissue adhesives. In one case, fatal intraoperative anaphylaxis occurred in response to local application of fibrin sealant (Oswald et al. 2003). The formation of aprotinin-specific antibodies following application of fibrin glues is not uncommon: in one study of children undergoing operations for congenital heart disease, 49% developed aprotinin-specific antibodies at 6 weeks after exposure to bovine aprotinin in fibrin glue and 12% still had aprotinin-specific antibodies at 1 year after exposure to bovine aprotinin in fibrin glue (Scheule et al. 1998).

The prevalence and seriousness of such adverse effects highlight the drawbacks of using human and bovine proteins in tissue adhesives. Moreover, a practical limitation of fibrin-based tissue adhesives is that they require approximately 20 min of preparation time (Conrad and Yoskovitch 2003), so the time of use must be correctly anticipated. This also places a constraint on the utility of fibrin sealants in bleeding emergencies. Finally, fibrin tissue adhesives demonstrate relatively poor adhesion to tissue in comparison to synthetic cyanoacrylate adhesives and gelatin–resorcinol–formaldehyde/glutaraldehyde tissue adhesives (Albes et al. 1993). For these reasons, there is clinical interest in developing both alternative biological sealants and synthetic sealants for tissue reconstruction.

10.3 Cyanoacrylate-Based Biomaterials as Tissue Glues

Cyanoacrylate tissue adhesives are currently the principal synthetic polymer sealants in clinical usage. The preparation of alkyl alpha-cyanoacrylates was first described in 1949 for the production of "hard, clear, glass-like resins" (Ardis 1949a, b), and the adhesive properties of alpha-cyanoacrylates were discovered in the 1950s (Joyner and Hawkins 1955). Cyanoacrylates subsequently achieved widespread availability and household usage as "superglues," due to their fast-setting properties. The cyanoacrylate adhesive family also has found numerous applications in the automotive and construction industries. Cyanoacrylates were first used for medical applications in 1960, when the use of cyanoacrylate adhesives for small vessel surgery was first described (Carton et al. 1960). In 1962, clinical applications of cyanoacrylate glues in massive liver resection surgery (Marable and Wagner 1962) and bronchial closure (Healey et al. 1962) were reported. In the following year, cyanoacrylates were utilized for nephrotomy closure (Mathes and Terry 1963), gastrointestinal surgery (Seidenberg et al. 1963), and ophthalmic closure (Ellis and Levine 1963; Bloomfield et al. 1963). Cyanoacrylate tissue adhesives have been commercially available since the 1980s in Europe and Canada, but were initially restricted from the medical market in the United States due to concerns over histotoxicity and carcinogenicity. In 1998, the FDA approved Dermabond® (J&J/Ethicon, Somerville, NJ) as the first synthetic cyanoacrylate tissue adhesive product for the United States market.

Cyanoacrylates are distinct among adhesives in that they are single-component systems that polymerize at room temperature without the addition of a catalyst, evaporation of a solvent, heat, or pressure (Coover et al. 1959). These adhesives

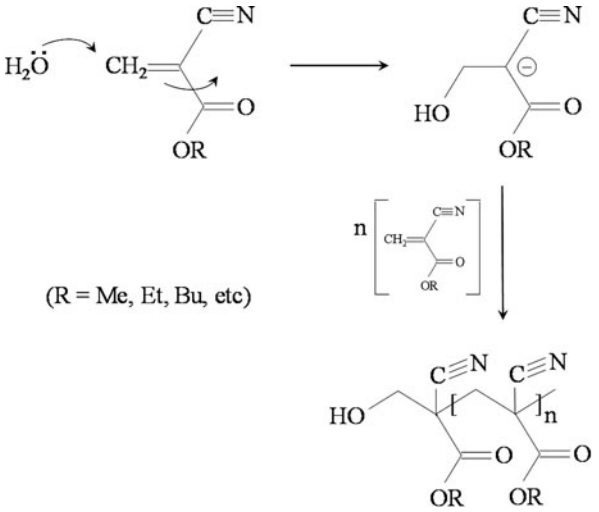

Fig. 10.4 Mechanism of anionic polymerization of cyanoacrylate tissue adhesive. The ethylene bond of the cyanoacrylate monomer is polarized due to the electron withdrawing capacity of the nitrile and alkoxylcarbonyl groups. A weak base, such as water from tissue fluid, can initiate and complete the anionic polymerization process

require no external initiation for curing; cyanoacrylates can rely on small amounts of water to initiate the polymerization reaction and bonding can occur within seconds. The uniqueness of cyanoacrylate glues derives from the extreme reactivity of the cyanoacrylate monomer (Fig. 10.4). The electron withdrawing capacity of the nitrile and the alkoxylcarbonyl groups of the monomer results in the double bond being very polarized and amenable to nucleophilic attack. This permits a weak base, such as the water from tissue fluid, to initiate and complete the anionic polymerization process quickly. The polymerization reaction is exothermic, and the rate of polymerization is inversely proportional to the amount of monomer. The reaction rate is also inversely proportional to the length of the alkyl side chain.

The basic cyanoacrylate monomer is a low-viscosity liquid. On contact with moist tissue, the cyanoacrylate polymerizes into a solid film that bridges apposed wound edges. Cyanoacrylate glues achieve adhesion through two independent mechanisms: molecular interaction via covalent bonding to the tissue surface and mechanical interlocking of the poly(cyanoacrylate) with underlying tissues. Cyanoacrylates form primary chemical bonds with the tissue surface, by covalently bonding to functional groups in proteins, in particular amine groups. The adhesive creates physical or mechanical bonds by penetration of cyanoacrylate monomers into cracks and channels in the tissue surface. Strong mechanical interlocks form as the polymerization process commences and the adhesive sets; this results in strong mechanical bonds between closely approximated tissues. The combination of chemical and mechanical bonding establishes the bond strength of cyanoacrylate tissue adhesives. In general, the strength and physical properties of cyanoacrylate

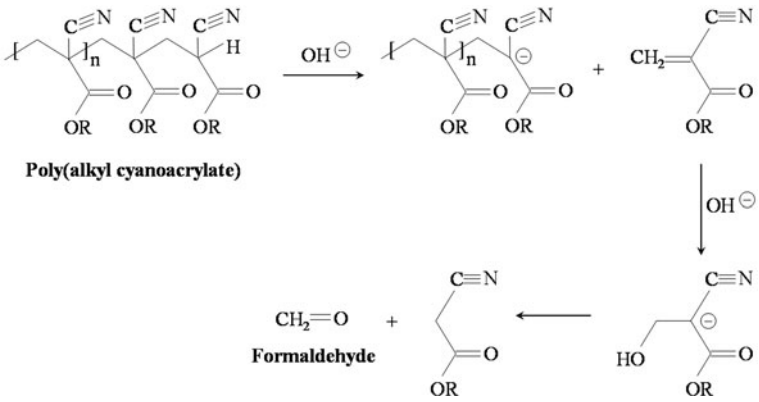

Fig. 10.5 Mechanism of hydrolytic degradation of cyanoacrylate polymer. Water associated with tissue can induce cyanoacrylate hydrolysis, releasing formaldehyde and alkyl cyanoacetate as degradation products

adhesives are determined the by the length and complexity of the alkyl side chain. Short, straight-chain derivatives (such as butyl-cyanoacrylate) form tighter and stronger bonds in comparison to complex, long-chain derivatives (such as octyl-cyanoacrylate). The tight bonds formed by shorter chain derivatives tend to be brittle and fracture prematurely when used as a topical bridge; this results in lower tensile strength of the polymerized short-chain derivatives than that of long-chain derivatives (Quinn 2005). Because of the brittle nature and lower bursting strength failure of shorter chain butyl-cyanoacrylate glues, when device failure occurs resulting in wound dehiscence, it tends to be a cohesive failure such that the adhesive breaks in the middle. In contrast, when device failure occurs with the longer chain octyl-cyanoacrylate glues, it tends to be an interfacial failure such that the adhesive peels away from the tissue surface (Singer et al. 2004).

Cyanoacrylate glues undergo hydrolytic degradation which takes place through non-enzymatic reactions; the main degradation products are formaldehyde and the corresponding alkyl cyanoacetate (Fig. 10.5). Degradation takes place by break-down of the polymer backbone and occurs because the methylene hydrogen in the polymer is highly activated inductively by the electron-withdrawing neighboring groups. The degradation rate of cyanoacrylate polymers decreases with an increase in length of the alkyl side chain, as a result of steric hindrance (Vezin and Florence 1980). An alternative degradation mechanism has also been proposed (Lenaerts et al. 1984), in which the cyanoacrylate polymer degrades by hydrolysis of the ester group to produce cyanoacrylic acid and alcohol (Fig. 10.6). This reaction may occur in the physiological environment and may be catalyzed by enzymatic activity.

A listing of commercially available cyanoacrylate tissue adhesives, along with their approved indications, is given in Table 10.4. Cyanoacrylates are approved for external closure of topical skin incisions and trauma-induced skin lacerations; the commercial cyanoacrylate glue Omnex® (J&J/Ethicon, Somerville, NJ) is

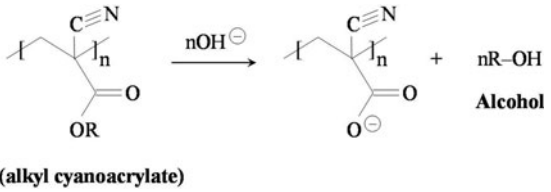

Fig. 10.6 Alternative mechanism of degradation of cyanoacrylate polymer. The ester group is hydrolyzed to produce cyanoacrylic acid and alcohol

Table 10.4 Commercially available cyanoacrylate-based tissue adhesives

Commercial product	Approved indications	Constituents
Indermil® (Covidien)	• Closure of topical skin incisions and trauma-induced skin lacerations • Additional approved claim as barrier to microbial penetration	*n*-Butyl-2-cyanoacrylate
Histoacryl® and Histoacryl® Blue (Tissueseal)	• Closure of topical skin incisions and trauma-induced skin lacerations	*n*-Butyl-2-cyanoacrylate
Dermabond® (J&J/Ethicon)	• Closure of topical skin incisions and trauma-induced skin lacerations • Additional approved claim as barrier to microbial penetration	2-Octyl-cyanoacrylate
Omnex® (J&J/Ethicon)	• Hemostasis for vascular reconstruction	2-Octyl-cyanoacrylate/butyl lactoyl cyanoacrylate

approved for internal hemostasis during vascular reconstruction surgery. When used for skin closure, the cyanoacrylates are recommended to be used with deep dermal sutures, because dehiscence can occur if the cyanoacrylates are the only means of skin attachment. In addition to their surgical adhesive indications, the 2-octyl-cyanoacrylate glue Dermabond® (J&J/Ethicon, Somerville, NJ) and the *n*-butyl-2-cyanoacrylate glue Indermil® (Covidien, Mansfield, MA; Fig. 10.7) are approved for use as barriers against common bacterial microbes including certain staphylococci, pseudomonads, and *Escherichia coli*. However, cyanoacrylate-based tissue adhesives have found numerous off-label uses in a variety of surgical disciplines.

The chief clinical application of cyanoacrylates is for external skin closure; cyanoacrylates have played an important role in enabling fast, painless, and cosmetically acceptable closure of topical wounds. Because the polymerized cyanoacrylate

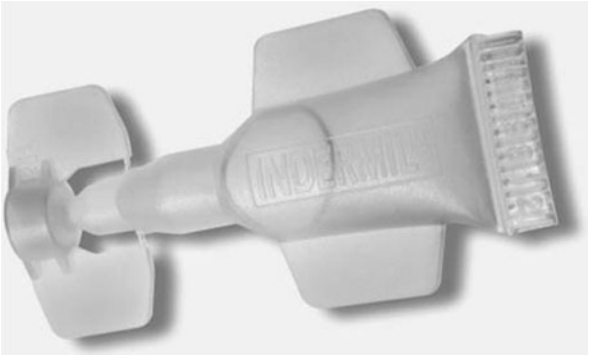

Fig. 10.7 Indermil® tissue glue composed of *n*-butyl-2-cyanoacrylate. The system is approved both as a surgical adhesive and a microbial barrier (Food and Drug Administration)

is waterproof, it requires no dressing. When used as a skin adhesive, the cyanoacrylate remains in place for approximately 7–10 days and then slowly sloughs off as skin cells regenerate and the natural healing process proceeds. Multiple clinical trials have confirmed the efficacy of cyanoacrylate glues in the management of lacerations and incisions (Quinn et al. 1993; Simon et al. 1997). A large, multi-center randomized controlled trial compared over 900 lacerations and surgical incisions closed with octyl-cyanoacrylate or a standard closure device (mostly sutures) and demonstrated that wound closure was faster using the cyanoacrylate adhesive, while the rates of wound infection, wound dehiscence, and optimal cosmetic results at 3 months were comparable (Singer et al. 2002). In a clinical study of cyanoacrylate adhesives for topical closure in pediatric patients, butyl-cyanoacrylate glues were utilized for the repair of scalp, face, and limb lacerations in over 1,500 children, with excellent cosmetic results (Mizrahi et al. 1988).

Cyanoacrylate-based tissue adhesives have also been used successfully for skin closure in hand surgery (Sinha et al. 2001) and topical closure in head and neck surgery (Laccourreye et al. 2005). In craniofacial surgery, cyanoacrylates have been successful in external lip closure for sutureless repair of congenital cleft lip (Spauwen et al. 2006). Cyanoacrylates have been used in neurosurgery for external wound closure in lumbar and cervical procedures (Hall and Bailes 2005), as well as scalp closure following craniotomies and shunt insertions (Wang et al. 1999). In plastic and reconstructive surgery, cyanoacrylate glues have been applied topically during body contouring surgery (Nahas et al. 2004), breast reduction surgery (Scott et al. 2007), and facial cosmetic surgery (Toriumi et al. 1998) including eyelid lifts (Greene et al. 1999). In general surgery, cyanoacrylates have been demonstrated for topical closure of laparascopic cholecystectomy incisions (Jallali et al. 2004) and inguinal herniorrhaphy incisions (Switzer et al. 2003); in obstetrics, cyanoacrylates have shown efficacy for external repair of perineal lacerations and episiotomy incisions (Bowen and Selinger 2002; Rogerson et al. 2000). Cyanoacrylate adhesives have even found use in interventional cardiology, where the glues have been used to

close wounds following cardiac device implantation (Pachulski et al. 2005), as well as cardiac surgery, where the glues demonstrate microbial barrier effects during skin closure of sternal incisions (Souza et al. 2008).

In vascular surgery, the cyanoacrylate glue Omnex® (J&J/Ethicon, Somerville, NJ) has been utilized for its approved indication to control bleeding during vascular reconstruction. This cyanoacrylate-based adhesive has been demonstrated to facilitate hemostasis of polytetrafluoroethylene (PTFE) vascular grafts, Dacron vascular grafts, and autologous vascular grafts (Brunkwall et al. 2007). The efficacy of cyanoacrylate glues for vascular reconstruction has been reported for both arteriovenous shunts and femoral bypass grafts (Schenk et al. 2005; Lumsdan et al. 2006). It should be noted that the *n*-butyl-cyanoacrylate product Trufill® n-BCA (J&J/Ethicon, Somerville, NJ) is also approved as a vascular occlusive agent for embolization of cerebral arteriovenous malformations, although this is not strictly a tissue reconstruction application.

Beyond their approved indications for external skin closure and vascular anastomotic closure, cyanoacrylate-based tissue adhesives have also been applied off-label in a variety of surgical fields. Cyanoacrylates have found utility in ophthalmology for treatment of corneal perforations (Taravella and Chang 2001), sealing of corneal incisions (Chen et al. 2007), and closure of scleral tunnel incisions (Kim et al. 1995). Cyanoacrylate glues have been utilized in hernia repair surgery to secure polypropylene hernia meshes (Jourdan and Bailey 1998). In gastroenterology, cyanoacrylates have been injected endoscopically to control bleeding from gastic varices (Greenwald et al. 2003). The cyanoacrylate glues have been employed in urology to seal nephrostomy tube sites (Sofer et al. 2003) and treat urinary fistulas (Bardari et al. 2001). In thoracic surgery, cyanoacrylate adhesives have been used in endoscopic repair of bronchial dehiscence following lung transplantation surgery (Maloney et al. 2001). In orthopedic surgery, there are case reports of cyanoacrylate glues for the fixation of osteochondral fractures of the knee (Gul et al. 2006), as well as fixation of talar osteochondral fractures (Yilmaz and Kuyurtar 2005). Bone repair with cyanoacrylates has also been accomplished in head and neck surgery, where the glues have been delivered endoscopically for fixation of zygomatic fractures (Cheski and Matthews 1997). Cyanoacrylate glues have additionally been employed in tympanoplasty and myringoplasty surgeries for repair of the tympanic membrane (Samuel et al. 1997).

Although cyanoacrylate-based tissue adhesives are unique single-component systems that are efficiently applied in a wide range of surgical procedures, these glues have significant and serious drawbacks because of limited biocompatibility. Cyanoacrylates are cytotoxic to connective tissue fibroblast cells (Ciapetti et al. 1994) and cultured tendon cells (Evans et al. 1999). In experimental implantation models, cyanoacrylates have been shown to induce acute inflammation and a prolonged foreign body giant cell response when applied subcutaneously (Toriumi et al. 1991). When used in experimental ophthalmic surgery for scleral tunnel incisions, cyanoacrylate glues provoke a severe inflammatory response that inhibits collagen remodeling and therefore interferes with wound healing (Kim et al. 1995). In experimental models of nerve anastomosis, cyanoacrylates cause a foreign body

inflammatory reaction and retractile fibrosis, reducing the nerve diameter by up to two-thirds (Wieken et al. 2003). In clinical neurosurgery, there are case reports of cyanoacrylates causing late complications following application to the frontal and lateral base of the skull; these serious complications include therapy-resistant fistulas, chronic sinusitis, and otogenic meningitis after *n*-butyl-2-cyanoacrylate glues were used for dural repair (Chilla 1987).

Both *n*-butyl-2- cyanoacrylate and 2-octyl-cyanoacrylate induce harmful histological changes in pancreatic tissue (Lämsä et al. 2008); there is one clinical case report of an inflammatory tumor of the pancreas, induced by endoscopic injection of cyanoacrylate glue for gastric varices (Sato et al. 2004). Necrosis associated with cyanoacrylate adhesives has been shown to contribute to thrombotic reactions (Papatheofanis 1989). Moreover, cyanoacrylates have been noted to inhibit new bone formation, cause a foreign body reaction, and impede fracture healing in experimental bone repair (Ekelund and Nilsson 1991). These effects raise questions regarding the routine use of cyanoacrylate adhesives for internal tissue bonding. Indeed, concerns have recently been raised regarding the hazards of cyanoacrylate use to both patients and healthcare workers; reported toxic effects of cyanoacrylates in the workplace include dermatologic, allergic, and respiratory conditions (Leggat et al. 2007).

The cytotoxic, histotoxic, and inflammatory effects of cyanoacrylates may be due to the release of their degradation products, including formaldehyde. The production of formaldehyde inside the body represents a major issue regarding the suitability of cyanoacrylates for internal surgical wound closure. Formaldehyde has been classified as a human carcinogen by the International Agency for Research on Cancer, a panel of the World Health Organization. It is classified as a probable human carcinogen by the United States Environmental Protection Agency (1987). One experimental study in laboratory animals has shown that *n*-butyl-2-cyanoacrylate tissue adhesives induce the formation of cancerous soft tissue sarcomas (Reiter 1987); this raises further questions about the potential carcinogenicity of cyanoacrylate glues. Given these considerations, it is prudent to limit the use of cyanoacrylates to their approved indications: external closure of topical skin wounds and hemostasis during vascular reconstruction.

Beyond their biological limitations, cyanoacrylates are also characterized by shortcomings in mechanical performance. After polymerizing, cyanoacrylate adhesives become brittle and are subject to fracturing when used in skin creases or long incisions. Cyanoacrylates are not as strong as 3/0 and some 4/0 sutures, so there is an increased risk of wound dehiscence when cyanoacrylates are used alone to close high-tension wounds (Singer et al. 2008). A study comparing wound closure using *n*-butyl-2-cyanoacrylate versus sutures in children with groin incisions suggests that closure of these high-tension wounds with cyanoacrylates may result in a higher rate of wound dehiscence after repair (van den Ende et al. 2004); dehiscence of the wound occurred in 26% of the cyanoacrylate-treated group and 0% of the suture-treated group. Cyanoacrylates are most appropriate for external closure of low-tension surgical incisions and traumatic lacerations whose edges are easily approximated.

10.4 Crosslinked Protein-Based Biomaterials as Tissue Glues

Tissue adhesives based on crosslinked proteins were originally developed as less toxic alternatives to early cyanoacrylate glues. Crosslinked protein-based adhesives are typically composed of both natural and synthetic materials and are fabricated by combining a natural protein with chemical crosslinking agents. The two major crosslinked protein-based sealants utilized in clinical medicine are gelatin–resorcinol–formaledhyde glues and albumin–glutaraldehyde glues; both of these adhesive platforms will be reviewed below. In general, the crosslinked protein-based tissue adhesives are characterized by very strong tissue adhesion but suboptimal biocompatibility. These adhesives have found specific utility in emergency cardiothoracic surgery, particularly for aortic dissections, by virtue of their superior adhesive properties. However, their toxicity profiles have limited these adhesives from achieving wider approval or usage.

The use of crosslinked gelatin as a tissue adhesive was first described in the 1960s by two different groups (Braunwald and Tatooles 1965; Falb and Cooper 1966). A gelatin–resorcinol mixture crosslinked with formaldehyde was chosen because of its high bond strength even in the presence of moisture. In 1966, it was reported that a gelatin–resorcinol mixture crosslinked with either formaldehyde (GRF glue) or a combination of formaldehyde and glutaraldehyde (GRFG glue) controlled hemorrhage from the liver and kidneys in an experimental model (Tatooles and Braunwald 1966). The GRF and GRFG glues were also demonstrated to give satisfactory tensile bond strengths in hepatic and renal tissues in an animal model and favorable hemostatic effects in the aorta, atria, ventricles, and lungs (Braunwald et al. 1966). In 1967, crosslinked gelatin tissue adhesives were successfully used in experimental gastrointestinal surgery (Bonchek and Braunwald 1967) and urinary tract surgery (Bonchek et al. 1967). In 1968, gelatin crosslinked with formaldehyde was investigated as a potential tissue adhesive, and it was found that addition of resorcinol to the gelatin–formaldehyde mixture was necessary to improve bond strength (Cooper and Falb 1968). Gelatin–resorcinol–formaldehyde tissue adhesives were first utilized to treat aortic dissections in the late 1970s (Laurian et al. 1977). Although GRF tissue adhesives are now widely used in Japan and Europe to treat aortic dissections, these glues are not currently commercially available in the United States, due to concerns about possible toxicity and carcinogenicity of formaldehyde.

Curing of GRF tissue adhesives occurs by condensation reactions of formaldehyde with gelatin (Fig. 10.8) and resorcinol (Fig. 10.9); condensation of formaldehyde with resorcinol yields a three-dimensional crosslinked resin. In use, the GRF glue is prepared by warming a 3:1 mixture of gelatin and resorcinol to 45°C, and applying the warmed mixture to the operative site; an 18% formaldehyde solution is then added to polymerize the tissue adhesive. Crosslinking of the GRF glue takes place in approximately 30 s. The curing profile of GRF adhesives can be altered by adjusting the ratios of the ingredients. The GRF glues bond well to wet tissues and form covalent linkages with functional groups on the tissue surface. Bonding strength may be enhanced by the penetration of ingredients into the tissue, as well as the hydrophobicity of the resultant resin.

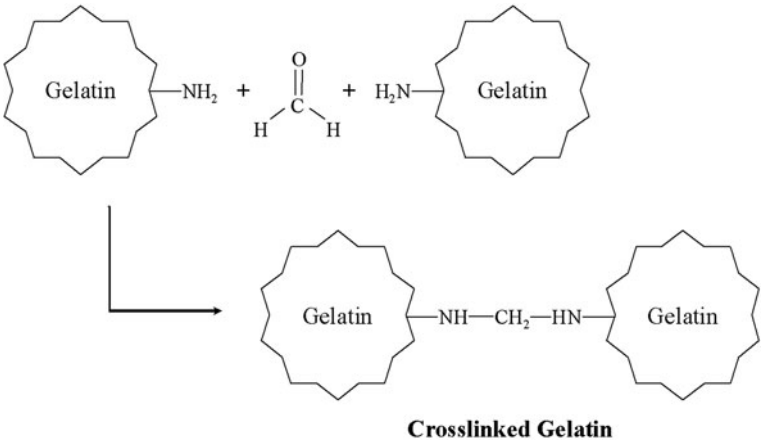

Fig. 10.8 Mechanism for curing of gelatin–resorcinol–formaldehyde tissue adhesives. Formaldehyde undergoes a condensation reaction with amine groups in gelatin protein to yield crosslinked gelatin

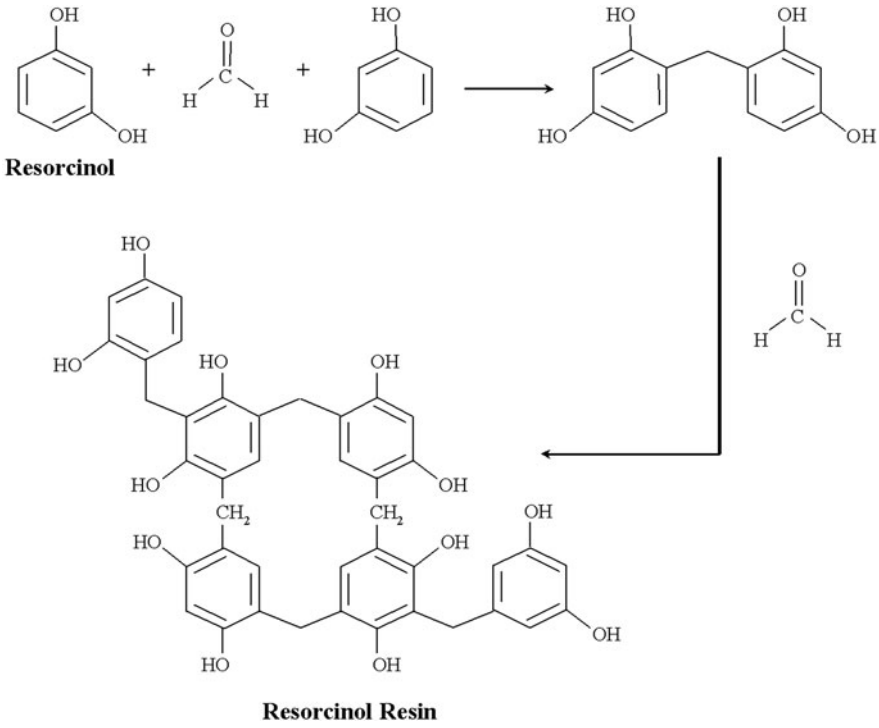

Fig. 10.9 Additional mechanism for curing of gelatin–resorcinol–formaldehyde tissue adhesives. Formaldehyde undergoes a condensation reaction with resorcinol to yield a three-dimensional crosslinked resorcinol resin

Currently, the principal clinical application of GRF tissue adhesive is for treatment of acute aortic dissections (Kunihara et al. 2008); several clinicians have noted the utility of GRF glue in difficult cases (Bachet et al. 1999; Neri et al. 1999). Because of its tissue bonding strength and crosslinked resin structure, the cured GRF polymer is exceptionally useful in reinforcing and reattaching the delicate structures of the dissected aortic wall. The GRF adhesive can be used to eliminate the abnormal dissection plane of the aortic vessel wall, as it glues together the layers of the aorta and strengthens the vessel wall to hold sutures more effectively. GRF glues have also been applied to remedy complications from aortic prostheses. In one clinical report, two patients presented with infected aortic bioprostheses complicated by annular abscesses; in each case, the aortic valve was replaced with a bioprosthesis and the annular abscesses were debrided and closed with the GRF glue, which completely sealed the abscess cavities (Stassano et al. 1994). GRF glues have additionally been employed in cardiac surgery for sutureless repair of left ventricular wall rupture (Iha et al. 1999; Okada et al. 2005) and ventricular septal defect (Isoda et al. 2004). In thoracic surgery, GRF adhesives have been applied following lung surgery to prevent air leakage (Takahashi et al. 2001); there is also one case report of successful closure of a bronchopleural fistula with GRF glue (Hasumi et al. 2003). In vascular surgery, GRF sealants have been demonstrated to facilitate hemostasis of ePTFE patch suture lines (Rittoo et al. 2001).

Despite its powerful ability to bind fragile tissue surfaces, GRF glue can cause substantial long-term damage and destruction to tissues. GRF adhesives are toxic to cardiovascular tissue, and devastating complications have occurred following the use of GRF glues in acute aortic dissection. Reported adverse outcomes include aortic root necrosis, aortic root redissection, pseudoaneurysm formation, and aortic regurgitation and insufficiency (Suzuki et al. 2006; Suehiro et al. 2002). In one clinical case, application of GRF glue for aortic dissection resulted in severe coronary artery narrowing which required bypass surgery (Martinelli et al. 2000). Given such potential outcomes, patients who receive GRF glues during surgery require careful long-term follow-up. Surgical application of GRF glues should be limited to special cases in which tissue integrity is poor, hemostasis is challenging, and high bonding strength is absolutely imperative.

A modified gelatin–resorcinol–aldehyde formulation has been developed to avoid the toxicity and potential carcinogenicity of formaldehyde (Ennker et al. 1994a, b). In this modified tissue adhesive, known as GR-DIAL, the formaldehyde component is replaced with two dialdehydes: glutaraldehyde (pentane-1,5-dial) and glyoxal (ethanedial). The GR-DIAL glue is commercially available in Europe under the trade name Gluetiss® (Geister Medizintechnik GmbH, Germany) and is indicated for treatment of aortic dissection.

Albumin–glutaraldehyde sealants derive conceptually from GRF glues, as the albumin–glutaraldehyde agent not only serves as a tissue sealant, but also acts to strengthen friable tissues (Chao and Torchiana 2003). Glutaraldehyde-crosslinked albumin was investigated as a sealant for polyester vascular prostheses in the 1990s (Chafke et al. 1996); commercial albumin–glutaraldehyde tissue adhesives were introduced shortly thereafter. In 1997, the surgical adhesive BioGlue® (Cryolife,

Atlanta, GA) received FDA approval in the United States under a humanitarian device exemption for use in acute aortic dissection. In 2001, BioGlue® received FDA approval for general use as a hemostatic adjunct in cardiac and vascular surgery. The albumin–glutaraldehyde sealant has broader indications in Europe, where BioGlue® received approval for vascular surgery in 1998, for pulmonary surgery in 1999, and for general surgical procedures in 2002. Under the CE mark, indicated soft tissues for BioGlue® are cardiac, vascular, pulmonary, genitourinary, dural, alimentary (esophageal, gastrointestinal, and colorectal), and other abdominal tissues (pancreatic, splenic, hepatic, biliary). Additionally, BioGlue® is allowed in Europe for the fixation of surgical meshes in hernia repair. In 2008, the albumin–glutaraldehyde glue received European approval for periosteal fixation following endoscopic browplasty or brow lift, a reconstructive plastic surgery procedure.

Curing of albumin/glutaraldehyde tissue adhesives occurs by condensation reactions between albumin and glutaraldehyde (Fig. 10.10). Glutaraldehyde reacts with amine groups in the albumin protein, particularly amine groups within lysine amino acid residues, yielding a crosslinked albumin network. In practice, the adhesive is a two-component system, comprised of stoichiometrically equivalent doses of 45% bovine serum albumin and 10% glutaraldehyde (typically delivered in a 4:1 volume ratio). The two solutions are mixed as they are delivered, combining to form an adhesive polymer on the target tissue; no advance preparation is required. The glue begins to polymerize within 20–30 s and reaches its bonding strength within 2 min. Albumin–glutaraldehyde tissue adhesives form covalent linkages with functional

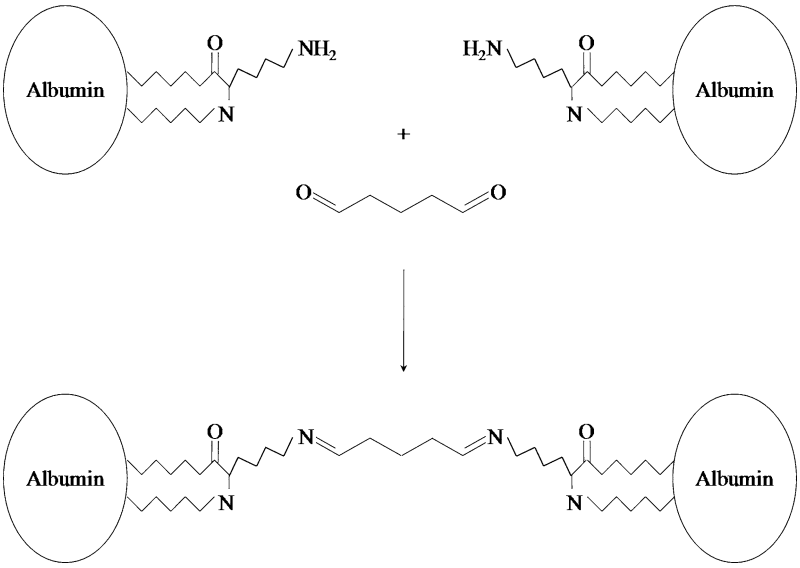

Fig. 10.10 Mechanism for curing of albumin–glutaraldehyde tissue adhesives. Glutaraldehyde undergoes a condensation reaction with amine groups in albumin protein, particularly amines in lysine amino acid residues. The result is a crosslinked albumin network

groups on the tissue surface. These glues also adhere to synthetic graft materials through mechanical bonding within the interstices of the graft matrix. Albumin–glutaraldehyde glues degrade very slowly, and one clinical report has demonstrated that the albumin–glutaraldehyde polymer persists at the repair site for up to 2 years after application (Yuen and Kaye 2005).

Albumin–glutaraldehyde adhesives are primarily utilized in the clinic for repair of acute aortic dissection (Raanani et al. 2004). Like GRF glue, albumin–glutaraldehyde glue reinforces flimsy tissue into a tougher and more workable consistency; the treated tissue is firm and easy to suture. Albumin–glutaraldehyde tissue adhesives have also been used for a wide array of cardiac surgical procedures, including coronary artery bypass grafting, valve procedures, ventricular aneurysm repair, closure of ventricular septal defect, and correction of congenital conditions (Passage et al. 2002). In addition, the albumin–glutaraldehyde glues have been employed as hemostatic and structural adjuncts to reduce bleeding from cardiac and vascular anastomoses (Coselli et al. 2003) and have been applied to attach Teflon patches during sutureless repair of ventricular free wall rupture (Leva et al. 2006). Albumin–glutaraldehyde sealants have additionally found utility for hemostasis during left ventricular assist device implantation (Goldstein and Beauford 2003). In thoracic surgery, albumin–glutaraldehyde adhesives have been used to seal lung lacerations, close bronchopleural fistulas, prevent lymph leakage, and prevent air leakage from suture or staple lines on pulmonary parenchyma (Potaris et al. 2003; Passage et al. 2005).

In the abdominal cavity, albumin–glutaraldehyde sealant has been applied to seal the kidney (Nadler et al. 2006) and spleen (Biggs et al. 2006) and has been utilized during minimally invasive surgery to remove ovarian cysts (Ehrlich et al. 2007). In the lower gastrointestinal tract, albumin–glutaraldehyde glue has been shown to reduce leakage from stapled anastomoses during hemorrhoid surgery (Anghelacopoulos et al. 2006) and has additionally been used to close anal fistulas (de la Portilla et al. 2007). In neurosurgery, albumin–glutaraldehyde sealant has been demonstrated to be effective in reducing cerebrospinal fluid leakage from dural defects and diaphragmatic defects (Dusick et al. 2006); the sealant has been used off-label for fixation of deep brain stimulation electrodes (Bjarkam et al. 2008). Albumin–glutaraldehyde glue has also been employed for tissue closure during middle ear surgery (Sen et al. 2006) and nasal surgery (Friedman and Schalch 2008). Finally, albumin–glutaraldehyde adhesives have been applied in facial plastic surgery for brow fixation following endoscopic brow lift procedures (Sidle et al. 2005).

While albumin–glutaraldehyde tissue adhesives share many of the functional benefits of GRF tissue adhesives, they also share many of the same limitations. Although albumin–glutaraldehyde adhesives avoid the use of formaldehyde, significant toxicity can still result from the glutaraldehyde component of these sealants. Polymerized albumin/glutaraldehyde glue releases levels of glutaraldehyde that are capable of inducing cytotoxic effects in vitro to cultured human embryo fibroblasts and mouse myoblasts. The glue also releases amounts of glutaraldehyde sufficient to induce adverse effects in vivo, including high-grade inflammation, edema, and

toxic necrosis in lung and liver tissue, as well as medium-grade inflammation in aortic tissue (Furst and Banerjee 2005). There are several case reports of late tissue toxicity and tissue scarring in patients who received albumin–glutaraldehyde glue; dense fibrosis and significant acute inflammation with foreign body giant cells were observed in these cases (Calafiore et al. 2002; Erasmi and Wohlschlager 2002).

Use of albumin–glutaraldehyde tissue adhesives for aortic dissection repair is associated with a risk of aortic wall necrosis, leading to aortic root redissection (Kazui et al. 2001). Albumin–glutaraldehyde glue impairs aortic vascular tissue growth and causes stricture when applied circumferentially around aortic anastomoses; for this reason, albumin–glutaraldehyde glue is contraindicated for cardiovascular anastomoses in pediatric patients (LeMaire et al. 2002). Stenosis of the superior vena cava has additionally been reported following nearby application of albumin–glutaraldehyde glue (Economopoulos et al. 2004). Other reported adverse outcomes of albumin–glutaraldehyde adhesive application in cardiothoracic procedures include mediastinal cyst formation (Szafrenek et al. 2006), lung fibrosis (Haj-Yahia et al. 2007), and aortic pseudoaneurysm formation (Ngaage et al. 2005).

Migration and embolization of the albumin–glutaraldehyde polymer can also cause serious complications. Albumin–glutaraldehyde glue can leak through suture holes in aortic tissue and vascular grafts (LeMaire et al. 2005) and migrate to block distal blood vessels. In one clinical report, embolization of the glue led to blockage of the right and left coronary arteries, resulting in a fatal right ventricular heart attack (Mahmood et al. 2004). In another report, two patients experienced acute loss of blood perfusion to the limbs, due to embolization of albumin–glutaraldehyde polymer after aortic dissection repair (Bernabeu et al. 2005). One patient required surgery to restore blood flow to the leg, and the other patient required surgery to restore blood flow to the arm. In addition, migration of the glue has resulted in cardiac valve malfunction. In one case report, a patient experienced blockage of a mechanical mitral valve leaflet following albumin–glutaraldehyde glue application (Devbhandari et al. 2006), and in another case, a patient experienced malfunction of a prosthetic aortic valve due to albumin/glutaraldhehyde adhesive (Shapira et al. 2006).

Moreover, glutaraldehyde may exhibit nerve toxicity, and adverse reactions have been noted following the use of albumin–glutaraldehyde sealant in neurosurgical procedures, as well as in the vicinity of peripheral nerves. Albumin–glutaraldehyde glue has been demonstrated in vivo to cause acute phrenic nerve injury leading to diaphragmatic paralysis, along with coagulation necrosis leading to cardiac conduction tissue damage (LeMaire et al. 2007). A clinical study of 75 pediatric neurosurgical patients found a strong association between the use of albumin–glutaraldehyde adhesive and postoperative wound complications; a 10-fold increase in complications prompted the investigators to stop the use of albumin–glutaraldehyde glue in pediatric neurosurgery (Klimo et al. 2007). Observed reactions included both inflammatory and infectious complications, and the investigators proposed that the intense inflammatory response triggered by albumin–glutaraldehyde glue creates an ideal environment for bacterial growth. Indeed, albumin–glutaraldehyde sealant has even been associated with an increased risk of sepsis following treatment of

anal fistulas (Abbas and Tejirian 2008). Finally, the bovine albumin component of albumin–glutaraldehyde glue could act as an immunogen and sensitize patients to bovine products (Van Belleghem et al. 2004). Taken together, these reports suggest that routine use of albumin–glutaraldehyde tissue adhesives is unwise. Tissue necrosis, neurotoxicity, infectious complications, and dense inflammatory adhesions are possible long-term outcomes that must be weighed against short-term benefits. Like GRF glues, albumin–glutaraldehyde glues should be limited to clinical situations in which strong tissue bonding is absolutely necessary and no satisfactory alternatives exist.

10.5 Polyethylene Glycol (PEG)-Based Biomaterials for Wound Closure

New tissue adhesives based on polyethylene glycol (PEG) have been developed to provide highly biocompatible, bioresorbable, synthetic hydrogels for wound closure. PEG hydrogel-based tissue adhesives are advantageous relative to other synthetically derived sealants, including cyanoacrylates, GRF glues, and albumin–glutaraldehyde glues, because PEG is much more compatible with biological tissues, and PEG hydrogels are readily degraded by hydrolysis. In addition, synthetic PEG-based adhesives avoid the risks associated with biological fibrin glues, including viral transmission and sensitization; moreover, PEG-based sealants circumvent the potential immunogenicity of bovine albumin–glutaraldehyde glues. PEG polymers have a long history of clinical use as drug delivery agents for therapeutic proteins (Caliceti and Veronese 2000). PEG conjugation reduces the immunogenicity of proteins and imparts "stealth" properties; PEG-modified proteins are non-immunogenic, even with repeated infusions (Abuchowski et al. 1977a, b). PEG polymers are thus well known in clinical medicine as biocompatible materials. Three major PEG-based tissue adhesives that have been designed for clinical medicine are photopolymerizable PEG sealants, PEG–PEG sealants, and PEG–trilysine sealants; all three of these adhesive platforms will be reviewed below. In general, the PEG-based sealants are characterized by excellent biocompatibility, but are high swelling with very fast degradation profiles that limit their functionality in wound reinforcement.

Hydrogel adhesives based on water-soluble, photopolymerizable macromers were developed in the early 1990s; these bioresorbable hydrogels are formed by photopolymerization of poly(ethylene glycol)-co-poly(α-hydroxy acid) diacrylate macromers (Sawhney et al. 1993). In 1994, photopolymerized PEG sealants were reported to prevent post-surgical adhesion formation and allow intra-abdominal healing in experimental models (Hill-West et al. 1994; Sawhney et al. 1994). In 1995, photopolymerizable PEG adhesives were demonstrated to seal human blood vessel anastomoses without inducing thrombogenicity (Dumanian et al. 1995). By 1997, the photopolymerized hydrogel adhesives were found to be effective for sealing bronchial and parenchymal air leaks in experimental lung surgery (Ranger et al. 1997). On May 26, 2000, the FDA approved the commercial sealant FocalSeal®-L

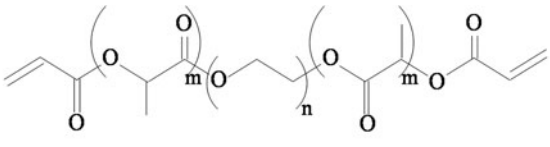

$AA\text{-}(LA)_m\text{-}(PEG)\text{-}(LA)_m\text{-}AA$

Primer Macromer

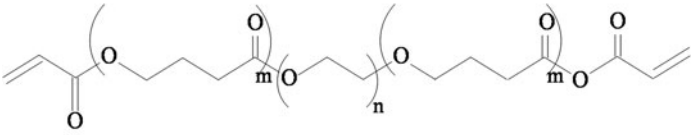

$AA\text{-}(TMC)_m\text{-}(PEG)\text{-}(TMC)_m\text{-}AA$

Sealant Macromer

Fig. 10.11 Chemical structures of primer and sealant macromers used in photopolymerizable PEG tissue adhesives. In each macromer, polyethylene glycol (PEG) is linked on each end to either trimethylene carbonate (TMC) or lactate (LA) hydolyzable segments and end-capped with polymerizable acrylate groups (AA)

(Focal Incorporated, Lexington, MA) for sealing air leaks on the lungs following surgical removal of cancerous lung tumors. The photopolymerizable tissue adhesive also received CE Mark approval for sealing air leaks following lung surgery.

Each macromer of the commercial photopolymerizable adhesive consists of PEG modified with biodegradable and photo-reactive elements. In each macromer, poly(ethylene glycol) is linked on both ends to hydrolyzable trimethylene carbonate or lactate oligomeric segments and then end-capped with polymerizable acrylate groups (Fig. 10.11). The macromers are amphiphilic in nature, with hydrophobic end regions on the central PEG chain, and form micellar structures in aqueous solution. The formation of such preorganized configurations in aqueous solutions enables the macromers to undergo rapid photopolymerization and gelation. During clinical use, the macromers are applied to the target tissue in two parts: a primer solution to provide tissue bonding and a sealant solution to provide desired mechanical properties. Both components are introduced as aqueous solutions to the target site. The primer layer is first brushed onto the tissue surface to allow the low-viscosity solution to flow into tissue interstices. The sealant solution is then mixed with the primer solution using a brush to provide a transition layer. The thicker sealant layer is then flowed in a continuous manner over the application area, and the macromers are photopolymerized.

To enable photopolymerization, the macromers are formulated in buffered saline solutions containing triethanolamine and eosin Y as the photoinitiator (Sawhney and

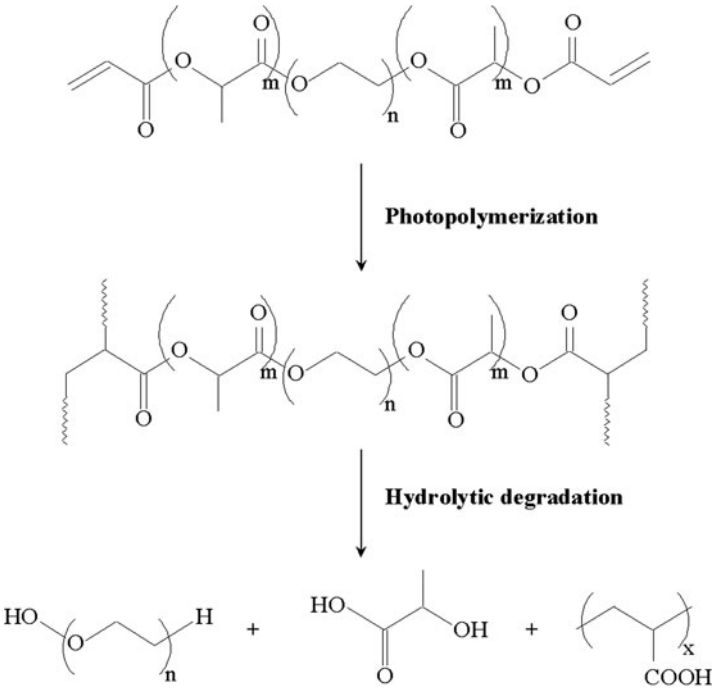

Fig. 10.12 Photopolymerization and biodegradation reactions of poly(ethylene glycol)-co-poly(L-lactide) diacrylate monomer. The degradation products are soluble and biocompatible

Hubbell 1999). The polymerization is initiated using visible blue-green light illumination from a xenon arc lamp (470–520 nm) for 40 s at an intensity of 100 mW cm^{-2}. The macromers crosslink to form a clear, flexible, and adherent hydrogel network. Because the sealant is polymerized in situ, the polymer conforms to the tissue surface. The hydrogel expands upon contact with body fluids and reaches its equilibrium swell volume within 24 h; the hydrogel contains 95% water at equilibrium. Following implantation, the poly(L-lactide) and poly(trimethylene carbonate) segments of the hydrogel degrade by hydrolysis (Fig. 10.12); the sealant thus degrades by dissolution rather than fragmentation. The biodegradation products are water soluble and biocompatible; the components are sufficiently low in molecular weight to be cleared through the kidneys or locally metabolized.

Photopolymerizable PEG tissue adhesives have been utilized clinically in their approved application for sealing air leaks following pulmonary resection (Maccharini et al. 1999; Wain et al. 2001); the adhesives have also been used to treat air leaks in patients suffering lung injury at cardiac reoperation (Gillinov and Lytle 2001). In addition, there is a clinical report of successful use of photopolymerized PEG adhesives for repairing ventricular wall rupture following mitral valve replacement (Fasol et al. 2004). In experimental models, the sealants have demonstrated efficacy for repairing acute aortic dissection (Tanaka et al. 1999),

Fig. 10.13 CoSeal® PEG–PEG tissue sealant. The sealant is a two-component system, comprising two functionalized star-branched PEGs. Upon mixing, the PEGs react to form a covalently bonded three-dimensional matrix. The sealant can be delivered as a sprayed barrier, as shown (Food and Drug Administration)

coronary artery anastomoses (White et al. 2000), inguinal hernia (Kato et al. 2005), pancreatic-jejunal anastomoses (Argyra et al. 2009), and intestinal anastomoses (Sweeney et al. 2002), as well as for prevention of peritendinous adhesions following flexor tendon repair surgery (Ferguson and Rinker 2006). However, despite desirable characteristics of biocompatibility, biodegradability, and potential versatility in surgical applications, the photopolymerizable PEG adhesives have failed to achieve widespread clinical use. The requirement for additional equipment (a blue-green visible light lamp) in the operating room may limit the ease of use, and ultimately reduce the clinical acceptability of photopolymerizable sealants.

A second PEG-based sealant system is the PEG–PEG platform. A rapidly gelling synthetic PEG–PEG tissue sealant, formed by reacting two multifunctional four-arm star-branched PEG molecules, was first reported in 2001. The sealant, composed of tetra-succinimidyl-derivatized poly(ethylene glycol) and tetra-thiol-derivatized poly(ethylene glycol), demonstrated adhesion to carotid arteries, collagen membranes, and PTFE grafts in vitro (Wallace et al. 2001). In subsequent clinical studies, the PEG–PEG tissue adhesive was successful in sealing suture lines of the aorta and coronary artery bypass grafts (Marc Hendrikx et al. 2001), as well as prosthetic vascular grafts (Glickman et al. 2002). On December 14, 2001, the commercial sealant CoSeal® (Cohesion Technologies, Palo Alto, CA) received FDA approval as a hemostatic adjunct during vascular reconstruction surgery (Fig. 10.13). The PEG–PEG sealant also received CE Mark approval for adjunctive hemostasis in vascular reconstructions.

The commercial PEG–PEG system is comprised of two PEG powder components: powdered pentaerythritol poly(ethylene glycol) ether tetra-succinimidyl glutarate and powdered pentaerythritol poly(ethylene glycol) ether tetra-thiol (Fig. 10.14). The molecular weight of each four-arm star-branched PEG is approximately 10,000. Immediately prior to clinical use, the powder components are dissolved in an aqueous buffer; the two components are then mixed as they are delivered to the tissue site. Upon mixing, the functional groups on multiple arms of the PEGs react to form a covalently bonded three-dimensional matrix. The sulfur group of the multi-arm PEG thiol nucleophilically attacks the carbonyl group attached

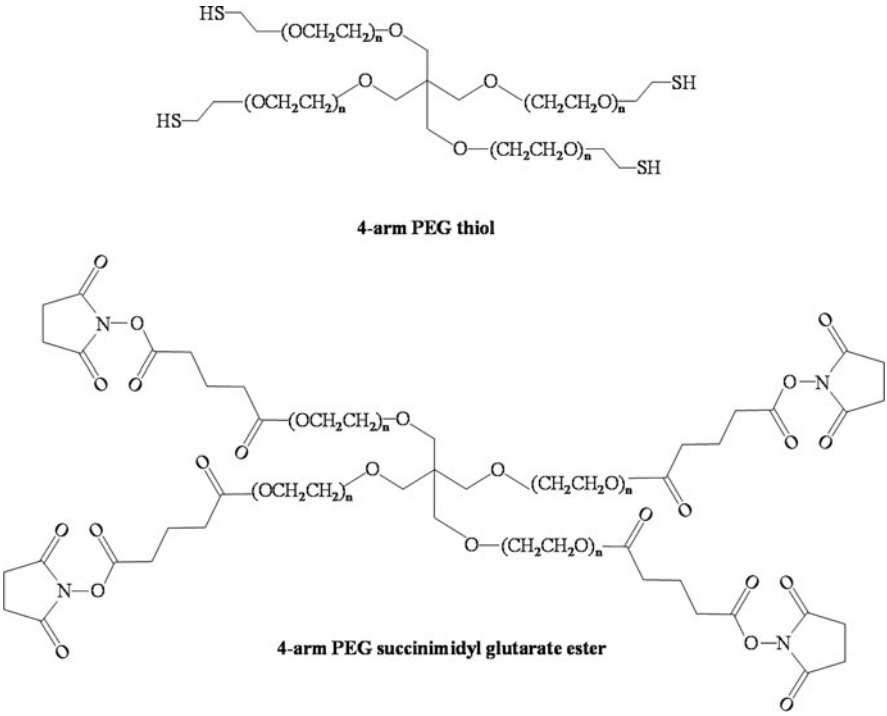

Fig. 10.14 Chemical structures of multifunctional star-branched four-arm PEG polymers used in PEG–PEG tissue adhesives. The two components of the PEG–PEG system are pentaerythritol poly(ethylene glycol) ether tetra-thiol and pentaerythritol poly(ethylene glycol) ether tetra-succinimidyl glutarate

to *N*-hydroxysuccinimide in the multi-arm PEG succinimidyl ester. The hydrogel is formed by the release of *N*-hydroxysuccinimide and concurrent formation of a thioester bond between the two substituted multi-arm PEGs (Fig. 10.15). There is also a small amount of disulfide bond formation between thiol groups. The functionalized PEG end groups additionally react with functional groups (particularly amine groups) in the tissue matrix to form covalent bonds, providing a chemical linkage between the PEG–PEG hydrogel and the surrounding tissue. When applied to prosthetic vascular grafts, the PEG–PEG hydrogel partially penetrates the irregular graft surface and creates a mechanical bond.

The PEG–PEG tissue sealant provides sealing within 60 s; the mean time to complete anastomotic sealing during placement of prosthetic vascular grafts is 16.5 s. Following implantation, the PEG–PEG hydrogel absorbs water and swells up to four times its original volume within 24 h; application of the sealant should therefore be avoided near anatomic structures that are sensitive to compression. The hydrogel is biodegradable and contains two hydrolyzable bonds: the thioester between the two multi-arm PEGs and an O-ester that is within one of the PEGs and glutarate. The sealant is fully resorbed within 4 weeks.

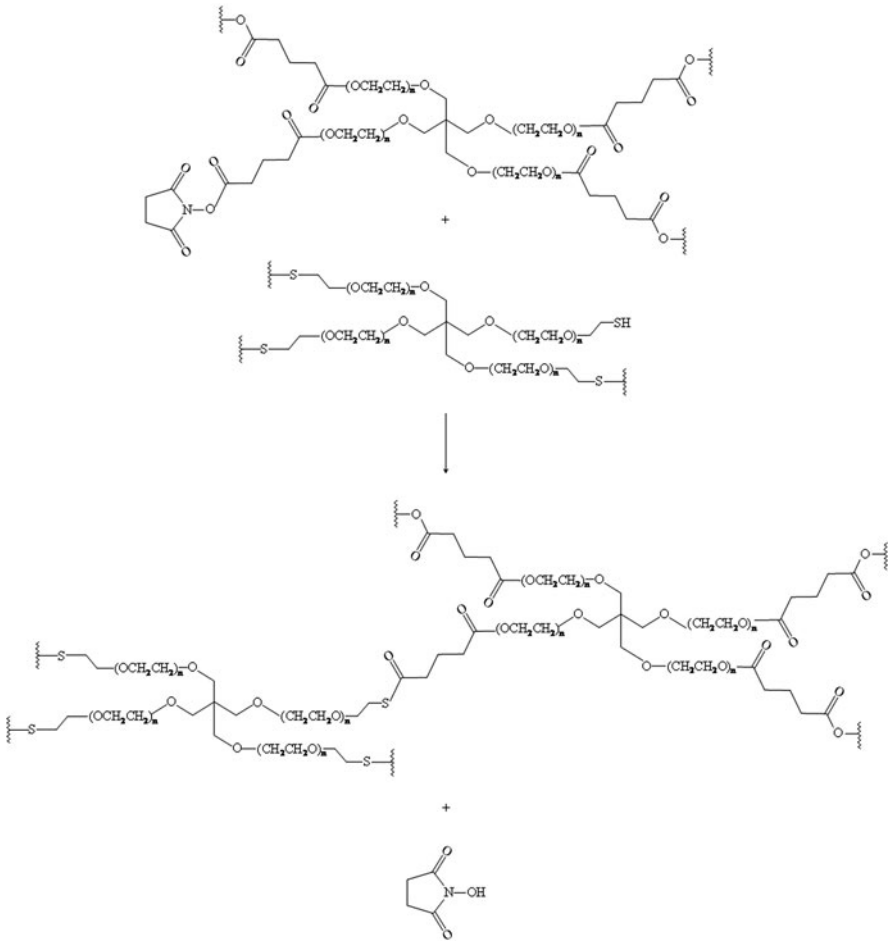

Fig. 10.15 Reaction of multifunctional star-branched four-arm PEG polymers to form PEG–PEG tissue adhesives. The sulfur group of the multi-arm PEG thiol nucleophilically attacks the carbonyl group attached to *N*-hydroxysuccinimide in the multi-arm PEG succinimidyl ester. The hydrogel is formed by the release of *N*-hydroxysuccinimide and concurrent formation of a thioester bond between the two substituted multi-arm PEGs

Beyond its indicated use for adjunctive hemostasis of peripheral vascular anastomoses, the PEG–PEG system has demonstrated efficacy for minimizing anastomotic bleeding during aortic reconstruction (Hagberg et al. 2004). In addition, PEG–PEG hydrogels have been successfully applied as sprayed barriers to reduce postoperative adhesion formation following uterine surgery (Mettler et al. 2008), as well as adult and pediatric cardiac surgery (Konertz et al. 2003; Napoleone et al. 2007). The major limitations of the PEG–PEG sealant are its high degree of swell and its relatively weak adhesion to tissue. On anastomotic closures, both cyanoacrylate glue and albumin–glutaraldehyde glue demonstrate greater mechanical integrity than the

Fig. 10.16 DuraSeal® PEG–trilysine tissue adhesive. The sealant is a two-component system, comprising a PEG ester and a trilysine amine. The two solutions mix as they are sprayed onto dural tissue, and the components crosslink to form a watertight seal. The system also contains blue dye to allow visualization of hydrogel coverage on the tissue surface (Food and Drug Administration)

PEG–PEG sealant and are capable of resisting higher loads before failure (Saunders et al. 2009). On the cut tissue surface of the kidney, fibrin sealant adheres more effectively than PEG–PEG sealant (Bernie et al. 2005). A practical limitation of the PEG–PEG system is the requirement for preparation and dissolution of the powdered PEGs into aqueous buffer prior to use; this may limit the convenient use of the sealant in the operating room.

A third PEG-based adhesive biomaterial is the PEG–trilysine system. A novel hydrogel sealant, composed of a PEG ester and trilysine amine, was described in 2003 as an effective agent for dural closure to prevent cerebrospinal fluid leakage following neurosurgery (Preul et al. 2003). In a preliminary clinical study conducted in 2005, the PEG–trilysine tissue adhesive demonstrated 100% closure of intraoperative cerebrospinal fluid leaks (Boogarts et al. 2005). The commercial PEG–trilysine sealant DuraSeal® (Confluent Surgical, Waltham, MA) was granted FDA approval on April 7, 2005, as an adjunct to sutured dural repair during cranial surgery to provide watertight closure (Fig. 10.16).

The commercial sealant is supplied as a two-component system, comprised of a PEG ester powder and a trilysine amine solution. The PEG component is dissolved in an aqueous solution immediately prior to clinical use. The two solutions mix as they are sprayed onto the dural tissue, and the components crosslink to form a watertight hydrogel seal. The sealant system also contains FD&C blue dye #1 to allow visualization of hydrogel coverage and thickness. The hydrogel absorbs water following implantation and swells by approximately 50% in volume; the sealant therefore should not be applied to confined bony structures where nerves are present, since neural compression can result due to hydrogel swelling. The tissue adhesive degrades hydrolytically within 4–8 weeks and the degradation products are readily cleared by the kidneys. The PEG–trilysine system has continued to demonstrate 100% efficacy in stopping cerebrospinal fluid leakage in patients undergoing neurosurgical procedures (Cosgrove et al. 2007).

10.6 Emerging Biomaterials for Wound Closure

A number of original adhesive platforms are currently being pursued for soft tissue repair and regeneration. Several of these innovative sealant technologies have demonstrated promise in experimental models of wound closure, but they have not yet reached clinical use. Three families of novel tissue adhesives are described below: naturally inspired tissue adhesives, polysaccharide-based tissue adhesives, and dendrimeric tissue adhesives. These emerging sealants are directed toward a variety of clinical applications, including external skin closure, gastrointestinal surgery, orthopedic surgery, and ophthalmic surgery.

Naturally occurring adhesive structures, such as frog glues, mussel proteins, and sticky gecko feet, have provided inspiration for unique new tissue sealants. For instance, the Australian frog *Notaden bennetti* secretes an exudate which rapidly forms a tacky elastic solid. This protein-based material acts as a pressure-sensitive adhesive that functions in wet conditions, and covalent crosslinking does not seem to be necessary for the glue to set (Graham et al. 2005). The frog glue demonstrated efficacy in repairing torn meniscal tissue of the knee in an ex vivo model and showed superior mechanical strength to both gelatin and fibrin glues (Szomor et al. 2008). This recently discovered biological glue may be considered for meniscal repairs in the future.

Marine and freshwater mussels also secrete specialized protein adhesives for rapid and durable attachment to wet surfaces. Mussels exude tough byssal threads (Fig. 10.17) and coat these threads with adhesive proteins to attach to natural and man-made structures. Glues based on mussel adhesive proteins may thus be ideal for achieving adhesion to wet tissue substrates. Adhesive proteins extracted from *Mytilus edulis* mussel have demonstrated success in vitro for bonding porcine skin (Ninan et al. 2003) and porcine small intestinal submucosa (Ninan et al. 2007); however, the mussel protein extracts required excessively long cure times. Synthetic polymers containing mussel protein functionality have been designed as a strategy for creating effective adhesives. The amino acid L-3,4- dihydroxylphenylalanine (DOPA) contributes to mussel protein solidification through oxidation and crosslinking reactions (Strausberg and Link 1990); DOPA is formed in mussel proteins by post-translational hydroxylation of the amino acid tyrosine (Fig. 10.18).

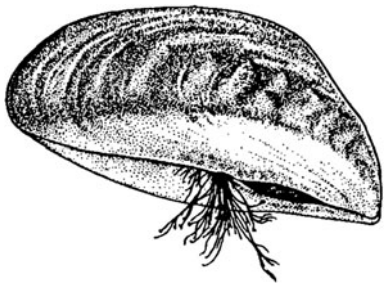

Fig. 10.17 Adhesive byssal threads of the mussel (National Oceanic and Atmospheric Administration). The tough byssal threads are coated with mussel adhesive proteins to enable attachment to natural and man-made surfaces

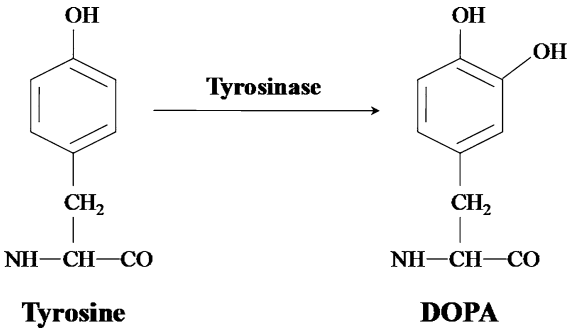

Fig. 10.18 Post-translational modification of tyrosine residues in the *Mytilus edulis* mussel adhesive protein. Hydroxylation of tyrosine residues creates L-3,4-dihydroxylphenylalanine (DOPA) residues, which are essential for adhesive protein crosslinking

Biomimetic DOPA-functionalized PEG polymers have been shown to crosslink upon exposure to oxidizing reagents and successfully bond porcine skin in vitro (Burke et al. 2007).

While frog glues and mussel adhesive proteins have inspired novel sealants based on their chemical compositions, the sticky footpad of the gecko lizard (Fig. 10.19) has inspired new tissue adhesives based on its nanostructure. The gecko footpad is covered with a dense array of fibrils (setae), which maximize interfacial adhesion to surfaces (Autumn et al. 2000). Individual setae operate by van der Waals forces; the intermolecular attraction allows geckos to adhere to vertical and inverted surfaces. A biodegradable and biocompatible tissue adhesive has been designed to mimic the nanotopography of the gecko foot (Mahdavi et al. 2008). The gecko-inspired tissue adhesive is manufactured from a poly(glycerol-co-sebacate acrylate) (PGSA) elastomeric surface. The PGSA surface is etched into an array of nanoscale pillars to mimic the nanopatterns of the gecko foot, and the etched polymer is subsequently coated with oxidized dextran to allow tissue bonding. Applied as a tissue tape, the

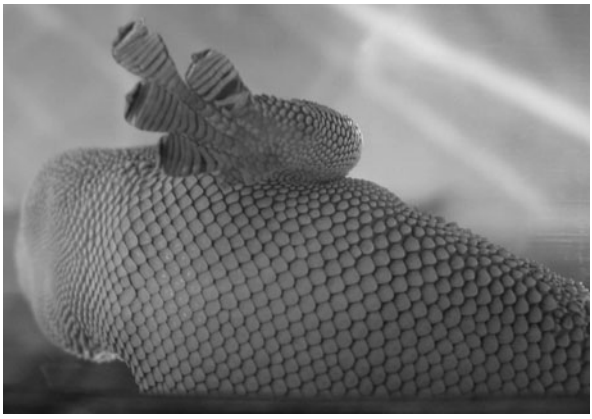

Fig. 10.19 Adhesive footpads of the Madagascar gecko lizard (Montreal Biodome)

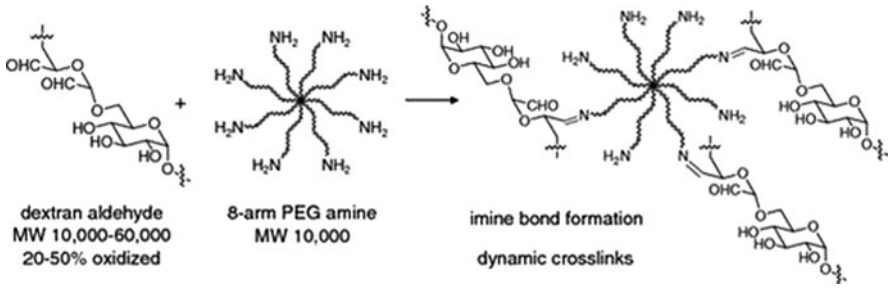

Fig. 10.20 Foundation chemistry for dextran-based tissue adhesives. The oxidized polysaccharide dextran aldehyde reacts with an eight-arm star PEG amine to form a crosslinked hydrogel network

gecko-inspired adhesive has demonstrated efficacy in binding porcine intestinal tissue in vitro and rat abdominal tissue in vivo. The gecko-like tissue adhesive may provide the basis for an entirely new family of nanopatterned surgical adhesives.

Surgical glues composed of functionalized natural polysaccharides, including chondroitin and dextran, are showing early success as biocompatible sealants. The biopolymer chondroitin sulfate is a major component of cartilage extracellular matrix and may provide an ideal foundation for designing biomaterials for cartilage repair. A photopolymerizable hydrogel composed of chondroitin sulfate functionalized with methacrylate and aldehyde groups has shown success in binding articular cartilage defects in vivo (Wang et al. 2007). The chondroitin sulfate–methacrylate–aldehyde hydrogel is non-cytotoxic, non-inflammatory, and able to encapsulate cartilage cells, making it a promising platform for cartilage reconstruction. In addition, a photopolymerizable polysaccharide-based sealant composed of hyaluronic acid functionalized with methacrylate groups has shown efficacy in sealing experimental corneal incisions (Miki et al. 2002). Finally, a polysaccharide-based sealant composed of dextran aldehyde and multi-arm PEG amine has been developed for wound closure (Fig. 10.20). The two components undergo a Schiff base reaction to form a crosslinked hydrogel. This two-component tissue adhesive system crosslinks in water, cures rapidly (<1 min) at room temperature, adheres to moist tissue, and degrades hydrolytically. The dextran-based tissue adhesive is non-cytotoxic to fibroblasts cell lines and non-inflammatory to macrophage cell lines (Bhatia et al. 2007a). In addition, the dextran-based sealant requires no external photoinitiator or other extra equipment and has demonstrated efficacy in an ex vivo model of corneal closure (Bhatia et al. 2007b). The polysaccharide-based tissue adhesive successfully seals corneal incisions to pressures of >10 psi (500 mmHg) and is non-cytotoxic to bovine corneal endothelial cells. Another advantage of this sealant, in terms of clinical acceptance, is that dextran has a long history of clinical use as a plasma expander.

Highly branched dendritic macromers have provided the basis for a new class of hydrogel sealants with unique physical and mechanical properties (Grinstaff 2008). Dendrimers possess three main structural components: a central core, internal branching layers, and peripheral functional groups. Unlike linear polymers in which

growth is accomplished by adding a single monomer, dendritic polymers grow by branching each monomer, leading to multiple additions. When used to construct hydrogel scaffolds, dendritic macromers allow increased crosslink density of the scaffold without significantly increasing the polymer concentration, as compared to linear polymer analogs; this approach leads to improved mechanical properties and minimal swelling of the hydrogel.

Biodendrimeric tissue adhesives, based on peptide dendrons functionalized with terminal cysteine residues, have been developed for ophthalmic applications. When the cysteine-terminated peptide dendrons are mixed with PEG dialdehyde, a hydrogel forms as a consequence of thiazolidene linkages between the two macromers (Wathier et al. 2004). These biodendrimeric sealants have been successful in sealing ex vivo corneal incisions and securing ex vivo corneal transplants (Wathier et al. 2006). A photocrosslinkable biodendrimeric tissue adhesive has also been created from tri- block copolymers; these hybrid dendritic-linear copolymers consist of a PEG core and methacrylated poly(glycerol succinic acid) dendrimer terminal blocks. The photopolymerized dendrimeric sealant is effective in sealing experimental full thickness corneal lacerations (Degoricija et al. 2007) and securing ex vivo laser in situ keratomileusis (LASIK) flaps (Kang et al. 2005). In addition, the photocrosslinkable dendrimer adhesive attaches to experimental cartilage defects (Degoricija et al. 2008) and encapsulates chondrocyte cells (Söntjens et al. 2006). Dendrimer-based sealants may thus be a promising new technology for cartilage repair.

It is fitting to discuss the status of tissue sealants in a volume on biomaterials for medical usage, as the needs and applications for tissue adhesives extend far beyond trauma. Any condition requiring surgical intervention, such as coronary artery disease, COPD, or lung cancer, could potentially benefit from effective bioadhesives. Currently available tissue adhesives, including fibrin sealants, cyanoacrylate glues, crosslinked protein sealants, and PEG hydrogels, have been utilized in a wide variety of surgical procedures to aid in hemostasis and wound closure. The oldest and most widely used tissue adhesives make use of known biological pathways (fibrin sealants) or known industrial products (cyanoacrylate glues). Yet these traditional classes of sealants are associated with trade-offs between functionality and biocompatibility. Biological fibrin glues are tissue-friendly but more prone to tearing, due to their relatively poor tissue adhesion; these sealants carry additional risks of viral transmission and sensitization. Synthetically derived glues such as cyanoacrylates, GRF glues, and albumin–glutaraldehyde glues demonstrate extremely strong tissue adhesion and are more resistant to tearing, but they exhibit much higher tissue toxicity and poor biodegradability. PEG-based adhesives are tissue friendly and readily biodegradable, but they do not adhere as strongly as cyanoacrylates and crosslinked-protein glues, and they can swell considerably following implantation.

An optimal tissue sealant would exhibit all of the advantages of existing tissue adhesives, while avoiding the disadvantages and adverse effects. Such a sealant would combine biocompatibility and biodegradability with strong tissue adhesion and favorable physical properties. The perfect sealant must meet stringent mechanical and biological performance requirements; novel tissue adhesives are

constantly being formulated to address these challenges. New technology platforms include naturally inspired adhesives, polysaccharide-based tissue adhesives, and dendrimeric adhesives. These emerging sealants demonstrate encouraging results in experimental models of wound closure, and they may soon realize clinical use. Continued development of adhesive biomaterials for tissue reconstruction will require a detailed understanding of both polymer properties and the biological environment. In addition, biomaterials scientists must be aware of the practical realities of the operating room and the trauma bay. When medicine, polymer science and biology are brought to bear on tissue adhesive design, the resulting biomaterials will save and enhance the lives of patients worldwide. The remaining chapter will focus on the world's youngest and smallest patients, our newborns. Perinatal conditions affecting this population are the tenth leading global killer.

References

Abbas MA, Tejirian T (2008) Bioglue for the treatment of anal fistula is associated with acute anal sepsis. Dis Colon Rectum 51:1155

Abuchowski A, McCoy JR, Palczuk NC et al (1977b) Effect of covalent attachment of polyethylene glycol on immunogenicity and circulating life of bovine liver catalase. J Biol Chem 252:3582

Abuchowski A, van Es T, Palczuk NC et al (1977a) Alteration of immunological properties of bovine serum albumin by covalent attachment of polyethylene glycol. J Biol Chem 252:3578

Albes JM, Krettek C, Hausen B et al (1993) Biophysical properties of the gelatin-resorcin-formaldehyde/glutaraldehyde adhesive. Ann Thorac Surg 56:910

American Society for Testing and Materials (2008) Annual book of ASTM standards. Volume 13.01 medical and surgical materials and devices; anesthetic and respiratory equipment; manufacture of pharmaceutical products. ASTM, Philadelphia, PA

Anghelacopoulos SE, Tagarakis GI, Pilpilidis I et al (2006) Albumin-glutaraldehyde bioadhesive ("Bioglue") for prevention of postoperative complications after stapled hemorrhoidopexy: a randomized controlled trial. Wien Klin Wochenschr 118:469

Ardis AE (1949a) Preparation of monomeric alkyl alpha-cyanoacrylates. US Patent 2,467,926

Ardis AE (1949b) Preparation of monomeric alkyl alpha-cyanoacrylates. US Patent 2,467,927

Argyra E, Polymeneas G, Karvouni E et al (2009) Sutureless pancreatojejunal anastomosis using an absorbable sealant: evaluation in a pig model. J Surg Res 153:282

Autumn K, Liang YA, Hsieh ST et al (2000) Adhesive force of a single gecko foot-hair. Nature 405:681

Bachet J, Goudot B, Dreyfus GD et al (1999) Surgery for acute type A aortic dissection: the Hopital Foch experience (1977–1998). Ann Thorac Surg 67:2006

Bar-Hava I, Krissi H, Ashkenazi J et al (1999) Fibrin glue improves pregnancy rates in women of advanced reproductive age and in patients in whom in vitro fertilization attempts repeatedly fail. Fertil Steril 71:821

Bardari F, D'Urso L, Muto G (2001) Conservative treatment of iatrogenic urinary fistulas: the value of cyanoacrylic glue. Urology 58:1046

Bayfield MS, Spotnitz WD (1996) Fibrin sealant in thoracic surgery. Pulmonary applications, including management of bronchopleural fistula. Chest Surg Clin N Am 6:576

Beierlein W, Scheule AM, Antoniadis G et al (2000) An immediate, allergic skin reaction to aprotinin after reexposure to fibrin sealant. Transfusion 40:302

Bergel S (1909) Uber Wirkungen des Fibrins. Dtschr Med Wochenschr 35:633

Bernabeu E, Castellá M, Barriuso C et al (2005) Acute limb ischemia due to embolization of biological glue after repair of type A aortic dissection. Interact Cardiovasc Thorac Surg 4:329

Bernie JE, Ng J, Bargman V et al (2005) Evaluation of hydrogel tissue sealant in porcine laparoscopic partial-nephrectomy model. J Endourol 19:1122
Berruyer M, Amiral J, Ffrench P et al (1993) Immunization by bovine thrombin used with fibrin glue during cardiovascular operations. Development of thrombin and factor V inhibitors. J Thorac Cardiovasc Surg 105:892
Bhatia SK, Arthur SD, Chenault HK et al (2007a) Interactions of polysaccharide-based tissue adhesives with clinically relevant fibroblast and macrophage cell lines. Biotechnol Lett 29:1645
Bhatia SK, Arthur SD, Chenault HK et al (2007b) Polysaccharide-based tissue adhesives for sealing corneal incisions. Curr Eye Res 32:1045
Biedner B, Rosenthal G (1996) Conjunctival closure in strabismus surgery: vicryl versus fibrin glue. Ophthalmic Surg Lasers 27:967
Biggs G, Hafron J, Feliciano J (2006) Treatment of splenic injury during laparoscopic nephrectomy with BioGlue, a surgical adhesive. Urology 66:882
Binder PS (1985) Selective suture removal can reduce postkeratoplasty astigmatism. Ophthalmology 92:1412
Bjarkam CR, Jorgensen RL, Jensen KN et al (2008) Deep brain stimulation electrode anchoring using BioGlue(R), a protective electrode covering, and a titanium microplate. J Neurosci Methods 168:151
Bloomfield S, Barnert AH, Kanter P (1963) Use of Eastman-910 monomer as an adhesive in ocular surgery. II. Effectivenessin closure of limbal wounds in rabbits. Amer J Ophthalmol 55:946
Bonchek LI, Braunwald NS (1967) Experimental evaluation of a cross-linked gelatin adhesive in gastrointestinal surgery. Ann Surg 165:420
Bonchek LI, Fuchs JC, Braunwald NS (1967) Use of a cross-linked gelatin tissue adhesive in surgery of the urinary tract. Surg Gynecol Obstet 125:1301
Boogaarts JD, Grotenhuis JA, Bartels RH et al (2005) Use of a novel absorbable hydrogel for augmentation of dural repair: results of a preliminary clinical study. Neurosurgery 57(1 suppl):146
Bove JR (1978) Fibrinogen – is the benefit worth the risk? Transfusion 18:129
Bowen ML, Selinger M (2002) Episiotomy closure comparing enbucrilate tissue adhesive with conventional sutures. Int J Gynaecol Obstet 78:201
Braunwald NS, Gay W, Tatooles CJ (1966) Evaluation of crosslinked gelatin as a tissue adhesive and hemostatic agent: an experimental study. Surgery 59:1024
Braunwald NS, Tatooles CJ (1965) Use of a cross linked gelatin tissue adhesive to control hemorrhage from liver and kidney. Surg Forum 16:345
Bruce J, Krukowski ZH, Al-Khairy G et al (2001) Systematic review of the definition and measurement of anastomotic leak after gastrointestinal surgery. Br J Surg 88:1157
Brunkwall J, Ruemenapf G, Florek HJ et al (2007) A single arm, prospective study of an absorbable cyanoacrylate surgical sealant for use in vascular reconstructions as an adjunct to conventional techniques to achieve haemostasis. J Cardiovasc Surg (Torino) 48:471
Buchta C, Hedrich HC, Macher M et al (2005) Biochemical characterization of autologous fibrin sealants produced by CryoSeal® and Vivostat® in comparison to the homologous fibrin sealant product Tissucol/Tisseel®. Biomaterials 26:6233
Burke SA, Ritter-Jones M, Lee BP (2007) Thermal gelation and tissue adhesion of biomimetic hydrogels. Biomed Mater 2:203
Busuttil RW (2003) A comparison of antifibrinolytic agents used in hemostatic fibrin sealants. J Am Coll Surg 197:1021
Caers J, Reekmans A, Jochmans K et al (2003) Factor V inhibitor after injection of human thrombin (tissucol) into a bleeding peptic ulcer. Endoscopy 35:542
Calafiore AM, DiGiamarco G, Vitolla G (2002) Aortic valve exposure through a combined right atrial-ascending aortic approach in redo cases. Ann Thorac Surg 73:318
Caliceti P, Veronese FM (2000) Pharmacokinetic and biodistribution properties of poly(ethylene glycol)-protein conjugates. Adv Drug Deliv Rev 55:1261

Carton CA, Kessler LA, Seidenberg B et al (1960) A plastic adhesive method of small blood vessel surgery. World Neurol 1:356
Chafke N, Gasser B, Lindner, V et al (1996) Albumin as a sealant for a polyester vascular prosthesis: its impact on the healing sequence in humans. J Cardiovasc Surg (Torino) 37:431
Chao H-H, Torchiana DF (2003) BioGlue: albumin/glutaraldehyde sealant in cardiac surgery. J Card Surg 18:500
Chen WL, Lin CT, Hsieh CY et al (2007) Comparison of the bacteriostatic effects, corneal cytotoxicity, and the ability to seal corneal incisions among three different tissue adhesives. Cornea 26:1228
Cheski PJ, Matthews TW (1997) Endoscopic reduction and internal cyanoacrylate fixation of the zygoma. J Otolaryngol 26:75
Chilla R (1987) Late histoacryl-induced complications of dura surgery in the frontal and lateral base of the skull. HNO 35:250
Ciapetti G, Stea S, Cenni E et al (1994) Cytotoxicity testing of cyanoacrylates using direct contact assay on cell cultures. Biomaterials 15:63
Conrad K, Yoskovitch A (2003) The use of fibrin glue in the correction of pollybeak deformity. Arch Facial Plast Surg 5:522
Cooper CW, Falb RD (1968) Surgical adhesives. Ann NY Acad Sci 146:214
Coover HW Jr, Joyner FB, Shearer NH et al (1959) Chemistry and performance of cyanoacrylate adhesives. SPE Tech Papers 5:92
Coselli JS, Bavaria JE, Fehrenbacher J et al (2003) Prospective randomized study of a protein-based tissue adhesive used as a hemostatic and structural adjunct in cardiac and vascular anastomotic repair procedures. J Am Coll Surg 197:243
Cosgrove GR, Delashaw JB, Grotenhuis JA et al (2007) Safety and efficacy of a novel polyethylene glycol hydrogel sealant for watertight dural repair. J Neurosurg 106:52
Cronkite EP, Lozner EL, Deaver, J (1944) Use of thrombin and fibrinogen in skin grafting. JAMA 124:976
Currie LJ, Sharpe JR, Martin R (2001) The use of fibrin glue in skin grafts and tissue-engineered skin replacements: a review. Plast Reconstr Surg 108:1713
de la Portilla F, Rada R., León E et al (2007) Evaluation of the use of BioGlue in the treatment of high anal fistulas: preliminary results of a pilot study. Dis Colon Rectum 50:218
Degoricija L, Bansal PN, Söntjens SH et al (2008) Hydrogels for osteochondral repair based on photocrosslinkable carbamate dendrimers. Biomacromolecules 9:2863
Degoricija L, Johnson CS, Wathier M et al (2007) Photo cross-linkable biodendrimers as ophthalmic adhesives for central lacerations and penetrating keratoplasties. Invest Ophthalmol Vis Sci 48:2037
Detweiler MB, Detweiler JG, Fenton J (1999) Sutureless and reduced suture anastomosis of hollow vessels with fibrin glue: a review. J Invest Surg 12:245
Devbhandari MP, Chaudhery Q, Duncan AJ (2006) Acute intraoperative malfunction of aortic valve due to surgical glue. Ann Thorac Surg 81:1499
Dumanian GA, Dascombe W, Hong C et al (1995) A new photopolymerizable blood vessel glue that seals human vessel anastomoses without augmenting thrombogenicity. Plast Reconstr Surg 95:901
Dusick JR, Mattozo CA, Esposito F et al (2006) BioGlue for prevention of postoperative cerebrospinal fluid leaks in transsphenoidal surgery: a case series. Surg Neurol 66:371
Economopoulos GC, Dimitrakakis GK, Brountzos E et al (2004) Superior vena cava stenosis: a delayed BioGlue complication. J Thorac Cardiovasc Surg 127:1819
Ehrlich PF, Teitelbaum DH, Hirschl RB et al (2007) Excision of large cystic ovarian tumors: combining minimal invasive surgery techniques and cancer surgery – the best of both worlds. J Pediatr Surg 42:890
Ekelund A, Nilsson OS (1991) Tissue adhesives inhibit experimental new bone formation. Int Orthop 15:331
Ellis RA, Levine AM (1963) Experimental sutureless ocular surgery. Amer J Ophthalmol 55:733

Ennker IC, Ennker J, Schoon D et al (1994a) Formaldehyde-free collagen glue in experimental lung gluing. Ann Thorac Surg 57:1622
Ennker IC, Ennker J, Schoon D et al (1994b) The impact of gelatin-resorcinol glue on aortic tissue: a histomorphologic evaluation. J Vasc Surg 20:34
Enzmann H (1982) Sensibilisierung bei der Verwendung von Fibrinkleber. Laryngol Rhinol Otol 61:302
Erasmi AW, Wohlschlager C (2002) Inflammatory response after BioGlue application. Ann Thorac Surg 73:1025
Evans CE, Lees GC, Trail IA (1999) Cytotoxicity of cyanoacrylate adhesives to cultured tendon cells. J Hand Surg (Br) 24:658
Falb RD, Cooper CW (1966) Adhesives in surgery. New Scientist 308
Fasol R, Wild T, El Dsoki S (2004) Left ventricular rupture after mitral surgery: repair by patch and sealing. Ann Thorac Surg 77:1070
Ferguson RE, Rinker B (2006) The use of a hydrogel sealant on flexor tendon repairs to prevent adhesion formation. Ann Plast Surg 56:54
Friedman M, Schalch P (2008) Middle turbinate medialization with bovine serum albumin tissue adhesive (BioGlue). Laryngoscope 118:335
Fürst W, Banerjee, A (2005) Release of glutaraldehyde from an albumin-glutaraldehyde tissue adhesive causes significant in vitro and in vivo toxicity. Ann Thorac Surg 79:1522
Gillinov AM, Lytle BW (2001) A novel synthetic sealant to treat air leaks at cardiac reoperation. J Card Surg 16:255
Glickman M, Gheissari A, Money S et al; CoSeal Multicenter Vascular Surgery Study Group (2002) A polymeric sealant inhibits anastomotic suture hole bleeding more rapidly than gelfoam/ thrombin: results of a randomized controlled trial. Arch Surg 137:326
Goldstein DJ, Beauford RB (2003) Left ventricular assist devices and bleeding: adding insult to injury. Ann Thorac Surg 75:S42
Graham LD, Glattauer V, Huson MG et al (2005) Characterization of a protein-based adhesive elastomer secreted by the Australian frog Notaden bennetti. Biomacromolecules 6:3300
Greene D, Koch RJ, Goode RL (1999) Efficacy of octyl-2- cyanoacrylate tissue glue in blepharoplasty. A prospective controlled study of wound-healing characteristics. Arch Facial Plast Surg 1:292
Greenwald BD, Caldwell SH, Hespenheide EE et al (2003) N-2-butyl- cyanoacrylate for bleeding gastric varices: a United States pilot study and cost analysis. Am J Gastroenterol 98:1982
Grey EG (1915) Fibrin as a haemostatic in cerebral surgery. Surg Gynecol Obstet 21:452
Grinstaff MW (2008) Dendritic macromers for hydrogel formation: tailored materials for ophthalmic, orthopedic, and biotech applications. J Polym Sci A Polym Chem 46:383
Gul R, Khan F, Maher Y et al (2006) Osteochondral fractures in the knee treated with butyl-2-cyanoacrylate glue. A case report. Acta Orthop Belg 72:641
Hagberg RC, Safi HJ, Sabik J et al (2004) Improved intraoperative management of anastomotic bleeding during aortic reconstruction: results of a randomized controlled trial. Am Surg 70:307
Haj-Yahia S, Mittal T, Birks E et al (2007) Lung fibrosis as a potential complication of the hemostatic tissue sealant, biologic glue (Bioglue). J Thorac Cardiovasc Surg 133:1387
Hall LT, Bailes JE (2005) Dermabond for wound closure in lumbar and cervical neurosurgical procedures. Neurosurgery 56:S147
Haring R (1972) Current status of tissue adhesives in Germany. In: Matsumoto T (ed) Tissue adhesives in surgery. Medical Examination Publ, New York, NY
Hasumi T, Yamanaka S, Yamanaka H et al (2003) Clinical experience of gelatin-resorcin-formal (GRF) glue for acute empyema with bronchopleural fistula. Kyobu Geka 56:82
Healey JE Jr, Sheena, KS, Gallager HS et al (1962) The use of a plastic adhesive in the technique of bronchial closure. Surg Forum 13:153
Heneghan MA, Byrne A, Harrison PM (2002) An open pilot study of the effects of a human fibrin glue for endoscopic treatment of patients with acute bleeding from gastric varices. Gastrointest Endosc 56:422

Hill-West JL, Chowdhury SM, Sawhney AS et al (1994) Prevention of postoperative adhesions in the rat by in situ photopolymerization of bioresorbable hydrogel barriers. Obstet Gynecol 83:59
Hino M, Ishiko O, Honda KI et al (2000) Transmission of symptomatic parvovirus B19 infection by fibrin sealant used during surgery. Br J Haematol 108:194
Hvass U, Chatel D, Frikha I et al (1995) Left ventricular free wall rupture. Long-term results with a pericardial patch and fibrin glue repair. Eur J Cardiothorac Surg 9:75
Iha K, Arakaki K, Horikawa Y et al (1999) Sutureless technique for subacute left ventricular free wall rupture: a case report of an 85-year-old. Ann Thorac Cardiovasc Surg 5:265
Isoda S, Imoto K, Uchida K et al (2004) Sandwich technique via right ventricle incision to repair postinfarction ventricular septal defect. J Card Surg 19:149
Jallali N, Haji A, Watson CJ (2004) A prospective randomized trial comparing 2-octyl cyanoacrylate to conventional suturing in closure of laparoscopic cholecystectomy incisions. J Laparoendosc Adv Surg Tech 14:209
Jourdan IC, Bailey ME (1998) Initial experience with the use of N-butyl 2- cyanoacrylate glue for the fixation of polypropylene mesh in laparoscopic hernia repair. Surg Laparosc Endosc 8:291
Joyner FB, Hawkins GF (1955) Method of making alpha-cyanoacrylates. US Patent 2,721,858
Kang PC, Carnahan MA, Wathier M et al (2005) Novel tissue adhesives to secure laser in situ keratomileusis flaps. J Cataract Refract Surg 31:1208
Kato Y, Yamataka A, Miyano G et al (2005) Tissue adhesives for repairing inguinal hernia: a preliminary study. J Laparoendosc Adv Surg Tech A 15:424
Kawamura M, Sawafuji M, Watanabe M et al (2002) Frequency of transmission of human parvovirus B19 infection by fibrin sealant used during thoracic surgery. Ann Thorac Surg 73:1098
Kazui T, Washiyama N, Bashar AH et al (2001) Role of biologic glue repair of proximal aortic dissection in the development of early and midterm redissection of the aortic root. Ann Thorac Surg 72:509
Kim JC, Bassage SD, Kempski MH et al (1995) Evaluation of tissue adhesives in closure of scleral tunnel incisions. J Cataract Refract Surg 21:320
Kim HJ, Kang SW, Lim HC et al (2007) The role of transforming growth factor-beta and bone morphogenetic protein with fibrin glue in healing of bone-tendon junction injury. Connect Tissue Res 48:309
Kitazawa H, Sato H, Adachi I et al (1997) Microdialysis assessment of fibrin glue containing sodium alginate for local delivery of doxorubicin in tumor-bearing rats. Biol Pharm Bull 20:278
Kjaergard HK, Fairbrother JE (1996) Controlled clinical studies of fibrin sealant in cardiothoracic surgery – a review. Eur J Cardiothorac Surg 10:727
Klimo P Jr, Khalil A, Slotkin JR et al (2007) Wound complications associated with the use of bovine serum albumin-glutaraldehyde surgical adhesive in pediatric patients. Neurosurgery 60:305
Kober BJ, Scheule AM, Voth V et al (2008) Anaphylactic reaction after systemic application of aprotinin triggered by aprotinin-containing fibrin sealant. Anesth Analg 107:406
Konertz WF, Kostelka M, Mohr FW et al (2003) Reducing the incidence and severity of pericardial adhesions with a sprayable polymeric matrix. Ann Thorac Surg 76:1270
Koveker G, De Vivie ER, Helberg KD et al (1981) Clinical experience with fibrin glue in cardiac surgery. Thorac Cardiovasc Surg 29:287
Kunihara T, Shiiya N, Matsuzaki K et al (2008) Recommendation for appropriate use of GRF glue in the operation for acute aortic dissection. Ann Thorac Cardiovasc Surg 14:88
Laccourreye P, Cauchois R, Sharkawy EL et al (2005) Octylcyanoacrylate (Dermabond) for skin closure at the time of head and neck surgery: a longitudinal prospective study. Ann Chir 130:624
Lämsä T, Jin HT, Sand J et al (2008) Tissue adhesives and the pancreas: biocompatibility and adhesive properties of 6 preparations. Pancreas 36:261
Lau WY, Leung KL, Zhu XL (1995) Laparoscopic repair of perforated peptic ulcer. Br J Surg 82:814

Laurian C, Gigou F, Guilmet D (1977) Gelatin resorcin formaldehyde glue in vascular surgery. Nouv Presse Med 6:3221
Leggat PA, Smith DR, Kedjarune U (2007) Surgical applications of cyanoacrylate adhesives: a review of toxicity. ANZ J Surg 77:209
LeMaire SA, Carter SA, Won T et al (2005) The threat of adhesive embolization: BioGlue leaks through needle holes in aortic tissue and prosthetic grafts. Ann Thorac Surg 80:106
LeMaire SA, Ochoa LN, Conklin LD et al (2007) Nerve and conduction tissue injury caused by contact with BioGlue. J Surg Res 143:286
LeMaire SA, Schmittling ZC, Coselli JS et al (2002) BioGlue surgical adhesive impairs aortic growth and causes anastomotic strictures. Ann Thorac Surg 73:1500
Lenaerts V, Couvreur P, Christiaens-Leyh D et al (1984) Degradation of poly (isobutyl cyanoacrylate) nanoparticles. Biomaterials 5:65
Leva C, Bruno PG, Gallorini C et al (2006) Complete myocardial revascularization and sutureless technique for left ventricular free wall rupture: clinical and echocardiographic results. Interact. Cardiovasc Thorac Surg 5:408
Lumsden AB, Heyman ER; Closure Medical Surgical Sealant Study Group (2006) Prospective randomized study evaluating an absorbable cyanoacrylate for use in vascular reconstructions. J Vasc Surg 44:1002
Macchiarini P, Wain J, Almy S et al (1999) Experimental and clinical evaluation of a new synthetic, absorbable sealant to reduce air leaks in thoracic operations. J Thorac Cardiovasc Surg 117:751
Mahdavi A, Ferreira L, Sundback C et al (2008) A biodegradable and biocompatible gecko-inspired tissue adhesive. Proc Natl Acad Sci USA 105:2307
Mahmood Z, Cook DS, Luckraz H et al (2004) Fatal right ventricular infarction caused by Bioglue coronary embolism. J Thorac Cardiovasc Surg 128:770
Maloney JD, Weigel TL, Love RB (2001) Endoscopic repair of bronchial dehiscence after lung transplantation. Ann Thorac Surg 72:2109
Marable SA, Wagner DE (1962) The use of rapidly polymerizing adhesives in massive liver resection. Surg Forum 13:264
Marc Hendrikx M, Mees U, Hill AC et al (2001) Evaluation of a novel synthetic sealant for inhibition of cardiac adhesions and clinical experience in cardiac surgery procedures. Heart Surg Forum 4:204
Marchac D, Sandor G (1994) Face lifts and sprayed fibrin glue: an outcome analysis of 200 patients. Br J Plast Surg 47:306
Martinelli L, Graffigna A, Guarnerio M et al (2000) Coronary artery narrowing after aortic root reconstruction with resorcin-formalin glue. Ann Thorac Surg 70:1701
Martinowitz U, Saltz R (1996) Fibrin sealant. Curr Opin Hematol 3:395
Martinowitz U, Schulman S, Horoszowski H et al (1996) Role of fibrin sealants in surgical procedures on patients with hemostatic disorders. Clin Orthop Relat Res 328:65
Martinowitz U, Spotnitz WD (1997) Fibrin tissue adhesives. Thromb Haemostas 78:661
Mathes GL, Terry JW Jr (1963) Non-suture closure of nephrotomy. J Urol 89:122
Matras H, Chiari F, Kletter G et al (1977) Zur klebung von mikrogefagefassanastomosen (Eine experimentelle studie). Proceedings of the 13th annual meeting. Dtsch Gesfplast Wiederhestell 357
Matras H, Dinges HP, Lassman H et al (1972) Zur nahtlosen interfaszikular-en Nerven- transplantation im Tier experiment. Wien Med Wochenschr 122:517
Mettler L, Hucke J, Bojahr B et al (2008) A safety and efficacy study of a resorbable hydrogel for reduction of post-operative adhesions following myomectomy. Hum Reprod 23:1093
Miki D, Dastgheib K, Kim T et al (2002) A photopolymerized sealant for corneal lacerations. Cornea 21:393
Miura S, Mii Y, Miyauchi Y et al (1995) Efficacy of slow-releasing anticancer drug delivery systems on transplantable osteosarcomas in rats. Jpn J Clin Oncol 25:61
Mizrahi S, Bickel A, Ben-Layish EB (1988) Use of tissue adhesives in the repair of lacerations in children. J Pediatr Surg 23:312

Moralee SJ, Carney AS, Cash MP et al (1994) The effect of fibrin sealant haemostasis on post-operative pain in tonsillectomy. Clin Otolaryngol 19:526
Muntean W, Zenz W, Finding K (1994) Inhibitor to factor V after exposure to fibrin sealant during cardiac surgery in a two-year-old child. Acta Paediatr 83:84
Nadler RB, Loeb S, Rubenstein RA et al (2006) Use of BioGlue in laparoscopic partial nephrectomy. Urology 68:416
Nagaki Y, Hayasaka S, Kadoi C et al (2003) Bacterial endophthalmitis after small-incision cataract surgery. Effect of incision placement and intraocular lens type. J Cataract Refract Surg 29:20
Nahas FX, Solia D, Ferreira LM et al (2004) The use of tissue adhesive for skin closure in body contouring surgery. Aesthetic Plast Surg 28:165
Napoleone CP, Oppido G, Angeli E et al (2007) Resternotomy in pediatric cardiac surgery: CoSeal initial experience. Interact Cardiovasc Thorac Surg 6:21
Neri E, Massetti M, Capannini G et al (1999) Glue containment and anastomosis reinforcement in repair of aortic dissection. Ann Thorac Surg 67:1510
Ngaage DL, Edwards WD, Bell MR et al (2005) A cautionary note regarding long-term sequelae of biologic glue. J Thorac Cardiovasc Surg 129:937
Ninan L, Monahan J, Stroshine RL et al (2003) Adhesive strength of marine mussel extracts on porcine skin. Biomaterials 24:4091
Ninan L, Stroshine RL, Wilker JJ et al (2007) Adhesive strength and curing rate of marine mussel protein extracts on porcine small intestinal submucosa. Acta Biomater 3:687
Ochsner MG (1998) Fibrin solutions to control hemorrhage in the trauma patient. J Long Term Effects Med Implants 8:161
Okada K, Yamashita T, Matsumori M et al (2005) Surgical treatment for rupture of left ventricular free wall after acute myocardial infarction. Interact. Cardiovasc Thorac Surg 4:203
Oswald AM, Joly LM, Gury C et al (2003) Fatal intraoperative anaphylaxis related to aprotinin after local application of fibrin glue. Anesthesiology 99:762
Pachulski R, Sabbour H, Gupta R et al (2005) Cardiac device implant wound closure with 2-octyl cyanoacrylate. J Interv Cardiol 18:185
Papatheofanis FJ (1989) Cytotoxicity of alkyl-2- cyanoacrylate adhesives. J Biomed Mater Res 23:661
Passage J, Jalali H, Tam RK et al (2002) BioGlue surgical adhesive – an appraisal of its indications in cardiac surgery. Ann Thorac Surg 74:432
Passage J, Tam R, Windsor M et al (2005) Bioglue: a review of the use of this new surgical adhesive in thoracic surgery. ANZ J Surg 75:315
Pickleman J, Watson W, Cunningham J et al (1999) The failed gastrointestinal anastomosis: an inevitable catastrophe? J Am Coll Surg 188:473
Potaris K, Mihos P, Gakidis I (2003) Preliminary results with the use of an albumin-glutaraldehyde tissue adhesive in lung surgery. Med Sci Monit 9:P179
Powe NR, Schein OD, Gieser SC et al (1994) Synthesis of the literature on visual acuity and complications following cataract extraction with intraocular lens implantation. Cataract patient outcome research team. Arch Ophthalmol 112:239
Preul MC, Bichard WD, Spetzler RF (2003) Toward optimal tissue sealants for neurosurgery: use of a novel hydrogel sealant in a canine durotomy repair model. Neurosurgery 53:1189
Quinn JV (2005) Clinical approaches to the use of cyanoacrylate tissue adhesives. In: Quinn JV (ed) Tissue adhesives in clinical medicine, 2nd edn. BC Decker Inc, Hamilton, Canada
Quinn J, Drzewiecki A, Li M et al (1993) A randomized, controlled trial comparing a tissue adhesive with suturing in the repair of pediatric facial lacerations. Ann Emerg Med 22:1130
Raanani E, Georghiou GP, Kogan A (2004) ′BioGlue′ for the repair of aortic insufficiency in acute aortic dissection. J Heart Valve Dis 13:734
Radosevich M, Goubran HA, Burnouf T (1997) Fibrin sealant: scientific rationale, production methods, properties, and current clinical use. Vox Sang 72:133
Ranger WR, Halpin D, Sawhney AS et al (1997) Pneumostasis of experimental air leaks with a new photopolymerized synthetic tissue sealant. Am Surg 63:788

Reiter A (1987) Induction of sarcomas by the tissue-binding substance Histoacryl-blau in the rat. Z Exp Chir Transplant Kunstliche Organe 20:55

Rittoo D, Sintler M, Burnley S et al (2001) Gelatine-resorcine-formol glue as a sealant of ePTFE patch suture lines. Int Angiol 20:214

Rogerson L, Mason GC, Roberts AC (2000) Preliminary experience with twenty perineal repairs using Indermil tissue adhesive. Eur J Obstet Gynecol Reprod Biol 88:139

Rousou J, Gonzalez-Lavin L, Cosgrove D et al (1989) Randomized clinical trial of fibrin sealant in patients undergoing resternotomy or reoperation after cardiac operations. J Thorac Cardiovasc Surg 97:194

Samuel PR, Roberts, AC, Nigam A (1997) The use of Indermil (n-butyl cyanoacrylate) in otorhinolaryngology and head and neck surgery. A preliminary report on the first 33 patients. J Layngol Otol 111:536

Sato T, Yamazaki K, Toyota J et al (2004) Inflammatory tumor in pancreatic tail induced by endoscopic ablation with cyanoacrylate glue for gastric varices. J Gastroenterol 39:475

Saunders MM, Baxter ZC, Abou-Elella A et al (2009) BioGlue and Dermabond save time, leak less, and are not mechanically inferior to two-layer and modified one-layer vasovasostomy. Fertil Steril 91:560

Sawhney AS, Hubbell JA (1999) In situ photopolymerized hydrogels for vascular and peritoneal wound healing. In: Morgan JR, Yarmush ML (eds) Tissue engineering methods and protocols. Humana Press, Totowa, NJ

Sawhney AS, Pathak CP, Hubbell JA (1993) Bioerodible hydrogels based on photopolymerized poly(ethylene glycol)-co-poly(α-hydroxy acid) diacrylate macromers. Macromolecules 26:581

Sawhney AS, Pathak CP, van Rensburg JJ et al (1994) Optimization of photopolymerized bioerodible hydrogel properties for adhesion prevention. J Biomed Mater Res 28:831

Schenk WG 3rd, Burks SG, Gagne PJ (2003) Fibrin sealant improves hemostasis in peripheral vascular surgery: a randomized prospective trial. Ann Surg 237:871

Schenk WG 3rd, Goldthwaite CA Jr, Burks S et al (2002) Fibrin sealant facilitates hemostasis in arteriovenous polytetrafluoroethylene grafts for renal dialysis access. Am Surg 68:728

Schenk WG 3rd, Spotnitz WD, Burks SG et al (2005) Absorbable cyanoacrylate as a vascular hemostatic sealant: a preliminary trial. Am Surg 71:658

Scheule AM, Beierlein W, Wendel HP et al (1998) Fibrin sealant, aprotinin, and immune response in children undergoing operations for congenital heart disease. J Thorac Cardiovasc Surg 115:883

Sciscione AC, Manley JS, Pollock M et al (2001) Intracervical fibrin sealants: a potential treatment for early preterm premature rupture of the membranes. Am J Obstet Gynecol 184:368

Scott GR, Carson CL, Borah GL (2007) Dermabond skin closures for bilateral reduction mammaplasties: a review of 255 consecutive cases. Plast Reconstr Surg 120:1460

Seguin JR, Frapier J-M, Colson R et al (1991) Fibrin sealants improve surgical results of type A acute aortic dissections. Ann Thorac Surg 52:745

Seidenberg B, Garrow E, Pimental R et al (1963) Studies on the use of plastic adhesive in gastrointestinal surgery. Ann Surg 158:721

Sen A, Green KM, Khan MI et al (2006) Cerebrospinal fluid leak rate after the use of BioGlue in translabyrinthine vestibular schwannoma surgery: a prospective study. Otol Neurotol 27:102

Sentovich SM (2003) Fibrin glue for anal fistulas: long-term results. Dis Colon Rectum 46:498

Shaffrey CI, Spotnitz WD, Shaffrey ME et al (1990) Neurosurgical applications of fibrin glue: augmentation of dural closure in 134 patients. Neurosurgery 26:207

Shapira Y, Raanani E, Sagie A (2006) ″BioGlue″ as a possible cause of acute blocked mechanical mitral valve leaflet. J Cardiovasc Surg (Torino) 47:581

Sharma A, Kaur R, Kumar S et al (2003) Fibrin glue versus N-butyl-2- cyanoacrylate in corneal perforations. Ophthalmology 110:291

Sidle DM, Loos BM, Ramirez AL et al (2005) Use of BioGlue surgical adhesive for brow fixation in endoscopic browplasty. Arch Facial Plast Surg 7:393

Simon HK, McLario DJ, Bruns TB et al (1997) Long-term appearance of lacerations repaired using a tissue adhesive. Pediatrics 99:193
Singer AJ, Quinn JV, Hollander JE (2008) The cyanoacrylate topical skin adhesives. Am J Emerg Med 26:490
Singer AJ, Quinn JV, Hollander JE et al; TraumaSeal Study Group (2002) Closure of lacerations and incisions with octyl- cyanoacrylate: a multi-center randomized clinical trial. Surgery 131:270
Singer AJ, Zimmerman T, Rooney J et al (2004) Comparison of wound bursting strength and surface characteristics of FDA approved tissue adhesives for skin closure. J Adhes Sci Technol 18:19
Sinha S, Naik M, Wright V et al (2001) A single blind, prospective, randomized trial comparing n-butyl 2- cyanoacrylate tissue adhesive (Indermil) and sutures for skin closure in hand surgery. J Hand Surg (Br) 26:264
Sofer M, Greenstein A, Chen J et al (2003) Immediate closure of nephrostomy tube wounds using a tissue adhesive: a novel approach following percutaneous endourological procedures. J Urol 169:2034
Söntjens SH, Nettles DL, Carnahan, MA et al (2006) Biodendrimer-based hydrogel scaffolds for cartilage tissue repair. Biomacromolecules 7:310
Souza EC, Fitaroni RB, Januzelli DM et al (2008) Use of 2-octyl cyanoacrylate for skin closure of sternal incisions in cardiac surgery: observations of microbial barrier effects. Curr Med Res Opin 24:151
Spauwen PH, de Laat WA, Hartman EH (2006) Octyl-2- cyanoacrylate tissue glue (Dermabond) versus Monocryl 6 × 0 sutures in lip closure. Cleft Palate Craniofac J 43:625
Stassano P, Rispo G, Losi M et al (1994) Annular abscesses and GRF glue. J Card Surg 9:357
Strausberg RL, Link R (1990) Protein-based medical adhesives. Trends Biotechnol 8:53
Suehiro K, Hata T, Yoshitaka H et al (2002) Late aortic root redissection following surgical treatment for acute type A aortic dissection using gelatin-resorcin-formalin glue. Jpn J Thorac Cardiovasc Surg 50:195
Suzuki S, Imoto K, Uchida K et al (2006) Aortic root necrosis after surgical treatment using gelatin-resorcinol- formaldehyde (GRF) glue in patients with acute type A aortic dissection. Ann Thorac Cardiovasc Surg 12:333
Sweeney T, Rayan S, Warren H (2002) Intestinal anastomoses detected with a photopolymerized hydrogel. Surgery 131:185
Switzer EF, Dinsmore RC, North JH Jr (2003) Subcuticular closure versus Dermabond: a prospective randomized trial. Am Surg 69:434
Szafranek A, Podila SR, Al-Khyatt W et al (2006) Aseptic mediastinal cyst caused by BioGlue 7 months after cardiac surgery. J Thorac Cardiovasc Surg 131:1202
Szomor ZL, Murrell GAC, Appleyard RC et al (2008) Meniscal repair with a new biological glue: an ex vivo study. Tech Knee Surg 7:261
Takahashi N, Tsunematsu K, Sugawara, H et al (2001) The estimation of the effectiveness of GRF glue in the respiratory. Kyobu Geka 54:141
Tanaka K, Takamoto S, Ohtsuka T et al (1999) Application of AdvaSeal for acute aortic dissection: experimental study. Ann Thorac Surg 68:1308
Taravella MJ, Chang CD (2001) 2-Octyl cyanoacrylate medical adhesive in treatment of a corneal perforation. Cornea 20:220
Tatooles CJ, Braunwald NS (1966) The use of crosslinked gelatin as a tissue adhesive to control hemorrhage from liver and kidney. Surgery 60:857
Thompson DF, Davis TW (1997) The addition of antibiotics to fibrin glue. South Med J 90:681
Toriumi DM, O'Grady K, Desai D et al (1998) Use of octyl-2- cyanoacrylate for skin closure in facial plastic surgery. Plast Reconstr Surg 102:2209
Toriumi DM, Raslan WF, Friedman M et al (1991) Variable histotoxicity of histoacryl when used in a subcutaneous site: an experimental study. Laryngoscope 101:339

Tredwell S, Jackson JK, Hamilton D et al (2006) Use of fibrin sealants for the localized, controlled release of cefazolin. Can J Surg 49:347
United States Environmental Protection Agency (1987) Assessment of health risks to garment workers and certain home residents from exposure to formaldehyde. Office of Pesticides and Toxic Substances, UnitedStates Environmental Protection Agency, Washington, DC
Vaiman M, Eviatar E, Segal S (2002) Effectiveness of second-generation fibrin glue in endonasal operations. Otolaryngol Head Neck Surg 126:388
Van Belleghem Y, Forsyth RG, Narine K et al (2004) Bovine glue (BioGlue) is catabolized by enzymatic reaction in the vascular dog model. Ann Thorac Surg 77:2177
van den Ende ED, Vriens PW, Allema JH et al (2004) Adhesive bonds or percutaneous absorbable suture for closure of surgical wounds in children. Results of a prospective randomized trial. J Pediatr Surg 39:1249
van der Ham AC, Kort WJ, Weijma IM (1992) Effect of antibiotics in fibrin sealant on healing colonic anastomoses in the rat. Br J Surg 79:525
Varley GA, Meisler DM (1991) Complications of penetrating keratoplasty: graft infections. Refract Corneal Surg 7:62
Vezin WR, Florence AT (1980) In vitro heterogeneous degradation of poly(n-alkyl alpha-cyanoacrylates). J Biomed Mater Res 14:93
Wain JC, Kaiser LR, Johnstone DW (2001) Trial of a novel synthetic sealant in preventing air leaks after lung resection. Ann Thorac Surg 71:1623
Walker KG, Bell SW, Rickard MJFX et al (2004) Anastomotic leakage is predictive of diminished survival after potentially curative resection for colorectal cancer. Ann Surg 240:255
Wallace DG, Cruise GM, Rhee WM et al (2001) A tissue sealant based on reactive multifunctional polyethylene glycol. J Biomed Mater Res 58:545
Wang GJ, Goldthwaite CA Jr, Burks S et al; Orthopaedic Investigators Group (2003a) Fibrin sealant reduces perioperative blood loss in total hip replacement. J Long Term Eff Med Implants 13:399
Wang GJ, Goldthwaite CA Jr, Burks S et al; Orthopaedic Research Group (2003b) Experience improves successful use of fibrin sealant in total knee arthroplasty: implications for surgical education. J Long Term Eff Med Implants 13:389
Wang MY, Levy ML, Mittler MA et al (1999) A prospective analysis of the use of octyl-cyanoacrylate tissue adhesive for wound closure in pediatric neurosurgery. Pediatr Neurosurg 30:186
Wang DA, Varghese S, Sharma B et al (2007) Multifunctional chondroitin sulphate for cartilage tissue-biomaterial integration. Nat Mater 6:385
Wathier M, Johnson CS, Kim T et al (2006) Hydrogels formed by multiple peptide ligation reactions to fasten corneal transplants. Bioconj Chem 17:873
Wathier M, Jung, PJ, Carnahan MA et al (2004) Dendritic macromers as in situ polymerizing biomaterials for securing cataract incisions. J Am Chem Soc 126:12744
White JK, Titus JS, Tanabe H et al (2000) The use of a novel tissue sealant as a hemostatic adjunct in cardiac surgery. Heart Surg Forum 3:56
Wieken K, Angioi-Duprez K, Lim A et al (2003) Nerve anastomosis with glue: comparative histologic study of fibrin and cyanoacrylate glue. J Reconstr Microsurg 19:17
Woolverton CJ, Fulton JA, Salstrom SJ et al (2001) Tetracycline delivery from fibrin controls peritoneal infection without measurable systemic antibiotic. J Antimicrob Chemother 48:861
World Health Organization (2008) The global burden of disease: 2004 update. WHO Press, Geneva
Yilmaz C, Kuyurtar F (2005) Fixation of a talar osteochondral fracture with cyanoacrylate glue. Arthroscopy 21:1009
Yin Q, Kemp GJ, Yu LG (2001) Neurotrophin-4 delivered by fibrin glue promotes peripheral nerve regeneration. Muscle Nerve 24:345
Young JZ, Medawar PB (1940) Fibrin suture of peripheral nerves. Lancet 275:126
Yuen T, Kaye AH (2005) Persistence of Bioglue® in spinal dural repair. J Clin Neurosci 12:100

Chapter 11
Prematurity

Prematurity and low birth weights are the 10th leading cause of death worldwide. In 2004, the neonatal conditions of prematurity and low birth weight were responsible for 1.2 million deaths, or 2% of all deaths globally (World Health Organization 2008). Because prematurity and low birth weights cause mortality within the first few days of life, these conditions account for a disproportionately high 11% of all years of life lost globally (World Health Organization 2008). In fact, such neonatal conditions account for more years of life lost globally than any of the other top causes of death. Prematurity, also known as preterm birth, occurs when an infant is born at less than 37 weeks gestational age; premature birth is associated with underdevelopment of vital organs such as the lungs. A major cause of morbidity and mortality in preterm infants is respiratory failure, resulting from a deficiency in lung surfactant. Although many conditions contribute to death of premature babies, respiratory distress syndrome is the leading cause of death in preterm infants (Rodriguez et al. 2002). Approximately 80% of infants born before 27 weeks of gestation will develop respiratory distress syndrome (Behrman and Stith 2007). As such, this chapter will focus on the role of biomaterials in alleviating respiratory distress in preterm infants. Currently, premature babies with respiratory distress syndrome are given animal-derived surfactant preparations. While animal-derived surfactant is effective in treating respiratory distress syndrome, it is expensive to produce and supplies are limited. This is a critical shortcoming, since preterm birth is a major contributor to neonatal mortality in developing countries. In addition, animal-derived preparations carry a theoretical risk of transmission of viral or other infectious agents and may exhibit batch-to-batch variation. To address these issues, biomaterials are now being developed as synthetic surfactants; such preparations incorporate synthetic phospholipids and essential hydrophobic surfactant protein analogs. In contrast to animal surfactants, synthetic biomaterial surfactants can be produced in a large quantity at reasonable cost. These emerging biomaterials could be used widely to treat infant respiratory distress and decrease mortality of preterm babies.

11.1 Lung Surfactant and Respiratory Distress in Infants

During fetal growth, the breathing of amniotic fluid in and out is essential for stimulating lung development (Behrman and Stith 2007). Breathing movements begin

S.K. Bhatia, *Biomaterials for Clinical Applications*,
DOI 10.1007/978-1-4419-6920-0_11, © Springer Science+Business Media, LLC 2010

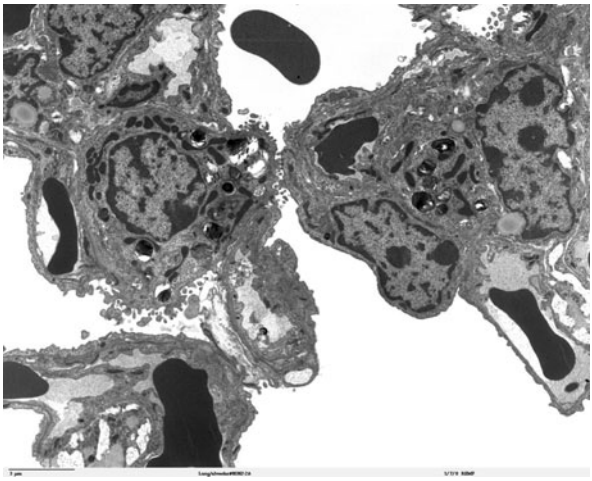

Fig. 11.1 Transmission electron microscope image of a thin section cut through the alveolar sac region of the mouse lung. The alveolar cell shown has vesicles which contain surfactant, a macroaggregate of phospholipids and proteins that support normal breathing. The surfactant is released by exocytosis and forms a thin monolayer on the wall of the alveoli. This layer cannot be visualized in a TEM image, as no fixative adequately preserves it, but it can be seen inside the surfactant vesicles in the cytoplasm. This layer helps to reduce surface tension, thereby preventing collapse of the alveoli during exhalation, and reduces the energy needed during inhalation (Louisa Howard and Michael Binder, Dartmouth College)

as early as 10 weeks of gestation, but tend to be erratic and occur only 30–40% of the time up to 30 weeks of gestation. A critical component of lung function is surfactant, a soap-like substance that helps keep the air sacs (alveoli) open throughout the normal cycle of inhalation and exhalation (Fig. 11.1). Surfactant is typically manufactured by the lungs at 30–32 weeks of gestation. Thus, infants born before 28–30 weeks gestation may have underdeveloped lungs, insufficient surfactant, and disrupted breathing patterns.

Pulmonary surfactant is required for normal respiration. In normal lungs, surfactant functions to reduce the work of breathing; stabilize alveolar inflation and deflation to optimize gas exchange; and reduce the driving force for pulmonary edema (Notter and Wang 2008). The physiological roles of surfactant are summarized in Table 11.1. Surfactant is produced and recycled by type II alveolar cells and packaged by the cells into structures called lamellar bodies. The surfactant is then extruded into alveolar spaces, where the lamellar bodies unfold into a complex lining of the alveolar sac. The majority of the extensive alveolar surface in mammals (approximately 1 m^2/kg body weight) is covered by this thin aqueous surfactant-containing layer, also known as the hypophase (Notter and Wang 2008). The surfactant layer reduces the surface tension of the fluid that lines the air space. Surface tension is a small force in many macroscopic systems, but it is highly important in the lungs. During respiration, the large surface area of the alveoli is contracted by inspired air, resulting in a large liquid–air interface with associated surface tension forces. In the lungs, surface tension is responsible for roughly

Table 11.1 Physiological actions and properties of functional lung surfactant

Physiological actions of functional lung surfactant
- Reduces the work of breathing (increases lung compliance)
- Increases alveolar stability against collapse during expiration (reduces atelectasis)
- Improves the uniformity of alveolar inflation during inspiration
- Reduces the hydrostatic driving force for pulmonary edema

Biophysical properties of functional lung surfactant
- Adsorbs rapidly to the air–water interface
- Reaches very low minimum surface tensions during dynamic film compression
- Varies surface tension with surface area during dynamic cycling
- Respreads effectively at the interface during successive cycles

Notter and Wang (2008)

two-thirds of the elastic recoil forces. Surfactant is thus essential for preventing alveolar collapse throughout the respiratory cycle.

Natural lung surfactant is a complex mixture of lipids and proteins, including several phospholipids, neutral lipids, and surfactant-specific proteins. The composition of surfactant by weight is approximately 85–95% phospholipid, 6–8% biologically active protein, and 4–7% neutral lipid, as detailed in Table 11.2. The most abundant single component of lung surfactant is the disaturated phospholipid dipalmitoyl phosphatidylcholine (DPPC), which makes up about one-third of total phospholipids (Notter 2000). DPPC is the major surface-active component of surfactant (Clements 1977) and stabilizes the lungs by reducing the deflating force in the alveolus. In addition to DPPC, lung surfactant contains various unsaturated and saturated phospholipids. Phosphatidylcholine (PC) is the most prevalent class, accounting

Table 11.2 Approximate composition of endogenous pulmonary surfactant

85–90% *Phospholipids*
- 80% Phosphatidylcholine (PC)
  - 40–50% Dipalmitoyl phosphatidylcholine (DPPC)
  - 10–15% Other disaturated PCs
  - 35–45% Unsaturated PCs
- 15% Anionic phospholipids – phosphatidylglycerol (PG), phosphatidylinositol (PI), phosphatidylserine (PS)
- 5% Other phospholipid classes – phosphatidylethanolamine (PE), sphingomyelin (Sph)

7–10% *Apoproteins*
- SP-A
- SP-B
- SP-C
- SP-D

4–7% *Neutral lipids*
- Cholesterol
- Cholesterol esters, glycerides

Notter (2000)

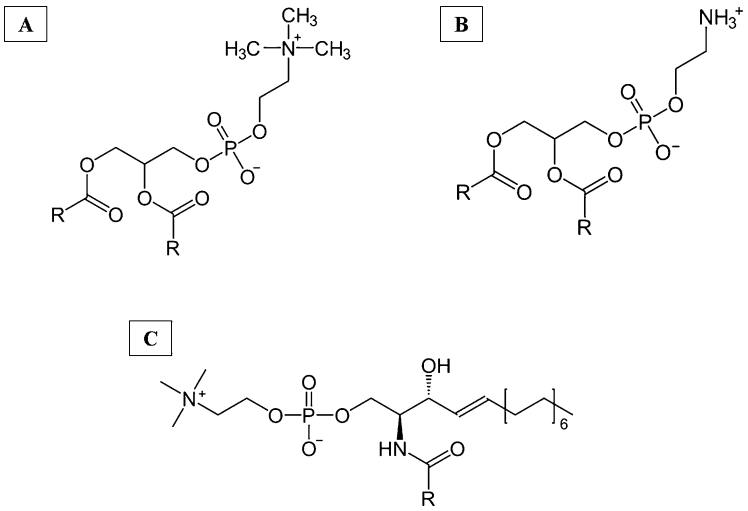

Fig. 11.2 Chemical structures of phospholipids contained in lung surfactant. **a** Phosphatidylcholine. **b** Phosphatidylethanolamine. **c** Sphingomyelin. All of these phospholipids are zwitterionic near neutral pH

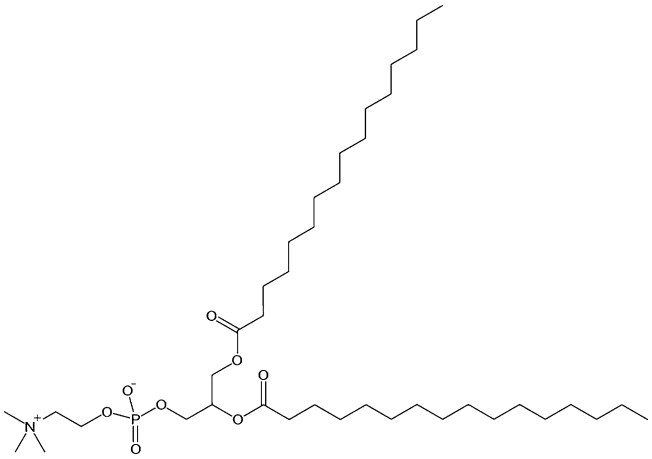

Fig. 11.3 Chemical structure of dipalmitoyl phosphatidylcholine (DPPC), the major surface-active component of lung surfactant

for 80% of total lung surfactant when DPPC is included (Notter 2000). Other phospholipid classes are present in smaller amounts: phosphatidylglycerol (PG), phosphatidylinositol (PI), phosphatidylserine (PS), phosphatidylethanolamine (PE), and sphingomyelin (SPH). Chemical structures of these phospholipids are given in Figs. 11.2, 11.3, and 11.4. PC, PE, and SPH are zwitterionic near neutral pH, while PG, PI, and PS are anionic. However, the properties of pulmonary surfactant are

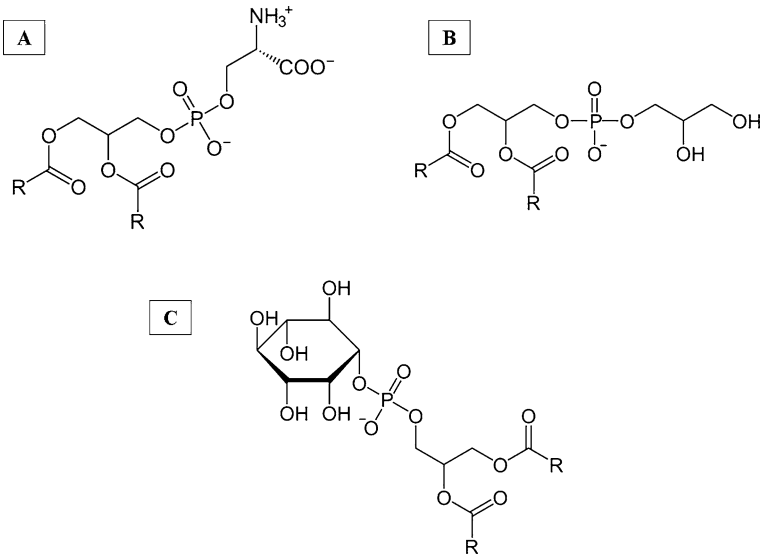

Fig. 11.4 Chemical structures of phospholipids contained in lung surfactant. **a** Phosphatidylserine. **b** Phosphatidylglycerol. **c** Phosphatidylinositol. All of these phospholipids are anionic near neutral pH

not determined by phospholipids alone; surfactant proteins play an important role in the biologic activity of lung surfactant. Four native surfactant proteins have been identified, named surfactant proteins (SP)-A, B, C, and D. The properties of these proteins are detailed in Table 11.3. The small hydrophobic molecules SP-B and SP-C are tightly bound to phospholipids and contribute to the surface tension-lowering properties of pulmonary surfactant. Both SP-B and SP-C increase the adsorption of surface-active lipids to the air–liquid interface and are critical for spreading of the surfactant film across the interface (Johansson and Curstedt 1997). SP-B and SP-C together account for 1.5% by weight of surfactant isolates (Notter 2000). SP-A and SP-D are larger hydrophobic proteins and may have significant functions in surfactant metabolism and in the lung host defense. SP-A is the most abundant protein and makes up about 5% of lung surfactant by weight, while SP-D is much less abundant (Notter 2000).

Molecular interactions between the proteins and lipids within surfactant generate specific surface properties and allow surfactant to modify pulmonary pressure–volume mechanics (Notter and Wang 2008). Secreted surfactant in the alveolar hypophase contains a heterogeneous population of phospholipid-rich aggregates with incorporated apoproteins. These aggregates vary from tens of nanometers to several microns in size, with larger aggregates having the greatest surface activity and highest apoprotein content. During breathing, surfactant adsorbs from the hypophase to form a highly active interfacial film, which lowers and modulates alveolar surface tension. Through its surface tension-lowering effects, surfactant increases lung compliance ($\Delta V/\Delta P$, the change in volume for a given change in

Table 11.3 Molecular characteristics of lung surfactant proteins

Surfactant protein (SP)	Selected structural and functional characteristics
SP-A	• MW 26–38 kD (monomer), 228 AA in length in humans • Most abundant surfactant apoprotein, relatively hydrophobic • Acidic glycoprotein with multiple posttranslational isoforms • C-type lectin and member of the collectin family of host-defense proteins • Oligomerizes to an active octadecamer (six trimer subunits) • Aggregates and orders lipids • Necessary for tubular myelin formation (along with SP-B and calcium) • Helps regulate surfactant re-uptake/recycling in type II alveolar cells
SP-B	• MW 8.5–9 kD (monomer), 79 AA in length in humans (active peptide) • Overall hydrophobic in nature, with two to three amphipathic helical regions • Sequence includes multiple charged AA (10 positive Arg/Lys residues) • Forms dimers of presumptive functional significance in humans • Necessary for tubular myelin formation (along with SP-A and calcium) • Disrupts and fuses lipid bilayers and promotes lipid insertion into surface films • Enhances adsorption, film spreading, and dynamic surface activity of lipids; most active SP in increasing adsorption and overall dynamic surface activity
SP-C	• MW 4.2 kD (monomer), 35 AA in length in humans (active peptide) • Most hydrophobic surfactant protein • Forms dimers and other oligomers of uncertain functional significance • Human form has two palmitoylated cysteine residues • Contains only two charged AA at neutral pH (two Arg/Lys residues) • Primarily alpha-helical in structure, with a length that spans a lipid bilayer • Interacts biophysically primarily with phospholipid fatty chains • Disrupts and fuses lipid bilayers • Enhances adsorption, film spreading, and surface activity of lipids
SP-D	• MW 39–46 kD (monomer), 355 AA in length in humans • Has significant structural similarity to SP-A • Oliogomerizes to a dodecamer (four trimer subunits) • C-type lectin and member of the collectin family of host-defense proteins • Not implicated in lung surfactant biophysics • May participate in surfactant metabolism in addition to host defense

Notter and Wang (2008)

pressure) and reduces the non-flow component of respiratory work. Essentially, the proteins and lipids in surfactant not only prevent the air spaces from completely collapsing on exhalation, they also allow re-opening and inflation of the air spaces with a lower amount of force.

In preterm babies with surfactant deficiency, the alveoli collapse during breathing and are very difficult to expand. The result is respiratory distress syndrome, manifested in infants by rapid and labored breathing, rapid heart rate, chest wall

retractions, grunting respirations, and flaring of the nostrils. These symptoms appear immediately or within a few hours after delivery (Beers et al. 2006). Infants with respiratory distress syndrome exhibit crackling or diminished breath sounds, as well as diminished peripheral pulses and poor color on physical examination. Gas exchange within the lungs is impaired, so that blood oxygen levels fall and carbon dioxide levels rise, leading to blood acidosis and hypoxia. The chest x-ray demonstrates decreased lung volumes (a bell-shaped chest), along with a small, discrete uniform infiltrate ("ground-glass" appearance).

The lungs of infants suffering from respiratory distress syndrome are stiff, requiring high pressures for ventilation. The lungs are also structurally immature, with a decreased number of gas-exchange units and thicker walls. As the disease progresses, repeated collapse and expansion of the lungs can lead to disruption of airway epithelium, impairment of lung mechanics, and further blockage of gas exchange (Curstedt and Johansson 2005). The surfactant-deficient lungs show bleeding, overdistension of the airways, and damage to the lining cells; alveolar injury additionally induces leakage from the lungs. Microscopically, the lungs demonstrate collapsed air spaces alternating with hyper-expanded areas; vascular congestion; and waxy hyaline membranes composed of fibrin and cellular debris. The hyaline membranes line the collapsed alveoli, and respiratory distress syndrome is sometimes called "hyaline membrane disease."

Eventually, infants with respiratory distress syndrome can develop cyanosis, lethargy, irregular breathing, and prolonged cessations of breathing (apnea). In severe cases, the respiratory muscles fatigue and ventilatory failure ensues. Complications of respiratory distress syndrome include intraventricular hemorrhage within the brain; white matter injury in the brain; tension pneumothorax of the lungs; bronchopulmonary dysplasia and chronic lung damage; sepsis; and ultimately neonatal death (Beers et al. 2006). Severe hypoxemia can also result in multiple organ failure and death. Clearly, a deficiency of lung surfactant can have devastating effects on premature infants.

Preterm babies with respiratory distress syndrome are treated with supplemental oxygen; mechanical ventilation; and intratracheal administration of exogenous surfactant through an endotracheal tube. A number of animal-derived surfactant preparations have been developed, as listed in Table 11.4. Such exogenous surfactants are created with improvements in overall mortality, morbidity, and resource utilization (Horbar et al. 1993a; Schwartz et al. 1994). Animal-derived surfactants are typically prepared either from extracts of lavaged animal lung surfactant or from extracts of processed animal lung tissue. The natural proteins SP-B and SP-C are found in all animal-derived surfactant products and are central to the efficacy of such preparations; in contrast, SP-A and SP-D are not retained in the preparation of any commercial animal-derived surfactants (Pfister and Soll 2005). Animal-derived surfactant therapies have been evaluated in clinical trials for very low birth weight infants and premature infants and have been shown to decrease mortality; reduce the severity of respiratory distress syndrome; decrease the likelihood of pneumothorax; and increase survival without chronic lung disease (Soll and McQueen 1992). For instance, one of the most commonly used surfactants is Survanta®, derived from

Table 11.4 Commercial animal-derived surfactant preparations in clinical use

Surfactant product	Source	Composition
Survanta® (beractant) – Abbott Laboratories	Organic solvent extract of processed bovine lung tissue, supplemented with phospholipids	• 25 mg/ml phospholipids (including 11.0–15.5 mg/ml disaturated phosphatidylcholine) • 0.5–1.75 mg/ml triglycerides • 1.4–3.5 mg/ml free fatty acids • <1.0 mg/ml protein • Suspended in 0.9% sodium chloride
Curosurf® (poractant) – Dey Laboratories	Organic solvent extract of processed bovine lung tissue	• 76 mg/ml phospholipids (including 55 mg/ml phosphatidylcholine, of which 30 mg is dipalmitoyl phosphatidylcholine) • 1 mg/ml protein, of which 0.2 mg/ml is SP-B • Suspended in 0.9% sodium chloride
Infasurf® (calfactant) – Forest Laboratories	Organic solvent extract of lavaged calf lung surfactant	• 35 mg/ml phospholipids (including 26 mg/ml phosphatidylcholine, of which 16 mg is dipalmitoyl phosphatidylcholine) • 0.65 mg/ml protein, of which 0.26 mg/ml is SP-B • Suspended in 0.9% sodium chloride

cow lungs, which can decrease the risk of death in very low birth weight infants by 30% (Schwartz et al. 1994).

However, animal-derived natural surfactants have several practical limitations. Any animal product has the potential to transmit viruses or other infectious agents derived from an animal source. Furthermore, infants receiving animal-derived surfactant are exposed to animal proteins and inflammatory mediators; such animal proteins may be seen as foreign by the infant's developing immune system and trigger an inflammatory response. Antibodies to these animal proteins may inactivate the exogenous surfactant as well as the native pulmonary surfactant (Strayer et al. 1991). In experimental in vivo models, antibodies developed against animal-derived SP-B caused respiratory distress and acute inflammatory and exudative lung lesions, including hyaline membranes (Robertson et al. 1991). Animal-derived surfactants thus raise concerns for adverse immunologic or infectious complications, along with the possibility of lung damage. Moreover, the levels of SP-B and SP-C found in the commercial surfactant preparations vary from batch to batch and are reduced compared to levels found in native pulmonary surfactant (van Eijk et al. 1995; Seeger et al. 1993). It has been argued that the concentration of surfactant proteins in these preparations may sometimes be too low to support the optimal adsorption of phospholipids at the air–fluid interface (Pfister and Soll 2005). Finally, surfactant preparations derived from animal lungs are expensive and in limited supply. Because of these issues with animal-derived surfactants, there is increasing interest in synthetic surfactant preparations to treat infants with respiratory distress syndrome.

11.2 Biomaterials as Synthetic Surfactants for the Lungs

New biomaterials are currently under investigation for use as synthetic surfactants and may overcome the limitations associated with animal-derived surfactant preparations. Synthetic surfactants could be more effective and safer, with no danger of infectious propagation or adverse reactions. Synthetic surfactant substitutes could also be produced in high quantities at lower costs, which may be particularly valuable for developing countries. In addition, synthetic surfactant proteins or their functional analogs might provide an opportunity to standardize the protein composition and thereby optimize surfactant function (Walther et al. 1998). Synthetic protein–lipid surfactants produced by molecular design would have a highly reproducible composition and ultimately provide an animal-free option. The appropriate protein content of synthetic surfactants will be critical to their clinical success; indeed, early non-protein-containing synthetic surfactants such as colfosceril palmitate were shown to be clinically inferior to animal-derived surfactants (Horbar et al. 1993b). Newer surfactant preparation composed of synthetic phospholipids and essential hydrophobic surfactant protein analogs or mimics have been formulated. These surfactant protein mimics have been produced by peptide synthesis and recombinant technology to provide an emerging class of synthetic surfactants that may be an efficacious alternative to animal-derived surfactants.

Two categories of synthetic surfactant preparations have been created: those containing SP-B mimics or analogs and those constituting SP-C analogs. (Native SP-B is too large and structurally complex to be synthesized, and native SP-C is structurally unstable in pure form.) Lucinactant (Surfaxin®, Discovery Laboratories, Inc., Warrington, PA) is a synthetic surfactant formulation that contains phospholipids and a peptide fragment that mimics polypeptide segments of SP-B. The peptide is called sinapultide (also known as KL4 peptide) and is designed to mimic a repeating pattern of hydrophobic and hydrophilic residues in the C-terminal part of SP-B. Sinapultide consists of a stretch of four hydrophobic leucines (L) interspersed with cationic lysine (K) to create a 21-residue sequence KLLLLKLLLLKLLLLKLLLLK, which is believed to stabilize the phospholipid layer by interactions with the lipid heads and the acyl chains (Cochrane and Revak 1991). Lucinactant is a combination of DPPC, palmitoyloleoyl-phophatidylglycerol, palmitic acid, and KL4 peptide (Cochrane et al. 1996).

The cationic peptide sinapultide resists inhibition to a greater extent than animal-derived surfactants (Manalo et al. 1996). In addition, sinapultide induces surface phase separation of model lung surfactant monolayers and enhances their ability to sustain high surface pressures (Ma et al. 1998). The KL4 synthetic peptide does not adversely affect the surfactant-related physiological functions of human pulmonary type II alveolar cells in culture (Romero et al. 2005). Compared to the animal-derived beractant, lucinactant protects human airway epithelial cells from inflammation and injury following exposure to hyperoxia (Zhu et al. 2008). The safety and efficacy of lucinactant has been further demonstrated using in vivo studies. In a simian model of respiratory distress syndrome, the KL4-containing surfactant exhibited homogeneous pulmonary distribution (Merritt et al. 1995). In

preterm rhesus monkeys, lucinactant successfully expanded the pulmonary alveoli and promoted gas exchange (Revak et al. 1996). Among preterm lambs with severe respiratory distress syndrome, lucinactant produced improvements in gas exchange and lung mechanics similar to those observed with the animal-derived poractant (Gastiasoro-Cuesta et al. 2006). When given to newborn babies with respiratory distress syndrome, lucinactant improved the arterial-to-alveolar oxygen tension ratio (Cochrane et al. 1996).

Lucinactant has recently progressed into controlled clinical trials for preterm infants. In a multi-center, randomized, controlled trial of lucinactant versus poractant for very premature infants at high risk for respiratory distress syndrome, lucinactant and poractant were similar in terms of safety and efficacy for the prevention and treatment of respiratory distress syndrome among preterm infants (Sinha et al. 2005). In another multi-center, randomized, masked comparison trial of lucinactant, colfosceril palmitate, and beractant for the prevention of respiratory distress syndrome among very preterm infants, lucinactant decreased respiratory distress syndrome-related mortality rates more effectively than both colfosceril and beractant (Moya et al. 2005). For preterm infants treated with lucinactant, the respiratory distress syndrome-related mortality rate by 14 days of life was 4.7%, compared with 9.4% for colfosceril-treated infants and 10.5% for beractant-treated infants. One-year follow-up of infants from both lucinactant trials indicated that the peptide-based surfactant is at least as good, if not superior, to animal-derived surfactants for prevention of respiratory distress syndrome (Moya et al. 2007). Survival through 1 year corrected age was higher for infants who received lucinactant than for infants who received animal-derived surfactants (beractant and poractant). The mortality rates were 24.6% for the lucinactant group and 26.7% for the animal-derived surfactant group. Clearly the lucinactant formulation, containing KL4 peptide to mimic the C-terminal fragment of SP-B, has the potential to replace animal-derived surfactants and lessen mortality of premature infants. As of late 2009, Surfaxin® was under review by the Food and Drug Administration.

Another synthetic peptide analog for SP-B has been created, utilizing an N-terminal segment of the SP-B surfactant protein (Fig. 11.5). SP-B_{1-25}, which contains the N-terminal residues 1–25 of SP-B, mimics the biophysical properties of full-length SP-B_{1-78} (Longo et al. 1993; Gupta et al. 2000). When added

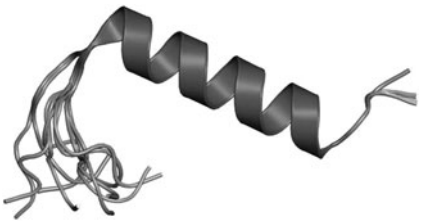

Fig. 11.5 Three-dimensional structure of the N-terminal fragment of SP-B, which contains an amphipathic helical region (Jawahar Swaminathan and Macromolecular Structure Database staff at the European Bioinformatics Institute)

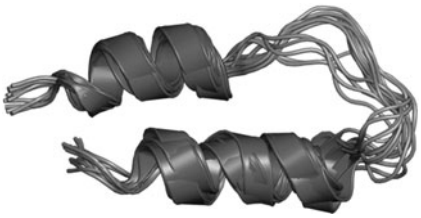

Fig. 11.6 Three-dimensional structure of a mini-protein construct (Mini-B) based on the primary structures of the N-terminal and C-terminal domains of SP-B. Mini-B incorporates residues 8–25 and 63–78 of SP-B, retaining two amphipathic helical regions (Jawahar Swaminathan and Macromolecular Structure Database staff at the European Bioinformatics Institute)

to phospholipids, SP-B_{1-25} induces monolayers in a fashion similar to full-length SP-B (Lipp et al. 1996). The SP-B_{1-25} peptide fragment is also relatively resistant to plasma inhibition in preterm rabbit models (Gupta et al. 2001). This peptide has been disulfide-linked into a homodimer, dSP-B_{1-25}, as native SP-B exists as a homodimer. The dimeric dSP-B_{1-25} analog demonstrates improved surface activity over the monomeric SP-B_{1-25}, and the dimeric analog has shown promise in vivo. Preterm rabbits given dSP-B_{1-25} and synthetic phospholipids had consistently higher tidal volumes than those given either animal-derived beractant or monomeric SP-B_{1-25} (Walther et al. 2002). Dimeric SP-B analogs that capture the N-terminal fragment show encouraging biochemical characteristics and have the potential to improve outcomes as compared to animal-derived surfactants, but these formulations have not yet been tested in humans.

Both the N-terminal and C-terminal domains of full-length SP-B are active sites of interaction with surfactant lipids (Waring et al. 1989). As such, an SP-B analog has been created which incorporates structures from both the N-terminal and C-terminal portions of SP-B (Waring et al. 2005). The construct, called Mini-B, is a 34 amino acid peptide which is designed to retain major amphipathic regions of SP-B; the construct includes residues 8–25 and 63–78 of human SP-B (Fig. 11.6). Critical N-terminal and C-terminal regions are joined in Mini-B via a beta-sheet/loop domain. The Mini-B construct is disulfide-bonded between Cys-8 and Cys-78 and between Cys-11 and Cys-71, analogous to the disulfide connectivities in native SP-B (residue numbers refer to the full-length sequence of human SP-B). Mini-B reproduces key in vitro and in vivo functions of native SP-B. For instance, in model surfactant lipid mixtures, SP-B exhibits high activity, with spread films showing near-zero minimum surface tensions. In a surfactant-deficient rat model, Mini-B enables oxygenation and dynamic compliance that compare favorably with results obtained using full-length SP-B (Waring et al. 2005).

Mini-B has additionally been evaluated as part of a fully synthetic exogenous surfactant (Walther et al. 2007). The novel synthetic surfactant contains Mini-B and DEPN-8, a phospholipase-resistant C16:0 diether phosphonolipid analog of DPPC. DEPN-8 and Mini-B display direct intermolecular interactions, and the DEPN-8 + Mini-B surfactant is more resistant to degradation than an animal-derived calf

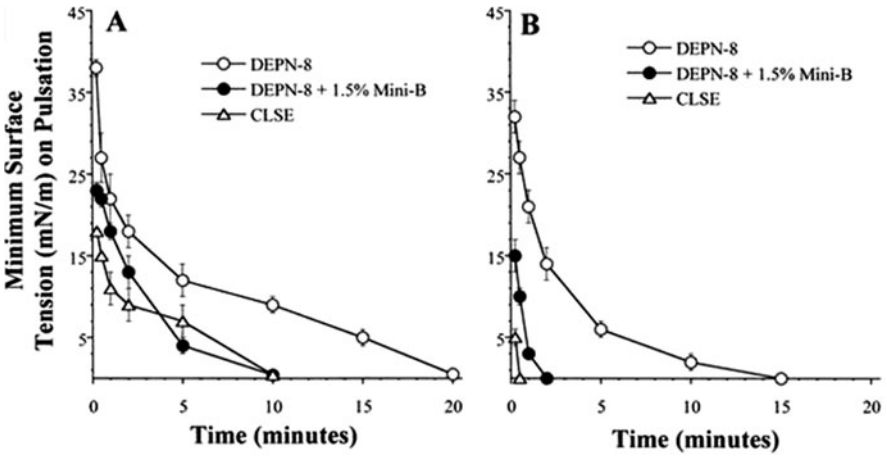

Fig. 11.7 Dynamic surface activity of synthetic lung surfactant and animal-derived lung surfactant, as measured on a pulsating bubble surfactometer. In this study, synthetic lung surfactants were composed of a diether phosphonolipid (DEPN-8), plus a mini-protein construct (Mini-B) related to native SP-B. The animal-derived preparation was a calf lung surfactant extract (CLSE). The study reveals a high dynamic surface activity for both the synthetic surfactant DEPN-8+1.5% Mini-B and the animal-derived CLSE. **a** 0.5 mg/ml phosphonolipid [phospholipid], **b** 2.5 mg/ml phosphonolipid [phospholipid] (Walther et al. 2007)

lung surfactant extract (Walther et al. 2007). Moreover, the synthetic DEPN-8 + Mini-B formulation demonstrates high dynamic surface activity, comparable to calf lung surfactant extract (Fig. 11.7). The DEPN-8 + Mini-B surfactant is resistant to the inhibitory effects of plasma proteins (Fig. 11.8). Surfactants containing Mini-B may thus be viable substitutes for animal-derived surfactants in the treatment of respiratory distress syndrome.

In terms of SP-C analogs, both full-length and truncated forms have been evaluated for use as synthetic surfactants. SP-C is a smaller protein than SP-B and is primarily alpha-helical in structure (Fig. 11.9). Native SP-C contains only 35 amino acid residues; the sequence of residues of 5–31 or 6–32, which contain the hydrophobic helical structure in the native protein, is necessary for biophysical activity (Takei et al. 1996). For the design of functional SP-C analogs, the formation of a transmembrane alpha-helix is more important than recapitulating the exact amino acid sequence (Johansson et al. 1995). A major challenge for the development of SP-C analogs is that the native molecule is extremely hydrophobic and exhibits structural instability in pure form. The native poly-valyl stretch within SP-C does not promote helix formation in vitro; rather, the poly-valyl sequence favors the formation of aggregates, with the peptide in a beta-sheet conformation (Johansson et al. 1995). To preserve the alpha-helical secondary structure and biophysical activity, an SP-C analog has been created which replaces the poly-valyl part of SP-C with a poly-leucyl stretch. The poly-Leu substituted SP-C analog, also known as SP-C(Leu), is virtually identical to native SP-C in its secondary alpha-helical

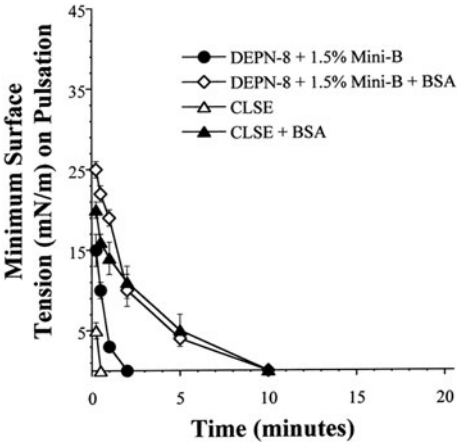

Fig. 11.8 Surface activity of synthetic lung surfactant and animal-derived lung surfactant in the presence of bovine serum albumin, as measured on a pulsating bubble surfactometer. In this study, synthetic lung surfactants were composed of a diether phosphonolipid (DEPN-8), plus a mini-protein construct (Mini-B) related to native SP-B. The animal-derived preparation was a calf lung surfactant extract (CLSE). Surfactant concentrations were 2.5 mg/ml phosphonolipid [phospholipid]. The study reveals a high overall surface activity for both the synthetic surfactant DEPN-8+1.5% Mini-B and the animal-derived CLSE, with both reaching minimum surface tensions of <1 mN/m by 10 min of bubble pulsation. Both preparations are resistant to the inhibitory effects of the plasma protein albumin (Walther et al. 2007)

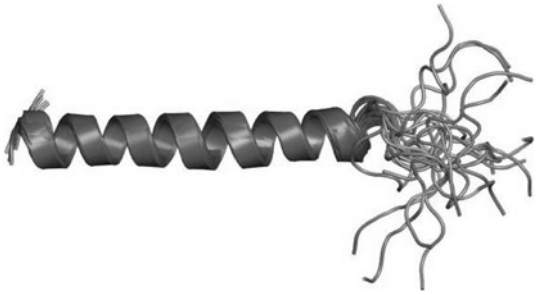

Fig. 11.9 Three-dimensional structure of SP-C, which contains a hydrophobic helical region (Jawahar Swaminathan and Macromolecular Structure Database staff at the European Bioinformatics Institute)

structure and surface-spreading properties in vitro (Nilsson et al. 1998). However, SP-C(Leu)/lipid mixtures show only a modest effect on dynamic lung compliance in preterm rabbit models. This may result from the fact that SP-C(Leu) oligomerizes into dimers, tetramers, hexamers, and higher-order oligomers, which makes it difficult to suspend SP-C(Leu)/lipid mixtures at high concentrations.

A modified SP-C (Leu) analog has been synthesized in an attempt to circumvent peptide oligomerization. The modified peptide, called SP-C(LKS), incorporates three lysines into the SP-C(Leu) sequence that cover the helix circumference and reduce peptide–peptide interactions (Palmblad et al. 1999). The SP-C(LKS)

peptide, combined with lipids, exhibits rapid absorption and spreading and can be suspended to high concentrations. Yet this preparation again does not significantly improve lung compliance in premature rabbit models; it is possible that the introduction of positively charged lysine residues disrupts peptide/membrane interactions (Curstedt and Johansson 2005). An alternative SP-C analog, named SP-C33, has been designed with one positive charge in the N-terminal portion of the alpha-helical chain (Johansson et al. 2003). Synthetic surfactants containing SP-C33/lipid mixtures can be suspended at high concentrations, and the SP-C33/lipid surfactants increase lung compliance in preterm rabbit models to levels similar to those obtained with animal-derived surfactants. However, rabbits receiving the SP-C33/lipid surfactant still exhibited alveolar instability.

Another novel synthetic surfactant preparation uses recombinant SP-C. Lusupultide (Venticute®, Altana Pharma, Konstanz, Germany) utilizes a full-length 34 amino acid human SP-C sequence, but replaces the cysteines in positions 4 and 5 replaced by phenylalanine, and replaces the methionine in position 32 with isoleucine to simplify the structure. In vitro, lusupultide effectively lowers surface tension. In vivo, surfactant based on this recombinant SP-C improves lung function in premature newborn rabbits and lambs (Davis et al. 1998). The effects of lusupultide on lung mechanics and compliance are similar to those of animal-derived surfactants. A clinical trial of lusupultide has been conducted in patients with acute respiratory distress syndrome; the synthetic surfactant improved gas exchange but did not improve survival during the treatment period (Spragg et al. 2003). Further optimization of SP-C analogs and recombinant SP-C formulations may be required for the creation of effective surfactants. In addition, studies are required to determine whether SP-C formulations can be improved by the addition of SP-B analogs or modification of lipid content.

Finally, non-natural bioinspired structures that capture both the amino acid sequence patterning and the three-dimensional structure of natural surfactant proteins have been designed for replacement of SP-B and SP-C (Wu et al. 2003; Seurynck et al. 2005). One of these polymers is a poly-*N*-substituted glycine (peptoid) with alpha-chiral side chains. The peptoids adopt a helical secondary structure and are resistant to enzymatic degradation. Peptoids have been created to mimic both the SP-B fragment SP-B_{1-25} (Seurynck et al. 2005) and the SP-C analog SP-C(Leu) (Wu et al. 2003). Formulations of these non-natural molecules with the lipid mixture DPPC:palmitoyloleoyl-phosphatidylglycerol:palmitic acid improve surfactant film morphology and dynamic adsorption and decrease surface tension in vitro. Very recently, dimeric peptoid analogs of native SP-B have been synthesized through "click"-mediated (1,3-dipolar cycloaddition) dimerization (Dohm et al. 2009). A family of "clicked" peptoid dimers has been developed to mimic d SP-B_{1-25}; in these dimeric structures, two amphipathic cationic helices are linked by an achiral octameric chain. The "clicked" dimers enhanced surface activity in lipid films relative to disulfide-bonded and monomeric SP-B fragments (Dohm et al. 2009). The performance of these artificial surfactants in vivo has not yet been evaluated.

Effective synthetic surfactant preparations based on designer peptides and phospholipids could eventually supplant animal-derived surfactant preparations for the treatment of respiratory distress syndrome. As pharmacologic products, synthetic exogenous surfactants possess significant advantages, including improved compositional and activity reproducibility, easier and less-costly quality control, freedom from infectious agents, and reduced cultural concerns relating to animal products. Much progress has been made in the development of synthetic surfactants, resulting from an increased understanding of the molecular mechanisms involved in the formation and preservation of the surfactant film at the alveolar lining. Stable and relatively simple peptides have been created to mimic the functions of SP-B and SP-C, and formulations based on these peptides have shown promise in laboratory, preclinical, and clinical studies. Future research on synthetic surfactants must focus on optimization of peptide structures and surfactant formulations. In addition, the biological interactions and metabolic fate of synthetic surfactants must be established. Well-designed synthetic surfactants could not only reduce deaths from respiratory distress syndrome but also be used as carriers for antibiotics, specific antibodies, or other drugs, for treatment of various lung diseases. The clinical impact of these preparations must be studied more extensively, and their clinical performance must be improved, with the goal of further reductions in morbidity and mortality of preterm infants.

Overall, novel biomaterials for the treatment of premature infants are a worthwhile investment. Between 1950 and 1990, the life expectancy for low birth weight infants increased by 12 years; this life expectancy improvement is primarily due to new medical technologies, including special ventilators and artificial surfactants (Cutler and McClellan 2001). From an economic perspective, every $1 spent on technological innovations for low-birth weight infants has produced an estimated $6 economic gain (Cutler and McClellan 2001). The benefits of medical technology for premature infants clearly outweigh the costs. Research advances in synthetic surfactants and other biomaterials are critical for eliminating infant mortality and protecting the youngest members of the global community.

References

Beers MH, Porter RS, Jones TV et al (2006) Merck manual of diagnosis and therapy, 18th edn. Wiley, New York, NY

Behrman RE, Stith A (2007) Preterm birth: causes, consequences, and prevention. National Academies Press, Washington, DC

Clements JA (1977) Functions of the alveolar lining. Am Rev Respir Dis 115:67

Cochrane CG, Revak SD (1991) Pulmonary surfactant protein B (SP-B): structure-function relationships. Science 254:566

Cochrane CG, Revak SD, Merritt TA et al (1996) The efficacy and safety of KL4- surfactant in preterm infants with respiratory distress syndrome. Am J Respir Crit Care Med 153:404

Curstedt T, Johansson J (2005) New synthetic surfactants – basic science. Biol Neonate 87:332

Cutler DM, McClellan M (2001) Is technological change in medicine worth it? Health Affairs 20:11

Davis AJ, Jobe AH, Häfner D et al (1998) Lung function in premature lambs and rabbits treated with a recombinant SP-C surfactant. Am J Respir Crit Care Med 157:553

Dohm MT, Seurynck-Servoss SL, Seo J et al (2009) Close mimicry of lung surfactant protein B by "clicked" dimers of helical, cationic peptoids. Biopolymers 92:538

Gastiasoro-Cuesta E, Alvarez-Diaz FJ, Rey-Santano C et al (2006) Acute and sustained effects of lucinactant versus poractant-alpha on pulmonary gas exchange and mechanics in premature lambs with respiratory distress syndrome. Pediatrics 117:2334

Gupta M, Hernández-Juviel JM, Waring AJ et al (2000) Comparison of functional efficacy of surfactant protein B analogues in lavaged rats. Eur Respir J 16:1129

Gupta M, Hernandez-Juviel JM, Waring AJ et al (2001) Function and inhibition sensitivity of the N-terminal segment of surfactant protein B (SP-B1-25) in preterm rabbits. Thorax 56:871

Horbar JD, Wright EC, Onstad L (1993a) Decreasing mortality associated with the introduction of surfactant therapy: an observational study of neonates weighing 601 to 1300 grams at birth. The Members of the National Institute of Child Health and Human Development Neonatal Research Network. Pediatrics 92:191

Horbar JD, Wright LL, Soll RF et al (1993b) A multicenter randomized trial comparing two surfactants for the treatment of neonatal respiratory distress syndrome. National Institute of Child Health and Human Development Neonatal Research Network. J Pediatr 123: 757

Johansson J, Curstedt T (1997) Molecular structures and interactions of pulmonary surfactant components. Eur J Biochem 244:675

Johansson J, Nilsson G, Strömberg R et al (1995) Secondary structure and biophysical activity of synthetic analogues of the pulmonary surfactant polypeptide SP-C. Biochem J 307:535

Johansson J, Some M, Linderholm BM et al (2003) A synthetic surfactant based on a poly-Leu SP-C analog and phospholipids: effects on tidal volumes and lung gas volumes in ventilated immature newborn rabbits. J Appl Physiol 95:2055

Lipp MM, Lee KY, Zasadzinski JA et al (1996) Phase and morphology changes in lipid monolayers induced by SP-B protein and its amino-terminal peptide. Science 273:1196

Longo ML, Bisagno AM, Zasadzinski JA et al (1993) A function of lung surfactant protein SP-B. Science 261:453

Ma J, Koppenol S, Yu H et al (1998) Effects of a cationic and hydrophobic peptide, KL4, on model lung surfactant lipid monolayers. Biophys J 74:1899

Manalo E, Merritt TA, Kheiter A et al (1996) Comparative effects of some serum components and proteolytic products of fibrinogen on surface tension-lowering abilities of beractant and a synthetic peptide containing surfactant KL4. Pediatr Res 39:947

Merritt TA, Kheiter A, Cochrane CG (1995) Positive end-expiratory pressure during KL4 surfactant instillation enhances intrapulmonary distribution in a simian model of respiratory distress syndrome. Pediatr Res 38:211

Moya FR, Gadzinowski J, Bancalari E et al (2005) A multicenter, randomized, masked, comparison trial of lucinactant, colfosceril palmitate, and beractant for the prevention of respiratory distress syndrome among very preterm infants. Pediatrics 115:1018

Moya F, Sinha S, Gadzinowski J et al (2007) One-year follow-up of very preterm infants who received lucinactant for prevention of respiratory distress syndrome: results from 2 multicenter randomized, controlled trials. Pediatrics 119:e1361

Nilsson G, Gustafsson M, Vandenbussche G et al (1998) Synthetic peptide-containing surfactants – evaluation of transmembrane versus amphipathic helices and surfactant protein C poly-valyl to poly-leucyl substitution. Eur J Biochem 255:116

Notter RH (2000) Lung surfactants: basic science and clinical applications. CRC Press, New York, NY

Notter RH, Wang Z (2008) Lung surfactants. In: Wnek GE, Bowlin GL (eds) Encyclopedia of biomaterials and biomedical engineering, 2nd edn. Informa Healthcare, New York, NY

Palmblad M, Johansson J, Robertson B et al (1999) Biophysical activity of an artificial surfactant containing an analogue of surfactant protein (SP)-C and native SP-B. Biochem J 339:381

Pfister RH, Soll RF (2005) New synthetic surfactants: the next generation? Biol Neonate 87:338

Revak SD, Merritt TA, Cochrane CG et al (1996) Efficacy of synthetic peptide-containing surfactant in the treatment of respiratory distress syndrome in preterm infant rhesus monkeys. Pediatr Res 39:715

Robertson B, Kobayashi T, Ganzuka M et al (1991) Experimental neonatal respiratory failure induced by a monoclonal antibody to the hydrophobic surfactant-associated protein SP-B. Pediatr Res 30:239

Rodriguez RJ, Martin RJ, Fanaroff AA (2002) Respiratory distress syndrome and its management. In: Fanaroff AA, Martin RJ (eds) Neonatal-perinatal medicine: diseases of the fetus and infant, 7th edn. Mosby, St Louis, MO

Romero EJ, Moya FR, Tuvim MJ et al (2005) Interaction of an artificial surfactant in human pulmonary epithelial cells. Pediatr Pulmonol 39:167

Schwartz RM, Luby AM, Scanlon JW et al (1994) Effect of surfactant on morbidity, mortality, and resource use in newborn infants weighing 500 to 1500 g. N Engl J Med 330:1476

Seeger W, Grube C, Günther A et al (1993) Surfactant inhibition by plasma proteins: differential sensitivity of various surfactant preparations. Eur Respir J 6:971

Seurynck SL, Patch JA, Barron AE (2005) Simple, helical peptoid analogs of lung surfactant protein B. Chem Biol 12:77

Sinha SK, Lacaze-Masmonteil T, Valls i Soler A et al (2005) A multicenter, randomized, controlled trial of lucinactant versus poractant alfa among very premature infants at high risk for respiratory distress syndrome. Pediatrics 115:1030

Soll RF, McQueen MC (1992) Respiratory distress syndrome. In: Sinclair JC, Bracken MB (eds) Effective care of the newborn infant. Oxford University Press, Oxford

Spragg RG, Lewis JF, Wurst W et al (2003) Treatment of acute respiratory distress syndrome with recombinant surfactant protein C surfactant. Am J Respir Crit Care Med 167:1562

Strayer DS, Hallman M, Merritt TA (1991) Immunogenicity of surfactant. II. Porcine and bovine surfactants. Clin Exp Immunol 83:41

Takei T, Hashimoto Y, Aiba T et al (1996) The surface properties of chemically synthesized peptides analogous to human pulmonary surfactant protein SP-C. Biol Pharm Bull 19:1247

van Eijk M, De Haas CG, Haagsman HP (1995) Quantitative analysis of pulmonary surfactant proteins B and C. Anal Biochem 232:231

Walther FJ, Hernández-Juviel J, Bruni R et al (1998) Protein composition of synthetic surfactant affects gas exchange in surfactant-deficient rats. Pediatr Res 43:666

Walther FJ, Hernandez-Juviel JM, Gordon LM et al (2002) Dimeric surfactant protein B peptide sp-b(1-25) in neonatal and acute respiratory distress syndrome. Exp Lung Res 28:623

Walther FJ, Waring AJ, Hernandez-Juviel et al (2007) Dynamic surface activity of a fully synthetic phospholipase-resistant lipid/peptide lung surfactant. PLoS One 2:e1039

Waring A, Taeusch W, Bruni R et al (1989) Synthetic amphipathic sequences of surfactant protein-B mimic several physicochemical and in vivo properties of native pulmonary surfactant proteins. Peptide Res 2:308

Waring AJ, Walther FJ, Gordon LM et al (2005) The role of charged amphipathic helices in the structure and function of surfactant protein B. J Pept Res 66:364

World Health Organization (2008) The global burden of disease: 2004 update. WHO Press, Geneva

Wu CW, Seurynck SL, Lee KY et al (2003) Helical peptoid mimics of lung surfactant protein C. Chem Biol 10:1057

Zhu Y, Miller TL, Chidekel A et al (2008) KL4- surfactant (Lucinactant) protects human airway epithelium from hyperoxia. Pediatr Res 64:154

Chapter 12
Conclusion

Biomaterials science is a multidisciplinary success story, having benefitted from advances in biomedical knowledge, as well as engineering and the physical sciences. Innovative biomaterials can allow individuals to live longer and healthier lives, as demonstrated by the technologies and case studies contained within this book. Biomaterials have sufficient versatility to tackle infectious diseases, chronic degenerative diseases, developmental disorders, and traumatic injuries. While this volume focused on 10 specific disease pathologies, the biomaterial devices described will have therapeutic potential for a multitude of disease processes. For instance, biomaterials for targeted delivery of chemotherapy will allow effective treatment of lung cancer along with several other cancers. Polymer-based vaccine adjuvants may help in preventing the spread of HIV/AIDS and numerous other infectious diseases. Biomaterials for nerve regeneration will have clinical applications that extend well beyond stroke, to various additional neurodegenerative diseases. When biomaterials are designed with an eye toward clinical needs, the resulting innovations will address the world's most prevalent diseases, yet will also find utility for related disease processes. It has been predicted that "ultimately, almost every human in technologically advanced societies will host a biomaterial" (Gristina 1981). Biomaterials scientists have the responsibility to create technologies that will reach both the developed world and the developing world. Modern discoveries in biomaterials and medical devices will rely on continual progress in molecular biology, polymer science, mechanical engineering, chemical engineering, and clinical practice.

Biomaterials scientists and engineers not only possess the capacity to solve critical healthcare problems, but also bear the duty to tackle these issues. The role of engineering in advanced healthcare is increasingly being recognized, as evidenced by the National Academy of Engineering's recent report on Grand Challenges for Engineering. In preparing this report, the National Academy of Engineering convened a panel of the most accomplished scientists and engineers of their generation; their goal was to identify the top societal challenges awaiting engineering solutions in the twenty-first century (National Academy of Engineering 2008). Of the 14 priorities identified as "Grand Challenges" by the panel, 3 fell into the realm of

S.K. Bhatia, *Biomaterials for Clinical Applications*,
DOI 10.1007/978-1-4419-6920-0_12, © Springer Science+Business Media, LLC 2010

healthcare. Specifically, the following three healthcare endeavors were recognized as priority areas for engineering:

- Advance health informatics
- Engineer better medicines
- Reverse-engineer the brain

Novel biomaterials will have a beneficial impact on all three of these "Grand Challenges": improved diagnostic platforms will advance health informatics; new drug delivery systems will enable better medicines; and emerging tissue-engineered scaffolds will reveal structure–function relationships in the brain and other organs. Ultimately, such emerging biomaterials will lessen the burden of disease worldwide, relieve the suffering inflicted by disease, and safeguard the well-being of the global community. Biomaterials scientists and engineers therefore have a clear directive to ensure the health of future generations and thereby ensure the future itself.

References

Gristina AG (1981) Biomaterial-centered infection: microbial adhesion versus tissue integration. Science 237:1588

National Academy of Engineering (2008) Grand challenges for engineering. National Academies Press, Washington, DC

Index

S.K. Bhatia, *Biomaterials for Clinical Applications*,
DOI 10.1007/978-1-4419-6920-0,